ТЕХНІКА ТА ЕНЕРГЕТИКА

Співзасновники:
Національний університет біоресурсів і природокористування України
ТОВ «Наукові журнали»

Рік заснування: 2010

Рекомендовано до друку та поширення
через мережу Інтернет Вченою радою
Національного університету біоресурсів і природокористування України
(протокол № 8 від 27 квітня 2022 р.)

Свідоцтво про державну реєстрацію
друкованого засобу масової інформації
серії КВ № 25126-15066 ПР від 17 лютого 2022

Журнал входить до переліку наукових фахових видань України
Категорія «Б». Галузь наук – Технічні.
Спеціальність: 131 – «Прикладна механіка», 133 – «Галузеве машинобудування»
(Наказ Міністерства освіти і науки України від від 17 березня 2020 року № 409)

Журнал представлено у міжнародних наукометричних базах даних,
репозитаріях та пошукових системах: Index Copernicus International,
Google Scholar, Фахові видання України,
Національна бібліотека України імені В. І. Вернадського,
AGRIS, BASE, Academic Resource Index ResearchBib

Адреса редакції:
Національний університет біоресурсів і природокористування України
вул. Героїв Оборони, 15, м. Київ, 03041, Україна
E-mail: info@technicalscience.com.ua
www: https://technicalscience.com.ua/uk

MACHINERY & ENERGETICS

Co-founders:
National University of Life and Environmental Sciences of Ukraine
LLC "Scientific Journals"

Year of foundation: 2010

Recommended for printing and distribution
via the Internet by the Academic Council
of National University of Life and Environmental Sciences of Ukraine
(Minutes No. 8 of April 27, 2022)

Certificate of state registration
of the print media
Series KV No. 25126-15066 PR of February 17, 2022

The journal is included in the list of Professional Scientific Publications of Ukraine
Category "B". Branch of sciences – Technical.
Specialty: 131 – "Applied mechanics", 133 – "Branch mechanical engineering
(Order of the Ministry of Education and Science of Ukraine of March 17, 2020, No. 409)

The journal is presented international scientometric databases, repositories and scientific systems: Index Copernicus International,
Google Scholar, Professional publications of Ukraine,
Vernadsky National Library of Ukraine, AGRIS, BASE,
Academic Resource Index ResearchBib

Editors office address:
National University of Life and Environmental Sciences of Ukraine
03041, 15 Heroiv Oborony, Kyiv, Ukraine
E-mail: info@technicalscience.com.ua
www: https://technicalscience.com.ua/en

Редакційна колегія

Editorial Board

ЗМІСТ

CONTENTS

Machinery & Energetics
Vol. 13, No. 2. 2022

Journal homepage:
https://technicalscience.com.ua/en

UDC 631.362.34
DOI: 10.31548/machenergy.13(2).2022.9-19

Elchyn Aliiev[1,2*], Krystyna Lupko[2]

[1]Institute of Oilseed Crops NAAS
69093, 1 Instytutska Str., v. Soniachne, Zaporizhzhia District, Zaporizhzhia Region, Ukraine

[2]Dnipro State Agrarian and Economic University
49600, 25 Serhii Efremov Str., Dnipro, Ukraine

Results of Numerical Modelling of the Process of Separation of Seed Material of Small-Seeded Crops on a Cylindrical Cell Trier

Abstract. The relevance of this study is conditioned upon the need to increase the amount of high-quality seed material of small-seeded crops, which cannot be achieved without an important process of separation. The separation is based on technical and technological principles of separation of seed material, depending on the differences in physical and mechanical properties of individual components of seed material. Cylindrical triers are used to separate seeds according to their length. The purpose of the study was to find the theoretical regularities of changes in the technological parameters of separation of the seed material of small-seeded crops from the structural and mode parameters of a cylindrical seed trier by numerical modelling. The solution of the set problems was implemented in the STAR-CCM+ programme based on the finite element method. Considering the physical and mechanical properties of the seed material, as a result of the study, a visualisation of the separation process was obtained depending on the research factors: the rotation frequency of the trier cylinder, the diameter of the cylinder, and the number of seeds and impurities in the seed mixture. According to the simulation results, the dependence of the relative content of impurities ε on factors under study was obtained in the form of second-order regression equations. Using the Mathematica programme, a compromise problem was solved, which lies in minimising the multiplicative function of the research criteria, and the rational constructive and technological parameters of the trier separator were found. The material of this paper is intended for scientists, graduate students, designers of agricultural machinery, students, and specialists in agricultural production

Keywords: mechanisation, separators, seed material, separation process

Article's History: Received: 14.12.2021; Revised: 21.03.2022; Accepted: 27.04.2022

INTRODUCTION

At various stages of seed processing of small-seeded crops, a separation process is used, the basis of which is the technical and technological principles of seed separation, based on differences in the physical and mechanical properties of individual components, among which one should note the shape, size, mass, specific weight, surface condition, and other properties inherent in the main seed and impurities. Carefully selected seed cleaning equipment has a considerable impact on the quality of its separation.

To separate the seeds, which differ in length, seed cleaning machines, namely cylindrical triers, are used. Their working body is a cylinder with an inner shell surface and a collection hopper installed on the axial support of the cylinder. The principle of operation of the trier is based on the rotation of the cylinder, during which seeds with different geometric sizes fall into the cells [1]. Long seeds have low resistance at rest and are carried towards rotation of the cylinder and fall out of the shell at a certain angle. Short seeds have high resting resistance and fall out of the pods, but at a different angle. All the seeds must fall out of the pods, and this depends on the structural parameters of the equipment, which include the rotation frequency of the cylinder and its diameter.

The purpose of this study was to find the theoretical regularities of changes in the technological parameters of separation of seed material of small-seeded crops from the structural and operational parameters of the cylindrical cell trier by numerical modelling and establishing rational structural and technological parameters of the trier separator.

In connection with the growing needs for high-quality visualisation with the possibility for the viewer to immerse

Suggested Citation:
Aliiev, E., & Lupko, K. (2022). Results of numerical modelling of the process of separation of seed material of small-seeded crops on a cylindrical cell trier. *Machinery & Energetics,* 13(2), 9-19.

*Corresponding author

himself in a virtual environment, a preliminary feasibility study was performed, the purpose of which was to find the advantages and disadvantages associated with visualisation in a virtual environment of the CAVE type [2]. The study [3] described the development of a method for predicting events that occur when the diesel fuel flow hits the walls of the combustion chamber. A mathematical model of the films on the walls of the chamber formed as a result of spraying was constructed. The paper [4] investigated the experimental data on the distribution of solid particles in horizontal pipelines, which were modelled using computational fluid dynamics (CFD) and the discrete element method (DEM). In [5], using the STAR-CCM+ software package, conditions for increasing the efficiency of removing small particles from the cyclone were applied. The paper [6] describes an attempt to visualise the behaviour of the flow in various geometric conditions of the pipe. The authors obtained the values of pressure and velocity contours on various parts of the pipe in which water is the medium.

Models of ideal extrusion and mixing, diffusion, and combined models have become widespread among modern researchers [7; 8].

A scientific originality of this study lies in the use of numerical modelling to investigate the separation of seed material of small-seeded crops on a cylindrical trier.

MATERIALS AND METHODS

Based on the above-mentioned studies, it was proposed to solve the problems in the STAR-CCM+ programme, which is based on the finite element method.

The numerical modelling is performed using the following methods and approaches [9]: analysis of the structure of material flows, empirical method, approach of the mechanics of continuous media, statistical method, entropy-information method.

As a seed model, mustard seeds were accepted, the physical and mechanical properties of which were as follows: Poisson's ratio – 0.5; Young's modulus – 0.2 MPa; density – 700 kg/m^3; coefficient of rest friction – 0.8; normal recovery factor – 0.5; tangent coefficient of recovery – 0.5; the coefficient of rolling resistance – 0.3. The model of the mustard seed is a sphere. Therewith, the seeds can have an effective diameter within the $d_g \in [dgmax_{gmin}]$ range, where d_{gmin} 0.001 m is the minimum value of the effective seed diameter, m; d_{gmax}=0.003 m is the maximum value of the effective seed diameter, m.

The seed mixture was presented in the form of two components: seeds of the main crop and impurities [10].

The following physical and mechanical properties were adopted as a model of impurities in the seed mixture: Poisson's ratio – 0.5; Young's modulus – 0.2 MPa; density – 700 kg/m^3; coefficient of rest friction – 0.8; normal recovery factor – 0.5; tangent coefficient of recovery – 0.5; the coefficient of rolling resistance – 0.3. In this case, the effective diameter of impurities obeys the normal distribution. Therewith, impurities can have an effective diameter within the $d_g \in [dgmax_{gmin}]$ range, where d_{gmin}=0.002 m is the minimum value of the effective diameter of the impurity, m; d_{gmax}=0.004 m is the maximum value of the effective diameter of the admixture, m.

The properties of the environment were as follows: environment – air; dynamic viscosity – 1.85508·10-5 Pa·s; turbulent Prandtl number – 0.9; acceleration of free fall – 9.8 m/s^2; temperature – 293 K; pressure – 101,325 Pa. The calculation scheme of the cylindrical cell trier is presented in Figure 1.

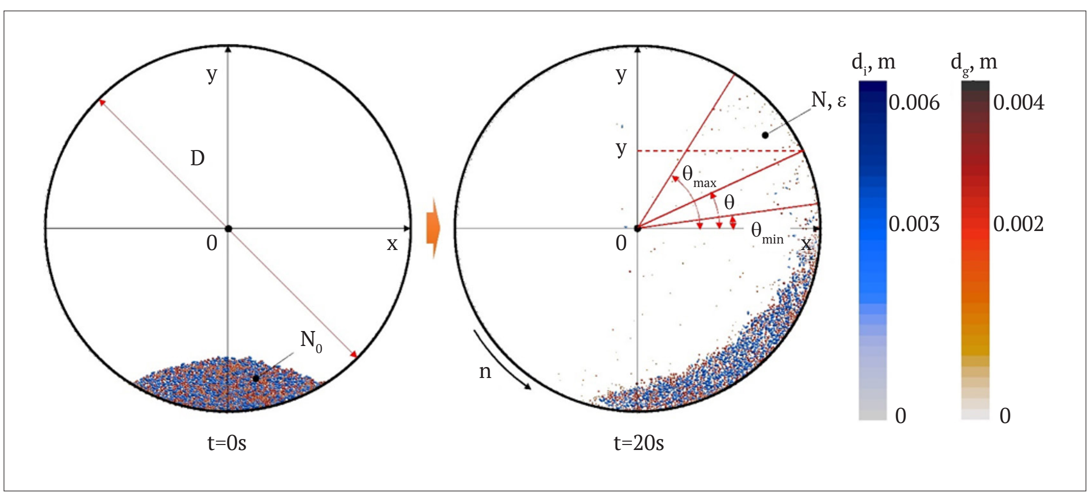

Figure 1. Calculation scheme of a cylindrical shell trier for numerical modelling in the STAR-CCM+ software package

Factors for numerical modelling are the diameter of the trier separator cylinder *D*, its rotation frequency *n* and the number of seeds in the seed mixture N_0 at the initial time. The levels of variation by factors are presented in Table 1. Numerical modelling was implemented using a fully factorial experiment. The total number of experiments was 5^3=125.

Table 1. Levels of variation by numerical modelling factors

Level	Factor		
	Trier cylinder diameter D, m (x_1)	Trier cylinder rotation frequency n, rpm (x_2)	The number of seeds and impurities in the seed mixture N_0, pcs (x_3)
-1.0	0.2	30.0	1,000
-0.5	0.3	37.5	2,000
0	0.4	45.0	3,000
+0.5	0.5	52.5	4,000
+1.0	0.6	60.0	5,000

The minimum θ_{min} and maximum θ_{max} values were determined from the list of values of the angle θ of seed exit from the pod.

The number of all components of the seed mixture N, which were within the minimum θ_{min} and maximum θ_{max} angles of rotation of the trier separator cylinder, was chosen as a performance criterion.

The criterion for evaluating the quality of the separation process was the relative content of impurities θ in the seed mixture, which was within the minimum θ_{min} and maximum θ_{max} rotation angles of the trier separator cylinder.

As a result of data processing in the Mathematica software package, it was necessary to establish the dependence of the above-mentioned criteria of the separation process on research factors in the form of second-order regression equations.

Statistical processing of the obtained data in the Mathematica software package consisted in determining the Student's criterion [11] for each coefficient of the regression equation and comparing it with the table value. If the calculated value is less than the table value, then the coefficient of the regression equation is insignificant and can be ignored.

The obtained regression equation was checked for adequacy using the Fisher test [12] and the correlation coefficient [13-15].

RESULTS AND DISCUSSION

The dependence of the values of the minimum θ_{min} and the maximum θ_{max} values of the angles of seed exit from the cell of the trier cylinder on research factors, which was obtained using the Mathematica programme, has the following coded form:

$$\begin{gathered}\theta_{min} = 0,311838 - 0,0758691\, x_1 - 0,0252283 x_1^2 + \\ +0,246916 x_2 - 0,00964664\, x_1 x_2 + 0,0125726 x_2^2 + \\ +\, 0,104465\, x_3 - 0,00984237\, x_1 x_3 + \\ +0,081428\, x_2 x_3 + 0,0366488\, x_3^2\,,\end{gathered} \tag{1}$$

$$\begin{gathered}\theta_{max} = 0,989517 + 0,277431 x_1 - 0,0739117 x_1^2 + \\ +0,499129\, x_2 + 0,0953195 x_1 x_2 - 0,0359794\, x_2^2 - \\ -\, 0,00436025 x_3 + 0,00296865 x_1 x_3 - \\ -0,00305847 x_2 x_3 - 0,0160532 x_3^2\,.\end{gathered} \tag{2}$$

Statistical processing of Equations (1) and (2) are presented in Tables 2 and 3, respectively.

Table 2. Results of statistical processing of Equation (1)

Coefficient	Value	Error	Student's t-test	Probability
a_{00}	0.311838	0.00917538	33.9864	$4.14411 \cdot 10^{-43}$
a_{10}	-0.0758691	0.0046433	-16.3395	$1.0548 \cdot 10^{-24}$
a_{20}	0.246916	0.00536162	46.0524	$2.41186 \cdot 10^{-51}$
a_{30}	0.104465	0.00536162	19.4839	$7.70832 \cdot 10^{-29}$
a_{12}	-0.00964664	0.00656662	-1.46904	0.146645
a_{13}	-0.00984237	0.00656662	-1.49885	0.138754
a_{23}	0.081428	0.00758248	10.739	$4.843 \cdot 10^{-16}$
a_{11}	-0.0252283	0.00804243	-3.1369	0.00256524
a_{22}	0.0125726	0.00906279	1.38727	0.170097
a_{33}	0.0366488	0.00906279	4.04388	0.000141885

Table 3. Results of statistical processing of Equation (2)

Coefficient	Value	Error	Student's t-test	Probability
a_{00}	0.989517	0.0229487	43.1186	$1.52231 \cdot 10^{-49}$
a_{10}	0.277431	0.0116135	23.8887	$6.77808 \cdot 10^{-34}$
a_{20}	0.499129	0.0134101	37.2205	$1.49665 \cdot 10^{-45}$
a_{30}	-0.00436025	0.0134101	-0.325148	0.746114
a_{12}	0.0953195	0.0164239	5.80371	$2.10038 \cdot 10^{-7}$
a_{13}	0.00296865	0.0164239	0.180752	0.857125
a_{23}	-0.00305847	0.0189647	-0.161272	0.872379
a_{11}	-0.0739117	0.0201151	-3.67444	0.000484351
a_{22}	-0.0359794	0.0226671	-1.58729	0.1173
a_{33}	-0.0160532	0.0226671	-0.708216	0.481343

Comparing the calculated Student's criterion with the tabular $t_{0.05}(125)=1.98$, insignificant regression coefficients were rejected. As a result, the Equations (1) and (2) are transformed as follows:

$$\theta_{\min} = 0{,}311838 - 0{,}0758691x_1 - 0{,}0252283\, x_1^2 + +0{,}246916\, x_2 + 0{,}104465x_3 + 0{,}081428x_2x_3 + +0{,}0366488x_3^2\,, \quad (3)$$

$$\theta_{\max} = 0{,}989517 + 0{,}277431\, x_1 - -0{,}0739117\, x_1^2 + 0{,}499129\, x_2 + 0{,}0953195\, x_1x_2 \quad (4)$$

By substituting the expressions for research factors into equations (3-4) instead of x_1–x_3 in an explicit form, one can obtain the dependence of the values of the minimum $\theta_{\min}$ and the maximum $\theta_{\max}$ of the values of the angles of seed exit from the cell of the trier cylinder on the research factors in a decoded form:

$$\theta_{\min} = -0{,}0858955 + 0{,}12522 \cdot D - 0{,}630707 \cdot D^2 + +0{,}00831824 \cdot n - 0{,}000124883\, N_0 + 2{,}71427 \cdot \cdot 10^{-6} n \cdot N_0 + 9{,}1622 \cdot 10^{-9} \cdot N_0^2\,, \quad (5)$$

$$\theta_{\max} = -0{,}786462 + 1{,}43559 \cdot D - 1{,}84779 \cdot D^2 + + 0{,}020566 \cdot n + 0{,}0317732 \cdot D \cdot n \quad (6)$$

Graphical interpretation of dependences (5-6) is presented in Figures 2-4.

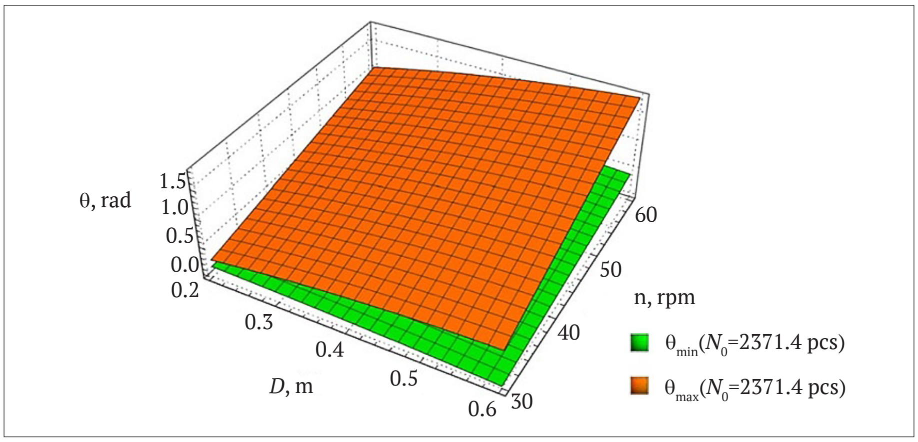

Figure 2. The dependence of the values of the minimum $\theta_{\min}$ and the maximum $\theta_{\max}$ values of the angles of seed exit from the cell of the trier cylinder on the diameter of the trier cylinder D and the rotation frequency of the trier cylinder n

Figure 2 demonstrates that with an increase in the rotation frequency of the cylinder and an increase in its diameter, the values of the angles of seed exit from the cell of the trier cylinder increase. The maximum seed exit angle is observed at the maximum rotation frequency of the cylinder, namely n=60 rpm and the maximum diameter D=0.6 m, and is $\theta_{\max}$=1.5 rad. The smallest value of the maximum seed exit angle is observed at the minimum rotation frequency of the cylinder, namely n=30 rpm and the smallest diameter D=0.2 m, and is $\theta_{\max}$=0.3–0.4 rad. Figure 2 shows that with an increase in the cylinder rotation frequency, the minimum seed departure angle $\theta_{\min}$ increases, which is 0.4 rad at a cylinder rotation frequency n=60 rpm. At the minimum rotation frequency of the cylinder, namely n=30 rpm, the minimum seed exit angle $\theta_{\min}$ is 0 rad. This is because at the minimum rotation frequency of the cylinder, the seed material practically does not move in the cylinder and does not reach the region $\theta_{\min}$.

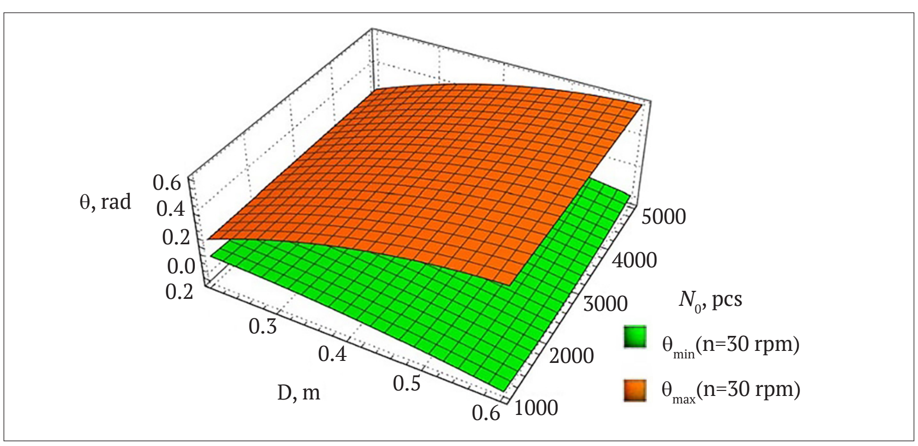

Figure 3. Dependence of the values of the minimum $\theta_{\min}$ and maximum $\theta_{\max}$ values of the angles of seed exit from the cell of the trier cylinder on the diameter of the trier cylinder D and the number of seeds and impurities in the seed mixture N_0

Figure 3 shows that as the diameter of the cylinder D decreases and the number of seeds in the mixture N increases, the value of the minimum seed exit angle θ_{min} increases. This is explained by the fact that at the minimum value of the diameter of the cylinder D, namely D=0.2 m, the seed material is practically not moved or is moved forming a thick layer of seed material, among which a dead layer is formed. On the contrary, the maximum angle of exit of the seed from the cell θ_{max} increases with an increase in the diameter of the cylinder D. This is explained by the fact that the seed material is better distributed on the inner surface of the cylinder and forms a thin layer that is easier to move when the trier cylinder rotates. The amount of seed material does not affect the maximum angle of exit of the seed from the cell θ_{max} at different values of the diameter of the cylinder D.

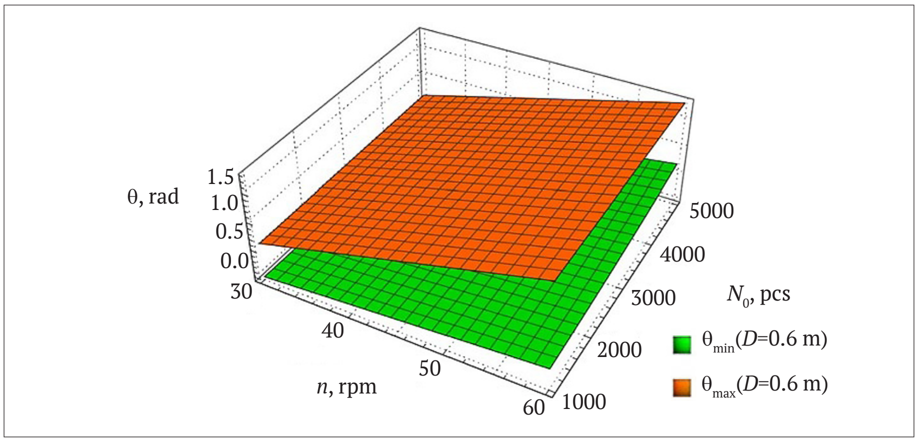

Figure 4. The dependence of the values of the minimum θ_{min} and the maximum θ_{max} values of the angles of seed exit from the cell of the trier cylinder on the rotation frequency of the trier cylinder n and the number of seeds and impurities in the seed mixture N_0

Figure 4 shows that the values of the minimum θ_{min} and maximum θ_{max} of the seed exit angles increase with an increase in the rotation frequency of the trier cylinder n. The values of the minimum seed exit angle θ_{min} increase with an increase in the rotation frequency of the trier cylinder n, and these values also depend on the number of seeds and impurities in the seed mixture N_0. Figure 4 demonstrates that with an increase in the amount of seed material, the minimum angle θ_{min} of seed exit from the pod increases. This is explained by the fact that at a higher rotation frequency of the trier cylinder n, more seed material is distributed over the inner surface of the trier cylinder in the direction of rotation of the cylinder, and the smaller the dead layer of seed material is formed.

The maximum angle of exit of the seed from the cell θ_{max} also increases with an increase in the rotation frequency of the trier cylinder n. The amount of seed material does not affect the maximum angle of exit of the seed from the cell θ_{max}.

Statistical analysis of Equations (5) and (6) in the variation range under study showed that the Pearson correlation coefficient is 0.82 and 0.85, respectively. In turn, Fisher's criterion was $F_{(7)}=2.27<F_t=2.49$ and $F_{(8)}=2.17<F_t=2.49$, respectively. This confirms the adequacy of the obtained models.

The dependence of the values of the number of all components of the seed mixture N that were within the minimum θ_{min} and maximum θ_{max} angles of rotation of the trier separator cylinder on the research factors, which was obtained using the Mathematica programme, has the following coded form:

$$N = 235{,}731 - 47{,}14\,x_1 + 47{,}74\,x_1^2 + 165{,}44x_2 + \\ +59{,}26x_1x_2 + 29{,}8667\,x_2^2 + 170{,}96x_3 - \\ -88{,}6x_1x_3 + 90{,}6133x_2x_3 - 2{,}20952\,x_3^2 \quad (7)$$

Statistical processing of Equation (7) is presented in Table 4.

Table 4. Results of statistical processing of Equation (9)

Coefficient	Value	Error	Student's t-test	Probability
a_{00}	235.731	12.0203	19.6112	$5.36449 \cdot 10^{-29}$
a_{10}	-47.14	6.08299	-7.74948	$8.13362 \cdot 10^{-11}$
a_{20}	165.44	7.02403	23.5534	$1.54678 \cdot 10^{-33}$
a_{30}	170.96	7.02403	24.3393	$2.26924 \cdot 10^{-34}$
a_{12}	59.26	8.60264	6.88858	$2.72815 \cdot 10^{-9}$
a_{13}	-88.6	8.60264	-10.2992	$2.72282 \cdot 10^{-15}$
a_{23}	90.6133	9.93347	9.12202	$3.02192 \cdot 10^{-13}$
a_{11}	47.74	10.536	4.53111	0.000025749
a_{22}	29.8667	11.8728	2.51556	0.0143649
a_{33}	-2.20952	11.8728	-0.1861	0.852946

Comparing the calculated Student's criterion with the tabular $t_{0.05}(125)=1.98$, the insignificant regression coefficients were excluded. As a result, the Equation (7 is transformed as follows:

$$N = 235{,}731 - 47{,}14\,x_1 + 47{,}74x_1^2 + \\ +165{,}44x_2 + 59{,}26x_1\,x_2 + 29{,}8667\,x_2^2 + \\ +170{,}96x_3 - 88{,}6x_1x_3 + 90{,}6133\,x_2x_3 \qquad (8)$$

By substituting into equation (10) instead of x_1–x_3 the expressions for research factors in an explicit form, one obtains the dependence of the values of the number of all components of the seed mixture N that were within the minimum θ_{min} and maximum θ_{max} rotation angles of the trier separator cylinder on the research factors in a decoded form:

$$N = 534{,}531 - 1414{,}9\,D + 1193{,}5D^2 - \\ -17{,}88\,n + 19{,}753\,D\,n + 0{,}132741\,n^2 + \\ +0{,}03816\,N_0 - 0{,}2215\,D\,N_0 + 0{,}00302044\,n\,N_0 \qquad (9)$$

The optimal values of the factors under the condition of the maximum amount of all components of the seed mixture (N=816 pcs) are D=0.2 m, n=60 rpm, N_0=5,000 pcs.

The graphical interpretation of the dependence (9) is presented in Figures 5-7.

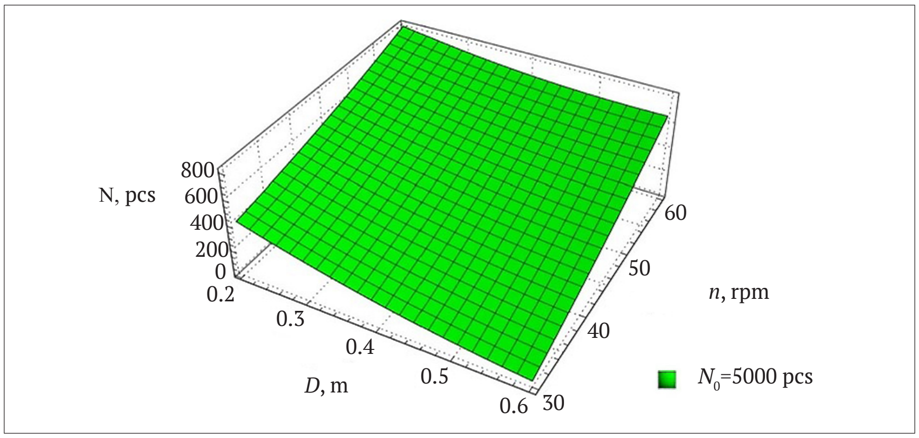

Figure 5. The dependence of the values of the number of all components of the seed mixture N, which were within the minimum θ_{min} and maximum θ_{max} rotation angles of the trier separator cylinder on the diameter of the trier cylinder D and the rotation frequency of the trier cylinder n

Figure 5 shows that the values of the number of all components of the seed mixture N increase with a decrease in the diameter of the cylinder and an increase in the frequency of rotation of the cylinder n. With an increase in the rotation frequency of the cylinder, the seed will reach the cells more often and, accordingly, the seed will be more efficiently separated into the main crop and impurities. The diameter of the trier cylinder D is also important because with a larger diameter, less seed material reaches the area between the minimum θ_{min} and maximum θ_{max} rotation angles of the trier separator cylinder.

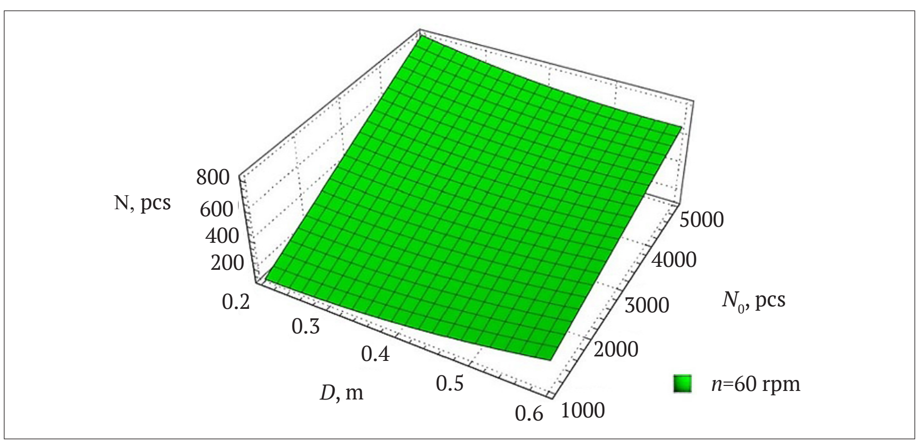

Figure 6. The dependence of the values of the number of all components of the seed mixture N, which were within the minimum θ_{min} and maximum θ_{max} rotation angles of the cylinder of the trier separator on the diameter of the cylinder of the trier D and the number of seeds and impurities in the seed mixture N_0

Figure 6 shows that the number of all components of the seed mixture N, which were within the minimum θ_{min} and maximum θ_{max} angles of rotation of the trier separator cylinder, increases with the increase in the total number of all components of the seed mass N_0. In addition, Figure 6 demonstrates that the number of all components of the seed mixture N, which were within the minimum θ_{min} and maximum θ_{max} angles of rotation of the cylinder of the trier separator, increases with an increase in the diameter of the cylinder D.

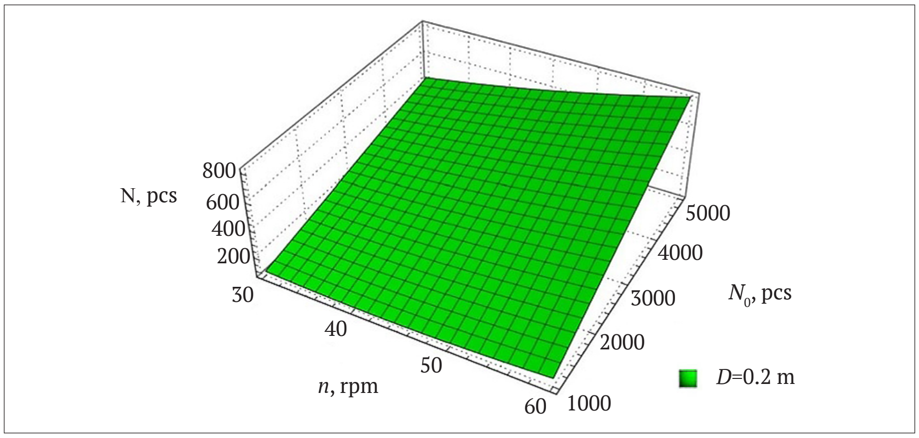

Figure 7. The dependence of the values of the number of all components of the seed mixture N, which were within the minimum θ_{min} and maximum θ_{max} angles of rotation of the cylinder of the trier separator, on the frequency of rotation of the cylinder of the trier n and the number of seeds and impurities in the seed mixture N_0

Figure 7 shows that the rotation frequency of the cylinder n at the minimum value N_0 (N_0=1,000 pcs) practically does not affect the value of the number of all components of the seed mixture N, which were within the minimum θ_{min} and maximum θ_{max} rotation angles of the trier separator cylinder. As the values of N_0 and the cylinder rotation frequency n increase, the values of the amount of seed material N increase. The amount of seeds and impurities in the seed material N_0 affects the amount of seed material N that was within the minimum θ_{min} and maximum θ_{max}: the greater the amount of N_0, the greater the amount of material reached the required limits.

Statistical analysis of Equation (9) in the variation range under study showed that the Pearson correlation coefficient is 0.83 and 0.85, respectively. In turn, Fisher's criterion was $F_{(7)}=2.11<F_t=1.87$ and $F_{(8)}=2.17<F_t=2.49$, respectively. This confirms the adequacy of the obtained models.

The dependence of the relative content of impurities ε in the seed mixture, which was within the minimum θ_{min} and maximum θ_{max} rotation angles of the trier separator cylinder, on the research factors, which was obtained using the Mathematica programme, has the following coded form:

$$\begin{aligned}\varepsilon = 11{,}9176 - 11{,}2438\, x_1 + 5{,}25111\, x_1^2 +\\ +1{,}25032\, x_2 + 0{,}95207\, x_1 x_2 - 0{,}203757\, x_2^2 +\\ +2{,}28584\, x_3 + 0{,}593043\, x_1 x_3 - 2{,}9289 x_2 x_3 +\\ +4{,}12055\, x_3^2\end{aligned} \quad (10)$$

Statistical processing of Equation (10) is presented in Table 5.

Table 5. Results of statistical processing of Equation (12)

Coefficient	Value	Error	Student's t-test	Probability
a_{00}	11.9176	0.866702	13.7505	$6.51748\cdot10^{-21}$
a_{10}	-11.2438	0.438604	-25.6353	$1.06553\cdot10^{-35}$
a_{20}	1.25032	0.506456	2.46876	0.0161966
a_{30}	2.28584	0.506456	4.51339	0.0000274407
a_{12}	0.95207	0.62028	1.5349	0.129661
a_{13}	0.593043	0.62028	0.956089	0.34257
a_{23}	-2.9289	0.716237	-4.08929	0.000121504
a_{11}	5.25111	0.759684	6.91222	$2.47842\cdot10^{-9}$
a_{22}	-0.203757	0.856067	-0.238015	0.812618
a_{33}	4.12055	0.856067	4.81335	$9.21338\cdot10^{-6}$

Comparing the calculated Student's criterion with the tabular $t_{0.05}(125)=1.98$, the insignificant regression coefficients were excluded. As a result, the Equation (10) is transformed as follows:

$$\begin{aligned}\varepsilon = 11{,}9176 - 11{,}2438 x_1 + 5{,}25111\, x_1^2 +\\ +1{,}25032\, x_2 + 2{,}28584 x_3 -\\ - 2{,}9289\, x_2 x_3 + 4{,}12055\, x_3^2\end{aligned} \quad (11)$$

By substituting into Equation (11) instead of x_1–x_3 the expressions for research factors in explicit form, one obtains the dependence of the relative content of impurities ε in the seed mixture, which was within the minimum θ_{min} and maximum θ_{max} rotation angles of the trier separator cylinder, on the research factors in decoded form:

$$\begin{aligned}\varepsilon = 44{,}321 - 161{,}241\, D + 131{,}278\, D^2 +\\ +0{,}376244\, n - 0{,}000644556\, N_0 -\\ -0{,}00009763\, n\, N_0 + 1{,}03014\cdot10^{-6} N_0^2\end{aligned} \quad (12)$$

The optimal values of the factors under the condition of the minimum relative content of impurities in the seed mixture (ε=3.02%) are D=0.6 m, n=30 rpm, N_0=1734 pcs.

A graphical interpretation of dependence (12) is presented in Figures 8-10.

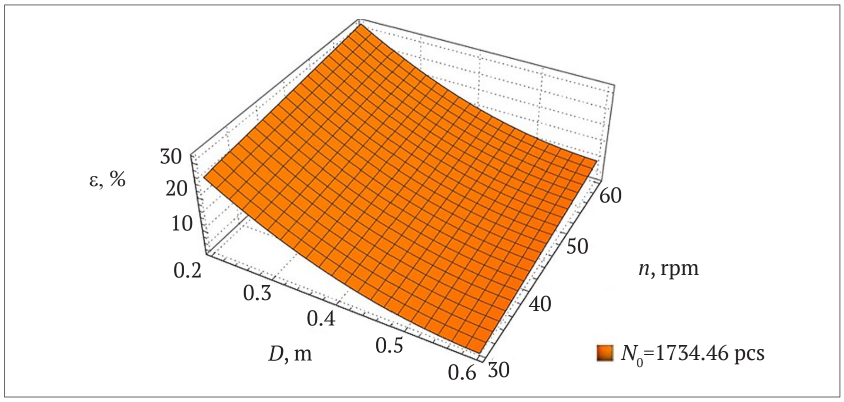

Figure 8. The dependence of the relative content of impurities ε in the seed mixture, which was within the minimum θ_{min} and maximum θ_{max} rotation angles of the trier separator cylinder on the diameter of the trier cylinder D and the rotation frequency of the trier cylinder n

Figure 8 shows that as the cylinder diameter D decreases, the relative content of impurities ε in the seed mixture increases. This is explained by the fact that with a smaller diameter, the efficiency of separating seed material is considerably reduced. The speed of rotation of the cylinder n also affects the relative content of impurities in the seed material. When the values of the frequency n increase, the relative content of impurities ε increases.

Figure 9 demonstrates that the relative content of impurities ε in the seed mixture increases with a decrease in the diameter of the cylinder and an increase in the number of seeds and impurities in the seed mixture N_0. The maximum amount of seed material (N_0=4,000 pcs, N_0=5,000 pcs) is more rationally divided using a cylinder with a larger diameter, namely D=0.5-0.6 m.

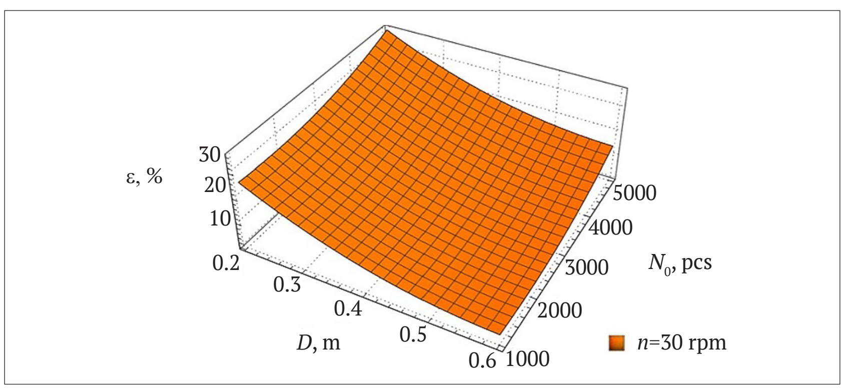

Figure 9. The dependence of the values of the relative content of impurities ε in the seed mixture, which was within the minimum θ_{min} and maximum θ_{max} angles of rotation of the cylinder of the trier separator on the diameter of the cylinder of the trier D and the number of seeds and impurities in the seed mixture N_0

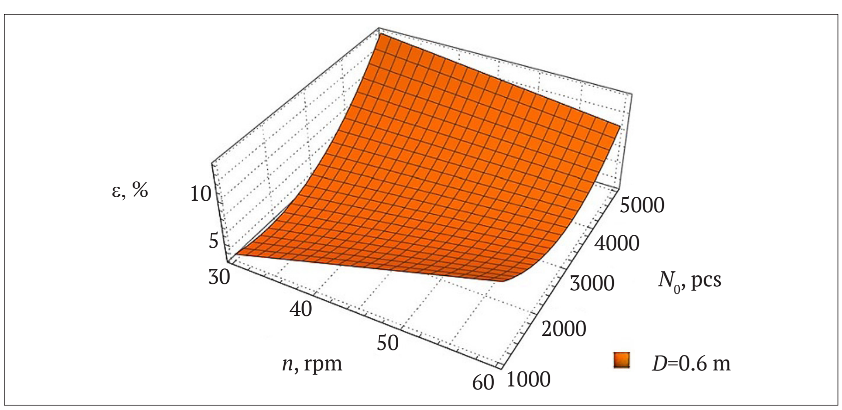

Figure 10. The dependence of the values of the relative content of impurities ε in the seed mixture, which was within the minimum θ_{min} and maximum θ_{max} rotation angles of the cylinder of the trier separator on the rotation frequency of the cylinder of the trier n and the number of seeds and impurities in the seed mixture N_0

Figure 10 shows that the largest values of the relative content of impurities ε occur in two cases: with the minimum value of the cylinder rotation frequency n=30 rpm and the maximum amount of seed mixture N_0=5,000 pcs, the relative content of impurities ε in the seed mixture is ε=13%; at the maximum value of the cylinder rotation frequency n=60 rpm and the minimum amount of seed mixture N_0=1,000 pcs, the relative content of impurities ε in the seed mixture is ε=12-14%.

Statistical analysis of equations (12) in the variation range under study showed that the Pearson correlation coefficient is 0.88 and 0.87, respectively. In turn, Fisher's criterion was $F_{(7)}=1.84<F_t=2.49$ and $F_{(8)}=1.98<F_t=2.49$, respectively. This confirms the adequacy of the obtained models.

Since the optimal values of factors according to individual research criteria do not coincide, the following compromise problem is to be solved:

$$\begin{cases} \varepsilon(D, n, N_0) \rightarrow min, \\ N(D, n, N_0) \rightarrow max. \end{cases} \quad (13)$$

Problem (13) will be solved by the method of scalar ranking by minimising the multiplicative function considering the importance coefficient of the private criterion:

$$\frac{\frac{N}{max(N)}}{\frac{\varepsilon}{max(\varepsilon)}} \rightarrow max$$

where *max* is the maximum function value.

Using the Mathematica programme, solving equation (14) together with (9) and (12) gives rational structural and technological parameters of the trier separator: D=0.58 m, n=46.8 rpm, N_0=2,722 pcs. With these parame-ters, the optimisation criteria were equal to N=251 units, ε=5.89%, θ_{min}=0.22 rad, θ_{min}=1.26 rad. Similar, but this time practical studies [16-17], were con-ducted by a scientist from Denmark, who investigated the behaviour of seed material during separation in a cylindrical trier. The author obtained a linear dependence between the rotation frequency of the cylinder and the angle of fall of the seeds from the cylinder pods. As a result, the scientist obtained the optimal values of the diameters of the pods and the frequency of rotation of the cylinder, namely: for three mixtures of hemp and rice, the optimal ranges of the diameter of the pods were 6.5-7 mm, and the frequency of rotation from 36.71 rpm to 42.60 rpm; for the three mixtures of hemp and wheat, the optimal value of the cell diameter was 6.5 mm, and the optimal range of rotation frequency was from 36.71 rpm to 39.73 rpm.

CONCLUSIONS

As a result of the numerical simulation of the process of separation of seed material of small-seeded crops on a cylindrical seed trimmer in the Star CCM+ software package, the dependence of the values of the minimum θ_{min} and maximum θ_{max} of the angles of seed exit from the seed cylinder trimmer on the research factors was obtained in the form of second-order regression equations. The number of all components of the seed mixture N, which were within the minimum θ_{min} and maximum θ_{max} angles of rotation of the trier separator cylinder, was chosen as a performance criterion. According to the simulation results, the dependence of the number of all components of the seed mixture N on research factors was obtained in the form of second-order regression equations. The criterion for evaluating the quality of the separation process was the relative content of impurities ε in the seed mixture, which was within the minimum θ_{min} and maximum θ_{max} rotation angles of the trier separator cylinder. According to the simulation results, the dependence of the relative content of impurities ε on factors under study was obtained in the form of second-order regression equations. Solving the compromise problem using the scalar ranking method by minimising the multiplicative function considering the importance coefficient of the private criterion in the Mathematica software package, which is reduced to minimising the relative content of impurities ε and maximising the number of all components of the seed mixture N that were within the minimum θ_{min} and maximum θmax angles of rotation of the cylinder, the rational design and technological parameters of the trier separator were obtained: D=0.58 m, n=46.8 rpm, N_0=2,722 pcs. With these parameters, the optimisation criteria were equal to N=251 units, ε=5.89%, θ_{min}=0.22 rad, θ_{min}=1.26 rad. Considering the obtained parameters, the next stage of research is to conduct an experiment using a laboratory setup to confirm the simulation results and further improve the existing trier separator by developing a mechatronic system that allows controlling the parameters of the trier and obtaining the optimal sorting result at the output.

REFERENCES

[1] Aliiev, E., & Lupko, K. (2021). Prerequisites for the creation of a mechatronic system of indented cylinders for the separation of fine seeds. *Scientific Horizons*, 24(3), 75-86.

[2] Broas, P. (2001). Advantages and problems of CAVE-visualisation for design purposes. In M. Lehtonen (Ed.), *Virtual prototyping VTT research programme 1998-2000* (pp. 73-81). Otaniemi: Technical Research Centre of Finland.

[3] Bai, C. (1996). *Modelling of spray impingement processes*. (Doctoral thesis, University of London, London, Great Britain).

[4] Kubicki, D., & Lo, S. (2012). Slurry transport in a pipeline – comparison of CFD and DEM models. In *Ninth international conference on CFD in the minerals and process industries* (pp. 1-6). Melbourne: University of Melbourne.

[5] Han, S.W., Lee, W.J., & Lee, S.J. (2012). Study on the particle removal efficiency of multi inner stage cyclone by CFD simulation. *World Academy of Science, Engineering and Technology*, 6, 411-415.

[6] Satish, G., Ashok, K.K., Vara, P.V., & Pasha, S.M. (2013). Comparison of flow analysis of a sudden and gradual change of pipe diameter using fluent software. *International Journal of Research in Engineering and Technology*, 2, 41-45.

[7] Ivanets, V.N., Bakin, I.A., & Belousov, G.N. (2002). Entropy approach to the evaluation of the process of mixing bulk materials. *Storage and Processing of Agricultural Raw Materials*, 11, 16-18.

[8] Bakin, I.A., Belousov, G.N., & Sablinsky, A.I. (2001). Modeling of the mixing process by the entropy-information method. In *New technologies in scientific research in education: Materials of the All-Russian scientific-practical conference* (pp. 34-40). Yurga: Yurga Technological Institute.
[9] Iguchi, M., & Ilegbusi, O.J. (2014). *Basic transport phenomena in materials engineering*. Dordrecht: Springer.
[10] Shevchenko, I., Aliev, E. (2018). Research on the photoelectronic separator seed supply block for oil crops. *INMATEH-Agricultural Engineering*, 1(54), 129-138
[11] Grzhybovsky, A. (2008). The choice of a statistical criterion for testing hypotheses. *Human Ecology*, 11, 48-57.
[12] Mocny, F. (2019). Analysis of nonparametric and parametric criteria for testing statistical hypotheses. *Statistics of Ukraine*, 1, 13-23.
[13] Prishenko, O., Chernogor, T., & Buhkalo, S. (2019). Some features of correlation analysis. In *Information technology: Science, technology, technology, education, health* (pp. 320-322). Kharkiv: V. N. Karazin Kharkiv National University.
[14] Buhkalo, C., Iglin, S., Glavcheva, Y., & Miroshnichenko, N. (2018). Possibilities of determining the components of complex projects. *Bulletin of the National Technical University "KhPI"*, 40, 46-52.
[15] Dreyper, N. (2006). *Applied regression analysis*. Moscow: Finance and statistics.
[16] Buus, O.T. (2013). *Analysis of the indented cylinder by the use of computer* vision (Doctoral thesis, University of Southern Denmark, Aarhus, Denmark).
[17] Tsysar, M. Zakora, O. Babak, A., Ivakhnenko, S., & Zanevsky, O. (2021). Dependence of the Static Strength of Type Ib Single Crystal Diamonds with Octahedral Habit on Their Size. *Scientific Herald of Uzhhorod University. Series "Physics"*, (50), 25-30.

СПИСОК ВИКОРИСТАНИХ ДЖЕРЕЛ

[1] Aliiev E., Lupko, K. Prerequisites for the creation of a mechatronic system of indented cylinders for the separation of fine seeds. *Scienti ic Horizons*. 2021. Vol. 24, No. 3. P. 75–86.
[2] Broas P. Advantages and problems of CAVE-visualisation for design purposes. *Virtual prototyping VTT research programme 1998–2000* / M. Lehtonen (Ed.). Otaniemi: Technical Research Centre of Finland, 2001. P. 73–81.
[3] Bai C. Modelling of spray impingement processes: Doctoral thesis, degree of doctor of philosophy. London: University of London, 1996. 449 p.
[4] Kubicki D., Lo S. Slurry transport in a pipeline – comparison of CFD and DEM models. *Ninth international conference on CFD in the minerals and process industries* (Melbourne, 10-12 December, 2012). Melbourne, 2012. P. 1–6.
[5] Han S.W., Lee W.J., Lee S.J. Study on the particle removal efficiency of multi inner stage cyclone by CFD simulation. *World Academy of Science, Engineering and Technology*. 2012. Vol. 6. P. 411–415.
[6] Satish G., Ashok K.K., Vara P.V., Pasha S.M. Comparison of flow analysis of a sudden and gradual changeof pipe diameter using fluent software. *International Journal of Research in Engineering and Technology*. 2013. Vol. 2. P. 41–45.
[7] Иванец В.Н., Бакин И.А., Белоусов Г.Н. Энтропийный поход к оценке процесса смешивания сипучих материалов. *Хранение и пераработка сельскохозяйственного сырья*. 2002. № 11. С. 16–18.
[8] Бакин И.А., Белоусов Г.Н., Саблинский А.И. Моделирование процесса смешивания энтропийно- информационным методом. *Новые технологи в научных исследованиях в образовании: материалы Всероссийской научно-практической конференции* (г. Юрга, 25 февраля 2001 г.). Юрга, 2001. С. 34–40.
[9] Iguchi M., Ilegbusi O.J. Basic transport phenomena in materials engineering. Dordrecht: Springer, 2014. 277 p.
[10] Shevchenko I., Aliev E. Research on the photoelectronic separator seed supply block for oil crops. INMATEH *Agricultural Engineering*. 2018. Vol. 1, No. 54. С. 129–138.
[11] Гржибовский А.М. Выбор статистического критерия для проверки гипотез. *Экология человека*. 2008. Вып. 11. С. 48–57.
[12] Моцний Ф.В. Аналіз непараметричних і параметричних критеріїв перевірки статистичних гіпотез. *Статистика України*. 2019. № 1. С. 13–23.
[13] Пріщенко О.П., Черногор Т.Т., Бухкало С.І. Деякі особливості проведення кореляційного аналізу. *Інформаційні технології: наука, техніка, технології, освіта, здоров'я*: тези доповідей XXVII міжнар. наук.-практ. конференції (Харків, 15–17 травня 2019). Харків, 2019. С. 320–322.
[14] Бухкало С.І., Іглін С.П., Главчева Ю.М., Мірошниченко Н.М. Можливості визначення компонентів складових комплексних проектів. *Вісник НТУ «ХПІ»*. 2018. Вип. 1316, № 40. С. 46–52.
[15] Дрейпер Н. Прикладной регрессионный анализ. Москва: Финансы и статистика, 2006. 57с.
[16] Buus O.T. Analysis of the indented cylinder by the use of computer vision: Doctoral thesis, degree of doctor of philosophy. Aarhus: University of Southern Denmark, 2013. 169 p.
[17] Tsysar, M. Zakora, O. Babak, A., Ivakhnenko, S., & Zanevsky, O. Dependence of the Static Strength of Type Ib Single Crystal Diamonds with Octahedral Habit on Their Size. *Scientific Herald of Uzhhorod University. Series "Physics"*. 2021. Vol. 50. P. 25-30.

Ельчин Бахтияр огли Алієв[1,2], Кристина Олегівна Лупко[2]

[1]Інститут олійних культур Національної академії аграрних наук України
69055, вул. Інститутська, 1, с. Сонячне, Запорізька обл., Україна

[2]Дніпровський державний аграрно-економічний університет
49600, вул. Сергія Єфремова, 25, м. Дніпро, Україна

Результати чисельного моделювання процесу сепарації насіннєвого матеріалу дрібнонасіннєвих культур на циліндричному чарунковому трієрі

Анотація. Актуальність дослідження зумовлена необхідністю збільшення кількості якісного насіннєвого матеріалу дрібнонасіннєвих культур, що неможливо досягти без важливого процесу сепарації. Сепарація заснована на техніко-технологічних принципах розділення насіннєвого матеріалу в залежності від відмінностей фізико-механічних властивостей окремих складових насіннєвого матеріалу. Для сепарації насіння за ознакою довжини призначені циліндричні трієри. Метою дослідження є визначення теоретичних закономірностей зміни технологічних параметрів процесу сепарації насіннєвого матеріалу дрібнонасіннєвих культур від конструктивно-режимних параметрів циліндричного чарункового трієра шляхом чисельного моделювання. Вирішення поставлених задач реалізовано в програмі STAR-CCM+ на базі методу кінцевих елементів. Враховуючи фізико-механічні властивості насіннєвого матеріалу, в результаті дослідження отримано візуалізацію процесу сепарації в залежності від факторів досліджень: частоти обертання циліндра трієра, діаметра циліндра та кількості насінин і домішок в насіннєвій суміші. За результатами моделювання отримано залежність у вигляді рівнянь регресії другого порядку відносного вмісту домішок ε від факторів досліджень. З використанням програми Mathematica вирішено компромісну задачу, яка полягає в мінімізації мультиплікативної функції критеріїв досліджень і визначені раціональні конструктивно-технологічні параметри трієрного сепаратора. Матеріал статті призначений для науковців, аспірантів, конструкторів сільськогосподарської техніки, студентів і фахівців сільськогосподарського виробництва

Ключові слова: механізація, сепаратори, насіннєвий матеріал, розділення

Machinery & Energetics
Vol. 13, No. 2. 2022

Journal homepage:
https://technicalscience.com.ua/en

UDC 620.9.004.18
DOI: 10.31548/machenergy.13(2).2022.20-31

Ievgen Antypov*, Anatoliy Mishchenko, Olena Shelimanova, Svitlana Tarasenko

National University of Life and Environmental Sciences of Ukraine
03041, 15 Heroiv Oborony, Kyiv, Ukraine

Analysis of the Influence of the Internal Heat Capacity of a Public Building on the Thermal Comfort Parameters of the Premises During the Operation of the Heating System in Alternating Mode

Abstract. In the climatic conditions of Ukraine, which are characterised by a long heating period, considerable energy requirements for heating lead to an increase in energy efficiency requirements. A substantial reduction in the energy consumption of buildings while ensuring comfort conditions will be facilitated by the inclusion of a model of human thermal comfort in the complex "heat source – fencing" system. The purpose of this study was to find the factors affecting the internal heat capacity and, accordingly, the thermal inertia of the building and further take these factors into account upon assessing the thermal condition and parameters of thermal comfort of building rooms. The object of this study was the educational and administrative building of the National University of Life and Environmental Sciences of Ukraine. Many studies were carried out, namely full-scale measurements of heat flows and temperatures on the surfaces of samples of the building's wall structure were carried out in a special climate complex that allows artificially creating external and internal thermal conditions of premises. It was found that the insulation of the structure with a layer of expanded polystyrene PSB-15, 100 mm thick, reduces heat losses through the wall panel by almost half. An algorithm for controlling the heat release process was developed, considering the internal heat capacity of the building. Compared to the "linear" dependence, this allows more accurately adjusting the schedule of heat carrier release to the heating system of a public building during the introduction of the alternating mode of its operation. The temperature deviation range is reduced by 4-6 °C, which allowed saving up to 10-12% of the consumed heat energy for the heating needs of the research object, provided that the normalised values of the internal temperature of the premises are maintained. Intermittent operation of the heating system of public buildings, the expediency of which is justified in this study, can be recommended for implementation in the structures of higher educational institutions of Ukraine

Keywords: thermal energy, energy requirements, energy efficiency, heating period, thermal inertia, control algorithm, heating system

Article's History: Received: 02.12.2021 Revised: 14.03.2022; Accepted: 27.04.2022.

INTRODUCTION

Buildings are one of the main consumers of primary energy carriers in the world [1]. Climatic conditions in Ukraine are characterised by a long heating period, which causes 85% of the energy demand for heating [2]. Therefore, energy efficiency requirements are increasing, which is reflected in the standards [3-5]. Most of the buildings in Ukraine belong to the buildings of mass development of the 1980s, during the construction of which the emphasis was placed on minimising capital costs during construction, while operating costs faded into the background, and therefore 80% of buildings do not meet modern energy efficiency requirements [6; 7]. The period from the 1990s to the present day is characterised by a constant increase in energy prices, which means that during the construction of buildings, considerable attention is already paid to operating costs, which is a late response to similar trends in Europe and the world.

According to the European Union Directive on the energy efficiency of buildings [8], a requirement has been introduced that all new public buildings put into operation from 2019 must meet the requirements presented for houses with almost zero energy consumption, which leads to an increase in energy efficiency and the use of renewable energy sources. Attention is being paid to the growth of thermal resistance of building fences, the relevance of economic assessment and assessment of its life cycle. This is conditioned upon the fact that in the EU, 1/3 of energy resources are

Suggested Citation:
Antypov, Ie., Mishchenko, A., Shelimanova, O., & Tarasenko, S. (2022). Analysis of the influence of the internal heat capacity of a public building on the thermal comfort parameters of the premises during the operation of the heating system in alternating mode. *Machinery & Energetics,* 13(2), 20-31.

*Corresponding author

spent on buildings, namely 60% of the energy consumed by the building is associated with operating costs [9].

Considering global trends in optimising energy demand and ensuring comfortable working conditions, the calculation of specific energy demand should be determined based on operating air temperature, or while observing the comfort indicator in various climatic conditions [10]. The global community pays special attention to thermal comfort issues, especially in the context of the need to reduce energy consumption. There are sections of the population that are particularly sensitive to thermal comfort requirements – these are children and the elderly; women and men feel differently under the same conditions. Therewith, special attention is paid to individual requirements for thermal comfort issues related to gender, age, etc. Hence, the transition from the paradigm of centralised microclimate quality assurance to personalised systems [11].

In Ukraine, thermal comfort is defined by several standards [12; 13]. The inclusion of the human thermal comfort model in the complex "heat source – fencing" system [14; 15] is an essential step towards reducing the energy consumption of buildings and ensuring a suitable level of thermal comfort, especially during the introduction of the alternating heating mode, which is an important step towards sustainable development. Therefore, the purpose of this study was to assess the impact of the level of thermal protection (heat capacity of the building) on the feeling of thermal comfort upon implementing the alternating heating mode. Such studies are important and relevant both in the context of improving the level of energy efficiency and increasing the quality of the microclimate.

LITERATURE REVIEW

Literature analysis has shown that the feasibility of introducing an intermittent (alternating) mode of operation of the heating system of a public building has been understudied. The available research results cover only a few isolated cases and do not provide an exhaustive answer to this question. The results of the study of the influence of thermal inertia of a room are presented in the paper [16], where consideration of the indicator of the internal heat capacity of a building, on the example of the educational and administrative building of the National University of Life and Environmental Sciences of Ukraine (NULES of Ukraine), avoids energy overspending at the level of about 10–12%. Therewith, it is also important to determine the operating time of the system in alternating mode and the depth of adjustment, provided that the parameters of room comfort are preserved. In this area, the authors V. Deshko, I. Bilous, N. Buyak, O. Golubenko, M. Gureev investigated the change in the comfort conditions of premises from the inertia of external enclosing structures of a building during the operation of the heating system in energy-saving modes [17], as well as the dependence of the comfort conditions of public buildings with different degrees of thermal protection of external enclosing structures in the operating conditions of the heating system of the structure in alternating mode [18], its influence on the dynamics of energy demand. Equally important was the assessment of the impact of ventilation on the overall energy consumption of the building. Thus, the authors of [19] studied the thermal environment in the room, the rate of air exchange, and the concentration of carbon dioxide before and after the energy modernisation of apartment buildings in Finland and Lithuania. The authors of the study [20] conducted a survey on the requirements and barriers in the implementation of ventilation systems in residential buildings with low energy consumption, as well as an assessment of operational problems from seven European countries that may arise in this case. The authors of the studies: [21] – conducted long-term measurements in recently built schools with low energy consumption in Sweden, [22] – characterised the design features of residential buildings in China, [23] – substantiated the feasibility of using adaptive thermal comfort methods for Iranian schoolchildren, [24] – investigated the parameters of residential adaptive comfort in a humid continental climate – Tianjin, China. Furthermore, the authors of [25] introduced the concept of controlling the thermal comfort of a building. The authors V. Nalyvaiko, I. Radko, A. Zhyltsov, O. Okushko, A. Mishchenko, I. Antypov studied the thermal comfort of the building after its thermal modernisation using renewable energy [26] and considering the provisions of the relevant standards [12; 13; 27]. However, the results of research in the studies listed above do not fully solve the problem of assessing the impact of the level of thermal protection (heat capacity of the building) on the feeling of thermal comfort when implementing an alternating heating mode, especially in terms of optimising the algorithm for controlling the heat release process considering the indicator of the internal heat capacity of the building and, accordingly, its thermal inertia, which is what this research is aimed at.

MATERIALS AND METHODS

The object of this study was the educational and administrative building of the National University of Life and Environmental Sciences of Ukraine. More detailed information about the thermophysical characteristics of enclosing structures and the operating mode of the building is given in the source [16].

To fulfil the purpose of this study, the influence of heat transfer resistance of external opaque enclosing structures (walls) of the structure on the efficiency indicators of the building's heating system was evaluated, considering the parameters of the external environment and the parameters of the microclimate of premises in dynamic mode. For this, two types of wall panels were manufactured and investigated – "with" and "without" insulation on its outer part, which were carried out in different years: before the introduction of standards [7], in 2011-2012, and after – in 2018-2020.

Thermophysical studies of the sample of the building's wall structure were performed in a special climate complex, which allows artificially creating external and internal thermal conditions of premises and comprises three compartments:

1. External, which simulates external climatic conditions (Fig. 1). 2. Internal, which simulates the microclimate of the premises. 3. Operator's room, which allows placing control and measuring equipment.

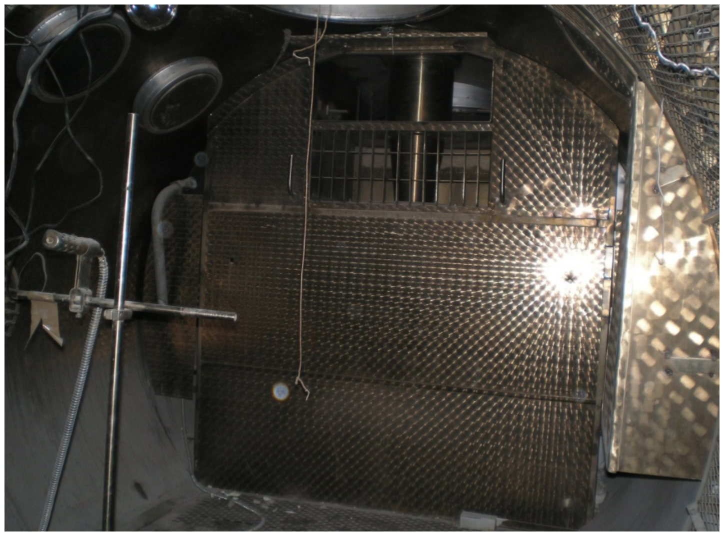

Figure 1. Appearance of the "cold" compartment of the climate chamber

The outer compartment was created based on the KTBV-8000/2 thermobaroclave, which has a powerful refrigerating unit, thanks to which the calculated values of the outdoor air temperature in the winter mode (-24 °C) were provided.

In stationary mode, the air temperature in the outer compartment was maintained by an automatic adjustment system with an accuracy of ±1.5 °C, in the inner compartment – up to ±1 °C. Humidity in the warm compartment of the camera was maintained in automatic mode with an accuracy of ±5%.

The given stationary thermal regime in the internal compartment was maintained using the EOS-2.00/220 electric convector and the BK-1500 air conditioner, which were turned on and off by the PTR-P semiconductor thermostat and the automatic temperature control system mounted in a separate unit.

The process of measuring heat flows and temperatures was controlled using the BS-2 Communication Unit, which has 300 input channels. Between the working compartments – external and internal – the tested product was located, mounted in a special cassette (Fig. 2a).

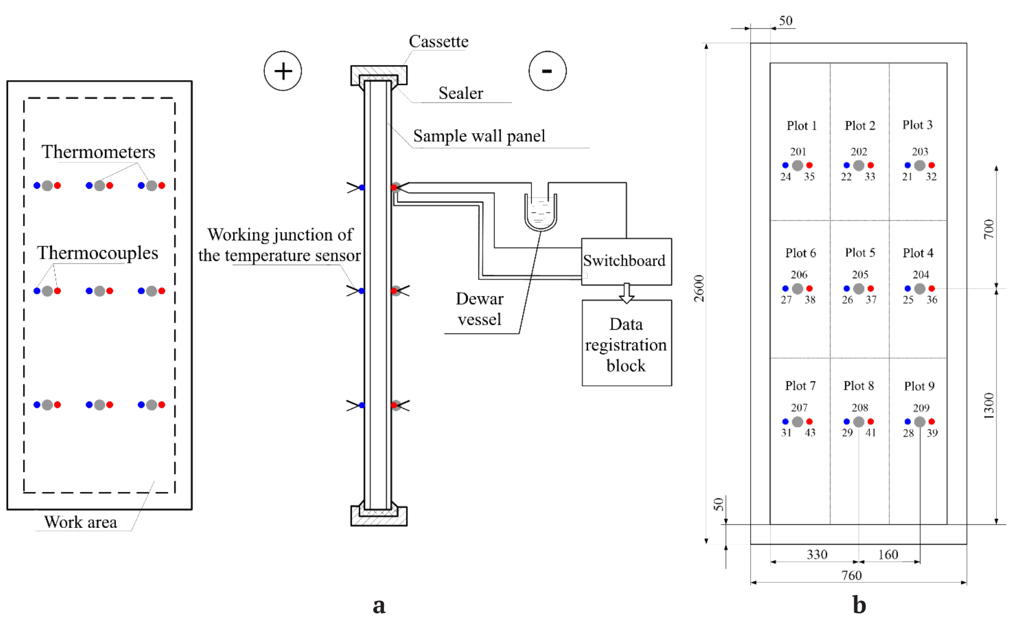

Figure 2. Installation diagram of the tested wall structure sample and placement of temperature and heat flow sensors on it (**a**) and placement diagram of primary temperature and heat flow converters on the surface of the wall panel sample tested (**b**): ● – heat flow sensors; ● – temperature sensors on the inner ("warm") side of the wall panel; ● – temperature on the outer ("cold") side of the wall panel

The readings of the measuring devices were taken remotely in the operator's compartment using the F70-78 measuring signal switch.

Chromel-Copel thermocouples with a relative measurement error of ±5% were used as temperature sensors. Primary temperature converters were tightly attached to the outer and inner surfaces of products at selected points. Plasticine with an application thickness of no more than 2 mm was used for fastening thermocouples. Therewith, the thermometric wire is led from the place of attachment of the sensitive element along the surface of the enclosing structure towards isotherms or the minimum temperature gradient for a length of at least 50 wire diameters. The free ends of the thermocouples were placed in a thermostat or Dewar vessel, while the latter must contain ice and water at the same time.

Thermobattery sensor PTP-1B.11.2.1.P.001.1.16.00.0 is a working tool for measuring surface heat flux density [28]. Since the thermal resistance of the sensor is negligible compared to the thermal resistance of the wall panel, it was not considered. For the same reason, the dimensions of the sensor (10×12×1.2 mm) in the wall plane also do not affect its temperature field.

The universal voltmeter B7-21A was used as a meter of the DC output signal. The voltmeter is designed to measure DC voltage in the range up to 10 MV. The accuracy class of the device is 0.2.

Experimental studies of energy-efficient fencing construction. For experiment No. 1, an experimental light hinged wall panel with overall dimensions of 760×2600 mm was manufactured. Panel thickness δ=100 mm.

The experimental panel was a three-layer panel with differentiation of layers by functions performed. Facing layers – external and internal – had the functions of weather protection and protection of insulation from mechanical damage. They were made of plywood sheets with a thickness δ=5 mm.

When choosing the insulation material, good thermal insulation was the decisive factor. Mineral wool [6] with a thickness δ=100 mm was used as insulation.

There was no monolithic connection between the plywood sheets and the heat insulator, which caused contact thermal resistances.

For experiment No. 2, polystyrene foam plates PSB-15, δ=100 mm thick, which repeated the dimensions of the wall panel, were attached to the previous wall panel from the side of the cold compartment of the climatic chamber using DRAGON polymer glue.

The conditions of experiment No. 1 and experiment No. 2 were the same: the temperature of the cold compartment of the camera was -24 °C, the temperature of the warm compartment was +16°C.

The method of determining the heat transfer resistance is based on the creation of stationary heat exchange conditions in the enclosing structure and the measurement of the air temperature in two compartments of the climate chamber, the heat flow density and the temperature of the surfaces of the structure under study, which were used to calculate the heat transfer resistance of the sample.

Since the wall panel was thermally relatively homogeneous (without substantial "cold bridges"), nine areas were selected for the experimental study, which were least affected by marginal outflows or inflows of heat in the chamber. 9 sections comprised the working zone (Fig. 2b), the boundaries of which were located at a distance of 50 mm from the edges of the sample under study. The locations of the sensors were marked on the sections with dots.

The test product was installed in the slot between the warm and cold compartments of the climate chamber. The contact surfaces with external fences were insulated with an effective heat-insulating material.

After checking the readiness of the equipment, the warm and cold compartments were isolated from the outside air by closing the airtight doors. The air temperatures in the warm and cold compartments were set on the regulating equipment, including refrigerating, heating, and air humidifying equipment.

The tested panel belongs to the non-inertial class, its exit to the stationary mode took place within three to four hours. The onset of stationary mode was recorded by stable indicators of thermocouples and heat meters. The sampling of experimental data in stationary mode for their further processing was made from the last six measurements (on six cycles), during which the temperature and heat fluxes remained practically constant.

Experimental studies of the parameters of thermal comfort of premises were carried out for five consecutive days, including Saturday and Sunday. Air temperature and humidity parameters were recorded by portable data loggers – Trotec BL30. Therewith, the measurement error was as follows: ±2°C – in the temperature range from 1°C to 50°C and ±3°C – in the range from -18°C to -1°C.

Evaluation of the influence of the resistance of the opaque enclosing structures of the building on the parameters of the thermal comfort of the premises and the energy consumption of the building using a numerical method. The total heat transfer and heat input were calculated according to [29], where dynamic impacts are considered by introducing the coefficient of use of heating inputs (accepted in the study) and the coefficient of use of cooling losses. The effect of inertia in the case of intermittent heating or its shutdown was considered separately.

The dimensionless coefficient of use of heating inputs $\eta_{H,\ gn}$ is calculated for each month according to [29] based on the ratio of heat inputs and losses and the numerical parameter a_H, which depends on the inertia of the building:

$$a_H = a_{H,O} + \frac{\tau}{\tau_{H,O}} \qquad (1)$$

where $a_{H,O}$ is the reference dimensionless numeric parameter, $a_{H,O}=1.0$; τ is the time constant of the building zone, h; $\tau_{H,O}$ is the reference time constant, which is taken as 15 h.

The time constant of the building zone τ, h, characterises the internal thermal inertia of the conditioned zone of the building, both for the heating period and for the cooling period:

$$\tau = \frac{C_m}{H_{tr,adj} + H_{ve,adj} + H_{ve,extra,adj}}, \qquad (2)$$

where C_m is the internal heat capacity of the building or building zone, W·h/K; $H_{tr, adj}$ is the representative value of the overall heat transfer coefficient of the transmission, W/K; $H_{ve, adj}$ is the representative value of the general coefficient of heat transfer by ventilation, W/K; $H_{ve, extra, adj}$ is the representative value of the overall heat transfer coefficient due to additional ventilation from night and/or natural cooling, W/K (for heating mode $H_{ve, extra, adj}$=0):

$$H_{ve,extra,adj} = \frac{\sum_{i=1}^{n}(\sum_{j=1}^{24} f_{ve,extra,j,k} H_{ve,extra,j,k})}{t}, \quad (3)$$

where is the total heat transfer coefficient due to added ventilation (night ventilation and/or natural cooling) from the *k*-th element, W/K, and the share of work for a specific j-th hour of the day of the *i*-th day of the month from the *k*-th element of added ventilation (if night ventilation and/or natural cooling works =1, otherwise 0.5); j is the calculation step in hours, from 1 to 24 h; *i*=1 to *n* is the calculation step in days (*n*=31 for January).

The building of the object under study belongs to the class of "massive" buildings – brickwork in two bricks with a reinforced concrete floor. In this case, the internal heat capacity of the building is calculated according to [29]:

$$C_m = CA_f \quad (4)$$

where C is the internal heat capacity of the building per unit area, taken according to the Table 15 [29], W·h/(m²·K); A_f is the conditioned area of the building, m².

In the case under study, for intermittent (alternating) heating mode, the energy consumption for heating $Q_{H, nd, interm}$, W·h, was found as follows:

$$Q_{H,nd,interm} = a_{H,red}\, Q_{H,nd,cont} \quad (5)$$

where $Q_{H, nd, cont}$ is the energy demand for continuous heating, W·h; $a_{H,red}$ is the dimensionless reduction coefficient for intermittent heating mode, with a minimum value $a_{H, red}$=$f_{H, hr}$ and a maximum value $a_{H, red}$=1:

$$a_{H,red} = 1 - b_{H,red}(\tau_{H,0}/\tau)\gamma_H(1 - f_{H,hr}), \quad (6)$$

where $f_{H,hr}$ is the share of the number of hours per week with a normal (permanent) set heating mode (not set on alternating or switched off); $b_{H, red}$ is the empirical correlation coefficient, $b_{H, red}$=3; τ is the time constant of the building zone, h; $\tau_{H,0}$ is the reference time constant for the heating mode, h; γ_H is the ratio of heat input and loss for the heating mode.

Adjustments for the non-use period. According to the data [16], it was found that in the building under study, periods of non-use during the heating period (on weekends and holidays) lead to a reduction in energy consumption during heating.

Energy consumption for heating was calculated, considering the period of non-use, $Q_{H, nd}$, W·h:

a) for the period of use (normal heating settings);

b) for setting the non-use period.

Linear interpolation was performed depending on the time fraction of the non-use mode compared to the maintenance mode:

$$Q_{H,nd} = (1 - f_{H,nocc})Q_{H,nd,occ} + f_{H,nocc}\, Q_{H,nd,nocc} \quad (7)$$

where $Q_{H, nd, occ}$ is the energy demand for heating, W·h, (either $Q_{H, nd, cont}$ or $Q_{H, nd, interm}$), assuming that on all days of the month, the adjustment and setting of the automatic air temperature controller in the room (e.g., the thermostat on the heating device) correspond to the settings of the period of use; $Q_{H, nd, nocc}$ is the energy demand for heating, W·h, (either $Q_{H, nd, cont}$ or $Q_{H,nd,interm}$), assuming that on all days of the month, the regulation and settings of the thermostat correspond to the settings of the period of non-use; $f_{H, nocc}$ is the fraction of a month with a period of non-use of heating (e.g., 10/31).

Additionally, according to the method [29], the influence of automatic control systems installed at the district heating point was investigated:

$$Q_{gen,out} = Q_{dis,in}/\eta_{ac}, \quad (8)$$

where $Q_{gen, out}$ is the produced/generated energy (output energy) from the generation (accumulation) subsystem, specifically based on phase-transition heat accumulators [30]; $Q_{dis, in}$ is the energy input to the distribution subsystem; η_{ac} is the efficiency of automatic adjustment.

RESULTS AND DISCUSSION

Figure 3 demonstrates the nature of changes in heat flows through the wall panel. Visual analysis shows that for experiment No. 1, the surface heat fluxes were 1.8 times greater than for experiment No. 2, at almost the same temperatures on the panel surface in the warm and cold compartments of the chamber.

The practical value of the obtained results, in terms of thermophysical studies of samples of the wall structure of the building, allows estimating the factual heat loss through the wall panel with an effective heat-insulating material [6] and bring the reference values to the operational values of its coefficient of thermal conductivity, considering the specific features of the real operating conditions of the structure. It was found that the insulation of the structure under study with a layer of expanded polystyrene PSB-15, 100 mm thick, reduces heat losses through the wall panel by almost half.

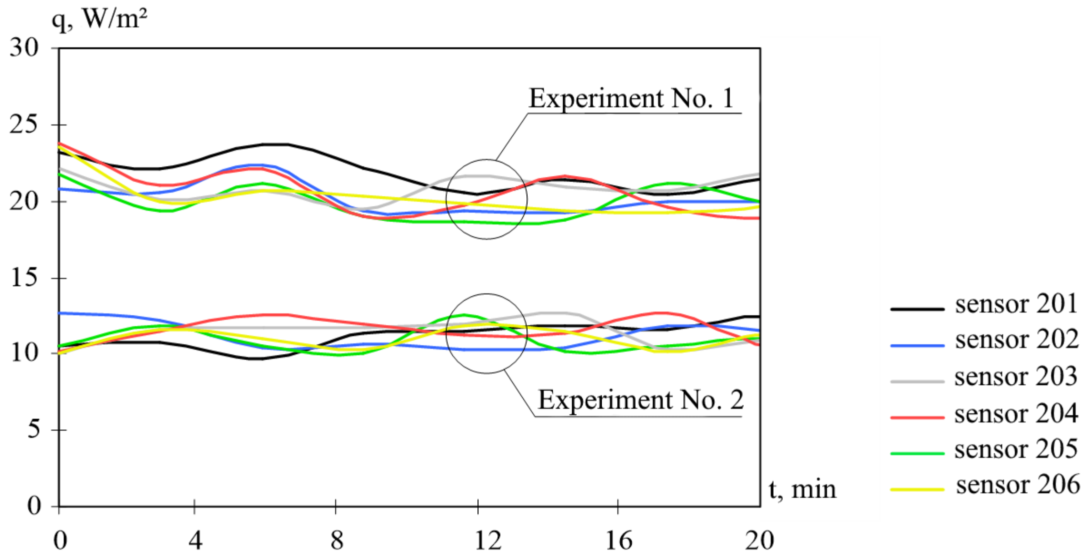

Figure 3. Graphs of changes in heat flows through the wall panel under study for experiment No. 1 – study of heat-insulating properties of a wall panel without insulation and for experiment No. 2 – study of heat-insulating properties of a wall panel with insulation – expanded polystyrene PSB-15.

Evaluating the influence of the resistance of the opaque enclosing structures of the building on the thermal comfort parameters of the premises using the numerical method according to [31], it was established that the used model considers the dynamic change of heat flows through the wall panels under study (Fig. 3), which were made of different structural materials. The results of calculations for [31] are presented in Figure 4.

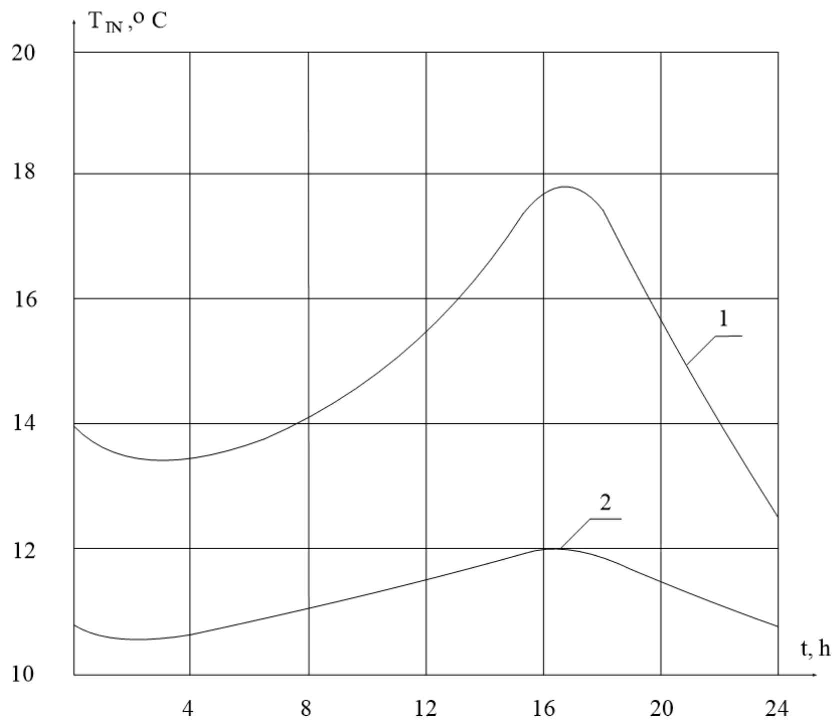

Figure 4. Temperature change on the inner surface of the wall of the room during the day: 1 – the enclosing structures made of multi-layered wall structures with insulation; 2 – the enclosing structures made of brickwork without insulation

Analysis of Figure 4 shows that when the operating mode of the heating system of a public building is introduced in the alternating mode, a substantial temperature change is observed on the inner surface of the enclosing structure. In the case of external walls made of multi-layer wall structures with insulation, the temperature drop reaches ±5°C, which meets the requirements [7], in contrast to the building's enclosing structures made of brickwork without insulation. The latter indicates a substantially lower indicator of the internal heat capacity of such a building.

The above (Fig. 3), in contrast to the results of research given in papers [17; 18], wherein, upon assessing the change in the comfort conditions of the premises from the inertia of the external enclosing structures of the building during the operation of the heating system in energy-saving modes [17], as well as the dependence of the comfort conditions of public buildings with different degrees of thermal protection of the external enclosing structures in the operating conditions of the building heating system in the regular mode [18], calculated (standardised) and not experimental (operational) values of the thermal conductivity coefficient were accepted. The results obtained in this study allow more accurately determining the factual temperature values on the inner surface of external enclosing structures (Fig. 4) and compare them with the minimum permissible ones [7] upon assessing the comfort conditions of the premises, which complements the results of the study [19], considering national standards [7; 12; 13].

Quasi-stable heating. For the object under study, the mode of intermittent (alternating) heating, as constant heating considering the set temperature value, in mode A and mode B was considered and investigated.

Mode A: the set temperature for calculation is the time average of the set temperature values for periods of constant heating and periods of alternating heating, since the time constant of the building is less than 0.2 of the duration of the shortest period with the alternating heating mode.

Thus, it was experimentally confirmed that an essential factor in the implementation of the regular heating mode is the thermal inertia of the building, which determines the time interval and the depth of adjustment [16] under the condition of maintaining the comfort parameters of the premises. When switching from constant mode to alternating mode, the average decrease in the temperature of the coolant and indoor air (from 18:00 to 4:00) was 8-10°C and >16°C (at the allowed 12°C), respectively. The recorded outdoor temperature was -3°C. Considering the structure of the external walls of the object under study, the "warm-up" time of the building, the heating system of which has been working for a long time in regular mode, with the achievement of the parameters of thermal comfort of the premises, was established. Thus, the duration of the heating of the "A" type building, when the heating system was operating in the "forced" mode, was 6.5 hours [16]. Savings in the consumed heat energy during the operation of the building's heating system in alternating mode amounted to 6-8%, the air temperature during this period was maintained at 12°C. An algorithm for controlling the heat release process was developed, considering the internal heat capacity of the building. Compared to the conventional "linear" dependence (inherent in type A buildings), this allows more accurately adjusting the schedule of heat carrier release (Fig. 5) to the heating system of a public building during the introduction of the alternating mode of its operation.

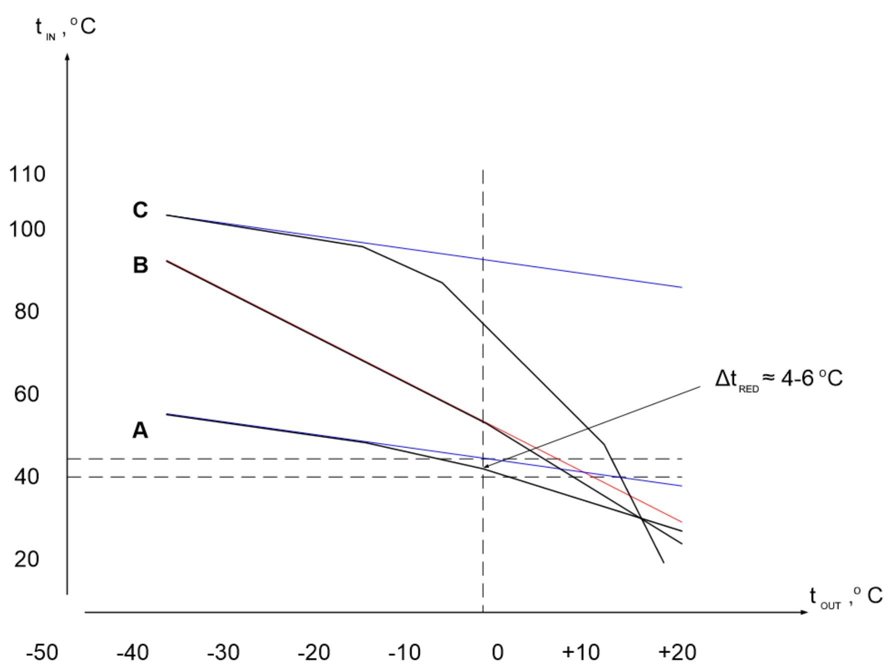

Figure 5. Temperature schedule of heat carrier release to the building's heating system, considering the outdoor air temperature and the internal heat capacity of the structure

Source: compiled by the author based on [16]

The temperature deviation range is reduced by 4-6°C, which allowed saving up to 10-12% of the consumed thermal energy for the heating needs of the educational and administrative building of NULES of Ukraine under the condition of supporting the normalised (for the alternating regime) values of the internal temperature of the premises.

Mode B: the set temperature for the calculation is the set temperature for the normal (continuous) heating mode, since the time constant of the building is more than three times the duration of the longest period with the alternating heating mode.

Comparing the data of the factual consumption by the educational and administrative building of the NULES of Ukraine with the calculated reduced to the factual number of degree-days of the heating period (for March 2019, Table 4 [16]) and the parameters of the comfort of the premises (temperature and air humidity), it was established that with an insignificant (+1.3°C) deviations of the indicators of the factual values of the internal air temperature in the premises of the building from the normalised values (18±2°C), an excess of the level of factual consumption of thermal energy was observed compared to the calculated value adjusted to the factual number of degree-days by 3.73 Gcal [16]. Thus, during the operation of the heating system of a public building in constant mode (Fig. 6a), there was an overspend of consumed thermal energy by 7.4% for the heating period of 2018-2019.

Given the structure of the enclosing structures of the object, the influence of heat transfer resistance on the performance indicators of the building heating system was investigated considering the parameters of the external environment and the microclimate of the premises in dynamic mode, a comparison was made of the specific energy consumption indicators of the building "before" the implementation of the heat release process management algorithm considering the indicator of its internal heat capacity (Fig. 6a) and "after" (Fig. 6b).

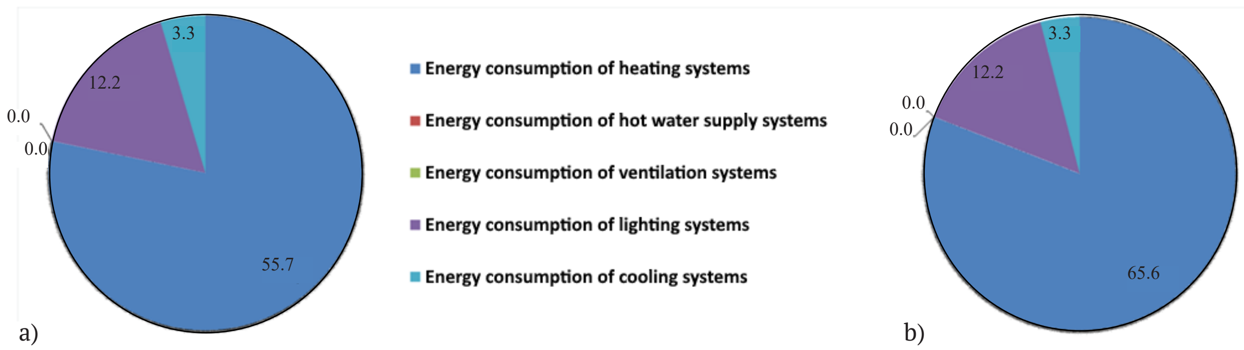

Figure 6. Specific indicators of the building's energy consumption "after" (a) and "before" (b) the implementation of the heat release process control algorithm, considering the indicator of its internal heat capacity, kW·h/m².

Therewith, the inclusion of the human thermal comfort model in the complex "heat source – fencing" system [14; 15] is an essential step towards reducing the energy consumption of buildings and ensuring a suitable level of thermal comfort, especially during the introduction of the alternating heating mode. The results obtained in this study regarding the assessment of the influence of the level of thermal protection (heat capacity of the building) on the feeling of thermal comfort of a person during the implementation of a regular heating mode, in contrast to the results of studies given in the papers [23-25], where the feasibility of using adaptive methods of thermal comfort is substanti-ated [23], and not the algorithms for its achievement, also consider the influence of the thermal inertia of the building, which determines the time interval and the depth of regula-tion, provided that the comfort parameters of the premises are observed and preserved, and not only their control [25]. This allows adjusting the coolant release schedule more accurately, according to the developed algorithm (Fig. 5) into the heating system of a public building during the introduction of the alternating mode of its operation, considering the outdoor air temperature and national standards [2; 29].

Given the factual indicators of savings in consumed heat energy during the operation of the building's heating system in alternating mode at the level of 6-8%, as well as the deviation of the factual values of the internal air temperature in the building from the normalised values, the total indicator of savings in consumed heat energy was 14-16% (Fig. 6), which complements the results of studies [14; 15; 32]. Considering the above, the intermittent (alternating) operation of the heating system of public buildings, the expediency of which is justi-fied in this study, can be recommended for implementation in the structures of higher educational institutions of Ukraine.

CONCLUSIONS

When assessing the thermal state of the building and the thermal comfort parameters of the rooms, those factors that affect its internal heat capacity and, accordingly, thermal inertia, are determined and considered. Reasonable expediency of implementing an intermittent (alternating) mode of operation of the heating system of public buildings and facilities of higher education institutions, namely:

1. It was experimentally confirmed that an essential factor in the implementation of the regular heating mode is the thermal inertia of the building, which determines the time interval and the depth of adjustment under the condition of maintaining the comfort parameters of the premises. When switching from constant mode to alternating mode, the average decrease in the temperature of the coolant and indoor air (from 18:00 to 4:00) was 8-10 °C and >16°C (at the allowed 12°C), respectively. The recorded outdoor temperature was -3°C.

2. Considering the structure of the external walls of the object under study, the "warm-up" time of the building, the heating system of which has been working for a long time in regular mode, with the achievement of the parameters of thermal comfort of the premises, was established. Thus, the duration of the heating of the "A" type building, when the heating system was operating in the "forced" mode, was 6.5 hours. Savings in the consumed heat energy during the operation of the building's heating system in alternating mode amounted to 6-8%, the air temperature during this period was maintained at 12°C.

3. Evaluating the influence of the resistance of the enclosing structures on the thermal comfort parameters of the premises using the numerical method, it was established that the used model considers the dynamic change

of heat flows through the wall panels under study, which were made of different materials, including in the alternating mode. Thus, in the case of external walls made of multi-layer wall structures with insulation, the temperature drop reaches ±5°C, in contrast to the building's enclosing structures made of brickwork without insulation.

4. An algorithm for controlling the heat release process was developed, considering the internal heat capacity of the building. Compared to the conventional "linear" dependence, this allows more accurately adjusting the schedule of heat carrier release to the heating system of a public building during the introduction of the alternating mode of its operation. The temperature deviation range is reduced by 4-6°C, which allowed saving up to 10-12% of the consumed thermal energy for the heating needs of the educational and administrative building of NULES of Ukraine under the condition of supporting the normalised values of the internal temperature of the premises.

5. Given the factual indicators of savings in consumed heat energy during the operation of the building's heating system in alternating mode at the level of 6-8%, as well as the deviation of the factual values of the internal air temperature in the building from the normalised values, the total indicator of savings in consumed heat energy was 14-16%.

In summary, intermittent (alternating) operation of the heating system of public buildings, the expediency of which is justified in this study, can be recommended for implementation in the structures of higher educational institutions of Ukraine. Therewith, the issue of establishing the limit time for cooling and "warm-up" of the building in the "forced" mode, considering the factual value of its thermal inertia under the operating conditions of the controller of the individual thermal point according to the developed algorithm for controlling the process of releasing heat into the building's heating system, requires further research.

REFERENCES

[1] 2020 Global status report for buildings and construction. Towards a zeroemission, efficient and resilient buildings and construction sector. (2020). Retrieved from https://wedocs.unep.org/bitstream/handle/20.500.11822/34572/GSR_ES.pdf.

[2] DSTU-N B V.1.1-27:2010 "Building climatology". (2011). Kyiv: Derzhspozhyvstandart Ukrainy.

[3] EN 13790:2008. Energy performance of buildings – Calculation of energy use for space heating and cooling. (2008). Brussels: European Committee for Standardization.

[4] EN 15217:2007. Energy performance of buildings – Methods for expressing energy performance and for energy certification of buildings. (2007). Brussels: European Committee for Standardization.

[5] EN 15603:2008. Energy performance of buildings – overall energy use and definition of energy ratings. (2008). Brussels: European Committee for Standardization.

[6] DSTU B V.2.6-189-2013 "Methods of choosing thermal insulation material for building insulation". (2013). Kyiv: Derzhspozhyvstandart Ukrainy.

[7] DBN B.2.6-31: 2016 "Thermal insulation of buildings". (2016). Kyiv: Derzhspozhyvstandart Ukrainy.

[8] Wang, Z., de Dear, R., Luo, M., Lin, B., He, Y., & Zhu, Y. (2018). Individual difference in thermal comfort: A literature review. *Building and Environment*, 138, 181-193.

[9] 2021 Global status report for buildings and construction. Towards a zeroemission, efficient and resilient buildings and construction sector. (2021). Retrieved from https://globalabc.org/sites/default/files/2021-10/GABC_Buildings-GSR-2021_BOOK.pdf.

[10] Lu, D.B., & Warsinger, D.M. (2020). Energy savings of retrofitting residential buildings with variable air volume systems across different climates. *Journal of Building Engineering,* 30, article number 101223.

[11] DSTU B EN 15261: 2012 "Calculation of microclimate parameters". (2012). Kyiv: Ministry of the Region of Ukraine.

[12] DSTU B EN ISO 7730: 2011 "Ergonomics of the thermal environment. Analytical definition and interpretation of thermal comfort on the basis of calculations of PMV and PPD indicators and criteria of local thermal comfort". (2012). Kyiv: Derzhspozhyvstandart Ukrainy.

[13] DSTU B EN 15251: 2011 "Calculated parameters of the microclimate of the premises for the design and evaluation of energy performance of buildings in relation to air quality, thermal comfort, lighting and acoustics". (2012). Kyiv: Derzhspozhyvstandart Ukrainy.

[14] Ding, Y., Zhang, Q., Yuan, T., & Yang, K. (2018). Model input selection for building heating load prediction: A case study for an office building in Tianjin. *Energy and Buildings,* 59, 254-270.

[15] Deshko, V., Buyak, N., Bilous, I., & Voloshchuk, V. (2020). Reference state and exergy based dynamics analysis of energy performance of the "heat source – human – building envelope". *Energy*, 200, article number 117534.

[16] Antypov, I.A., Mishchenko, A.V., Shelimanova, O.V., & Tarasenko, S.E. (2021). Analysis of the influence of the internal heat capacity of the ZVO building and weather-dependent regulation of ITP on the efficiency of the heating system in the next mode. *Energy and Automation*, 5, 46-61. doi: 10.31548/energiya2021.05.045.

[17] Deshko, V.I., Bilous, I.Y., Buyak, N.A., Golubenko, O.O., & Gureev, M.V. (2019). Influence of heat-inertial features of protections on comfort conditions at introduction of energy-saving modes of heating in buildings. *Scientific and Technical Collection "Utility Management of Cities",* 3(149), 44-50.

[18] Deshko, V.I., Bilous, I.Y., & Buyak, N.A. (2019). Influence of intermittent heating modes on the dynamics of energy consumption and comfort conditions of buildings with different levels of thermal protection. *Scientific News of NTUU KPI*, 4, 7-16.

[19] Leivo, V., Prasauskas, T., Du, L., Turunen, M., Kiviste, M., Aaltonen, A., Martuzevicius, D., & Haverinen-Shaughnessy, U. (2018). Indoor thermal environment, air exchange rates, and carbon dioxide concentrations before and after energy retro fits in Finnish and Lithuanian multi-family buildings. *STE*, 621, 398-406.
[20] Zukowska, D., Rojas, G., Burman, E., Guyot, G., Bocanegra-Yanez, M.C., Laverge, J., Cao, G., & Kolarik, J. (2020). Ventilation in low energy residences – a survey on code requirements, implementation barriers and operational challenges from seven European countries. *International Journal of Ventilation*, 20, 1-20.
[21] Simanic, B., Nordquist, B., Bagge, H., & Johansson, D. (2019). Indoor air temperatures, CO_2 concentrations and ventilation rates: Long-term measurements in newly built low-energy schools in Sweden. *Journal of Building Engineering*, 25, article number 100827.
[22] Gou, S., Nik, V.M., Scartezzini, J.L., Zhao, Q., & Li, Z. (2018). Passive design optimization of newly-built residential buildings in Shanghai for improving indoor thermal comfort while reducing building energy demand. *Energy and Buildings*, 169, 484-506. doi: 10.1016/j.enbuild.2017.09.095.
[23] Haddad, S., Osmond, P., & King, S. (2019). Application of adaptive thermal comfort methods for Iranian schoolchildren. *Building Research and Information*, 47(2), 173-189.
[24] Yangrui, S., Yuexia, S., Shugang, L., Zhe, T., Jing, H., Jungsoo, K., Parkinson, T., & de Dear, R. (2018). Residential adaptive comfort in a humid continental climate – Tianjin China. *Energy and Buildings*, 170, 115-121. doi: 10.1016/j.enbuild.2018.03.083.
[25] Esmaeilzadeh, A., Zakerzadeh, M.R., & Koma, A.Y. (2018). The comparison of some advanced control methods for energy optimization and comfort management in buildings. *Sustainable Cities and Society*, 43, 601-623. doi: 10.1016/j.scs.2018.08.038.
[26] Nalyvaiko, V., Radko, I., Zhyltsov, A., Okushko, O., Mishchenko, A., & Antypov, I. (2020). Investigation of thermal modernized building's microclimate with renewable energy. *ICoRES 2019*, 154, article number 07011.
[27] Directive (EU) 2018/844 of the European Parliament and of the Council "Amending Directive 2010/31/EU on the energy performance of buildings and Directive 2012/27/EU on energy efficiency". (2018, May). Retrieved from https://eur-lex.europa.eu/legal-content/EN/TXT/PDF/?uri=CELEX:32018L0844&from=IT.
[28] DSTU 3756-98 "Energy Saving. General Purpose Thermoelectric Heat Flow Converters. General Technical Conditions (61163)". (2020). Kyiv: Derzhspozhyvstandart Ukrainy.
[29] DSTU B A.2.2-12: 2015 "Energy Efficiency of Buildings. Method of Calculating Energy Consumption for Heating, Cooling, Ventilation, Lighting and Hot Water Supply". (2015). Kyiv: Derzhspozhyvstandart Ukrainy.
[30] Gorobets, V., Antypov, I., Trokhaniak, V., & Bohdan, Y. (2018). Experimental and numerical studies of heat and mass transfer in low-temperature heat accumulator with phase transformations of accumulating material. *MATEC Web of Conferences,* 240, article number 01009.
[31] Chernykh, L.F., Rodionova, T.Yu., Gorbonos, N.N., & Dats, P.A. (2006). *Method for determining the heat transfer resistance of enclosing structures*. Kyiv: NULES.
[32] Tsysar, M. Zakora, O. Babak, A., Ivakhnenko, S., & Zanevsky, O. (2021). Dependence of the Static Strength of Type Ib Single Crystal Diamonds with Octahedral Habit on Their Size. *Scientific Herald of Uzhhorod University. Series "Physics"*, (50), 25-30.

СПИСОК ВИКОРИСТАНИХ ДЖЕРЕЛ

[1] 2020 Global status report for buildings and construction. Towards a zeroemission, efficient and resilient buildings and construction sector. URL: https://wedocs.unep.org/bitstream/handle/20.500.11822/34572/GSR_ES.pdf.
[2] ДСТУ-Н Б В.1.1-27:2010 «Будівельна кліматологія». Київ: Держстандарт України, 2011. 130 с.
[3] EN 13790:2008. Energy performance of buildings – Calculation of energy use for space heating and cooling. Brussels: European Committee for Standardization, 2008. 53 p.
[4] EN 15217:2007. Energy performance of buildings – Methods for expressing energy performance and for energy certification of buildings. Brussels: European Committee for Standardization, 2007. 31 p.
[5] EN 15603:2008. Energy performance of buildings – overall energy use and definition of energy ratings. Brussels: European Committee for Standardization, 2008. 43 p.
[6] ДСТУ Б В.2.6-189-2013 «Методи вибору теплоізоляційного матеріалу для утеплення будівель». Київ: Держстандарт України, 2013. 55 с.
[7] ДБН В.2.6-31:2016 «Теплова ізоляція будівель». Київ: Держстандарт України, 2016. 33 с.
[8] Individual difference in thermal comfort: A literature review / Zh. Wang, et al. *Building and Environment*. 2018. Vol. 138. P. 181–193.
[9] 2021 Global status report for buildings and construction. Towards a zeroemission, efficient and resilient buildings and construction sector. URL: https://globalabc.org/sites/default/files/2021-10/GABC_Buildings-GSR-2021_BOOK.pdf.
[10] Lu D.B., Warsinger, D.M. Energy savings of retrofitting residential buildings with variable air volume systems across different climates. *Journal of Building Engineering*. 2020. Vol. 30. Article number 101223.
[11] ДСТУ Б EN 15261: 2012. «Розрахунок параметрів мікроклімату». Київ: Мінрегіон України, 2012. 81 с.
[12] ДСТУ Б EN ISO 7730:2011 «Ергономіка теплового середовища. Аналітичне визначення та інтерпретація теплового комфорту на основі розрахунків показників PMV I PPD і критеріїв локального теплового комфорту». Київ: Мінрегіон України, 2012. 74 с.

[13] ДСТУ Б EN 15251:2011 «Розрахункові параметри мікроклімату приміщень для проектування та оцінки енергетичних характеристик будівель по відношенню до якості повітря, теплового комфорту, освітлення та акустики». Київ: Мінрегіон України, 2012. 71 с.

[14] Ding Y., Zhang Q., Yuan T., Yang K. Model input selection for building heating load prediction: A case study for an office building in Tianjin. *Energy and Buildings*. 2018. Vol. 59. P. 254–270.

[15] Deshko . ., Buyak N., Bilous, ., Voloshchuk V. Reference state and exergy based dynamics analysis of energy performance of the heat source – human – building envelope. *Energy*. 2020. Vol. 200. Article number 117534.

[16] Антипов .О., іщенко А.., еліманова О.., Тарасенко .. Аналіз впливу внутрішньої теплоємності будівлі О та погодозалежного регулювання ТП на ефективність роботи системи опалення в черговому режимі. *Енергетика і автоматика*. 2021. № 5. . 46–61. doi : 10.31548/energiya2021.05.045.

[17] ешко .., ілоус .., уяк Н.А., Голубенко О.О., Гурєєв .. плив теплоінерційних особливостей огороджень на умови комфортності при впровадженні енергоощадних режимів опалення в будівлях. *Науково-технічний збірник «Комунальне господарство міст». Серія: технічні науки та архітектура*, 2019. Т. 3, 149. С. 44–50.

[18] ешко .., ілоус .., уяк Н.А. плив переривчастих режимів опалення на динаміку енергопотреби та умови комфортності будівель з різним рівнем теплового захисту. *Наукові вісті НТУУ КПІ*, 2019. 4. . 7–16.

[19] ndoor thermal environment, air exchange rates, and carbon dioxide concentrations before and after energy retro fits in Finnish and Lithuanian multi-family buildings / V. Leivo et al. *STE*. 2018. Vol. 621. P. 398–406.

[20] Ventilation in low energy residences–a survey on code reuirements, implementation barriers and operational challenges from seven European countries / D. ukowska et al. *International Journal of Ventilation*. 2020. Vol. 20. P.1–20.

[21] Simanic B., Norduist B., Bagge H., Johansson D. ndoor air temperatures, CO_2 concentrations and ventilation rates: Long-term measurements in newly built low-energy schools in Sweden. *Journal of Building Engineering*. 2019. Vol. 25. Article number 100827.

[22] Passive design optimization of newly-built residential buildings in Shanghai for improving indoor thermal comfort while reducing building energy demand / S. Gou, et al. *Energy and Buildings*. 2018. Vol. 169. P. 484–506. doi: 10.1016/.enbuild.2017 .09.095.

[23] Haddad S., Osmond P ., King S. Application of adaptive thermal comfort methods for ranian schoolchildren . *Building Research and Information*. 2019. Vol. 47, No. 2. P. 173–189.

[24] Residential adaptive comfort in a humid continental climate – Tianin China / . Song, et al. *Energy and Buildings*. 2018. Vol. 170. P. 115–121. doi: 10.1016/.enbuild.2018.03.083.

[25] Esmaeilzadeh A., akerzadeh M.R., Koma, A.Y. The comparison of some advanced control methods for energy optimization and comfort management in buildings. *Sustainable Cities and Society*. 2018. Vol. 43. P. 601–623. doi:10.1016/.scs.2018.08.038.

[26] nvestigation of thermal modernized building's microclimate with renewable energy / V. Nalyvaiko, et al. *ICoRES 2019*. 2020. Vol. 154. Article number 07011.

[27] Amending Directive 2010/31/E on the energy performance of buildings and Directive 2012/27/E on energy efficiency: Directive E 2018/844 of the European Parliament and of the Council. RL: https://eur-lex.europa.eu/legal-content/EN/TT/PDF/uriCELE:32018L0844fromT .

[28] ТУ 3756-98. «нергозбереження. Перетворювачі теплового потоку термоелектричні загального призначення. агальні технічні умови 61163». иїв: ержстандарт України, 2000. 54 с.

[29] ТУ А.2.2-12:2015 «нерг етична ефективність будівель. ето д розрахунку енергоспоживання при опаленні, охолодженні, вентиляції, освітленні та гарячому водопостачанні». иїв: ержстандарт України, 2015. 140 с.

[30] Gorobets V., Antypov ., Trokhaniak V., Bohdan Y. Experimental and numerical studies of heat and mass transfer in low-temperature heat accumulator with phase transformations of accumulating material. *MATEC Web of Conferences*. 2018. Vol. 240. Article number 01009.

[31] Черних Л.. , Родіонова Т.., Горбонос Н.Н., Дац П.А. Методика визначення опору теплопередачі огороджувальних конструкцій. иїв: НУіП, 2006. 12 с.

[32] Tsysar, M. Zakora, O. Babak, A., Ivakhnenko, S., & Zanevsky, O. Dependence of the Static Strength of Type Ib Single Crystal Diamonds with Octahedral Habit on Their Size. *Scientific Herald of Uzhhorod University. Series "Physics"*. 2021. Vol. 50. P. 25-30.

Євген Олексійович Антипов, Анатолій Васильович Міщенко,
Олена Віталіївна Шеліманова, Світлана Євгенівна Тарасенко

Національний університет біоресурсів і природокористування України
03041, вул. Героїв Оборони, 15, м. Київ, Україна

Аналіз впливу внутрішньої теплоємності громадської будівлі на параметри теплового комфорту приміщень при роботі системи опалення в черговому режимі

Анотація. У кліматичних умовах України, які характеризуються довгим опалювальним періодом, значні енергопотреби на опалення призводять до зростання вимог щодо енергоефективності. Суттєвому зниженню енергоспоживання будівель при забезпеченні умов комфортності сприятиме включення моделі теплового комфорту людини до складної системи «джерело тепла – огородження». Мета цього дослідження – визначення чинників, які впливають на внутрішню теплоємність та, відповідно, теплову інерцію будівлі і подальше врахування цих факторів при оцінці теплового стану та параметрів теплового комфорту кімнат будівлі. Об'єкт дослідження – навчально-адміністративний корпус НУБіП України. Проведено ряд досліджень, зокрема натурні виміри теплових потоків і температур на поверхнях зразків стінової конструкції будівлі виконувались в спеціальному кліматичному комплексі, який дозволяє штучно створювати зовнішні та внутрішні теплові умови приміщень. Показано, що утеплення конструкції шаром пінополістиролу ПСБ-15, товщиною 100 мм, дозволяє знизити теплові втрати через стінову панель майже вдвічі. Розроблено алгоритм управління процесом відпуску теплоти з урахуванням показника внутрішньої теплоємності будівлі. Порівняно з «лінійною» залежністю це дозволяє більш точно коригувати графік відпуску теплоносія в систему опалення громадської будівлі під час впровадження чергового режиму її роботи. Діапазон відхилення температур знижується на 4–6 °C, що дозволило заощадити до 10–12 % спожитої теплової енергії на потреби опалення об'єкту дослідження при умові збереження нормованих значень внутрішньої температури приміщень. Переривчастий режим роботи системи опалення громадських будівель, доцільність якого обґрунтована в даному дослідженні, може бути рекомендований до впровадження у спорудах закладів вищої освіти України

Ключові слова: теплова енергія, енергопотреби, енергоефективність, опалювальний період, теплова інерція, алгоритм управління, система опалення

Machinery & Energetics
Vol. 13, No. 2. 2022

Journal homepage:
https://technicalscience.com.ua/en

UDC 631.312:514.18
DOI: 10.31548/machenergy.13(2).2022.32-40

Tatiana Volina*, **Victor Nesvidomin, Andrii Nesvidomin, Vitalii Babka, Iryna Hryshchenko**

National University of Life and Environmental Sciences of Ukraine
03041, 15 Heroyiv Oborony Str., Kyiv, Ukraine

Movement of a Particle Along an Inclined Cylinder Rotating Around Its Axis

Abstract. It is well known that parts of agricultural machinery often have a cylindrical shape. This shape, for example, can be observed in the casing of lifting and transport machines, where the active working body rotates. Furthermore, drum grain dryers and triers use an inclined cylinder that rotates around its axis. In this case, the particles of the technological material interact with the rotating surface, which leads to their sliding, the nature of which depends on the value of the angle of inclination of the cylinder. In this study, the methods of differential geometry, vector algebra, theoretical mechanics, and numerical integration of differential equations consider the motion of a particle along the inner surface of an inclined cylinder rotating at a constant angular velocity around its axis. The axes of a fixed coordinate system are used to compose differential equations of motion. It was established that the proper initial conditions under which the particle would be stationary at a certain distance from the lower forming cylinder towards its rotation can be determined analytically. In case of movement along an inclined cylinder, the particle moves, among other things, in the axial direction, while reducing the amplitude of vibrations. Furthermore, it was found that the angle of inclination of the cylinder plays a significant role. If the latter is less than the angle of friction, then the vibrations stop, the movement of the particle stabilises, and it performs a rectilinear movement at a constant speed in the axial direction. If the angle of inclination of the cylinder is greater than or equal to the angle of friction, then the particle moves rapidly in the axial direction and its movement does not stabilise. The value of the angular velocity of rotation also plays a significant role. A certain amount of it provokes "sticking" of the particle, which does not depend on the inclination angle of the cylinder. The obtained analytical dependences can be used in the design of cylindrical working bodies of agricultural machines

Keywords: surface, rotational motion, sliding, angular velocity, differential equations, trajectory

Article's History: Received: 10.11.2021; Revised: 11.03.2022; Accepted: 27.04.2022.

INTRODUCTION

Cylindrical surfaces form an integral part of agricultural machinery. In lifting and transport machines, they play the role of a casing, inside which the active working body rotates (e.g., an auger). An inclined cylinder that rotates around its axis is used in drum grain dryers and cylindrical separators (triers). The interaction of material particles with the surface of the cylinder rotating around its axis leads to their sliding, the nature of which depends on the value of the inclination angle of the cylinder. An analytical description of the particle's sliding on the cylinder surface is a prerequisite for designing machines with such a nature of particle interaction with a moving surface, which indicates the relevance of this study.

Furthermore, at all times, the issues of increasing the durability of machines and their elements by improving reliability indicators have been extremely relevant. Thus, the article [1] describes the latest method of surface sulphidation developed. In [2], the method of surface hardening of parts using cementing and nitriding is highlighted. In [3], a method for applying a multi-layer coating is proposed. As the researchers note, such recommendations are insufficient to meet the needs of the present [4]. Notably, in all these and similar studies, the latest technologies of surface hardening are developed, which is a costly process.

Engineering practice often faces problems of geometric design of objects that are proposed to be solved in various ways, e.g., in multidimensional space by approximating the solution of differential equations [5], by multidimensional parabolic interpolation [6], by interpolating geometric space [7], etc. It is even easier to solve the inverse problem. In this case, the geometric design of technological objects is reduced to finding analytical dependencies of their interaction. Such interaction in mechanical engineering is the interaction between the working body

Suggested Citation:
Volina, T., Nesvidomin, V., & Nesvidomin, A., Babka, V., & Hryshchenko, I.(2022). Movement of a particle along an inclined cylinder rotating around its axis. *Machinery & Energetics,* 13(2), 32-40.

*Corresponding author

and the material. This occurs during grain separation [8], aspiration separation [9], soil fertilisation [10], etc. The motion of an individual particle cannot be identified with the motion of a material that comprises individual particles, but it allows identifying patterns of motion that can be transferred to the material in a certain way. Thus, [11] presents the results of studies of particle motion on rough surfaces, and [12] – in rotary scatterers.

However, the study of body motion in some cases can be reduced to a particle [13]. This applies to the case when the inertial forces from the rotation of a body can be ignored due to the small angular velocities of their rotation [14]. Using this approach, the motion of particles on the surface of a spherical segment rotating around a vertical axis was investigated [15]. Thus, the range of applied problems requiring an analytical description of the motion of a particle along a plane is expansive. Proceeding from the above, the purpose of this study was to search for patterns of motion of a material particle along the inner surface of a cylinder set at an angle to the horizon and rotating around the axis. Research on this area is made in the monograph [16, p. 468], but they have a limited nature of calculations and graphical constructions for objective reasons due to the lack of modern computer tools at that time.

MATERIALS AND METHODS

To fulfil the purpose set, the authors of this paper used methods of differential geometry, vector algebra, theoretical mechanics, and methods of numerical integration of differential equations. The parametric equations of a cylinder with a horizontal axis directed along the *OX* axis (Fig. 1) have the following form:

$$X = u; Y = R\,sin\,\alpha\,; Z = -R\,cos\,\alpha, \tag{1}$$

where R is the cylinder radius-constant value; α and u are the independent variable surfaces, and α is the angular coordinate, u is the linear coordinate (length of a rectilinear generating cylinder). The sign "–" in the above Equation (1) is taken so that the value α=0 corresponds to the lowest element of the cylinder, on which the particle will be in the initial position.

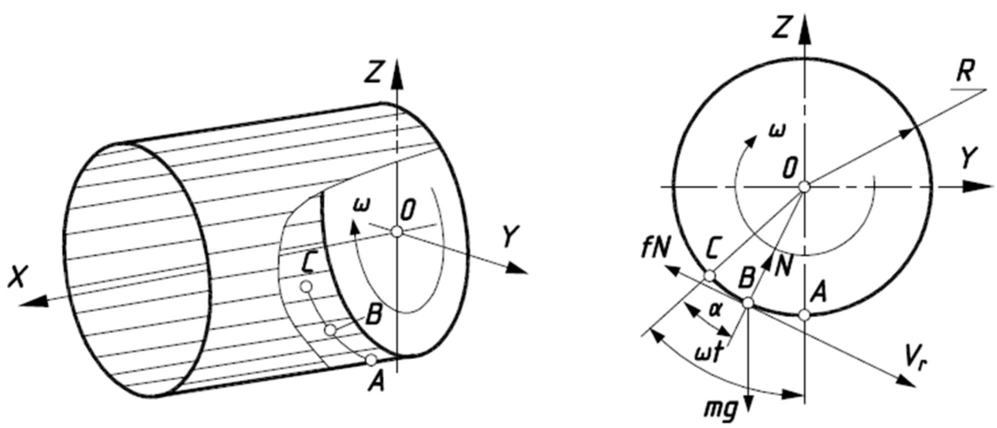

a) b)

Figure 1. Graphical illustrations for compiling the equations of motion of a particle along the inner surface of a horizontal cylinder that rotates around its axis: a) axonometric view of the cylinder; b) projection of the cylinder, when the *OX* axis is directed at the observer and the forces applied to the particle at point *B*

At the beginning of the movement, the particle is at point *A* on the lower base of the cylinder (Fig. 1). The cylinder will be rotated around the axis with a constant angular velocity ω. During time t, the cylinder will turn to the angle ωt and the lower generator of the cylinder will move to point *C*. During the same time, the particle will move along the surface of the cylinder, but will not reach point *C*, as it will slide along it (Fig. 1b). Suppose it reached point *B*, which corresponds to angular slip α. Since the axis of rotation of the cylinder is horizontal, it is obvious that the sliding trajectory will be an arc of a circle. If the cylinder is tilted, there will be a component of the force of gravity, which will make the particle slide towards the *OX* axis as well. First, the study considered the movement of a particle on the surface of a horizontal cylinder.

If one connects the independent variables α and u of the surface by a certain functional dependence, e.g., on time t, then Equations (1) will turn into equations of one variable, i.e., they will describe a line on the surface of the cylinder. This line will be considered as the sliding trajectory, and the dependences α=α(t) and $u=u(t)$ are unknowns that need to be found. To find them, one needs to compile a system of differential equations of motion of the particle in projections on the axis of the *OXYZ* coordinate system.

The equation of motion of the particle will be formulated in the following form: $m\overline{w}=\overline{F}$, where m is the particle mass, $\overline{w}$ is the vector of absolute acceleration, $\overline{F}$ is the resulting vector of forces applied to the particle. These forces are weight force mg (g=9.81 m/s^2 – acceleration of free fall), surface reaction N, and friction force $f{\cdot}N$ (f – friction coefficient). Next, the direction cosines are found, i.e., the unit direction vectors of action of these forces. The weight force is directed downwards, so the projections of the guide vector will be written as follows:

$$mg: \{0; 0; -1\} \tag{2}$$

The frictional force $f{\cdot}N$ is directed opposite to the velocity vector of the relative movement V_r – sliding. To find the speed V_r of relative motion, Equation (1) is differentiated with respect to time t. Therewith, it is implied that α=α(t) and $u=u(t)$, i.e., Equations (1) are no longer equations of the cylinder, but equations of a line on it, i.e., of a relative trajectory. To distinguish between line and surface equations, in the equations of the relative trajectory, the authors switch from uppercase letters to lowercase letters with the index "r":

$$x_r' = u'; y_r' = R\alpha' \cos\alpha\, ; z_r' = R\alpha' \sin\alpha \tag{3}$$

The relative sliding velocity of a particle on the surface of a cylinder is defined as the geometric sum of the components (3):

$$V_r = \sqrt{{x_r'}^2 + {y_r'}^2 + {z_r'}^2} = \sqrt{u'^2 + R^2\alpha'^2} \tag{4}$$

When dividing (3) by (4), it is possible to obtain a unit vector of the tangent to the relative trajectory in the projections on the axis of the *OXYZ* system. Given the opposite direction of the friction force $f{\cdot}N$ and the relative velocity vector V_r, the sign of the unit direction vector of the friction force must be changed to the opposite:

$$fN\colon\left\{-\frac{u'}{\sqrt{u'^2 + R^2\alpha'^2}}; -\frac{R\alpha' \cos\alpha}{\sqrt{u'^2 + R^2\alpha'^2}}; -\frac{R\alpha' \sin\alpha}{\sqrt{u'^2 + R^2\alpha'^2}}\right\} \tag{5}$$

Surface reaction N is directed from a point on the cylinder to the axis of rotation (Fig. 1b). If the radius vector of a point on a cylinder is determined by the second and third expressions of Equations (1), then the surface reaction is determined by the same expressions, but with the opposite sign. Having shortened the expressions by R, the projections of the unit reaction vector N will be written as follows:

$$N\colon\{0; -\sin\alpha\, ; \cos\alpha\} \tag{6}$$

At the angular rotation speed ω of the cylinder surface during the time t, a turn by an angle of $\theta=-\omega t$ (clockwise) will be made. The generator of the cylinder, which was in the lower position at point A, will take the position at point C (Fig. 1b). To rotate the cylinder (1) around the *OX* axis by an angle $\theta=-\omega t$, the known formulas are applied as follows:

$$\begin{aligned} X &= u; \\ Y &= R\sin\alpha\cos\theta + R\cos\alpha\sin\theta\, ; \\ Z &= R\sin\alpha\sin\theta - R\cos\alpha\cos\theta. \end{aligned} \tag{7}$$

After simplifications considering $\Theta=-\omega t$, equation (7) takes the following form:

$$\begin{aligned} X &= u; \\ Y &= -R\sin(\omega t - \alpha)\, ; \\ Z &= -R\cos(\omega t - \alpha). \end{aligned} \tag{8}$$

Equation (8) at α=α(t) and $u=u(t)$ are the equations of the absolute trajectory of the particle's motion. The cylinder turned to the angle $\theta=-\omega{\cdot}t$, and during this time the particle, sliding along the cylinder in the opposite direction, turned to the angle α=α(t) and took the position at point B (Fig. 1b). The absolute speed of the particle is found by differentiating equations (8), switching to the lowercase letters with the index "a":

$$\begin{aligned} x_a' &= u'; \\ y_a' &= -R(\omega - \alpha')\cos(\omega t - \alpha)\, ; \\ z_a' &= R(\omega - \alpha')\sin(\omega t - \alpha). \end{aligned} \tag{9}$$

By differentiating Equations (8), the projections of the absolute acceleration vector are found as follows:

$$\begin{aligned} x_a'' &= u''; \\ y_a'' &= R(\omega - \alpha')^2 \sin(\omega t - \alpha) + R\alpha''\cos(\omega t - \alpha)\, ; \\ z_a'' &= R(\omega - \alpha')^2 \cos(\omega t - \alpha) - R\alpha''\sin(\omega t - \alpha). \end{aligned} \tag{10}$$

The unit direction vector of the action of the friction force $f{\cdot}N$ (5) and the reaction N of the surface (6) were found for a stationary cylinder. The surface rotates at an angle $\theta=-\omega{\cdot}t$, and therefore the vectors must also be rotated by this angle. Otherwise, the correspondence to the location of the particle is lost. The rotation is performed by analogy with the rotation of the surface according to Equations (7). After such manipulations, the projections of vectors take the following form:

– of the unit direction vector of the friction force $f{\cdot}N$:

$$fN\colon\left\{-\frac{u'}{\sqrt{u'^2 + R^2\alpha'^2}}; -\frac{R\alpha' \cos(\omega t - \alpha)}{\sqrt{u'^2 + R^2\alpha'^2}}; \frac{R\alpha' \sin(\omega t - \alpha)}{\sqrt{u'^2 + R^2\alpha'^2}}\right\}. \tag{11}$$

– of the unit direction vector of the action of the reaction force N:

$$N\colon\{0; \sin(\omega t - \alpha)\, ; \cos(\omega t - \alpha)\} \tag{12}$$

Since the projections (10) of the absolute acceleration vector and the direction vectors of the applied forces of the particle weight mg (2), friction $f{\cdot}N$ (11) and reaction N (12) are known, the vector equation $m\bar{w}=\bar{F}$ must be formulated relative to the fixed *OXYZ* coordinate system:

$$\begin{aligned} mx_a'' &= -fN\frac{u'}{\sqrt{u'^2 + R^2\alpha'^2}}; \\ my_a'' &= -fN\frac{R\alpha' \cos(\omega t - \alpha)}{\sqrt{u'^2 + R^2\alpha'^2}} + N\sin(\omega t - \alpha)\, ; \\ mz_a'' &= -mg + fN\frac{R\alpha' \sin(\omega t - \alpha)}{\sqrt{u'^2 + R^2\alpha'^2}} + N\cos(\omega t - \alpha). \end{aligned} \tag{13}$$

By substituting acceleration expressions (10) into (13), a system of three equations will be obtained with three unknown dependencies: α=α(t), $u=u(t)$, and $N=N(t)$. It should be used in the case when the initial velocity u' of particle sliding is specified towards the *OX* axis. When $u''=u'=0$ (i.e., when a particle slides around a circle), the first Equation (13) turns into the identity 0=0. Having solved the system of the other two with respect to α″=α″(t) and $N=N(t)$, one obtains as follows:

$$\alpha'' = \frac{g}{R}[\sin(\omega t - \alpha) - f\cos(\omega t - \alpha)] - f(\omega - \alpha')^2. \tag{14}$$

$$N = m[R(\omega - \alpha')^2 + g\cos(\omega t - \alpha)]. \tag{15}$$

Equation (14) is differential and can be solved independently. It can be assumed that when the horizontal cylinder rotates, the particle located at the bottom (point A, Fig. 1b) will rotate with the cylinder without sliding to point C, and then it will slide down to a certain point below, and this process will be repeated. Numerical integration of

Equation (14) has shown that this assumption is valid only for small angular velocities. An essential role in numerical integration is played by the initial conditions, on which, as will be shown later, the nature of the particle's motion depends. The initial conditions provided that the particle at the initial moment is on the bottom of the cylinder and there is no sliding angular velocity, i.e., $\alpha=\alpha'=0$. In Figure 2, graphs of the change in the kinematic characteristics of the particle movement during 3 s at R=0.2 m, f=0.3 and different angular velocities of the cylinder rotation are plotted. Above is a graph of the change in the angle α, and below – the difference in the angles $\omega \cdot t-\alpha$. The horizontal section of the graph $\alpha=\alpha(t)$, which is repeated periodically, indicates that at this moment in time there is no sliding, the particle "sticks" and rotates together with the cylinder. "Sticking" (lifting up) periodically alternates with sliding (lowering down). The graph of the change in the angle difference $\omega \cdot t-\alpha$ shows the amplitude of oscillations in the angular dimension.

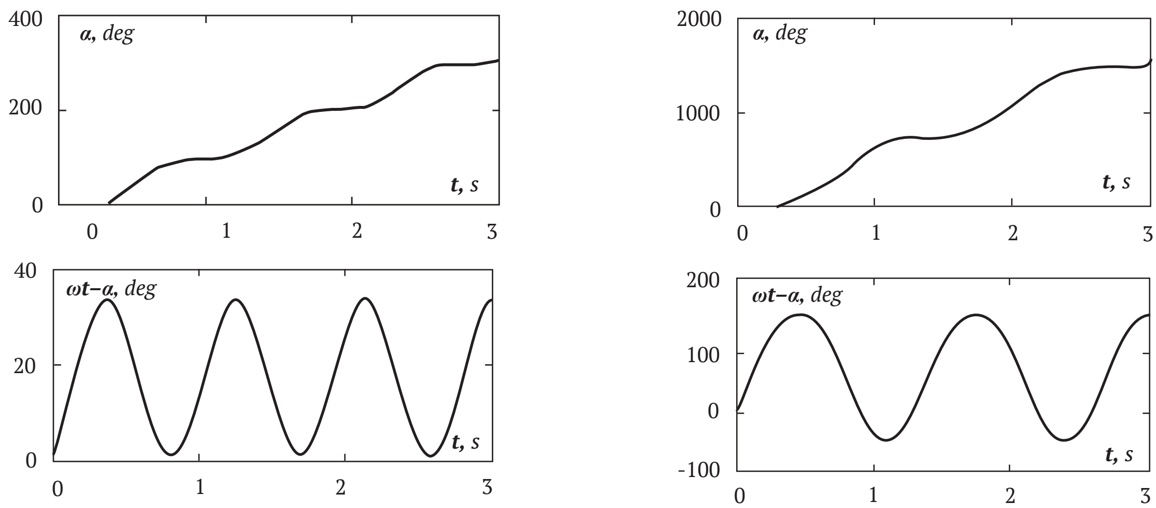

a) b)

Figure 2. Graphs of changes in the sliding angle α and the angle of deviation of the particle $\omega \cdot t-\alpha$ from the zero value in absolute motion: a) $\omega=2\ s^{-1}$; b) $\omega=10\ s^{-1}$

The graphs show that the amplitude of particle vibrations increases as the angular velocity of rotation of the cylinder increases. If at $\omega=2\ s^{-1}$ the particle turned by approximately 35° while rising and descended almost to zero (i.e., to the lower generator), then at $\omega=10\ s^{-1}$ these angles are 165° and –40°, respectively, i.e., the particle oscillates in a circle, covering more than half of its arc. With the further growth of the angular velocity ω of the cylinder rotation, the particle practically "sticks" and rotates together with it.

If, at the initial moment, the particle is given an angular speed of sliding $\alpha'=\omega$, i.e., at the beginning of the movement, its absolute speed of rotation will be equal to zero, then the further movement of the particle will differ from the considered cases. For instance, the authors of this paper took $\omega=10\ s^{-1}$ (the graph is presented in Figure 2b below for the initial conditions $\alpha=\alpha'=0$). Next, only one initial condition was changed: $\alpha=0$, $\alpha'=\omega$. This substitution substantially changed the nature of the vibrations – their amplitude decreased (Fig. 3a).

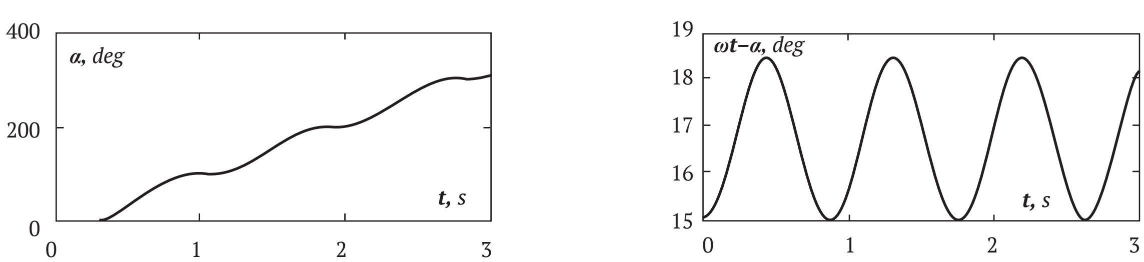

a) b)

Figure 3. Graphs of changes in the particle deviation angle $\omega \cdot t-\alpha$ from the zero value in absolute motion at $\omega=10\ s^{-1}$ and different initial conditions of integration: a) $\alpha'=\omega$, $\alpha=0$; b) $\alpha'=\omega$, $\alpha=-15°$

Theoretical studies have shown that when the angular speed of rotation of the cylinder increases, the particle does not "stick", but oscillates with the same amplitude (within 0° to 35°), i.e., the angular speed of rotation of the cylinder in this case does not affect the amplitude of oscillations. However, the second initial condition added to the first has an effect. In Figure 3b, a similar graph is plotted when $\alpha=-15°$, i.e., at the initial moment, the particle is not fed to the lower point of the cylinder, but slightly higher towards its rotation. The amplitude of vibrations has decreased and is within 15°...18.5°, while it is not difficult to notice that in both cases (Fig. 3a, b) vibrations occur relative to the midpoint, which in angular measurement is approximately 17°. If α=–17° is taken as the starting condition, then the amplitude of oscillations practically disappears, and the particle remains motionless in absolute motion. This is confirmed by the partial solution of differential Equation (14) for the corresponding initial conditions.

Let the solution of equation (14) be the dependence $\alpha=\omega\cdot t+\alpha_o$. Then $\alpha'=\omega$, $\alpha''=0$. Substituting these expressions into the differential Equation (14) satisfies it. One gets a simple equation:

$$-\sin\alpha_0 - f\cos\alpha_0 = 0,\ \text{hence}\ \alpha_0 = -\mathrm{Arctg}f. \qquad (16)$$

Thus, the angle α_o is equal to the angular friction of the particle on the cylinder surface. For the accepted value of f=0.3, the angle α_o= –16.7°. If these initial conditions are met ($\alpha'=\omega$ and $\alpha=\alpha_o= -Arctg\,f$), the particle will slide along the surface of the cylinder, remaining motionless in absolute motion at a certain height from the lower generator, which in the angular dimension corresponds to the angular friction.

To make differential equations of motion of a particle along an inclined cylinder rotating around its axis, one needs to rotate the cylinder and bring all the vectors of forces and absolute acceleration according to its position. Rotation will be performed around the *OY* axis by an angle β, clockwise, so that the direction of the particle sliding down along the generating lines of the cylinder coincides with the direction of the *OX* axis. The weight force vector is directed downwards, i.e., it does not change its direction. The vectors of the remaining forces and absolute acceleration are rigidly tied to the surface of the cylinder or to the lines (trajectories) on it, so they must be rotated in the same way as the cylinder.

After turning by the angle β, the following expressions are obtained:

are the parametric equations of the cylinder:

$$\begin{gathered} X = u\cos\beta - R\sin\beta\cos\alpha\,; \\ Y = R\sin\alpha\,; \\ Z = -u\sin\beta - R\cos\beta\cos\alpha\,; \end{gathered} \qquad (17)$$

are the projections of the absolute trajectory:

$$\begin{gathered} x_a = u\cos\beta - R\sin\beta\cos(\omega t-\alpha)\,; \\ y_a = -R\sin(\omega t-\alpha)\,; \\ z_a = -u\sin\beta - R\cos\beta\cos(\omega t-\alpha)\,; \end{gathered} \qquad (18)$$

are the projections of absolute acceleration:

$$\begin{gathered} x''_{a\beta} = R\sin\beta\,(\omega-\alpha')^2\cos(\omega t-\alpha) + u''\cos\beta - R\alpha''\sin\beta\sin(\omega t-\alpha)\,; \\ y''_{a\beta} = R(\omega-\alpha')^2\sin(\omega t-\alpha) + R\alpha''\cos(\omega t-\alpha)\,; \\ z''_{a\beta} = R\cos\beta\,(\omega-\alpha')^2\cos(\omega t-\alpha) - u''\sin\beta - R\alpha''\cos\beta\sin(\omega t-\alpha). \end{gathered} \qquad (19)$$

– of the unit direction vector of the friction force $f{\cdot}N$:

$$fN:\left\{\begin{matrix} \dfrac{R\alpha'\sin\beta\sin(\omega t-\alpha) - u'\cos\beta}{\sqrt{u'^2+R^2\alpha'^2}}; \\ -\dfrac{R\alpha'\cos(\omega t-\alpha)}{\sqrt{u'^2+R^2\alpha'^2}}; \\ \dfrac{R\alpha'\cos\beta\sin(\omega t-\alpha) + u'\sin\beta}{\sqrt{u'^2+R^2\alpha'^2}} \end{matrix}\right\}. \qquad (20)$$

– of the unit direction vector of the action of the reaction force N:

$$\{N:\ \sin\beta\cos(\omega t-\alpha)\,;\sin(\omega t-\alpha)\,;\cos\beta\cos(\omega t-\alpha)\} \qquad (21)$$

Similarly, as for a horizontal cylinder, a system of differential equations is compiled considering the rotated vectors (19–21):

$$\begin{gathered} m x''_{a\beta} = fN\frac{R\alpha'\sin\beta\sin(\omega t-\alpha) - u'\cos\beta}{\sqrt{u'^2+R^2\alpha'^2}} + N\sin\beta\cos(\omega t-\alpha)\,; \\ m y''_{a\beta} = -fN\frac{R\alpha'\cos(\omega t-\alpha)}{\sqrt{u'^2+R^2\alpha'^2}} + N\sin(\omega t-\alpha)\,; \\ m z''_{a\beta} = -mg + fN\frac{R\alpha'\cos\beta\sin(\omega t-\alpha) + u'\sin\beta}{\sqrt{u'^2+R^2\alpha'^2}} + N\cos\beta\cos(\omega t-\alpha). \end{gathered} \qquad (22)$$

Next, the authors substituted the acceleration expressions (19) into (22) and solved with respect to $\alpha''=\alpha''(t)$, $u''=u''(t)$ and $N=N(t)$:

$$\begin{gathered} \alpha'' = \frac{g}{R}\cos\beta\sin(\omega t-\alpha) - \frac{f\alpha'}{\sqrt{u'^2+R^2\alpha'^2}}[g\cos\beta\cos(\omega t-\alpha) + R(\omega-\alpha')^2]; \\ u'' = g\sin\beta - \frac{fu'}{\sqrt{u'^2+R^2\alpha'^2}}[g\cos\beta\cos(\omega t-\alpha) + R(\omega-\alpha')^2]; \\ N = m[g\cos\beta\cos(\omega t-\alpha) + R(\omega-\alpha')^2]. \end{gathered} \qquad (23)$$

RESULTS AND DISCUSSION

Using numerical integration, the kinematic characteristics of the movement of the particle along the inner surface inside the cylinder were obtained, and they substantially depend on two parameters: the angle of inclination β of the cylinder and the angular velocity ω of its rotation. In Figure 4, the absolute trajectories of the particle movement are plotted for a cylinder of radius *R*=0.2 m, tilted at an angle β=15° (smaller than the friction angle, which for *f*=0.3 is 16.7°).

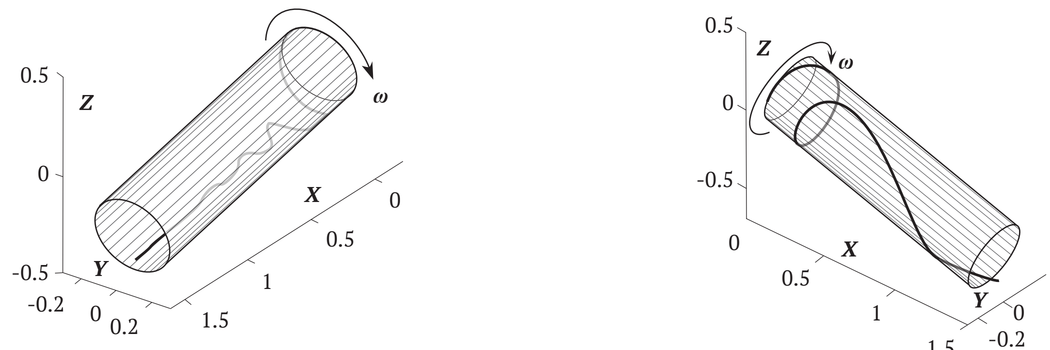

a) b)

Figure 4. Absolute trajectories of particle motion along the inner surface of the cylinder at different angular velocities of its rotation: a) ω=2 s^{-1}; b) ω=10 s^{-1}

In Figure 5, graphs of speed changes are plotted $u'=V_z$ towards the *OX* axis. In one case (Fig. 5a), the tilt angle is smaller than the friction angle, in the second (Fig. 5b) – it is larger.

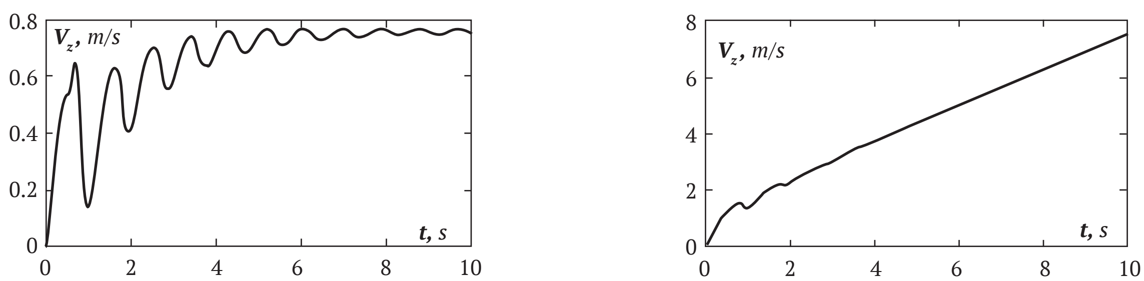

a) b)

Figure 5. Graphs of the change in speed $u'=V_z$ towards the cylinder axis at ω=5 s^{-1} for different angles β of its inclination: a) β=10°; b) β=20°

Analysing the image in Figures 4a and 5a, it can be concluded that the motion of the particle stabilises, its velocity in the axial direction approaches a constant value, and the trajectory approaches a straight line. Such stabilisation is possible up to a certain value of the angular velocity of the cylinder rotation. Figure 4b shows the absolute trajectory at ω=10 s^{-1}, which shows that the particle's oscillations are increasing. As the angular velocity ω increases further, the particle practically "sticks" and rotates together with the cylinder. At low angular speeds of rotation of the cylinder (i.e., before the particle "sticks"), speed stabilisation is possible only for cylinder tilt angles that are less than the angle of friction. Figure 5b shows a graph of the particle sliding speed in the axial direction at an angle β greater than the friction angle. It shows that the sliding velocity of the particle increases linearly.

"Sticking" of the particle occurs when the corresponding angular velocity of rotation of the cylinder is reached at any angles of its inclination. Figure 6 shows graphs of the change in the sliding angle α and the distance *u* of the particle movement in the axial direction at ω=20 s^{-1} and the angle of inclination β=45°.

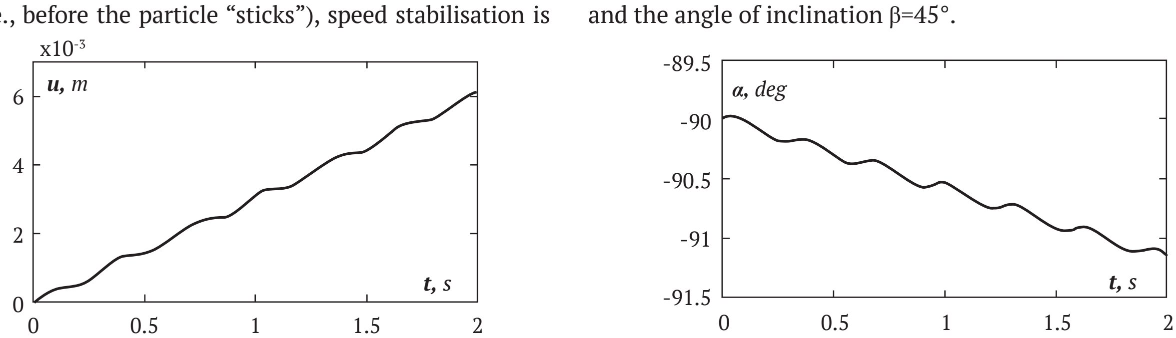

a) b)

Figure 6. Graphs of changes in the kinematic characteristics of particle motion at ω=20 s^{-1} and the inclination angle β=45°: a) graph of the dependence *u=u(t)*; b) dependence graph α=α(t)

The graphs show that the particle moves 6 mm in the axial direction during the time t=2 s and turns 1° in the angular dimension. It is clear that a further increase in the angular velocity of rotation of the cylinder will lead to complete "sticking" of the particle.

The results obtained considerably complement the similar results obtained in the monograph [16]. In the given study, the sliding trajectories of particles are plotted on the surface of an inclined cylinder, in contrast to the specified monograph, where they are plotted on a cylinder sweep. Furthermore, this study considered cases where the angle of inclination of the cylinder is less than or greater than the angle of friction, while the aforementioned study considered an angle less than the angle of friction. The results obtained show that with an increase in the angular velocity of rotation of the cylinder, "sticking" of the particle is possible, which was not considered in the cited monograph.

As it turned out, for the cylinder inclination angles smaller than the friction angle, it is possible to stabilise the motion, in which the particle slides in a straight line at a constant speed. A solution for this case and for a horizontal cylinder can be found by looking for the solution in the form $\alpha=\omega\cdot t+\alpha_o$, supplementing it with a constant velocity in the axial direction $u'=V_z=const$. Thus, $\alpha'=\omega$, $\alpha''=0$, $u''=0$. Substituting these data into the first two Equations (23), a system of two equations is obtained as follows:

$$0=\frac{g}{R}\cos\beta\,\sin(-\alpha_0)-\frac{f\omega g\cos\beta\cos(-\alpha_0)}{\sqrt{V_z^2+R^2\omega^2}};\qquad 0=g\sin\beta-\frac{fV_z g\cos\beta\cos(-\alpha_0)}{\sqrt{V_z^2+R^2\omega^2}}. \tag{24}$$

After solving system (24) with respect to α_o and V_z, one obtains:

$$\alpha_0=-\mathrm{Arctg}\sqrt{f^2\cos^2\beta-\sin\beta};\ V_z=R\omega\sqrt{\frac{1+f^2}{f^2\mathrm{ctg}^2\beta-1}}. \tag{25}$$

The obtained result (25) should be understood as follows: if a particle hits a cylinder at α_o with a relative angular velocity equal to the angular velocity of rotation of the cylinder, directed oppositely from the direction of its rotation and with a relative translational velocity along the V_z axis, then it continues to move at this speed along the cylinder without oscillation.

CONCLUSIONS

When a particle hits the inner surface of a horizontal cylinder, which rotates with an angular velocity ω around its axis, it begins to oscillate in the plane of the cylinder cross-section with a certain amplitude in the angular dimension. The magnitude of the amplitude depends on the point of impact of the particle, the coefficient of friction, and the initial absolute velocity. Under proper starting conditions, which are determined analytically, a particle in absolute motion can be stationary, being at a point in the cylinder at a certain distance from the lowest point in the angular dimension along the course of the cylinder rotation. When the cylinder is tilted at an angle β to the horizon, the particle begins to move in the axial direction, while the amplitude of vibrations decreases. The angle of inclination of the cylinder is important: at the angle β, which is smaller than the friction angle, the movement stabilises, the oscillations stop, and the particle moves in a straight line in the axial direction with a constant speed; at an angle β greater than or equal to the angle of friction, motion stabilisation does not occur, the particle moves accelerated in the axial direction. The value of the angular velocity of rotation is of great importance. When a certain value is reached, the particle practically "sticks" regardless of the angle of inclination of the cylinder. Experimental verification of data obtained as a result of theoretical research can serve as the basis of further research.

REFERENCES

[1] Tarelnyk, V., Martsynkovskyy, V., Gaponova, O., Konoplianchenko, I., Dovzyk, M., Tarelnyk, N., & Gorovoy, S. (2017). New sulphiding method for steel and cast iron parts. *IOP Conference Series: Materials Science and Engineering*, 233, article number 012049. doi: 10.1088/1757-899x/233/1/012049.

[2] Tarelnyk, V., Martsynkovskyy, V., Gaponova, O., Konoplianchenko, I., Belous, A., Gerasimenko, V., & Zakharov, M. (2017). New method for strengthening surfaces of heat treated steel parts. *IOP Conference Series: Materials Science and Engineering*, 233, article number 012048. doi: 10.1088/1757-899x/233/1/012048.

[3] Tarel'nik, V.B., Martsinkovskii, V.S., & Zhukov, A.N. (2017). Increase in the reliability and durability of metal impulse end seals. Part 1. *Chemical and Petroleum Engineering*, 53(1/2), 114-120. doi: doi: 10.1007/s10556-017-0305-y.

[4] Martsinkovsky, V., Yurko, V., Tarelnik, V., & Filonenko, Y. (2012). Designing thrust sliding bearings of high bearing capacity. *Procedia Engineering*, 39, 148-156. doi: 10.1016/j.proeng.2012.07.019.

[5] Konopatskiy, E., Voronova, O., Bezditnyi, A., & Shevchuk, O. (2020). About one method of numeral decision of differential equalizations in partials using geometric interpolants. In *Proceedings of the 30th international conference on computer graphics and machine vision* (pp. 213-219). St. Petersburg: Saint Petersburg State University.

[6] Konopatskiy, E.V., & Bezditnyi, A.A. (2020). Geometric modeling of multifactor processes and phenomena by the multidimensional parabolic interpolation method. *Journal of Physics: Conference Series*, 1441(1), article number 012063. doi: 10.1088/1742-6596/1441/1/012063.

[7] Konopatskiy, E., Bezditnyi, A., & Shevchuk, O. (2020). Modeling geometric varieties with given differential characteristics and its application. In *Proceedings of the 30th international conference on computer graphics and machine vision* (pp. 1-8). St. Petersburg: Saint Petersburg State University. doi: 10.51130/graphicon-2020-2-4-31.

[8] Abbou-ou-Cherif, E.M., Piron, E., Chateauneuf, A., Miclet, D., Lenain, R., & Koko, J. (2017). On-the-field simulation of fertilizer spreading. Part 1 – Modeling. *Computers and Electronics in Agriculture,* 142(A), 235-247. doi: 10.1016/j.compag.2017.09.006.
[9] Bulgakov, V., Nikolaenko, S., Holovach, I., Boris, A., Kiurchev, S., Ihnatiev, Y., & Olt, J. (2020). Theory of motion of grain mixture particle in the process of aspiration separation. *Agronomy Research*, 18(2), 1177-1188. doi: 10.15159/AR.20.069.
[10] Kobets, A.S., Ponomarenko, N.O., & Kharytonov, M.M. (2017). Construction of centrifugal working device for mineral fertilizer spreading. *INMATEH-Agricultural Engineering*, 51(1), 5-14.
[11] Golub, G.A., Szalay, K., Kukharets, S.M., & Marus, O.A. (2017). Energy efficiency of rotary digesters. *Progress in Agricultural Engineering Sciences*, 13(1), 35-49. doi: 10.1556/446.13.2017.3.
[12] Kurzthaler, C., Zhu, L., Pahlavan, A., & Stone, H. (2020). Particle motion nearby rough surfaces. *Physical Review Fluids*, 5, article number 082101(R). doi: 10.1103/PhysRevFluids.5.082101.
[13] Pylypaka, S., Klendiy, M., & Zaharova, T. (2019). Movement of the particle on the external surface of the cylinder, which makes the translational oscillations in horizontal planes. In *Advances in design, simulation and manufacturing* (pp. 336-345). Sumy: Sumy State University.
[14] Loveikin, V.S., & Romesevych, Yu.O. (2017). Dynamic optimization of a mine winder acceleration mode. *Naukovyi Visnyk Natsionalnoho Hirnychoho Universytetu*, 4, 55-61.
[15] Pylypaka, S., Nesvidomin, V., Volina, T., Sirykh, L., & Ivashyna, L. (2020). Movement of the particle on the internal surface of the spherical segment rotating about a vertical axis. *INMATEH-Agricultural Engineering*, 62(3), 79-86. doi: 10.35633/inmateh-62-08.
[16] Zaika, P.M. (1992). *Selected tasks of agricultural mechanics*. Kyiv: USHA Publishing House.

СПИСОК ВИКОРИСТАНИХ ДЖЕРЕЛ

[1] New sulphiding method for steel and cast iron parts / V. Tarelnyk et al. *IOP Conference Series: Materials Science and Engineering*. 2017. Vol. 233. Article number 012049. doi: 10.1088/1757-899x/233/1/012049.
[2] New method for strengthening surfaces of heat treated steel parts / V. Tarelnyk et al. *IOP Conference Series: Materials Science and Engineering*. 2017. 233, article number 012048. doi: 10.1088/1757-899x/233/1/012048.
[3] Increase in the reliability and durability of metal impulse end seals. Part 1. *Chemical and Petroleum Engineering*. Vol. 53, No. 1/2. P. 114–120. doi: doi: 10.1007/s10556-017-0305-y.
[4] Martsinkovsky V., Yurko V., Tarelnik V., Filonenk, Y. Designing thrust sliding bearings of high bearing capacity. *Procedia Engineering*. 2012. Vol. 39. P. 148–156. doi: 10.1016/j.proeng.2012.07.019.
[5] Konopatskiy E., Voronova O., Bezditnyi A., Shevchuk O. About one method of numeral decision of differential equalizations in partials using geometric interpolants. *Proceedings of the 30th international conference on computer graphics and machine vision* (Saint Petersburg, September 23–25, 2020). St. Petersburg, 2020. P. 213–219.
[6] Konopatskiy E.V., Bezditnyi A.A. Geometric modeling of multifactor processes and phenomena by the multidimensional parabolic interpolation method. *Journal of Physics: Conference Series*. 2020. Vol. 1441, No. 1. Article number 012063. doi: 10.1088/1742-6596/1441/1/012063.
[7] Konopatskiy E., Bezditnyi A., Shevchuk O. Modeling geometric varieties with given differential characteristics and its application. *Proceedings of the 30th international conference on computer graphics and machine vision* (Saint Petersburg, September 23–25, 2020). St. Petersburg, 2020. P. 1–8. doi: 10.51130/graphicon-2020-2-4-31.
[8] On-the-field simulation of fertilizer spreading. Part 1 – Modeling / E.M. Abbou-ou-Cherif et al. *Computers and Electronics in Agriculture*. 2017. Vol. 142(A). P. 235–247. doi: 10.1016/j.compag.2017.09.006.
[9] Theory of motion of grain mixture particle in the process of aspiration separation / V. Bulgakov et al. *Agronomy Research*. 2020. Vol. 18, No. 2. P. 1177–1188. doi: 10.15159/AR.20.069.
[10] Kobets A.S., Ponomarenko N.O., Kharytonov M.M. Construction of centrifugal working device for mineral fertilizer spreading. *INMATEH-Agricultural Engineering*. 2017. Vol. 51, No. 1. P. 5–14.
[11] Golub G.A., Szalay K., Kukharets S.M., Marus O.A. Energy efficiency of rotary digesters. *Progress in Agricultural Engineering Sciences*. 2017. Vol. 13, No. 1. P. 35–49. doi: 10.1556/446.13.2017.3.
[12] Kurzthaler C., Zhu L., Pahlavan A., Stone H. Particle motion nearby rough surfaces. *Physical Review Fluids*. 2020. Vol. 5. Article number 082101(R). doi: 10.1103/PhysRevFluids.5.082101.
[13] Pylypaka S., Klendiy M., Zaharova T. Movement of the particle on the external surface of the cylinder, which makes the translational oscillations in horizontal planes. *Advances in design, simulation and manufacturing* (Sumy, October 12–15, 2019). Sumy, 2019. P. 336–345
[14] Loveikin V.S., Romesevych Yu.O. (2017). Dynamic optimization of a mine winder acceleration mode. *Naukovyi Visnyk Natsionalnoho Hirnychoho Universytetu*. Vol. 4. P. 55–61.
[15] Movement of the particle on the internal surface of the spherical segment rotating about a vertical axis / S. Pylypaka et al. *INMATEH-Agricultural Engineering*. 2020. Vol. 62, No. 3. P. 79–86. doi: 10.35633/inmateh-62-08.
[16] Заика П.М. Избранные задачи земледельческой механики. Киев: Изд-во УСХА, 1992. 512 с.

**Тетяна Миколаївна Воліна, Віктор Миколайович Несвідомін,
Андрій Вікторович Несвідомін, Віталій Миколайович Бабка,
Ірина Юріївна Грищенко**

Національний університет біоресурсів і природокористування України,
03041, вул. Героїв Оборони, 15, м. Київ, Україна

Переміщення частинки по похилому циліндру, що обертається навколо власної осі

Анотація. Загальновідомо, що частини сільськогосподарських машин часто мають циліндричну форму. Таку форму, наприклад, має кожух підйомно-транспортних машин, в якому обертається активний робочий орган. Крім того, у барабанних зерносушарках та трієрах використовується похилий циліндр, що обертається навколо власної осі. При цьому частинки технологічного матеріалу взаємодіють з обертовою поверхнею, що призводить до їх ковзання, характер якого залежить від величини кута нахилу циліндра. У даному дослідженні методами диференціальної геометрії, векторної алгебри, теоретичної механіки та чисельного інтегрування диференціальних рівнянь розглядається рух частинки по внутрішній поверхні похилого циліндра, що обертається з постійною кутовою швидкістю навколо власної осі. Для складання диференціальних рівнянь руху використано осі нерухомої системи координат. Встановлено, що належні вихідні умови, при яких частинка буде нерухомою на певній відстані від нижньої твірної циліндра в напрямі його обертання, можуть бути визначені аналітично. У випадку руху по похилому циліндру частинка рухається в тому числі в осьовому напрямі з одночасним зменшенням амплітуди коливань. Крім того, з'ясовано, що значну роль має кут нахилу циліндра. Якщо останній менше за кут тертя, то коливання припиняються, рух частинки стабілізується та вона здійснює прямолінійний рух зі сталою швидкістю в осьовому напрямі. Якщо кут нахилу циліндра більше або дорівнює куту тертя, то частинка рухається прискорено в осьовому напрямі та її рух не стабілізується. Також значну роль має величина кутової швидкості обертання. Певна її величина провокує «залипання» частинки, яке не залежить від кута нахилу циліндра. Отримані аналітичні залежності можуть бути використані при проектуванні циліндричних робочих органів сільськогосподарських машин

Ключові слова: поверхня, обертальний рух, ковзання, кутова швидкість, диференціальні рівняння, траєкторія

Machinery & Energetics
Vol. 13, No. 2. 2022

Journal homepage:
https://technicalscience.com.ua/en

UDC 622.23
DOI: 10.31548/machenergy.13(2).2022.41-49

Volodymyr Gritsyuk[1*], Igor Nevliudov[1], Mykola Zablodskiy[2], Periasami Subramanian[3]

[1]Kharkiv National University of Radio Electronics
61166, 14 Nauky Ave., Kharkiv, Ukraine

[2]National University of Life and Environmental Sciences of Ukraine
03041, 15 Heroiv Oborony, Kyiv, Ukraine

[3]Tamil Nadu Agricultural University
641003, Lawley Road, Coimbatore, India

Estimation of Eddy Currents and Power Losses in the Rotor of a Screw Electrothermomechanical Converter for Additive Manufacturing

Abstract. 3D printing technologies for large-scale structures allow architects and builders to considerably expand the design boundaries of structures and increase the efficiency of their construction. Mobile robotic platforms for 3D printing are increasingly being implemented in the construction sector, as well as in the production of road surfaces, allowing to solve the problem of limited working space. The typical design of the extruder assembly of a robotic platform for 3D printing large-scale structures can be improved by combining an electric motor, an auger extruder, and a heater in one housing. The proposed auger-type electrothermomechanical converter uses an external auger rotor, which simultaneously performs the functions of an asynchronous motor rotor, a heating element, an actuator, and a protective housing. The purpose of this study was to evaluate the efficiency of using an auger converter as part of a mobile robotic platform for additive manufacturing. For converters operating in difficult conditions, the use of field calculation methods is relevant. In this study, a field calculation was performed using the finite element method and the spatial distribution of eddy currents in the section of the hollow ferromagnetic rotor was found. Pictures of the three-dimensional distribution of the z-component, the normal component of the density of eddy currents, as well as the distribution of the dissipated power density, which considers all types of losses in the rotor, were obtained using the Comsol Multiphysics software and computing complex. The practical value of the obtained results lies in the possibility of predicting optimal indicators of the influence of the thermal regime on the material, as well as the speed of rotation of the converter rotor. This will determine the mechanical properties of the material at the output of the device

Keywords: 3D printing, mobile robotic platform, numerical calculation, external auger rotor, extruder assembly, power density

Article's History: Received: 16.12.2021; Revised: 09.03.2022; Accepted: 27.04.2022.

INTRODUCTION

3D printing is a trending technology of modern times, and its application is constantly growing, as it reduces the cost of production. Additive manufacturing provides unique advantages in creating complex structures that are in high demand in the aerospace industry [1], biomedicine [2; 3], automotive [4] and other areas [5; 6]. One of the problems with 3D printing is that typical desktop printers are stationary and have limited working space. Mobile platforms for 3D printing solve this problem, allowing to move without restrictions [7].

To increase the efficiency and cost-effectiveness of the mobile robotic platform for 3D printing technology of large-scale structures, it is proposed to improve the design of the extruder assembly by combining an electric motor, an auger extruder, and a heater in one housing. This will not only save weight and size, but also substantially increase the efficiency and reliability of the entire system.

Apart from the freedom of design, additive manufacturing has enormous potential in the construction industry, as well as in the production and repair of road surfaces. For example, researchers at the Massachusetts Institute of

Suggested Citation:
Gritsyuk V., Nevliudov I., Zablodskiy M., & Subramanian, P. (2022). Estimation of eddy currents and power losses in the rotor of a screw electrothermomechanical converter for additive manufacturing *Machinery & Energetics* 13(2), 41-49.

*Corresponding author

Technology in [8] presented a large-scale digital construction platform (DCP) for on-site sensing, analysis, and digital production. The second version of DCP used a tracked electric car as a platform and was used to extrude foam when pouring walls, which is similar to the block construction method. In [9], the authors developed a mobile printing system comprising two robotic manipulators on a mobile base that prints cement objects of a fairly large size. Researchers from the Institute of Advanced Architecture of Catalonia (IAAC) presented the idea of mobile 3D printing, where three separate systems are used to print architectural structures using cement [10].

According to the concept of "self-repairing cities" [11; 12], a fleet of autonomous vehicles and drones will scan roads for cracks and eliminate them before potholes appear. By detecting a crack in the road, a robot with a 3D printer will be able to place asphalt in the crack to repair it, all within a minute. This approach can be used at night to avoid road closures that can disrupt traffic. The device is based on the Mendel 90 desktop RepRap printer but is equipped with a special extruder and a nozzle made of high-temperature photopolymer. Printing is performed with bituminous crumb with millimetre-sized particles, which is poured into a hopper, heated, and pushed through a nozzle using an auger. The extruder assembly has an internal heating sleeve. The pellets soften as they pass through the auger, due to an increase in temperature under the action of heating resistors, which leads to the leakage of liquid bitumen from the nozzle, as demonstrated in Figure 1a. Stepper motors, temperature, gradient, and auger rotation speed are controlled by simple electronics connected to a PC (Fig. 1b). The improved mechanical properties are a function of temperature, which may be due to microstructural changes in asphalt. This leads to the formation of fibres that cover the cracks, which increases the impact strength. During experiments, the authors [11] found that a temperature between 125°C and 135°C is optimal for creating continuous asphalt extrusion with a constant line width.

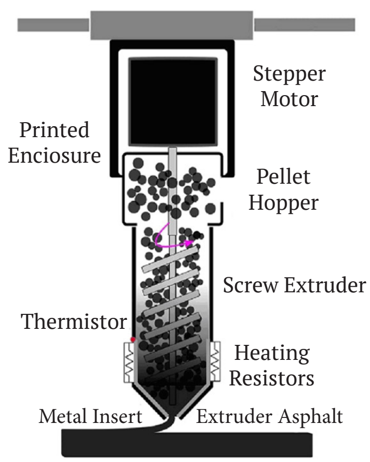

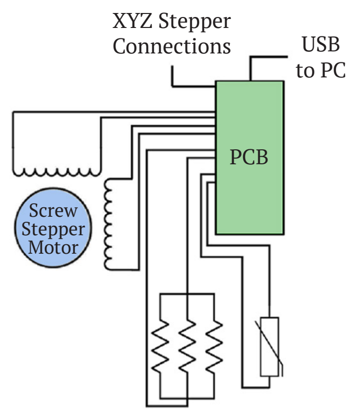

Figure 1. System design: extruder design (a), control electronics (b)

Source: [11]

The authors [11] believe that a fleet of autonomous vehicles will ensure the functioning of a new economic model underlying urban infrastructure that will help society. The improved and customisable properties of 3D-printed asphalt combined with the flexibility and efficiency of the platform will provide an advanced approach to the maintenance of urban infrastructure facilities.

Apart from roads, this will change the way hard-to-reach structures are repaired, such as flat roofs of buildings and other structures. The advantage of this method is not only the ability to reduce costs (other repair methods often require the construction of scaffolding and the closure or disconnection of infrastructure to gain access), but also the fact that repairs can be started earlier, before large-scale wear and tear occurs.

3D printing technology for large-scale structures can be improved by combining an electric motor, an auger extruder, and a heater in one housing. This will not only save weight and size, but also substantially increase the efficiency and reliability of the system due to functional integration and full use of the dissipative component of energy. The need for added heat sources will disappear, and the rotor-auger completely immersed in the material can transfer maximum thermal and mechanical energy to it.

The operability of the idea of combining an electric motor and a working body was demonstrated by the authors of the study [13], who showed the advantages of an energy-efficient industrial mixer for concrete production. The mixer is designed based on a synchronous electric motor with a massive rotor and permanent magnets. The mixing blades are installed directly on the shaft without gear transmission (Fig. 2). Devices of this design perform rotational and linear motion simultaneously and have a modular structure that can include any number of modules with a common three-phase winding [14-16]. As a rule, they are used for mixing and drilling [17; 18]; however, their potential applications range from machine tools to robotics and various devices used for assembly, gripping, moving, packing, shaking [15; 19].

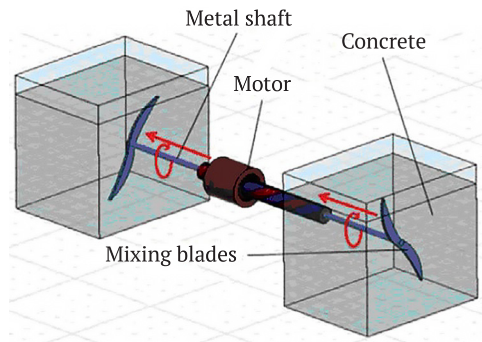

Figure 2. Design diagram of a permanent magnet motor

Source: [11]

For a clear comparison with the conventional electric motor used in industrial mixers, an asynchronous motor with equivalent mechanical power, rated rotational speed, and torque was chosen. The efficiency of a motor with a massive rotor and permanent magnets at full load is 94%, and the efficiency of an asynchronous motor is close to 87%.

The comparison is based on a paper presented at the conference on industrial and commercial energy use in 2013 [20]. Notably, the comparison of motors shown does not consider the heating losses of the massive rotor and stator, which should be used to heat and reduce the viscosity of the working medium [21; 22].

Therefore, to increase the efficiency, cost-effectiveness, and versatility of devices that provide transportation, mixing, pressing and heating operations, their use as links in the technological chain is important. As an alternative to the above approaches, a mobile robotic platform equipped with an auger-type electrothermomechanical converter (ETMC) is proposed. The proposed converter uses an external auger rotor, which simultaneously performs the functions of an asynchronous motor rotor, a heating element, an executive mechanism, and a protective housing (Fig. 3). Therefore, considering the "useful" losses of the electromagnetic system, the efficiency of electromechanical converters for technological purposes increases to 98-99% [23].

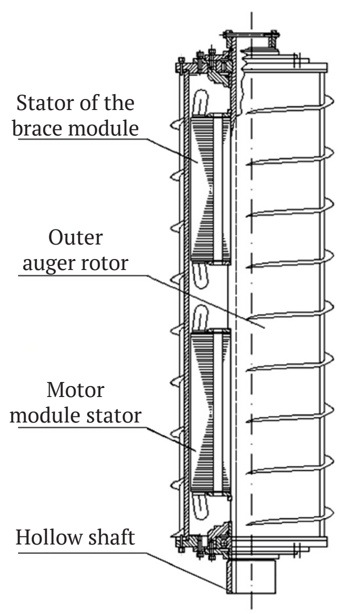

Figure 3. Design diagram of an auger-type ETMC

The auger-type ETMC uses the principle of self-regulation in energy conversion, according to which the distribution of thermal and mechanical energy into useful flows is carried out according to the value of the current slip, which depends on the ratio of electromagnetic moments of the engine and brake modules of the ETMC. When the stator winding of the motor module is connected to a voltage source, a rotating magnetic field is created, under the action of which eddy currents (EC) are induced in the adjacent zone of the external ferromagnetic rotor. As a result, an asynchronous electromagnetic moment is formed. The main mode can be considered the opposite direction of rotation of the fields, wherein the brake module works upon sliding $S_G>1$, i.e., in the mode of electromagnetic braking.

The study of the distribution of EC induced in electrically conductive media is of practical interest for a wide range of industrial applications. EC in vacuum chambers, cores of high-speed magnets and accelerating resonators cause many adverse effects. This primarily refers to heating the cores and electrically conductive structural elements and, accordingly, reducing the overall efficiency of the devices. At the same time, the assessment of the heat output that occurs in the conductors during the BC leak is important for various devices, such as induction furnaces, melting devices, soldering devices, etc. Especially relevant is the use of field calculation methods for electromechanical converters operating in difficult conditions. During the electromechanical conversion of energy into ETMC, a single physical force field occurs, the separate components of which are the fields of electromagnetic, thermal, and mechanical quantities.

Purpose of the study. For a preliminary assessment of the efficiency of using auger-type ETMCS as part of mobile robotic platforms for industrial 3D printing, it is necessary to analyse the distribution of EC in the ferromagnetic rotor as the main sources of heat generation. This will serve as important information for predicting the optimal temperature, gradient, and rotation speed of the auger extruder. In turn, these values will determine the mechanical properties of the material at the output of the device.

MATERIALS AND METHODS

When developing an auger-type ETMC, it is necessary to perform a quantitative analysis of the distribution of the EC density and the power density that is dissipated, to develop recommendations for choosing rational parameters and heating modes of the material. Conventional methods and approaches to calculating and analysing processes in ETMC, due to the specificity of functioning, do not provide the necessary reliability of the results. Methods that ensure high reliability of calculations are field and circle-field methods of analysis, which are invariant to the nature of electromagnetic connections of the object of research, consider the real geometry and properties of materials. Circle-field methods are used in the analysis of dynamic operating modes of electromechanical converters. The use of the field analysis method allows conducting refined studies of the parameters, characteristics, and operating modes of the ETMC, considering the design features and operating modes that do not lend themselves to reliable analysis by conventional, classical methods.

In the study of electromechanical converters, numerical methods for calculating the field are widely used, considering the features of the geometry and saturation of cores, among which the finite element method is particularly progressive. According to the finite element method, the study area is divided into sections. The solution of differential equations is reduced to solving a system of algebra equations that relate the values of the vector field potential at nodal points, obtained by dividing into sections. The method of conduction of toothed contours has become widespread, according to which the complete field of the machine is considered, taking into account its change in time during the mutual movement of the toothed cores. Electromagnetic processes are calculated by jointly solving a system of differential equations written in matrix form for the circuits of an electrical circuit that includes machine windings and external electrical circuits.

The highest accuracy of analysis is provided upon calculating a three-dimensional problem. This becomes possible when considering the majority of physical effects, which are more deeply manifested in conditions of full reproduction of the geometry of the device. The solution of a system of equations describing a three-dimensional electromagnetic and temperature field at any given time for any spatial point in the model can only be implemented by numerical methods. These methods are widely used in modern multiphysical modelling software packages Cedrat Flux, Comsol Multiphysics, Ansys, etc.

To fulfil this purpose, the mathematical model presented in [24; 25] was used. In this study, a three-dimensional modification of the finite-element model, implemented within the Comsol Multiphysics software and computing complex, has been implemented. Means of analysing the results of calculations of this particular complex allow obtaining comprehensive information about the processes that take place in the object under study. Therewith, Comsol Multiphysics is one of the most proven and affordable software products that implement the finite element method.

Calculation of the three-dimensional distribution of the EC was performed on the rotor section for the engine module of the experimental sample of the auger-type ETMC. The three-dimensional geometry of the model comprises the following design sections: a hollow external rotor, a toothed stator magnetic circuit, an air gap, and a stator winding. The angular velocity of the rotor is defined as the frequency of field sources according to the rotor coordinate system. The specific electrical conductivity of the rotor material was taken according to the reference data, considering the average temperature at the operating sliding of the engine module S=0.88. The nonlinearity of the magnetic properties of the massive rotor and stator core is considered by setting the corresponding magnetisation curves. Field sources are set by an extraneous current density in the sections of the stator grooves according to the three-phase winding connection scheme

RESULTS AND DISCUSSION

The result of solving the field problem in the form of a three-dimensional distribution of EC is presented in Figure 4. A single cross-section of a hollow rotor is given for a slip value of S=0.88 (n^2=90 rpm). The section is made in the "edge" zone of the hollow cylinder, and the value of the z-component of the density of the EC is determined by colouring it in different colours and intensities. The same figure shows the line along which the section of the rotor wall is made, presented in Figure 5.

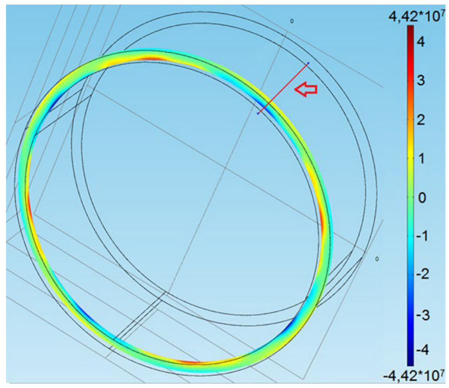

Figure 4. Distribution of the z-component of the EC density in the cross-section of the outer hollow rotor at S=0.88 (A/m^2)

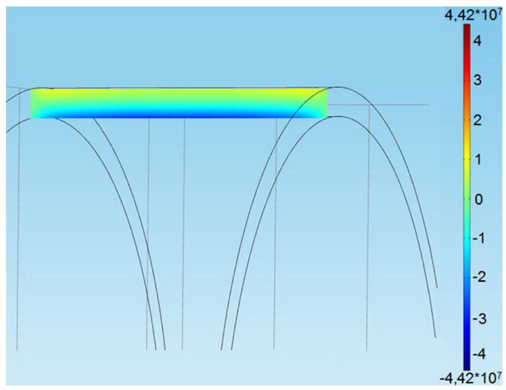

Figure 5. Distribution of the z-component of the EC density in the wall of the outer hollow rotor at S=0.88 (A/m^2)

The largest value of the normal component of the EC density slightly exceeds the maximum value (4.42 A/mm^2) of the z-component for S=0.88. On the three-dimensional picture of the distribution of the normal component (Fig. 6), internal areas of high density of EC are visible, which are conditioned upon the presence of the internal toothed-groove structure of the stator. That is, the main source of heat output is a layer of the inner surface of the rotor (4-5 mm), facing the source of the electromagnetic field.

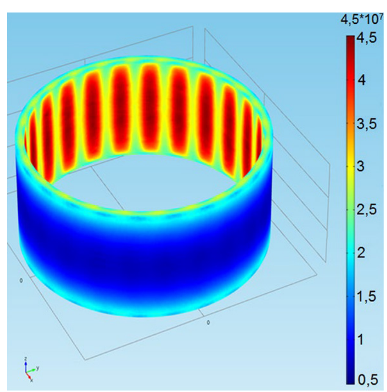

Figure 6. Distribution of the normal component of the EC density in the outer hollow rotor at S=0.88 (A/m^2)

The pattern of distribution of the dissipated power density, which considers all types of losses in the rotor, has a similar nature (Fig. 7). Preferably, the density of dissipated power on the outer surface of the rotor is within (10.5-20)·10^6 W/m^3. A considerable difference in the dissipated power density between the inner and outer surfaces of the rotor under operating conditions is not critical. The thermal energy of the rotor is actively transferred to the surrounding material, and the temperature gradient towards the cylinder wall thickness will stay small [22].

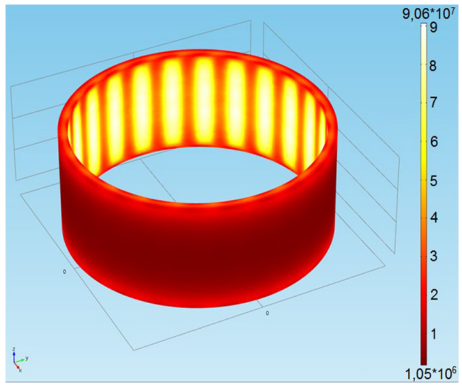

Figure 7. Distribution of the power density dissipated in the external hollow rotor at S=0.88 (W/m^3)

Note that the nature of the distribution of the dissipated power density in the rotor changes substantially with increasing field frequency, which affects the quality of thermal action on the material. This is conditioned upon a change in the configuration of the EC flow contours, probably due to a decrease in the depth of penetration of the electromagnetic field, as well as the influence of the edge effect.

The considerable scientific achievements of foreign authors in the field of research of electromagnetic and thermal processes in converters should be noted, which are the closest in terms of the ideology of creation. A sizeable number of publications investigate the physical fields in the core of electromechanical transducers with a ferromagnetic rotor using numerical methods. Thus, the authors of [26] performed a three-dimensional calculation of the finite element model of a rotational-linear converter, considering transients in the active part. The authors of studies [27-29] presented the analysis of the spiral motion engine using the method of Fourier series, which considers edge effects, the authors [30; 31] developed a technique for determining the parameters of the equivalent circuit of substitution, despite the small magnetisation inductance of the structure of the secondary conductive sleeve. In [32], a three-dimensional finite element analysis of a rotational linear motor is presented, which considers the longitudinal and transverse edge effects, the surface effect, and the influence of the thickness of the extreme sheets of a magnetic circuit. The study [33] contains simulation results for a two-module motor with an external rotor, namely the influence of the electric motor design on the torque and its pulsation is analysed. Calculations allow finding the electromechanical parameters for a particular engine that is being designed. In contrast to the above studies, this paper contains the results of calculating the three-dimensional distribution of eddy currents and the density of dissipated power, namely for an external ferromagnetic rotor. Furthermore, the calculation is performed considering the “useful” heat losses of the rotor used to heat the material. That is, the available electromechanical converters do not use the heating losses of the rotor and stator to heat and melt the working medium.

CONCLUSIONS

Additive manufacturing has enormous potential in the construction industry, as well as in the production and repair of road surfaces. Mobile platforms for 3D printing can solve the problem of limited workspace. To increase the efficiency and cost-effectiveness of the mobile robotic platform for 3D printing technology of large-scale structures, it is proposed to improve the design of the extruder assembly. This is achieved by combining an electric motor, auger extruder, and heater in one housing. This approach saves weight and size, as well as substantially increases the efficiency and reliability of the system due to functional integration and full use of the dissipative component of energy.

The proposed converter for a mobile robotics platform uses an external auger rotor, which simultaneously performs the functions of an asynchronous motor rotor, a heating element, an executive mechanism, and a protective housing. To pre-evaluate the efficiency of using an auger-type ETMC as part of a mobile robotic platform for industrial 3D printing, a finite element calculation of the spatial distribution of the EC in the hollow rotor section was performed for the motor module of an experimental sample of an auger-type ETMC. Estimating the levels of dissipated power density on the rotor surface allows discussing the prospects of the proposed approach for optimising the design of the extruder assembly of a mobile robotic platform for industrial 3D printing. The results of the spatial distribution of the rotor EC will allow improving the design of the ETMC, to ensure the set values of temperature and gradient, which determine the mechanical properties of the material at the output of the device.

Further research in this area should be a physical experiment, as well as a detailed analysis of the spatial configuration of contours B due to the direct impact on the quality of heat treatment of the material.

REFERENCES

[1] Katz-Demyanetz, A., Popov, V.V.Jr, Kovalevsky, A., Safranchik, D., & Koptyug, A. (2019). Powder-bed additive manufacturing for aerospace application: Techniques, metallic and metal/ceramic composite materials and trends. *Manufacturing Revew*, 6, article number 5.

[2] Yuk, H., Lu, B., Qu, K., Xu, J., Zhao, X., Lin, S., & Luo, J. (2020). 3D printing of conducting polymers. *Nature Communications*, 11, article number 1604. doi: 10.1038/s41467-020-15316-7.

[3] Birbara, N.S., Otton, J.M., & Pather, N. (2017). 3D modelling and printing technology to produce patient-specific 3D models. *Heart Lung Circulation*, 28(2), 302-313. doi: 10.1016/j.hlc.2017.10.017.

[4] Jankovics, D. (2019).Customization of automotive structural components using additive manufacturing and topology optimization. *IFAC-PapersOnLine*, 52(10), 212-217. doi: 10.1016/j.ifacol.2019.10.066.

[5] Kolomiets, A., Grobman, Y.J., Popov, Jr.V.V., Strokin, E., Senchikhin, G., & Tarazi, E. (2020). The titanium 3D printed flute: New prospects of additive manufacturing for musical wind instruments design. *Journal of New Music Research*, 50(1), 1-17. doi: 10.1080/09298215.2020.1824240.

[6] Wohlers, T.T., Campbell, I., Diegel, O., Huff, R., & Kowen, J. (2021). *Wohlers report 2020: 3D printing and additive manufacturing state of the industry*. Fort Collins: Wohlers Associates.

[7] Sauter, A., Nasirov, A., Fidan, I., Allen, M., Elliott, A., Cossette, M., & Singer, T. (2021). Development, implementation and optimization of a mobile 3D printing platform. *Progress in Additive Manufacturing*, 6(2), 231-241. doi: 10.1007/s40964-020-00154-2.

[8] Keating, S, Spielberg, N.A., Klein, J, & Oxman, N. (2014). A compound arm approach. In *Robotic Fabrication in Architecture* (pp. 99-110). Dordrecht: Springer. doi: 10.1007/978-3-319-04663-1_7.

[9] Efe Tiryaki, M., Zhang, X., & Pham, Q.C. (2018). Printing-while-moving: A new paradigm for large-scale robotic 3D Printing. *IEEE International Workshop on Intelligent Robots and Systems*, 4, 2286-2291. doi: 10.1109/IROS40897.2019.8967524.

[10] Hall, N. (2016). *IAAC Minibuilders small robots with big ambitions. 3D Print Ind, WA*. Retrieved from https://3dprintingindustry.com/news/iaac-minibuilders-small-robots-big-ambitions-83257/.

[11] Jackson, R.J., Wojcik, A., & Miodownik, M. (2018). 3D printing of asphalt and its effect on mechanical properties. *Materials & Design*, 160, 468-474. doi: 10.1016/j.matdes.2018.09.030.

[12] Johansson, A. (2016). *3D printing robot may be the solution to potholes, PSFK*. Retrieved from https://www.psfk.com/print-post?format=pdf&id=322046.

[13] Dobzhanskyi, O., Amiri, E., & Gouws, R. (2016). Comparison analysis of electric motors with two degrees of mechanical freedom: PM synchronous motor vs induction motor. In *II International Young Scientists Forum on Applied Physics and Engineering* (pp. 14-17). Kharkiv: Kharkiv National Agrarian University named after V.V. Dokuchaiev. doi: 10.1109/YSF.2016.7753750.

[14] Alwash, J.H., & Qaseer L.J. (2010). Three-dimension finite element analysis of a helical motion induction motor. *ACES*, 25(8), 703-712.

[15] Bolognesi, P. (2010). A novel rotary-linear permanent magnets synchronous machine using common active parts. In *15th IEEE Mediterranean Electrotechnical Conference* (pp. 1179-1183). Valletta: The University of Malta. doi: 10.1109/MELCON.2010.5476370.

[16] Bentia, I., & Szabo, L. (2010). Rotary-linear machines – A survey. *Journal of Computer Science and Control Systems*, 3, 11-14.

[17] Zhao, J., Liu, X., Xin, Z. & Han, Y. (2009). Research on the energy-saving technology of concrete mixer trucks. In *4th IEEE Conference on Industrial Electronics and Applications* (pp. 3551-3554). Xi'an: Xi'an University of Science and Technology.

[18] Szczygieł, M., & Kluszczyński, K. (2016). Rotary-linear induction motor based on the standard 3-phase squirrel cage induction motor – constructional and technological features. *Czasopismo Techniczne. Elektrotechnika*, 1, 395-406. doi: 10.4467/2353737XCT.15.059.3859.

[19] Bolognesi, P., Bruno, O., Landi, A., Sani, L., & Taponecco L. (2004). Electromagnetic actuators featuring multiple degrees of freedom: A survey. In *16th International Conference on Electrical Machines – ICEM 2004* (pp. 1-6). Cracow: Cracow University of Technology.

[20] Dobzhanskyi, O., & Gouws, R. (2017). 3-D Finite element method analysis of twin-armature permanent magnet motor with two degrees of mechanical freedom. *Springer Electrical Engineering*, 99(3), 997-1004.

[21] Zablodskiy, M., Zhiltsov, A., Kondratenko, I., & Gritsyuk, V. (2017). Conception of efficiency of heat electromechanical complex as hybrid system. Electrical and Computer Engineering (UKRCON). In *2017 IEEE First Ukraine Conference* (pp. 399-404). Kyiv: Taras Shevchenko National University of Kyiv. doi: 10.1109/UKRCON.2017.8100519.

[22] Zablodskiy, N., Pliugin, V., & Gritsyuk, V. (2014). Submersible electromechanical transformers for energy efficient technologies of oil extraction. *Progressive Technologies of Coal, Coalbed Methane, and Ores Mining*, 9, 223-227.

[23] Zablodskii, N.N., Plyugin, V.E., Gritsyuk, V.Y., & Grin, G.M. (2016). Polyfunctional electromechanical energy transformers for technological purposes. *Russian Electrical Engineering*, 87, 140-144. doi: 10.3103/S1068371216030123.

[24] Zablodskiy, M., Gritsyuk, V., Rudnev, Y., & Brozhko, R. (2019). Three-dimensional electromagnetic field model of an auger electromechanical converter with an external solid rotor. *Mining of Mineral Deposits*, 13(4), 99-106. doi: 10.33271/mining13.04.099.

[25] Zablodskiy, M., Gritsyuk, V., Rudnev, Y., Brozhko, R., & Tymofieieva, O. (2020). Analysis of 3D eddy current distribution in a hollow rotor of an electromechanical converter. In *IEEE 40th International Conference on Electronics and Nanotechnology* (pp. 561-564). Kyiv: Taras Shevchenko National University of Kyiv. doi: 10.1109/ELNANO50318.2020.9088777.

[26] Amiri, E. (2014). Circuit modeling of double-armature rotary-linear induction motor. In *IECON 2014-40th annual conference of the IEEE industrial electronics society* (pp. 431-436). Dallas: Dallas Theological Seminary.

[27] Mendrela, E.A., & Turowski, J. (1978). Rotary-linear induction motor. In *IEEE winter power meeting* (article number A78091-1). New York: Columbia University.

[28] Fleszar, J., & Mendrela, E.A. (1983). Twin-armature rotarylinear induction motor. *IEE Proceedings B (Electric Power Applications)*, 130(3), 186-192.
[29] Mendrela, E.A., & Geirczak, E. (1987). Double-winding rotary-linear induction motors. *IEEE Transactions on Energy Conversion*, EC–2(1), 48-54.
[30] Cathey, J.J. (1985). Helical motion induction motor. *Proceedings of the Institution of Electrical Engineers*, 132(2), 112-114.
[31] Rabiee, M., & Cathey, J.J. (1988). Verification of a field theory analysis applied to a helical motion induction motors. *IEEE Transactions on Magnetics*, 24(4), 127-138.
[32] Alwash, J.H., & Qaseer, L.J. (2010). Three-dimension finite element analysis of a helical motion induction motor. *Applied Computational Electromagnetics Society Journal*, 25(8), 703-712.
[33] Łukaniszyn, M., Kowol M., & Kołodziej, J. (2010). Performance analysis of a two-module reluctance motor with an axial flux. *Computer Applications in Electrical Engineering*, 8, 72-80.

СПИСОК ВИКОРИСТАНИХ ДЖЕРЕЛ

[1] Powder-bed additive manufacturing for aerospace application: Techniques, metallic and metal/ceramic composite materials and trends / A. Katz-Demyanetz et al. *Manufacturing Revew*. 2019. Vol. 6. Article number 5.
[2] 3D printing of conducting polymers / H. Yuk et al. *Natural Communication*. 2020. Vol. 11. Article number 1604. doi: 10.1038/s41467-020-15316-7.
[3] Birbara N.S., Otton J.M., Pather N. 3D modelling and printing technology to produce patient-specific 3D models. *Heart Lung Circulation*. 2019. Vol. 28, No. 2. P. 302–313. doi: 10.1016/j.hlc.2017.10.017.
[4] Jankovics D. Customization of automotive structural components using additive manufacturing and topology optimization. *IFAC-PapersOnLine*. 2019. Vol. 52, No 10. P. 212–217. doi: 10.1016/j.ifacol.2019.10.066.
[5] The titanium 3D printed flute: New prospects of additive manufacturing for musical wind instruments design / A. Kolomiets et al. *Journal of New Music Research*. 2020. Vol. 50, No. 1. P. 1–17. doi: 10.1080/09298215.2020.1824240.
[6] Wohlers report 2020: 3D printing and additive manufacturing state of the industry / T.T. Wohlers et al. Fort Collins: Wohlers Associates, 2021. 374 p.
[7] Development, implementation and optimization of a mobile 3D printing platform / A. Sauter et al. *Progress in additive manufacturing*. 2021. Vol. 6, No. 2. P. 231–241. doi: 10.1007/s40964-020-00154-2.
[8] Keating S, Spielberg N.A., Klein J, Oxman N. A compound arm approach. *Robotic Fabrication in Architecture*. Dordrecht: Springer, 2014. P. 99–110. doi: 10.1007/978-3-319-04663-1_7.
[9] Efe Tiryaki M., Zhang X., Pham Q.C. Printing-while-moving: A new paradigm for large-scale robotic 3D Printing. *IEEE International Workshop on Intelligent Robots and Systems*. 2018. Vol. 4. P. 2286–2291. doi: 10.1109/IROS40897.2019.8967524.
[10] Hall N. IAAC Minibuilders small robots with big ambitions. 3D Print Ind, WA. URL: https://3dprintingindustry.com/news/iaac-minibuilders-small-robots-big-ambitions-83257/.
[11] Jackson R.J., Wojcik A., Miodownik M. 3D printing of asphalt and its effect on mechanical properties. *Materials & Design*. 2018. Vol. 160. P. 468–474. doi: 10.1016/j.matdes.2018.09.030.
[12] Johansson A. 3D printing robot may be the solution to potholes, PSFK. URL: https://www.psfk.com/print-post?format=pdf&id=322046.
[13] Dobzhanskyi O., Amiri E., Gouws R. Comparison analysis of electric motors with two degrees of mechanical freedom: PM synchronous motor vs induction motor. *II international young scientists forum on applied physics and engineering* (Kharkiv, 10-14 Oct. 2016). Kharkiv, 2016. P. 14–17. doi: 10.1109/YSF.2016.7753750.
[14] Alwash J.H., Qaseer L.J. Three-dimension finite element analysis of a helical motion induction motor. *ACES*. 2010. Vol. 25, No 8. P. 703–712.
[15] Bolognesi P. A novel rotary-linear permanent magnets synchronous machine using common active parts. *15th IEEE Mediterranean Electrotechnical Conference*. (Valletta, 26–28 April 2010). Valletta, 2010. P. 1179–1183. doi: 10.1109/MELCON.2010.5476370.
[16] Bentia I., Szabo L. Rotary-linear machines – A survey. *Journal of Computer Science and Control Systems*. 2010. Vol. 3. P. 11–14.
[17] Zhao J., Liu X., Xin Z., Han Y. Research on the energy-saving technology of concrete mixer trucks. *4th IEEE Conference on Industrial Electronics and Applications*. (Xi'an, 25-27 May 2009). Xi'an, 2009. P. 3551–3554.
[18] Szczygieł M., Kluszczyński K. Rotary-linear induction motor based on the standard 3-phase squirrel cage induction motor – constructional and technological features. *Czasopismo Techniczne. Elektrotechnika*. 2016. Vol. 1. 395–406. doi: 10.4467/2353737XCT.15.059.3859.
[19] Electromagnetic actuators featuring multiple degrees of freedom: A survey / P. Bolognesi et al. *16th International Conference on Electrical Machines – ICEM 2004*. (Cracow, 20–25 May 2004). Cracow, 2004. P. 1–6.
[20] Dobzhanskyi O., Gouws R. 3-D Finite element method analysis of twin-armature permanent magnet motor with two degrees of mechanical freedom. *Springer Electrical Engineering*. 2017. Vol. 99, No. 3. P. 997–1004.
[21] Zablodskiy M., Zhiltsov A., Kondratenko I., Gritsyuk V. Conception of efficiency of heat electromechanical complex as hybrid system. Electrical and Computer Engineering (UKRCON). *2017 IEEE First Ukraine Conference*. (Kyiv, 29 May–2 June 2017). Kyiv, 2017. P. 399–404. doi: 10.1109/UKRCON.2017.8100519.

[22] Zablodskiy N., Pliugin V., Gritsyuk V. Submersible electromechanical transformers for energy efficient technologies of oil extraction. *Progressive Technologies of Coal, Coalbed Methane, and Ores Mining*. 2014. Vol. 9. P. 223–227.
[23] Zablodskii N.N., Plyugin V.E., Gritsyuk V.Y., Grin G.M. Polyfunctional electromechanical energy transformers for technological purposes. *Russian Electrical Engineering*. 2016. Vol. 87. P. 140–144. doi: 10.3103/S1068371216030123.
[24] Zablodskiy M., Gritsyuk V., Rudnev Y., Brozhko R. Three-dimensional electromagnetic field model of an auger electromechanical converter with an external solid rotor. *Mining of Mineral Deposits*. 2019. Vol. 13, No. 4. P. 99–106. doi: 10.33271/mining13.04.099.
[25] Analysis of 3D eddy current distribution in a hollow rotor of an electromechanical converter / M. Zablodskiy et al. *IEEE 40th International Conference on Electronics and Nanotechnology*. (Kyiv, 22–24 April 2020). Kyiv, 2020. P. 561–564. doi: 10.1109/ELNANO50318.2020.9088777.
[26] Amiri E. Circuit modeling of double-armature rotary-linear induction motor. *IECON 2014–40th Annual Conference of the IEEE Industrial Electronics Society* (Dallas, 29 Oct.–1 Nov. 2017). Dallas, 2014. C. 431–436.
[27] Mendrela E.A., Turowski J. Rotary-linear induction motor. *IEEE winter power meeting* (New York, 29 Jan–3 Feb. 1978). New York, 1978. Article number A78091-1.
[28] Fleszar J., Mendrela E.A. Twin-armature rotarylinear induction motor. *IEEE proceedings B (electric power applications)*. 1983. Vol. 130, No. 3. P. 186–192.
[29] Mendrela E.A., Geirczak E. Double-winding rotary-linear induction motors. *IEEE transactions on energy conversion*. 1987. Vol. EC–2, No. 1. P. 48–54.
[30] Cathey J.J. Helical motion induction motor. *Proceedings of the Institution of Electrical Engineers*. 1985. Vol. 132, No. 2. P. 112–114.
[31] Rabiee M., Cathey J.J. Verification of a field theory analysis applied to a helical motion induction motors. *IEEE transactions on magnetics*. 1988. Vol. 24, No. 4. P. 127–138.
[32] Alwash J.H., Qaseer L.J. Three-dimension finite element analysis of a helical motion induction motor. *Applied Computational Electromagnetics Society Journal*. 2010. Vol. 25, No. 8. P. 703–712.
[33] Łukaniszyn M., Kowol M., Kołodziej J. Performance analysis of a two-module reluctance motor with an axial flux. *Computer Applications in Electrical Engineering*. 2010. Vol. 8. P. 72–80.

Володимир Юрійович Грицюк[1], Ігор Шакирович Невлюдов[1], Микола Миколайович Заблодський[2], Періасамі Субраманіан[3]

[1]Харківський національний університет радіоелектроніки
61166, просп. Науки, 14, м. Харків, Україна

[2]Національний університет біоресурсів і природокористування України
03041, вул. Героїв Оборони, 15, м. Київ, Україна

[3]Державний аграрний університет Таміл Наду
641003, Лоулі Роуд, м. Коімбатур, Індія

Оцінка вихрових струмів і втрат потужності у роторі шнекового електротепломеханічного перетворювача для адитивного виробництва

Анотація. Технології 3D-друку великомасштабних структур дозволяють архітекторам і будівельникам значно розширити межі проектування конструкцій та підвищити ефективність їх будівництва. Мобільні робототехнічні платформи для 3D-друку все частіше впроваджуються в будівельній сфері, а також при виробництві дорожніх покриттів, дозволяючи вирішити проблему обмеженого робочого простору. Типова конструкція вузла екструдера робототехнічної платформи для 3D-друку великомасштабних структур може бути вдосконалена шляхом об'єднання електродвигуна, шнекового екструдера та нагрівача в одному корпусі. Пропонований шнековий електротепломеханічний перетворювач використовує зовнішній ротор-шнек, який одночасно виконує функції ротора асинхронного двигуна, нагрівального елемента, виконавчого механізму і захисного корпусу. Метою статті є оцінка ефективності використання шнекового перетворювача у складі мобільної робототехнічної платформи для адитивного виробництва. Для перетворювачів, які функціонують в складних умовах, актуальним є застосування польових методів розрахунку. В роботі проведено польовий розрахунок методом кінцевих елементів та визначено просторовий розподіл вихрових струмів на ділянці порожнистого феромагнітного ротора. Із використанням програмно-обчислювального комплексу Comsol Multiphysics отримано картини тривимірного розподілу z-складової, нормальної складової густини вихрових струмів, а також розподілу густини дисипованої потужності, що враховує всі види втрат в роторі. Практичне значення отриманих результатів полягає в можливості прогнозування оптимальних показників впливу теплового режиму на матеріал, а також швидкості обертання ротора перетворювача. Це в свою чергу, буде визначати механічні властивості матеріалу на виході пристрою

Ключові слова: 3D-друк, мобільна робототехнічна платформа, чисельний розрахунок, зовнішній шнековий ротор, вузол екструдера, густина потужності

Machinery & Energetics
Vol. 13, No. 2. 2022

Journal homepage:
https://technicalscience.com.ua/en

UDC 620.92(477)
DOI: 10.31548/machenergy.13(2).2022.50-61

Volodymyr Danylyshyn*, Mariia Koval

Technical and Economic Vocational College of the Lviv Polytechnic National University
79038, 87 Pasichna Str., Lviv, Ukraine

Development of Alternative Energy in the World and Ukraine

Abstract. The relevance of this study is conditioned upon the wide spread of alternative energy sources around the world and in Ukraine, as well as the need for theoretical development and practical implementation of modern methods for establishing non-standard energy mechanisms in Ukraine and in the world. The main purpose of this study was to analyse key trends in the development of alternative energy in Ukraine and the world in the current socio-economic conditions. The methodological approach in this paper was based on a combination of quantitative and qualitative methods of research on issues related to the analysis of key growth vectors of non-standard methods of energy production in modern conditions. During this study, results were obtained that indicate the existence of a clearly structured interrelation between the degree of development of alternative energy sources and the types of fuel used in them, including the presence of prospects for the development of alternative energy sources in the conditions of modern Ukraine, provided the high-quality investment support for projects that are being implemented for the development of alternative energy. The results obtained in this study, as well as the conclusions formulated on their basis, are of significant practical importance for various branches of Ukrainian and world industry, the real technological capabilities of which allow the use of renewable energy sources for their ability to meet the life needs of all types of industrial enterprises, for their further full functioning and solving any technological problems facing these enterprises

Keywords: green energy, biofuels, renewable energy sources, energy consumption, economic development, environmental problems

Article's History: Received: 08.11.2021; Revised: 03.03.2022; Accepted: 27.04.2022.

INTRODUCTION

Every year, "green" energy supplies an increasing part of the energy needs of the world's leading economies. At present, a new paradigm of world energy is being the developed, which entails the decisive contribution of renewable energy sources (RES) to the total energy consumption and the gradual displacement of conventional fossil energy resources. The category of non-conventional renewable energy sources (NRES), which are often called alternative, includes sources that have not yet become widespread in Ukraine and provide constant energy recovery due to natural processes. These are sources associated with natural processes in the lithosphere (geothermal energy), in the hydrosphere (diverse types of water energy), in the atmosphere (wind energy), in the biosphere (biomass energy), and in outer space (solar energy) [1].

The possibility of successful implementation and development of any technological innovation is determined mainly by a combination of several interrelated factors – these are real needs and opportunities to fully meet them. The energy-related issues only confirm the specified regularity. The situation on the global energy market is characterised by a gradual reduction of conventional energy resources, which indicates the need to find real alternatives, while the development of technological solutions contributes to the search for certain ways of using non-conventional raw materials for the production of energy that would be suitable for use. As a rule, this process involves certain costs for adapting equipment or transport to use this energy. However, the scale of production and use of alternative energy is not sufficient for full-scale replacement of conventional energy sources; qualitative characteristics of non-conventional energy sources also restrain this process [2]. At the same time, great attention should be paid to the quality of biofuel produced to meet the needs of non-conventional energy sources and their high-quality functioning, sufficient satisfaction of real economic needs.

There are many real problems of implementing alternative energy sources in various countries to meet the needs of industry and the residential sector. The expansion of the use of renewable sources of electric energy becomes possible due to significant technological advance in this area, which allowed reducing the cost of electricity production

Suggested Citation:
Danylyshyn, V., & Koval, M. (2022). Development of alternative energy in the world and Ukraine. *Machinery & Energetics* 13(2), 50-61.

*Corresponding author

by wind and solar power plants of diverse types [3]. Global trends in the spread of alternative energy sources are based on numerous advantages of energy of this kind, namely considerably lower cost of obtaining alternative energy, practicality in using alternative energy generation plants, as well as relative ease of installation of power generation plants. Therewith, the environmental friendliness of alternative energy sources and the absence of harmful emissions into the environment during their use are not the least important. Together, these factors necessitate the development of specific measures to expand the practice of using renewable energy sources in various industries of modern developed countries of the world. In this context, the growth of investment in the development of renewable energy sources in the world is of primary importance. In almost any country, especially in countries with unstable economic conditions, the energy complex exists thanks to investment. An important role in the financing of RES projects is played by the so-called "clean energy funds", as well as modern development banks (namely, the European Investment Bank, the Brazilian BNDES bank, etc.), as well as crowdfunding formations (e.g., the largest crowdfunding platform for RES is the WindCentrale, located in the Netherlands) [3; 4]. This study aims to investigate the main prospects for the development of alternative energy in the world and in Ukraine, considering the investment allocated for the development of RES and with an assessment of the prospects for the development of RES in Ukraine and the world.

MATERIALS AND METHODS

The methodological approach in this paper was based on a combination of quantitative and qualitative methods of research on issues related to the analysis of key growth vectors of non-standard methods of energy production in modern conditions. During this study, key trends in the development of alternative energy in the world and in Ukraine were evaluated, with the provision of a classification of RES. The RES were classified using the system of ideas that has developed to date on the volume of use of alternative energy obtained from various sources, for which the method of comparative data analysis was used.

The conducted quantitative study includes the investigation of a considerable amount of data from several Ukrainian and foreign sources, containing the results of developments of modern authors who have studied numerous issues related to the introduction of alternative energy sources in various industries and in the domestic sphere. The obtained data created a basis for further analysis, with the identification of key growth patterns of non-standard methods of energy production in Ukraine and the world. The study was accompanied by the provision of significant amounts of graphical and statistical information presented in the corresponding tables. This contributed to the objective presentation of research data and obtaining results that efficiently reflect the issues under study [5]. The qualitative method of scientific research involves a systematic analysis of all gathered scientific information to build a clear, structured picture of the presented information. This makes provision for the analysis of information presented in the form of diagrams reflecting the main stages of research with the results obtained, which allows drawing systematic conclusions about the key growth trends of non-standard methods of energy production in modern Ukraine and in the world. Thus, the structural interrelationship of qualitative and quantitative methods of scientific research used in the analysis of the development of alternative energy sources allows forming a clear picture of the work performed on the data obtained during research, as well as to form objective conclusions based on them [6].

The methodology of this study makes provision for the breakdown of the results of scientific research into certain sections corresponding to specific stages of scientific research. Thus, the entire sequence of studies performed was presented as an accurate system for displaying the data obtained. Various aspects of the development of alternative energy complexes in the world and in Ukraine were highlighted, including the dynamics of investment injections in the development of alternative energy, including key aspects of biofuel production for alternative power plants and facilities. Such a model of constructing the methodology of scientific research can be effectively used in the future to conduct further scientific developments in the field of analysing the prospects for the development of RES in the world and in Ukraine.

RESULTS

1. Trends in the development of alternative energy in the world and Ukraine

Currently, non-conventional and renewable energy sources have become essential criteria for economic development and energy security of the world community. The search for new and improvement of existing technologies, their modernisation to a cost-effective level and expansion of application areas is constantly being carried out. The use of renewable energy sources is due to many factors, the main ones being as follows:

– preventing energy instability in countries and reducing dependence on energy imports;

– considerable amount of harmful emissions into the environment from the operation of conventional energy sources and the need to reduce them;

– saving and increasing energy reserves.

Hydroelectric power plants, geothermal, solar, thermal energy, energy from heat pumps, etc. should be considered renewable energy sources [7] (Fig. 1).

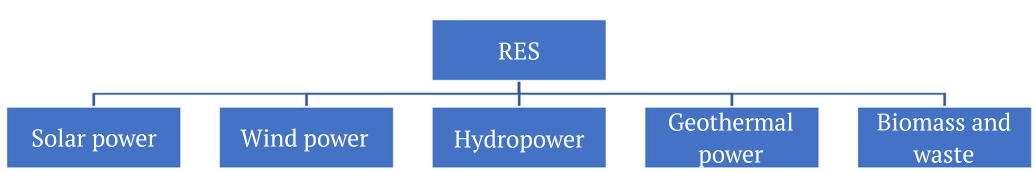

Figure 1. Classification of renewable energy sources

The RES share in the world's energy production is increasing every year, and their potential is several times higher than the level of global consumption of fuel and energy resources. The growth rate of energy production from non-conventional sources is also considerably higher than that of conventional types of energy. The rapid development of alternative energy is largely due to lower prices for equipment for solar and wind power plants, and a variety of biomass processing plants. The finding of significant amounts of investment infusions and, instead, the rapid development of alternative energy under the condition of a considerable decrease in the cost of the main energy carriers proves the need to gradually start the practice of using alternative energy sources in the world. The average annual investment growth in 2004-2016 was 12.5%. The absolute record was set in 2015, when the volume of investment in renewable energy sources amounted to 349 billion dollars at a time when world oil prices were almost at a historic low [8] (Fig. 2).

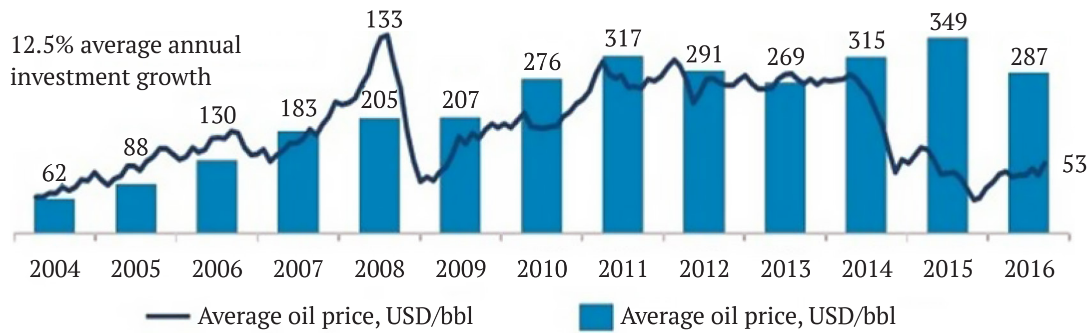

Figure 2. Dynamics of investment in renewable energy in the world

The contribution of renewable energy sources to the world's gross final energy consumption is about 18%, including biomass – 14%, or 76% of the total contribution of non-conventional energy sources (Fig. 3).

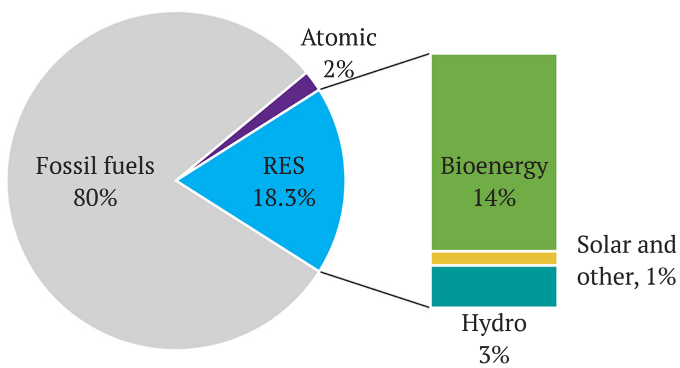

Figure 3. Structure of gross energy consumption in the world

The economic downturn in Ukraine in previous years was accompanied by high inflation and the crisis of the banking system, which created unfavourable conditions for the development of renewable energy in Ukraine. The economic situation in Ukraine has somewhat stabilised recently, and therefore the capacity of RES in Ukraine is growing every year (the decline in 2014 was associated with the loss of energy facilities in the Crimea and the ATO zone) [9] (Fig. 4).

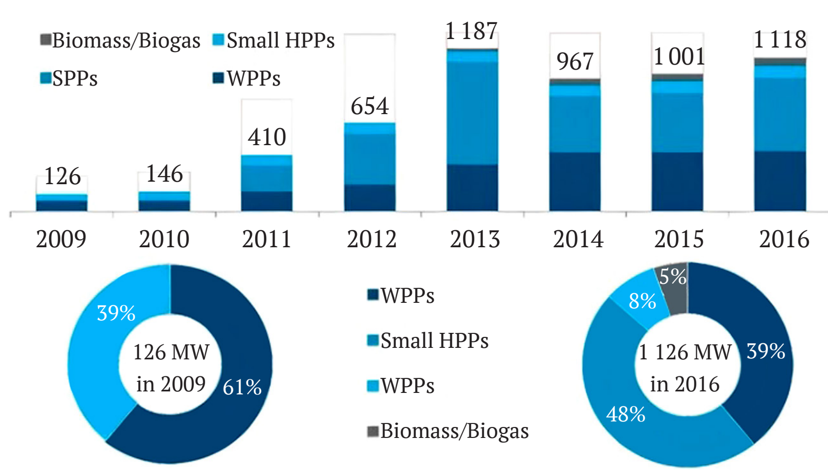

Figure 4. Capacity of renewable energy facilities in Ukraine

The average annual capacity parameter of RES in Ukraine is 31%. As of 01.01.2017, the capacity of alternative energy facilities operating in Ukraine under the "green tariff" was 1,117.7 MW. Bioenergy is one of the key RES sectors in Ukraine and the world.

2. Prospects for the development of bioenergy in Ukraine. Bioenergy is the production of energy from biomass of diverse types. Biomass is organic substances of plant (wood, straw, tree leaves, energy crops, and other plant residues of agricultural production) and animal (manure) origin. At present, technologies for processing biological raw materials are widely used to solve the problems of safe disposal of organic waste, reduce environmental pollution, and obtain alternative energy. The main trend of bioenergy lies in the search for the most effective technologies for the processing of organic waste with the utilisation of biomass due to methane fermentation with the production of biogas. For Ukraine, the use of biofuels is an effective way to get rid of external energy dependence (Fig. 5).

The main components of biomass potential in Ukraine are agricultural processing waste (straw, stems, leaves, manure, etc.) and energy crops (Table 1) [10].

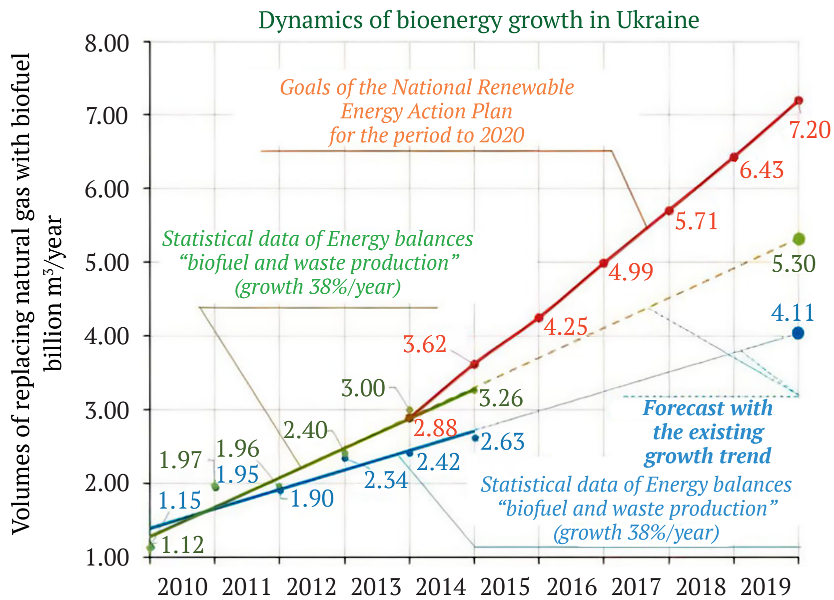

Figure 5. Growth dynamics of the bioenergy sector in Ukraine

Table 1. Energy potential of biomass in Ukraine

Type of biomass	Theoretical potential, million tonnes	Share available for energy, %	Economic potential, million tonnes of conventional fuel
Grain straw	35.1	30	5.22
Rapeseed straw	3.1	40	0.62
By-products of corn production for grain (stems, rods)	30.3	40	3.31
Sunflower by-products (stems, baskets)	21.2	40	1.74
Secondary agricultural waste (husk, pulp)	6.6	47	0.53
Wood biomass (firewood, felling residues, woodworking waste)	6.0	94	1.98
Wood biomass (dead wood, wood from forest belts, pruning of orchards and vineyards)	11.0	58	2.57
Biodiesel (from rapeseed)	–	–	0.27
Grain straw	36.2	35	6.77
Rapeseed straw	3.2	40	0.58
Corn production waste	32.4	35	3.45
Sunflower production waste	20.5	40	1.75
Secondary type waste	6.5	45	0.46
Wood biomass (firewood, felling residues, woodworking waste)	5.8	90	1.86
Wood biomass (dead wood, wood from forest belts, pruning of orchards and vineyards)	10.3	65	3.32
Biodiesel (rapeseed)	–	–	0.21
Bioethanol (corn and sugar beet)	–	–	0.63
Biogas from agricultural waste	1.4 billion m³	55	0.74
Biogas from landfills of household waste	0.4 billion m³	30	0.17

Table 1, Continued

Type of biomass	Theoretical potential, million tonnes	Share available for energy, %	Economic potential, million tonnes of conventional fuel
Industrial and municipal wastewater biogas	1.0 billion m^3	25	0.22
Energy crops:			
Poplar, willow, silvergrass	12.6	85	5.76
Peat	–	–	0.55
Corn (biogas)	2.8 billion m^3	85	2.89
Total	–	–	29.36

Source: [11]

Currently, Ukraine substantially falls behind European countries in the pace of bioenergy development. The percentage of biomass in total primary energy production in the state today is 1.2 %, and in gross current energy consumption – 1.78 %. Every year in Ukraine, about 2 million tonnes of biomass of various types are used for energy production. Therewith, the main contribution is made by wood – its share in the structure of annual biomass consumption is almost 80%. The energy potential of grain straw, fallen leaves, and rapeseed waste is least actively realised [12]. The main ways of obtaining energy from biomass are anaerobic fermentation, fermentation, combustion, hydrolysis, dry distillation, and gasification. The most promising and easy-to-use method is anaerobic fermentation, which produces biogas, and organic waste is a valuable biofertiliser when growing plants in agriculture. An analytical review of the literature sources suggests that biogas obtained during anaerobic fermentation of organic waste with the ability to recover is a highly efficient, non-conventional, and alternative energy source.

3. Anaerobic fermentation in biogas production.
The technology of biogas production is relatively simple, energy-saving, economically feasible, and environmentally friendly. In organic waste, under certain conditions, biochemical processes called anaerobic fermentation (fermentation) begin. As a result of these processes, not only biogas is obtained, but also valuable concentrated organic fertilisers.

The main sources of biomass used for the production of biogas are as follows: 1) crop production: grass, straw, fallen leaves, organic waste from agricultural processing; 2) animal husbandry: cattle, pig breeding, poultry farming; 3) solid waste landfills; 4) wastewater treatment.

If necessary, the fermentation material should be conditionally divided into the main (the fermentation of which occurs without the inclusion of auxiliary components) and additional. The key fermentation material is manure, young grass, and waste from industrial fruit processing, organic waste, food residues, fats, molasses, organic products that decompose naturally (biologically), household waste, etc., play an additional role. The yield of biogas, depending on the type of substrate, is presented in Tables 2-7.

Table 2. Biogas yield (substrate-silage and energy crops)

Substrate	Dry matter, %	Organic dry matter, %	Biogas output m^3/t	Methane CH_4 %
Clover silage (1st mowing, beginning of flowering)	35.0	88.6	185.1	55.1
Corn silage	33.0	95.8	185.3	52.2
Grass silage	40.0	89.2	208.3	54.1
Millet, waxy ripeness phase	35.0	88.5	162.7	53.0
Sugar beet leaf silage	18.0	80.5	88.2	54.4
Grain silage (whole plant), full grain	42.0	94.2	214.1	52.1
Wheat silage (whole plant)	40.0	93.6	187.7	52.4
Red clover silage (1st mowing)	30.0	87.0	140.1	55.3

Source: [11]

Table 3. Biogas yield (substrate – root crops, grain, seeds)

Substrate	Dry matter, %	Organic dry matter, %	Biogas output m^3/t	Methane CH_4 %
Double row barley	87.0	97.2	578.5	52.7
Dry corn	87.0	98.3	590.3	52.8
Oats	87.0	96.7	501.1	54.1
Beet and molasses chips	89.6	92.0	569.0	51.9
Fresh sugar beet	23.0	91.9	147.1	50.8
Rye	87.0	97.8	597.0	52.0
Sunflower	88.0	96.6	594.5	63.5
Wheat	87.0	98.1	598.2	52.8
Peas	87.0	96.3	581.4	55.0
Rapeseed	88.0	95.5	644.5	65.7
Potato starch	83.6	99.5	605.6	50.0
Fresh potatoes	26.0	93.4	177.1	51.4

Source: [11]

Table 4. Biogas yield (substrate-vegetable crops)

Substrate	Dry matter, %	Organic dry matter, %	Biogas output m^3/t	Methane CH_4 %
Vegetable waste	15.0	76.0	57.0	56.0
Onions	9.6	94.0	80.3	65.0
Onion peel	82.4	67.0	267.8	65.0
Carrot	11.9	88.3	73.3	52.0
Cauliflower	9.6	92.7	59.2	56.0
Fresh pumpkin	8.4	91.5	50.9	55.8

Source: [11]

Table 5. Biogas yield (substrate – fat, oil)

Substrate	Dry substances, %	Dry organic substances, %	Biogas output m^3/t	Methane CH_4 %
Fat	95.0	92.0	874.0	68.0
Glycerin	100.0	99.5	845.7	50.0
Linseed oil	99.9	99.9	1222.6	68.0
Rapeseed oil	99.9	99.9	1197.6	68.0
Soybean oil	99.9	99.9	1222.6	68.0
Sunflower oil	99.9	99.9	1222.6	68.0

Source: [11]

Table 6. Biogas yield (substrate – livestock waste)

Substrate	Dry matter, %	Organic dry matter, %	Biogas output m^3/t	Methane CH_4 %
Liquid pig manure	6.0	85.0	20.4	60.0
Pig manure with bedding	22.5	82.5	74.3	60.0
Liquid manure of fattening cattle	10.0	85.0	34.0	55.0
Fresh cow manure	25.0	80.0	90.0	50.0
Dairy cow manure	8.5	85.0	20.2	55.0
Manure of dairy cows with feeding residues	8.5	85.0	25.3	55.0
Horse manure	28.0	75.0	63.0	55.0
Chicken faeces, dry	40.0	75.0	80.0	55.0
Fresh chicken faeces	15.0	75.0	100.0	65.0

Source: [11]

Table 7. Biogas yield (substrate – food industry waste)

Substrate	Dry matter, %	Organic dry matter, %	Biogas output m^3/t	Methane CH_4 %
Soybean husk	90.0	95.1	516.7	52.7
Potato spent wash, fresh	6.0	86.7	35.0	56.3
Oat flakes	91.0	98.1	619.7	53.5
Brewer's spent grain	24.0	95.5	122.2	59.3
Bran	89.0	86.5	262.4	50.7
Apple pulp	22.0	97.6	111.6	51.7
Soy flour	87.0	93.3	551.6	61.2
Wheat spent wash, liquid	6.0	94.0	36.1	58.9
Corn gluten	90.5	97.9	597.1	66.0
Lactose	100.0	99.7	756.0	50.0
Whole cow's milk	13.5	94.7	114.9	62.8
Brewer's yeast, boiled	10.0	91.8	60.7	62.1
Old bread	65.0	97.2	482.0	52.8
Bakery waste	87.7	97.1	650.6	52.8
Cheese factory waste	79.3	94.0	673.8	67.5
Low-fat, wet food waste	14.4	81.5	75.4	59.8
High-fat food waste	18.0	92.3	126.5	62.0
Various food wastes	40.0	50.0	120.0	60.0

Source: [11]

Having analysed the tables, it can be concluded that the main sources of biogas production are products and waste from crop and animal husbandry. As a result of the analysis of the literature review, it was established that due attention was not paid to the processing of waste of plant origin, namely the disposal of fallen leaves and dry grass.

I believe that the use of fallen leaves is a promising direction for the production of biogas [13].

Anaerobic fermentation for the production of biogas is a complex biotechnological process, which for the effective course of methane fermentation of organic substances requires the interaction and fulfilment of the following conditions: the appropriate temperature regime of the process, a slightly alkaline reaction of the medium, the presence of methane-forming bacteria, an oxygen-free environment. Anaerobic fermentation in a bioreactor is a complex process that is influenced by external and internal factors (Fig. 6).

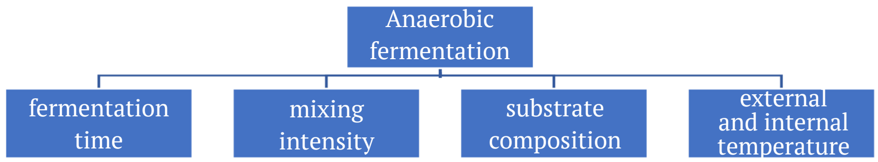

Figure 6. The main factors affecting the fermentation

One of the key factors of an effective fermentation process is the temperature regime of the fermenting biomass. In natural conditions, the production of biogas takes place at temperatures from 0°C to 97°C, but taking into account the process of optimizing the processing of organic waste for the production of biogas and biofertilisers, three temperature modes are distinguished: psychophilic temperature regime (20-25°C); mesophilic temperature regime (25-40°C); thermophilic temperature regime (more than 40°C) [11; 14; 15] (Table 8).

Table 8. C/N ratio of organic waste that can be raw material for obtaining biogas

Raw materials for biogas	Nitrogen, %	Carbon-nitrogen ratio, C/N
	Animal manure	
Cattle	1.7-1.8	16.6...25
Chicken	3.7... 6.3	7.3... 9.65
Horse	2.3	25
Pork	3.8	6.2... 12.5
Sheep's	3.8	33
	Farm waste	
Faeces	6...7.1	6...10
Kitchen waste	1.9	28.60
Potato skins	1.5	25
Cabbage	3.6	12.5
Tomatoes	3.3	12.5
	Plant dry waste	
Corn cobs	1.2	56.6
Grain straw	1.0	49.9
Wheat straw	0.5	100...150
Corn straw	0.8	50
Oat straw	N/A	50
Soybean	1.3	33
Alfalfa	2.8	16.6...17
Beet pulp	0.3...0.4	140...150
Other		
Grass	4	12
Sawdust	0.1	200...500
Fallen leaves	1.0	50

Source: [11]

Certain small particles, namely sand, clay, etc., collectively lead to the occurrence of sediment. In this case, the lightest materials end up on the surface of the raw material and create a hard film on its surface. This reduces gas formation, which is why plant residues should be thoroughly mixed before loading into the reactor: straw, grass, leaves, etc.

The humidity index of raw materials that appears in the reactor of the plant should not exceed 85% in winter and 92% in summer. To obtain the optimal humidity of raw materials, it is mixed with hot water in a volume determined by Formula (1):

$$OV = LF((B2 - B1) : (100 - B2)) \quad (1)$$

where LF is the amount of manure loaded, $B1$ is the primary humidity of manure, $B2$ is the expected humidity of raw materials, and OV is the total volume of water in litres.

The analysis of scientific and technical literature allowed determining the main conditions affecting the biogas production process, which requires improving the quality of equipment used to obtain the highest yield of biogas and improving the economic efficiency of converting biomass into organic fertilisers [16].

The process of processing organic substances into biogas is called methane fermentation. Its essence lies in anaerobic fermentation, which occurs due to the decomposition of biomass by bacteria (methanogens). There are 4 groups of bacteria involved in the formation of biogas. The metabolic products of each group of bacteria serve as nutrients for the next group. Bacteria of the first group convert organic compounds (protein, carbohydrates, fats) using enzymes into low-molecular compounds (amino acids, fatty acids, water). Next, acid-forming bacteria convert the above-mentioned low-molecular compounds into unstable fatty acids (acetic, formic, propionic), ethanol, carbon, and gases (carbon dioxide, hydrogen, hydrogen sulphide and ammonia). Water-producing bacteria handle converting higher fatty acids into vinegar and formic acids, carbon dioxide, and hydrogen. Microorganisms of the fourth group (methane-forming) process vinegar and formic acids into methane [17]. The process of anaerobic fermentation is accompanied by several biochemical reactions, and the process of biogas formation itself comprises three stages:

Stage I – hydrolysis – the decomposition of organic mass (2):

$$(C_6H_{10}O_5)n + nH_2O = nC_6H_{12}O_6; \qquad (2)$$

Stage II – acetonogenesis – the reproduction of acid-forming bacteria (3):

$$6H_{12}O_6 + 2CH_0O = 2CH_3COOH + 4H_2 + 2CO_2, \qquad (3)$$

Stage III – methanogenesis – the reproduction of methane-forming bacteria (4):

$$CH_0COOH = CH_4 + CO_2, 4H_2 + CO_2 = CH_4 + 2H_2O. \qquad (4)$$

At the end of the process, thanks to bacteria capable of creating methane, methane, carbon dioxide and water appear from acetic and formic acids, carbon, and hydrogen. At the same time, 90% of the total volume of methane must be produced at this stage, and 70% of methane is produced using acetic acid. Methane-forming bacteria are completely anaerobic [18-20].

Thus, the process of anaerobic fermentation is influenced by four factors:

– biological: the composition of the fermented mass, the composition of the microflora, the living conditions of organisms;

– physical: fermentation temperature, pressure in the biogas plant, hydraulic mode;

– chemical: concentration, acidity of the medium, volume and composition of the resulting biogas;

– organisational and technological: volume of loading biomass, residual substances.

Consequently, the nature and quality of the course of biochemical reactions largely determine the final quality of the resulting biofuel, which affects the efficiency of its further use.

DISCUSSION

It should be clearly understood that 80% of all energy produced on Earth is obtained by burning something, mainly minerals. And they, according to various estimates of scientists, will not last long: oil for 30-50 years, gas for 50-70 years, coal for about 300 years. Admittedly, considering the constant development of mining technologies, these figures can be extended for several more decades, and in the case of coal, possibly for several hundred. Innovative technologies in energy production will also reduce resource costs. New deposits are found or data on old ones are updated, revealing that the new reserves are slightly higher than previously estimated. But still, this will not solve the problem of depletion of the Earth's interior and environmental pollution. A lot of work needs to be done to avoid an energy crisis. And big steps have already been taken towards a new era [21].

In connection with the approaching threat of depletion of global hydrocarbon reserves, the international expert society declared bioenergy as the main trend in the development of the fuel market, which should become the foundation of the beginning of a new era of energy. In the next 30-40 years, it is bioenergy that will dominate the development of the global energy supply system [22]. The use of biofuels from renewable raw materials can reduce the consumption of oil resources, improve fuel performance, reduce environmental pollution and solve the problem of greenhouse gas emissions. Today, biofuel has substantial advantages over other types of conventional fuel. These include the possibility of obtaining biofuels by processing plant products, which does not adversely impact the structural and chemical composition of soils in crop rotation systems, as well as considerably lower carbon dioxide emissions into the environment than from conventional types of fuels. Furthermore, biofuels practically do not contain sulphur, which distinguishes them favourably from mineral-type analogues, and there is no harm from biofuels when they get to various biological objects, which also distinguishes biofuels from motor fuel. In general, biofuels are subject to complete biological decomposition, which determines their complete environmental friendliness and safety of use compared to motor fuels.

There are considerable differences in the characteristics of biofuel preparation compared to conventional hydrogen liquid fuels, and the same can be said about the composition of these two types of fuels. Therefore, a crucial task is to identify the influence of the properties of biofuels on the final performance of the engines in which it is used (operational, economic, environmental). Furthermore, when preparing biofuels, the stages of its production should be considered, from loading raw materials to obtaining the end product. In this context, the development of biofuel production in any state, high-quality and consistent management of all such processes should be considered as the primary goal of national and international cooperation in the field of energy globalisation, involving all the potential opportunities of different countries. Renewable energy fuel production programmes are often considered as preparing the economy for a possible long-term shortage of hydrocarbons. The development of fuel production from renewable energy sources is determined by the tasks of Sustainable Rural Development – biologisation and greening of agricultural production, consolidation of the rural population and preservation of the rural lifestyle, including by stimulating the production of agricultural products for non-production purposes [23].

The effective fermentation in the bioreactor occurs thanks to maintaining a constant temperature in strict accordance with the established mode of anaerobic fermentation: mesophilic or thermophilic and regular mixing of biomass. Thermophilic bacteria do not have considerably higher productivity compared to mesophilic ones. This circumstance determines the fact that with the same volume of biogas production per day, fermentation tanks hold much less. At the same time, considering the need to support a higher parameter of the fermentation mass temperature, the total heat energy consumption during the implementation of thermophilic processes increases substantially. Due to the low ambient temperature and poor insulation of the tank, a lot of thermal energy is consumed, so biogas is not enough to heat the fermentation mass. That is why, in the climatic conditions of Eastern and Western Europe, the work of fermentation chambers is mostly carried out in the mesophilic range of temperatures. The thermophilic fermentation process has many advantages, which include a significant rate of decomposition of raw materials, a very high yield of biogas, and almost complete destruction of pathogenic bacteria present in the raw material. The disadvantages of thermophilic decomposition are a substantial amount of energy allocated for the preparation of raw materials in the reactor, high sensitivity of the fermentation process at all stages to the slightest fluctuations in temperature changes, as well as poor quality of final biological fertilisers. During the application of the mesophilic fermentation regime, it is possible to preserve the substantial amino acid composition of biological fertilisers; therewith, the period of anaerobic fermentation increases considerably.

A mandatory factor in ensuring the high-quality flow of biochemical processes in the methane tank is a slightly alkaline fermentation reaction, while the 6-8 pH is considered satisfactory (the optimal value is set as 7-7.5 pH). A highly alkaline reaction leads to the undesirable appearance of hydrogen sulphide. In an environment of increased acidity (during fermentation of household waste, pig excrement), methane fermentation can be stopped in the absence of biogas release. One can set the real level of acid-alkaline balance with litmus paper. Its value will correspond to the colour that the paper acquires when it is immersed in fermentation raw materials. Another important factor affecting methane fermentation is the concentration of carbon and nitrogen in raw materials. If the C/N ratio is significant enough, then insufficient nitrogen will be a factor that can considerably limit the entire course of methane fermentation. If the specified concentration is insignificant, then a significant amount of ammonia is formed, which becomes toxic to bacteria. Numerous scientific experiments suggest that the highest yield of biogas when the ratio of carbon and nitrogen is reached in the range of 10-20, the optimal value may be due to the final type of raw material. To achieve high-quality biogas, it is necessary to mix raw materials until the desired C/N ratio is obtained. For the growth and vital activity of methane bacteria, the presence of organic and mineral nutrients in raw materials is necessary. The composition of carbon and hydrogen, the formation of biological fertilisers, requires a large amount of nitrogen, sulphur, phosphorus, potassium, calcium and magnesium, as well as certain trace elements – iron, manganese, molybdenum, zinc, cobalt, nickel, etc. Organic raw materials, namely animal manure, contain a sufficient amount of the above-mentioned elements [18; 20]. High-quality metabolism in raw materials is a mandatory factor for increased bacterial motility. This can only be achieved if the viscosity of the raw material is sufficient for the free movement of bacteria and gas bubbles between the liquid and the solids present in the raw material.

At the initial stage of anaerobic fermentation, hydrolysed bacteria decompose high-molecular compounds with the involvement of enzymes into low-molecular formations. Polymers (the formation of many molecules) gradually become one-dimensional (individual molecules). This process, called hydrolysis, proceeds slowly and is caused by the presence of extracellular enzymes, namely amylases, proteases, lipases, etc. The hydrolysis process will be affected by the pH level and time spent in the bioreactor.

At the stage of acetogenesis, acid-forming bacteria are engaged in uncoupling. This stage of methane fermentation is called the “oxidation phase”, in which the pH level decreases. Some molecules end up in bacterial cells, where their breakdown continues [22]. This process also involves aerobic bacteria that need oxygen residues, while creating the necessary anaerobic conditions for methane bacteria, and partially anaerobic bacteria. At this stage, unstable fatty acids (acetic, formic, butyric, propionic), low-molecular alcohols (ethanol, methanol), carbon and gases – carbon dioxide, hydrogen, hydrogen sulphide and ammonia – are produced. Next, water-producing bacteria from organic fatty acids form products to produce methane: acetic and formic acids, carbon dioxide, hydrogen. Microorganisms that reduce the volume of carbon (in the composition of organic acids) are extremely sensitive to changes in temperature conditions.

To date, many developed countries have already appreciated the great prospects that open up in obtaining motor fuel produced from renewable raw materials [22]. The result was an increase in the share of the United States, as well as several European Union states, in the world production of biotechnological products, which largely determined the prospects for the development of alternative energy in these countries. The relevance of the energy issue for the countries taking part in the global energy market is explained by its tension today and even more so in the future. Scientists find new ways of obtaining energy and improving already known extraction methods, politicians develop strategic plans for the large-scale implementation of achievements, economists calculate the effectiveness of projects and measures to save energy and increase energy efficiency, ecologists determine the ecological effect of preserving the share of natural renewable resources and reducing the level of environmental pollution environment In this case, all subjects interact in a certain way [18]. The effectiveness of the mechanism of this interaction obviously affects the quality of results and the speed of their achievement.

There are about several dozen countries in the world whose share of renewable energy sources in the total energy balance exceeds 25 % [24]. Among them are such countries as Iceland, Norway, Scotland, Denmark, Germany, and some other countries. According to the energy strategy adopted in the European Commonwealth, by 2020, the member states of this Commonwealth should ensure a 20% reduction in greenhouse gas emissions, an increase in the share of renewable energy to 20% and a 20% increase in energy efficiency. In the longer term, many countries will go much further. In particular, Germany plans to achieve a 60% share of renewable energy sources in the country's total energy balance and 80% in electricity production by 2050. The development of the modern renewable energy sector is taking place in the context of crisis phenomena in the global economy, although today this energy is one of the main ways to overcome the current economic crisis. Since 2015, wind power has occupied one of the leading positions in terms of capacity and volume of use of wind turbines in the world, which largely determined the possibilities of developing wind energy in the long term. Furthermore, the considerable growth rate of RES production was largely conditioned upon the massive support from the state. It allows some individual countries to produce and implement renewable energy, even in cases where key economic indicators are more than 50% worse than when using minerals and fuel resources.

CONCLUSIONS

Having analysed the energy potential of biomass in Ukraine, the main sources of biogas production are the products and wastes of plant and animal husbandry. As a result of the analysis of the literature review, it was established that the problems of the rational use of livestock waste were considered in many scientific papers. Along with this, due attention is not paid to the processing of waste of plant origin, namely the disposal of fallen leaves and dry grass. According to the authors, the use of fallen leaves is a promising area, and the raw material base itself is not sufficiently involved.

In the autumn, an environmental problem in the cities of Ukraine is the disposal of fallen leaves. The most common methods of disposal of fallen leaves in Ukraine are, at best, removal to landfills of solid household waste; in the worst-case scenario, it is incineration, which leads to atmospheric pollution and is prohibited by law. Removal of leaves to landfills requires significant costs, and upon incineration, harmful substances are released (nitrogen oxide, carbon monoxide, benzopyrene and formaldehydes, etc.). Therefore, the most appropriate solution to the problem of disposing of fallen leaves is biological destruction under anaerobic conditions. This method of disposal of fallen leaves is not only ecological, but also economically viable, since biogas produced during methane fermentation can be used as an alternative source of energy, and fermentation waste can be used as a valuable biological fertiliser.

The analysis of scientific and technical literature allowed finding the main factors influencing the anaerobic fermentation in the production of biogas from fallen leaves, which requires technological improvement of equipment to ensure maximum biogas yield and justify the economic efficiency of processing organic waste into biogas and organic fertilisers. Having considered modern designs of gas bioreactors, it can be concluded that the main criteria for choosing a methane tank for the disposal of fallen leaves are the possibility of its practical use, economic feasibility, and convenience of its maintenance upon operation. For obtaining biogas from fallen leaves, the most optimal design is an egg-shaped bioreactor. Its shape allows reducing hydraulic resistance upon mixing raw materials and avoiding stagnant zones due to the lack of corners in its design. To achieve high efficiency of the bioreactor and obtain the maximum amount of biogas per unit volume of biomass (fallen leaves), it is necessary to create optimal technological parameters in the bioreactor. Their formation is affected by the mixing and heating system of the substrate. When choosing a mixing system, it is necessary to consider its effect on the rate of methane formation and the fermentation time of biomass in the methane tank. An important aspect of the stability of the thermal regime in methane tanks is the heating of biomass and simultaneous thermal insulation of the bioreactor walls to reduce the impact of ambient temperature fluctuations.

REFERENCES

[1] Shishkina, I.A. (2012). Objective necessity of development of alternative energy in the world energy market. *Topical Issues of Economic Sciences*, 8, 36-43.

[2] Sheina, S.G., & Pirozhkova, A.P. (2021). Trends in the development of alternative energy in the world and Russia. *Engineering Bulletin*, 3, 1-12.

[3] Pankratieva, S.G., Rizak, E.V., & Chervyakova, M.V. (2021). Development of alternative energy in the world and in Russia, renewable energy sources and its role in providing consumers with energy. *Regional Economics and Management: Electronic Scientific Journal*, 4, 1-8.

[4] Bukarov, N.V., Vasilenko, V.V., & Pirozhnikova, A.P. (2019). Analysis of global investment in renewable energy. *Innovation and Investment*, 2, 12-15.

[5] Osina, A.V. (2018). Alternative energy sources. *International Journal of Applied Sciences and Technologies "Integral"*, 2, 102-105.
[6] Solodova, N.L., & Terentyeva, N.A. (2020). A little about biofuels. *Bulletin of Kazan University of Technology*, 7, 348-357.
[7] Pozubenkova, E.I., & Fomenko, O.V. (2017). Biofuel production management. *Nikon Readings*, 3, 26-27.
[8] Chebotariova, G.S., Strelkovskiy, V.A., & Blaginin, V.A. (2019). Renewable energy market: Development and profitability of companies. *The Manager*, 3(10), 58-69.
[9] Sorensen, S.B. (2017). *Renewable energy: Physics, engineering, environmental impacts, economics and planning*. London: Academic Press.
[10] Jones, L.E. (2017). *Renewable energy integration: Practical management of variability, uncertainty, and flexibility in power grids*. London: Academic Press.
[11] Shukla, V., & Kumar, N. (2020). *Environmental concerns and sustainable development. Volume 1: Air, water and energy resources*. Singapore: Springer.
[12] Sari, M.M., Temizel, C., Canbaz, C.H., Saputelli, L.A., & Torsaeter, O. (2021). *Sustainable materials for transitional and alternative energy*. Houston: Gulf Professional Publishing.
[13] Letcher, T. (2022). *Comprehensive renewable energy*. Oxford: Elsevier.
[14] Da Rosa, A.V., & Ordonez, J.C. (2021). *Fundamentals of renewable energy processes*. London: Academic Press.
[15] Jurasz, J., & Beluco, A. (2022). *Complementarity of variable renewable energy sources: A foundation for efficient grid integration*. London: Academic Press.
[16] Azar, A.T., & Kamal, N.A. (2021). *Design, analysis and applications of renewable energy systems*. London: Academic Press.
[17] Redko, A., Redko, O., & DiPippo, R. (2019). *Low-temperature energy systems with applications of renewable energy*. London: Academic Press.
[18] Raikar, S., Adamson, S. (2021). *Renewable energy finance*. London: Academic Press.
[19] Nguyen, K.H., & Kakinaka, M. (2019). Renewable energy consumption, carbon emissions, and development stages: Some evidence from panel cointegration analysis. *Renewable Energy*, 132, 1049-1057. doi: 10.1016/j.renene.2018.08.069.
[20] Child, M., Kemfert, C., Bogdanov, D., & Breyer, C. (2019). Flexible electricity generation, grid exchange and storage for the transition to a 100 % renewable energy system in Europe. *Renewable Energy*, 139, 80-101. doi: 10.1016/j.renene.2019.02.077.
[21] Scarlat, N., Dallemand, J.F., & Fahl, F. (2018). Biogas: Developments and perspectives in Europe. *Renewable Energy*, 129, 457-472. doi: 10.1016/j.renene.2018.03.006.
[22] Abedini, A., Amiri, H., & Karimi, K. (2020). Efficient biobutanol production from potato peel wastes by separate and simultaneous inhibitors removal and pretreatment. *Renewable Energy*, 160, 269-277. doi: 10.1016/j.renene.2020.06.112.
[23] Li, J., Zhao, R., Xu, Y., Wu, X., Bean, S.R., & Wang, D. (2022). Fuel ethanol production from starchy grain and other crops: An overview on feedstocks, affecting factors, and technical advances. *Renewable Energy*, 188, 223-239. doi: 10.1016/j.renene.2022.02.038.
[24] Bobyr, S. (2021). Theoretical Aspects of Hydrogen Diffusion in Metals. *Scientific Herald of Uzhhorod University. Series "Physics"*, (50), 31-38.

СПИСОК ВИКОРИСТАНИХ ДЖЕРЕЛ

[1] Шишкіна І. Об'єктивна необхідність розвитку альтернативної енергетики на світовому енергетичному ринку. *Актуальні питання економічних наук*. 2012. № 8. С. 36–43.
[2] Шеїна С.Г., Пірожкова А.П. Тенденції розвитку альтернативної енергетики у країнах світу. *Інженерний вісник Дона*. 2016. № 3. С. 1–12.
[3] Панкратьева С.Г., Різак Є.В., Червякова М.В. Розвиток альтернативної енергетики у світі та у Росії, відновлювані джерела енергії та його роль забезпеченні споживачів енергією. *Регіональна економіка та управління: електронний науковий журнал*. 2021. № 4. С. 1–8.
[4] Букаров Н.В., Василенко В.В., Пірожнікова А.П. Аналіз світових інвестицій у відновлювану енергетику. *Інновації та інвестиції*. 2019. № 11. С. 12–15.
[5] Осіна А.В. Альтернативні джерела енергії. *Міжнародний журнал прикладних наук та технологій «Integral»*. 2018. № 2. С. 102–105.
[6] Солодова Н.Л., Терентьєва Н.А. Трохи про біопаливи. *Вісник Казанського технологічного університету*. 2020. № 7. С. 348–357.
[7] Позубенкова Е.І., Фоменко О.В. Управління виробництвом біопалива. *Никоновські читання*. 2017. № 3. С. 26–27.
[8] Чеботарьова Г.С., Стрєлковський В.А., Благінін В.А. Ринок відновлюваної енергетики: розвиток та прибутковість компаній. *Керівник*. 2019. № 3. С. 58–69.
[9] Sorensen B. Renewable energy. London: Academic Press, 2017. 1056 p.
[10] Jones L. Renewable energy integration. London: Academic Press, 2017. 474 p.
[11] Shukla V., Kumar N. Environmental concerns and sustainable development. Volume 1: Air, water and energy resources. Singapore: Springer, 2020. 351 p.

[12] Sustainable materials for transitional and alternative energy / M.M. Sari et al. Houston: Gulf Professional Publishing, 2021. 242 p.
[13] Letcher T. Comprehensive renewable energy. Oxford: Elsevier, 2022. 4422 p.
[14] Da Rosa A., Ordonez J. Fundamentals of renewable energy processes. London: Academic Press, 2021. 924 p.
[15] Jurasz J., Beluco A. Complementarity of variable renewable energy sources. London: Academic Press, 2022. 720 p.
[16] Azar A., Kamal N. Renewable energy systems. London: Academic Press, 2021. 732 p.
[17] Redko A., Redko O., DiPippo R. Low-temperature energy systems with applications of renewable energy. London: Academic Press, 2021. 394 p.
[18] Raikar S., Adamson S. Renewable energy finance. London: Academic Press, 2021. 298 p.
[19] Nguyen K.H., Kakinaka M. Renewable energy consumption, carbon emissions, and development stages: Some evidence from panel cointegration analysis. *Renewable Energy*. 2019. No. 132. P. 1049–1057.
[20] Child M., Kemfet C., Bogdanov D., Breyer C. Flexible electricity generation, grid exchange and storage for the transition to a 100 % renewable energy system in Europe. *Renewable Energy*. 2019. No. 139. P. 80–101.
[21] Scarlat N., Dallermant J-F., Fahl F. Biogas: Developments and perspectives in Europe. *Renewable Energy*. 2018. No. 127. P. 457–472.
[22] Abedini A., Amiri H., Karimi K. Efficient biobutanol production from potato peel wastes by separate and simultaneous inhibitors removal and pre-treatment. *Renewable Energy*. 2020. No. 160. P. 269–277.
[23] Fuel ethanol production from starchy grain and other crops: An overview on feedstocks, affecting factors, and technical advances / J. Li et al. *Renewable Energy*. 2022. No. 188. P. 223–239.
[24] Bobyr, S. (2021). Theoretical Aspects of Hydrogen Diffusion in Metals. *Scientific Herald of Uzhhorod University. Series "Physics"*. 2021. Vol 50. P. 31-38.

Володимир Іванович Данилишин, Марія Орестівна Коваль

Техніко-економічний фаховий коледж Національного університету «Львівська політехніка»
79038, вул. Пасічна, 87, м. Львів, Україна

Розвиток альтернативної енергетики у світі та Україні

Анотація. Актуальність наукового дослідження зумовлена широким поширенням практики застосування установок альтернативної енергетики у масштабах усього світу загалом та України зокрема, а також необхідністю теоретичної розробки та практичного впровадження сучасних методик налагодження механізмів нестандартної енергетики в Україні та в світі. Головною метою цього дослідження є аналіз ключових тенденцій розвитку альтернативної енергетики в Україні та світі у сформованих на сьогоднішній день соціально-економічних умовах. Основу методологічного підходу у цій науково-дослідній роботі становить поєднання кількісного та якісного методів досліджень питань, пов'язаних з аналізом ключових напрямів росту нестандартних методів отримання енергії у сучасних умовах. У ході виконання даної науково-дослідної роботи було отримано результати, що свідчать про наявність чітко структурованого взаємозв'язку між ступенем розвитку альтернативних джерел енергії та типами використовуваного в них палива, а також про наявність значних перспектив розвитку альтернативних джерел енергії в умовах сучасної України за умови якісного інвестиційного забезпечення проектів, що реалізуються, з розвитку альтернативної енергетики. Результати, отримані в ході даного наукового дослідження, а також сформульовані на їх основі висновки, мають значне практичне значення для різних галузей української та світової промисловості, реальні технологічні можливості яких допускають використання відновлюваних джерел енергії для їх здатності відповідати потребам життєдіяльності всіх типів промислових підприємств, для їхнього подальшого повноцінного функціонування та вирішення будь-яких технологічних завдань, що стоять перед даними підприємствами

Ключові слова: «зелена» енергетика, біопаливо, відновлювані джерела енергії, енергоспоживання, економічний розвиток, екологічні проблеми

Machinery & Energetics
Vol. 13, No. 2. 2022

Journal homepage:
https://technicalscience.com.ua/en

UDC 514.18
DOI: 10.31548/machenergy.13(2).2022.62-72

Serhii Pylypaka[1], Mykola Klendii[2*], Tetyana Kresan[3]

[1]National University of Life and Environmental Sciences of Ukraine
03041, 15 Heroiv Oborony, Kyiv, Ukraine

[2]Separated subdivision of National University of Life and Environmental Sciences of Ukraine
“Berezhany Agrotechnical Institute”
47501, 20 Academichna Str., Berezhany, Ternopil region, Ukraine

[3]Separated subdivision of National University of Life and Environmental Sciences of Ukraine
“Nizhyn Agrotechnical Institute”
16600, 10 Shevchenko Str., Nizhyn, Chernihiv region, Ukraine

Study of the Movement of Soil Particles on the Surface of a Screw Tillage Working Body

Abstract. This study considers the interaction of soil particles with a screw tillage body, the working surface of which is made in the form of a deployed helicoid and substantially differs from the screw. Furthermore, the unfolded surface is characterised by manufacturability of the working body, since it is possible to calculate the geometric dimensions of a flat workpiece, which is formed into a finished product by simple bending with minimal plastic deformations. The purpose of this paper was to conduct theoretical and experimental studies of the movement of soil particles along the helical surface of the tillage working body, which is made in the form of a deployed helicoid. Mathematical modelling of the processes of movement of soil particles along the helical surface of a tillage working body was described based on general laws and principles of analytical and differential mathematics, theoretical and analytical mechanics. Experimental studies were carried out using a methodology with elements of mathematical statistics, mathematical methods of optimal planning of a multifactor experiment. The analysis of the results of experimental and theoretical studies was performed using applied computer programmes and systems. Experimental studies were conducted according to standard and independently developed methods.Results: a mathematical model of the movement of soil particles along the helical surface of the tillage body was developed, and it was established that when the angle of attack of the helical tillage working body increases, the lifting value of soil particles increases and the area of their dispersion by the helical surface increases. The value of the coefficient of friction does not substantially affect the shape of the trajectory of the soil particle. The quality of loosening the soil most depends on the angle of attack of the screw surface and the angular speed of rotation of the working body. The materials of this paper can be used by scientists for further research and practices in the selection of tillage units

Keywords: deployed helicoid, surface treatment, rectilinear formation, differential equations of motion, angular velocity, angle of attack, coefficient of friction, scattering area

Article’s History: Received: 05.01.2022; Revised: 01.04.2022; Accepted: 27.04.2022.

INTRODUCTION

For tillage, tools with disk working bodies are used. The profile of the treated soil and the size of the ridges depend on the size of the distance between the disks, the design parameters of the disks, and the angles of their installation. Tillage discs are set in such a way that the plane of placement of the blade and the direction of movement of the tillage unit form a given angle, i.e., the angle of attack. For better mixing of the soil and crop residue, the disk is also tilted from the vertical to the tilt angle, and therefore each disk must have its attachment to the harrow frame. If one uses a screw surface for tillage, it is also possible to provide surface tillage with a given depth and distance between the ridges of the tilled soil. However, the screw surface can now be fixed to the joint shaft. This simplifies the design of the working body.

Disk tillage tools, their designs, and calculation of their main parameters are covered in the studies [1-3].

Suggested Citation:
Pylypaka, S., Klendii, M., & Kresan, T. (2022). Study of the movement of soil particles on the surface of a screw tillage working body. *Machinery & Energetics,* 13(2), 62-72.

*Corresponding author

The study [4] thoroughly considers the design and calculation of disk tillage harrows. The study [5] considers the analytical expression of the model of installation of tillage disks for determining their geometric, structural, and technological parameters. In addition, other narrower studies investigated various possibilities for improving the quality of tillage with disc harrows [6-8]. The possibility of improving tillage units is considered in [9]. The studies [10; 11] investigated the motion of soil particles by the surface of disk tillage working bodies. The use of a helicoid for the calculation and manufacture of screw working elements is considered in the papers [12; 13]. The theory of design and construction of linear surfaces is covered in [14]. The study [15] justified the practical possibility of using a screw working body for tillage.

But presently, the process of tilling the soil with a screw working body remains unexplored, namely the study of the interaction of soil particles with a screw tillage body, the working surface of which is made in the form of an expanding helicoid, which are discussed in this paper.

The purpose of this study was to conduct theoretical and experimental studies of the movement of soil particles along the helical surface of the tillage working body, which is made in the form of a deployed helicoid.

MATERIALS AND METHODS

A screw working body that can be used for surface tillage is proposed in the form of a helicoid. The working turns of the surface of the screw organ are obtained by bending and then stretching the sweep ring along the axis. The surface obtained by this method differs from the screw. In a helical conoid, the rectilinear components of the helical surface are perpendicular to the axis, while in a spiral helicoid, they form an angle with the axis (Fig. 1a). The design parameters of the helical surface are the radius of the inner edge *r*, the radius of the outer (cutting) edge *R*, the pitch of the helical surface *H*, the angle of inclination of the generators. The inner and outer edges of the surface describe helical lines that have angles φR and φr. The presence of an angle of inclination of the generators contributes to the immersion of the helical surface into the soil if the axis of the helicoid is placed horizontally and at an angle β to the direction perpendicular to the direction of movement of the unit (Fig. 1b).

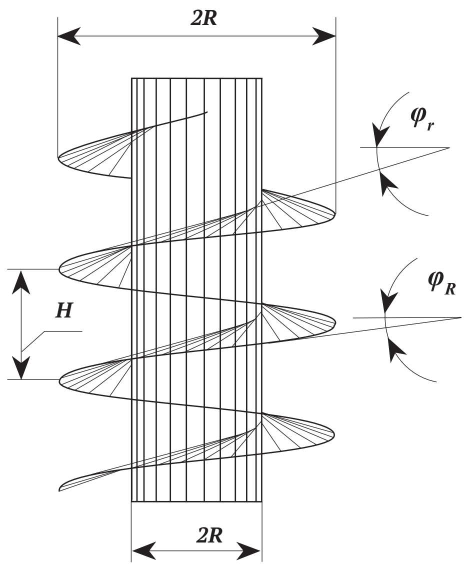

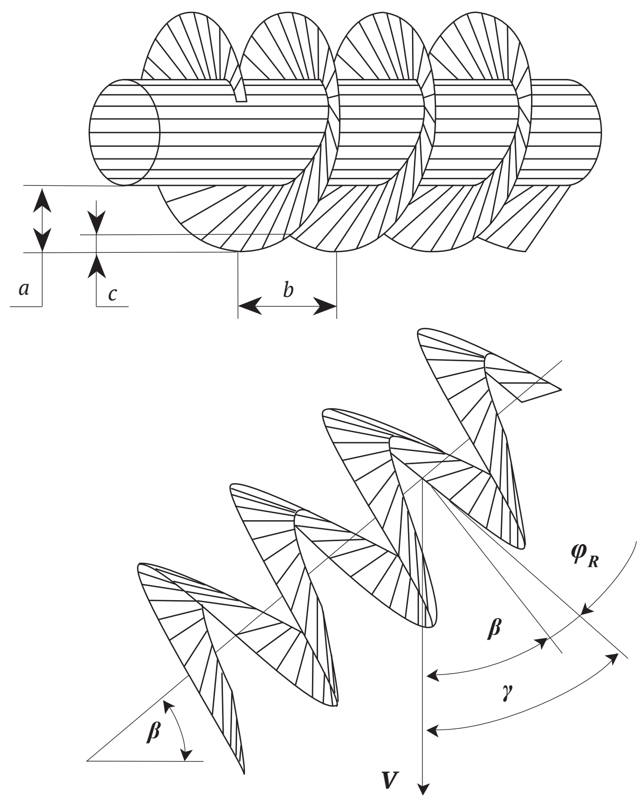

Figure 1. Surface of the working body for tillage: a) structural parameters of the surface; b) projections of the screw surface

Figure 1b presents the helical surface without a shaft, and the angle of attack γ is shown at one of the points of the cutting edge:

$$\gamma=\beta+\varphi_R, \quad (1)$$

The cultivation depth $a=R-r$, the height of the ridges on the bottom of the soil *c*, the value of the distance *b* between the ridges are determined by the design parameters of the helical surface and the angle of attack γ. The consequence of the operation of such a screw body is similar to the result of the operation of a disk tillage working body. When each disk harrow needs to be installed on a separate rack with the necessary angles of attack and roll for the disk to enter the soil, then the shape of the helical working surface ensures its entry into the soil with simpler structural manufacturing.

The helical surface equations have the following form:

$$X = h\alpha - u \sin\phi\,; \quad Y = p \sin\alpha - u \cos\phi \cos\alpha\,; \quad Z = p\cos\alpha + u\cos\phi \sin\alpha, \tag{2}$$

where α, u are the variable parameters of the helical surface, α is the angle of rotation of the surface point around the axis, which is placed on the cylindrical surface of radius p; u is the value of the generator from the point on the helical line to the point on the helical surface; h is a screw parameter; H is the pitch of the surface $H=2\pi h$; φ is the angle of inclination of the generating element, while:

$$\cos\phi = \frac{p}{\sqrt{p^2 + h^2}} \tag{3}$$

Based on this dependence, the Equation (2) is written as follows:

$$X = (A\alpha - u)\sin\phi\,; \quad Y = (A\sin\alpha - u\cos\alpha)\cos\phi\,; \quad Z = (A\cos\alpha + u\sin\alpha)\cos\phi, \tag{4}$$

where the constant $A = \sqrt{p^2 + h^2}$.

The surface of the screw working body, which is set at an angle of attack γ relative to the movement of the unit shall be presented as follows (Fig. 2a). Part of the helical surface at the boundaries of the processing depth a is located in the soil. The lowest point A of the helical surface (cutting edge) contacts the soil at the bottom of the furrow. Point B of the edge contacts the soil at the level of the field surface. When the working body moves with speed V_p, then also with the same speed , the soil hits the helical surface. This speed is divided into two mutually perpendicular components: V_t=$V_p$cos(β+φ_R) and V_n=$V_n$sin(β+φ_R). The value of the angle of attack γ=β+φ_R, for the helical surface is variable and depends on the depth of the location of the point of the edge of the helical surface in the soil. This is caused by a variable angle value φR. The limits of the change of the angle φR are insignificant (Fig. 1a), and therefore its value is taken as a constant value and equal at the lowest point of the edge:

$$\varphi_R = arctg(\frac{h}{R}) = arctg(\frac{A\sin\varphi}{R}) \tag{5}$$

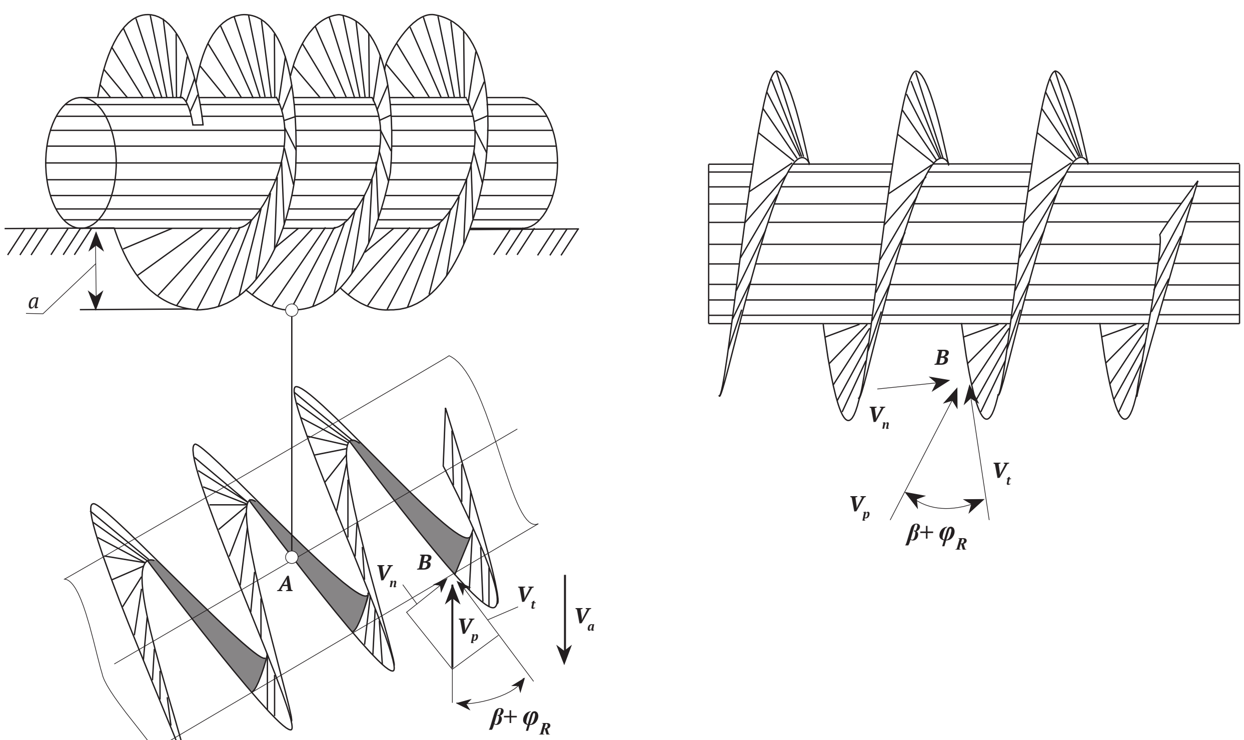

a) **b)**

Figure 2. Diagram of determining the particle speed

For calculations, the helicoid will not be turned to the angle β, but it will be assumed that the soil reaches it with the value of the velocity V_p when β=0 (Fig. 2b). This option allows describing the helical surface without turning it by the angle β, by replacing the rotation of the helicoid with the rotation of the speed vector of the harrow. That is, the helicoid is turned together with the vectors (Fig. 2a) back by the angle ($-\beta$). This allows using the parametric equations (3) of the helicoid without complications by rotating them by the angle β.

With the value of the transverse speed V_n, the soil particle enters the helical surface, and its angular speed of rotation depends on the value of the speed V_t. If the cutting edge of the helical surface rolls without sliding along the bottom of the furrow in the direction of movement of the tool, then with a certain assumption (the cutting edge of the working body is a helical line), V_t=Rω is written, where ω is the angular speed of rotation of the helical working body. Hence, ω is found as follows:

$$\omega = V_p \cos(\frac{\beta + \varphi_R)}{R} = V_R \cos\frac{\left[\beta + \mathrm{arctg}(\frac{A\sin\varphi}{R)}\right]}{R} \tag{6}$$

The magnitude of the velocity V_n and the angular velocity of rotation of the helicoid ω are considered upon solving the differential equations of particle motion by numerical methods.

If the surface variables u and α are set to depend on the amount of time the particle slides over the surface of the helicoid, then the equations of the trajectory of the particle will have the following form: $u=u(t)$ and $\alpha=\alpha(t)$.

Then Equations (3) transform into the equation of lines placed on the helical surface. For the difference between the equations of the surface and the equations of the line on it, uppercase letters were used in the expressions of the helical surface ("*X*", "*Y*", "*Z*"), and lowercase letters were used in the expressions of the line ("*x*", "*y*", "*z*"). When $u=u(t)$ and $\alpha=\alpha(t)$, equations (3) will record the trajectory of the material particle on the helical surface. At $u=const$, a helical line will be described on the surface of the helicoid. The radius R of its location is found as follows:

$$R^2 = \sqrt{Y^2 + Z^2} = (A^2 + u)^2 \cos^2 \phi \tag{5}$$

The value u with a known radius R is found as follows:

$$u = \frac{\sqrt{R^2 - A^2 \cos^2 \phi}}{\cos \phi} = \frac{\sqrt{R^2 - (p^2 + h^2) \cos^2 \phi}}{\cos \phi} \tag{6}$$

The following design parameters of the helicoid were adopted: $R=0.25$ m, $r=0.15$ m, $a=0.1$ m, $p=0.0721$, $h=0.0416$, $\varphi=30^0$. Next, the value u is found: $u=0.276$. If the value r is substituted instead of R, then $u=0.152$. Thus, the independent variable changes within $u=0.152...0.276$. Angle α changes within the limits of $\alpha=0...2\pi$.

According to the differentiation method (3), the projections of the particle sliding velocity along the helical surface are obtained as follows:

$$\begin{aligned} x' &= (A\alpha' - u') \sin \phi; \\ y' &= [\alpha'(u \sin \alpha + A \cos \alpha) - u' \cos \alpha] \cos \phi; \\ z' &= [\alpha'(u \cos \alpha - A \sin \alpha) + u' \sin \alpha] \cos \phi. \end{aligned} \tag{7}$$

The value of the relative velocity is obtained from (8):

$$V_r = \sqrt{x'^2 + y'^2 + z'^2} = \sqrt{(A\alpha' - u')^2 + u^2 \alpha'^2 \cos^2 \phi} \tag{8}$$

When the helical surface is in contact with the soil, it rotates with an angular velocity ω according to (4), and its value depends on the speed of movement of the unit $V_a=V_p$. During time t, the helical surface (3) will rotate through a certain angle $\psi=\omega \cdot t$. Parametric equations of a helicoid that record its position after turning an angle $\psi=\omega \cdot t$ (9):

$$\begin{aligned} X &= (A\alpha - u) \sin \phi; \\ Y &= (A \sin \alpha - u \cos \alpha) \cos \phi \cos \psi - (A \cos \alpha + u \sin \alpha) \cos \phi \sin \psi; \\ Z &= (A \sin \alpha - u \cos \alpha) \cos \phi \sin \psi + (A \cos \alpha + u \sin \alpha) \cos \phi \cos \psi. \end{aligned} \tag{9}$$

Having substituted the value $\psi=\omega \cdot t$ into (9) and simplified, the equation of a certain line on a helical surface, which is the absolute trajectory of motion, is as follows (10):

$$\begin{aligned} x &= [A\alpha - u] \sin \phi; \\ y &= -[A \sin(\omega t - \alpha) + u \cos(\omega t - \alpha)] \cos \phi; \\ z &= [A \cos(\omega t - \alpha) - u \sin(\omega t - \alpha)] \cos \phi. \end{aligned} \tag{10}$$

The differential equation of motion of a particle along a helical surface is written in the form of $\bar{m}w=\bar{F}$, which is written in projections on the coordinate axis, and therefore a system of equations is obtained.

The value of the absolute acceleration of the particle is obtained by differentiating the expressions of the absolute trajectory (10) over time t. The value of the vector of the absolute velocity of a particle has the following form:

$$\begin{aligned} x' &= (A\alpha' - u') \sin \phi; \\ y' &= -\left[\left(u' + A(\omega - \alpha')\right) \cos(\omega t - \alpha) - u(\omega - \alpha') \sin(\omega t - \alpha)\right] \cos \phi; \\ z' &= -[(u' + A(\omega - \alpha')) \sin(\omega t - \alpha) + u(\omega - \alpha') \cos(\omega t - \alpha)] \cos \phi. \end{aligned} \tag{11}$$

Having differentiated the Equation (11), the vector of the total acceleration of the particle projected on the coordinate axis is obtained:

$$\begin{aligned} x'' &= (A\alpha'' - u'') \sin \phi; \\ y'' &= (A\alpha'' - u'' + u(\omega - \alpha')^2) \cos(\omega t - \alpha) \cos \phi + \\ &+ (A(\omega - \alpha')^2 + 2u'(\omega - \alpha') - u\alpha'') \sin(\omega t - \alpha) \cos \phi; \\ z'' &= (A\alpha'' - u'' + u(\omega - \alpha')^2) \sin(\omega t - \alpha) \cos \phi - \\ &- (A(\omega - \alpha')^2 + 2u'(\omega - \alpha') - u\alpha'') \cos(\omega t - \alpha) \cos \phi. \end{aligned} \tag{12}$$

Projections of the guide unit vector of the force weight will be as follows:

$$\{0;\ 0;\ -1\} \tag{13}$$

The reaction of the surface, which is directed along the normal to it, is determined by the partial derivatives of Equations (3):

$$\begin{aligned} \frac{\partial X}{\partial u} &= -\sin \phi; \frac{\partial X}{\partial \alpha} = A \sin \phi; \\ \frac{\partial Y}{\partial u} &= -\cos \phi \cos \alpha; \frac{\partial Y}{\partial \alpha} = (u \sin \alpha + A \cos \alpha) \cos \phi; \\ \frac{\partial Z}{\partial u} &= \cos \phi \sin \alpha; \frac{\partial Z}{\partial \alpha} = (u \cos \alpha - A \sin \alpha). \end{aligned} \tag{14}$$

After multiplying the vectors (14) and reducing the resulting vector to unity, the value of the projections of the normal vector to the surface will have the following form:

$$\{-\cos \phi;\ \sin \phi \cos \alpha;\ -\sin \phi \sin \alpha\}. \tag{15}$$

To match the directions of the unit vector (15) and the direction of action of other forces acting on the soil particle at the moment of time t, it must also be rotated by the angle $\psi=\omega\cdot$ similarly to the rotation of the surface (9):

$$\{-\cos \phi;\ \sin \phi \cos(\omega t - \alpha);\ \sin \phi \sin(\omega t - \alpha)\}. \tag{16}$$

The force of friction is directed in the direction opposite to the relative sliding speed of the particle V_r. The value of the projections of the unit vector is determined by the ratio of the terms of the velocity (7) to its value modulo (8) with its subsequent rotation through the angle $\varphi=\omega t$:

$$\left\{\begin{matrix} \frac{(A\alpha'-u')}{\sqrt{(A\alpha'-u')^2+u^2\alpha'^2\cos^2\phi}}\sin\phi\,; \\ -\frac{u\alpha'\sin(\omega t-\alpha)+(u'-A\alpha')\cos(\omega t-\alpha)}{\sqrt{(A\alpha'-u')^2+u^2\alpha'^2\cos^2\phi}}\cos\phi\,; \\ \frac{u\alpha'\cos(\omega t-\alpha)-(u'-A\alpha')\sin(\omega t-\alpha)}{\sqrt{(A\alpha'-u')^2+u^2\alpha'^2\cos^2\phi}}\cos\phi \end{matrix}\right\}. \tag{17}$$

Next, the equation of motion of a particle $m\bar{w}=\bar{F}$ in projections is expanded onto the axes of the coordinate system, assuming that the friction force is directed opposite to vector (17):

$$\begin{gathered} mx''=-N\cos\phi-fN\frac{(A\alpha'-u')}{\sqrt{(A\alpha'-u')^2+u^2\alpha'^2\cos^2\phi}}\sin\phi\,; \\ my''=N\sin\phi\cos\alpha-fN\frac{u\alpha'\sin(\omega t-\alpha)+(u'-A\alpha')\cos(\omega t-\alpha)}{\sqrt{(A\alpha'-u')^2+u^2\alpha'^2\cos^2\phi}}\cos\phi\,; \\ mz''=-mg+N\sin\phi\sin(\omega t-\alpha)- \\ -fN\frac{u\alpha'\cos(\omega t-\alpha)-(u'-A\alpha')\sin(\omega t-\alpha)}{\sqrt{(A\alpha'-u')^2+u^2\alpha'^2\cos^2\phi}}\cos\phi. \end{gathered} \tag{18}$$

The equation (18) is solved with respect to other derivatives of the unknown coordinates, as well as the reaction force of the surface. After performing the simplifications, the result is as follows:

$$\begin{gathered} \alpha''=\frac{(2u'+A(\omega-\alpha'))(\omega-\alpha')\cos\phi-g\cos(wt-\alpha)}{u\cos\phi}-f\alpha'\sin\phi\frac{u(\omega-\alpha')^2\cos\phi+g\sin(wt-\alpha)}{\sqrt{(A\alpha'-u')^2+u^2\alpha'^2\cos^2\phi}}; \\ u''=g\cos\phi\sin(wt-\alpha)-fu'\sin\phi\frac{u(\omega-\alpha')^2\cos\phi+g\sin(wt-\alpha)}{\sqrt{(A\alpha'-u')^2+u^2\alpha'^2\cos^2\phi}}+ \\ +\frac{2Au'(\omega-\alpha')\cos\phi-Ag\cos(wt-\alpha)+(\omega-\alpha')^2(A^2+u^2\cos^2\phi)\cos\phi}{u\cos\phi}; \\ N=m\sin\phi\,[u(\omega-\alpha')^2\cos\phi+g\sin(wt-\alpha)]. \end{gathered} \tag{19}$$

The first two equations (19) are solved according to numerous methods in the *Simulink* environment of the *MatLab* system [16]. It was assumed that the helical surface, the design parameters of which are given earlier, moves with a speed of V_a=*9 km/h* ($V_a=V_p$=*2.5 m/s*). The angle of attack β=*40°*, the coefficient of friction f=*0.3* [17]. Having performed the calculations, it was found that: V_t=*1.62 m/s*; V_n=*1.9 m/s*, ω=*6.5* s^{-1}.

Considering at what point on the cutting edge the particle enters the helical surface, the initial integration conditions are chosen. This point is given by initial coordinates u_o and α_o. For the version under study, the value u_o=*0.276 m*. To find the value of αo, equation (3) must be solved:

$$\alpha_0=-\mathrm{Arccos}\frac{Az+u\sqrt{(A^2+u^2)\cos^2\phi-z^2}}{(A^2+u^2)\cos^2\phi} \tag{20}$$

The value z=*-0.15 m* corresponds to the surface of the field, and the value z=*-0.25 m* corresponds to the bottom of the furrow. After substituting these values into Equation (20), the values α_o=*-0.94* and α_o=*-1.83* are obtained.

The initial values u_o' and α_o' can be used to find the direction of entry of the soil particle on the helical surface.

It was established that the soil particle is captured by the helical surface, then moves along it, and therefore the angular velocity of sliding decreases due to friction [18].

The derivative of the coordinate u_o' denotes the linear velocity of the soil particle by the surface along the generatrix u and depends on the velocity V_n, equal to *1.9 m/s*. However, the direction of the velocity V_n differs from the direction of the generating helical surface. In addition, when the helical surface rotates, the speed of movement of the particle along the axis of rotation occurs. The soil particle enters the surface at a speed V_n and, additionally, the surface of the helicoid "runs into" the particle due to rotation. Therefore, $u_o'=V_n$=*-1.9 m/s* is taken as the initial value of the parameter u_o'. Figure 3 shows the trajectories of soil particle movement based on the results of integration of differential equations (19).

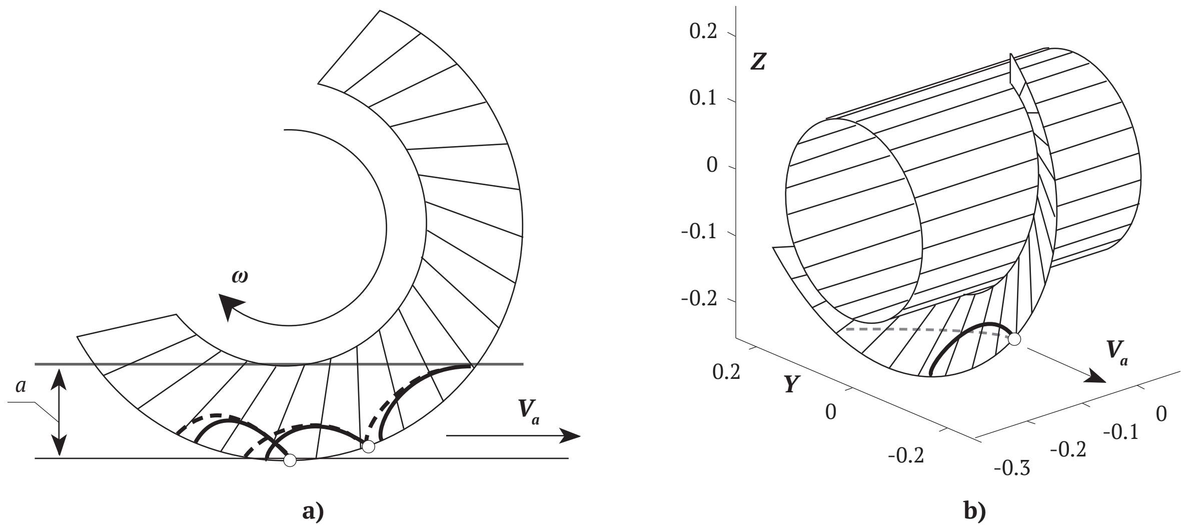

Figure 3. Relative and absolute trajectories of particle movement: a) helical surface; b) speed u_o'=-2.5 m/s

In Figure 3a, the helical surface is shown so that its axis is projected at a point. Soil particles are plotted along the spiral surface in three places: on the field surface, at an intermediate point, and at the bottom of the furrow. A solid line shows the movement of a soil particle without its interaction with other particles. However, in the real process, other soil particles act on the particle and force it to move along the helical surface. If the force of action of the particles balances the friction force, *f =0* is taken as the coefficient of friction. The dashed line shows the trajectories of soil particles at *f=0*. Figure 3a shows that the difference between the trajectories is insignificant.

Despite the position of the place where the soil particle enters the helical surface, the particle slides along it and approaches the shaft. If the speed of the unit is increased, this approximation increases. For example, in Figure 3b, the particle velocity was increased from *1.9 m/s* to *2.5 m/s*. Accordingly, the trajectory of the particle's movement is closer to the cylindrical shaft. As a result, the soil particles at the beginning of their movement, when sliding on the helical surface, approach the shaft. When the helical surface is immersed in the ground, the particles below press on the upper particles and the shaft gets in the way of the movement of the soil particles. Soil sticking will occur at the junction of the helical surface with the shaft. To avoid this, the shaft must be made latticed, as shown in Figure 4.

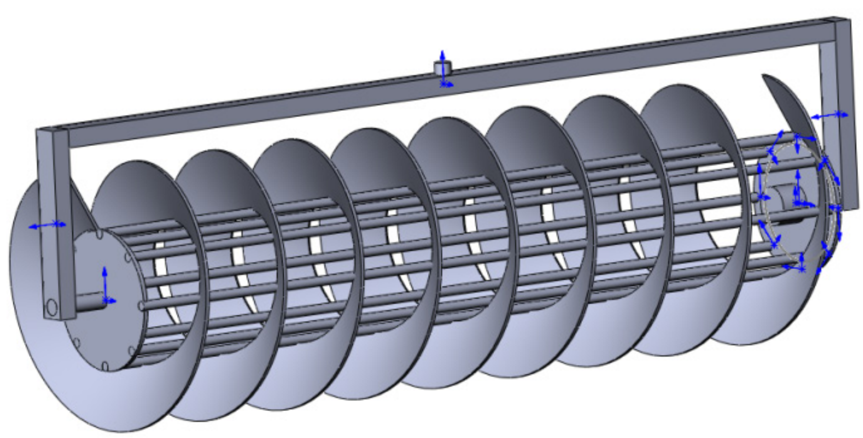

Figure 4. Grid shaft helicoid

Furthermore, the grid shaft additionally performs the function of a roller.

Figure 5 shows the kinematic characteristics of the movement of a soil particle that enters the helical surface at the field level (Fig. 3a). Solid lines show the dependence for *f=0.3*, and dashed lines for *f=0*.

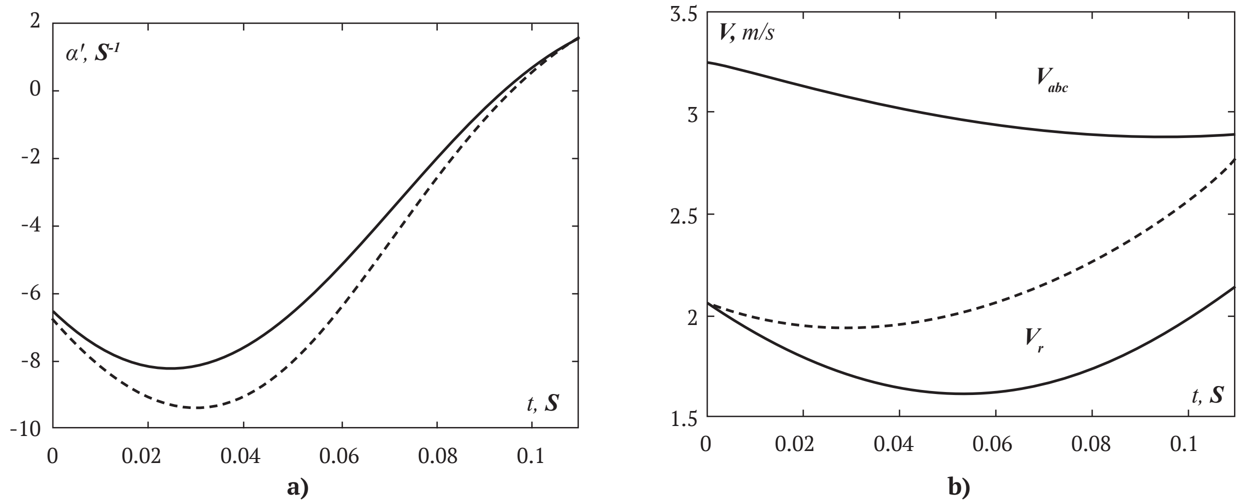

Figure 5. Graphs of changes in particle movement velocities at f=0.3 (solid) and f=0 (dashed) lines: a) angular velocity; b) relative and absolute speeds

An inherent feature of the movement of a soil particle is that at the beginning of the movement, the velocities decrease, and then gradually increase. The graphic dependences reflect the time interval (*t=0.11 s*) from the beginning of the particle's arrival on the helical surface until it leaves it.

RESULTS AND DISCUSSION

The analysis of helical linear surfaces (helicoids) showed that the surface of the expanding helicoid can also be used as an alternative to disk working bodies, since it can also provide surface tillage with a given depth and distance between the ridges of the tilled soil.

To determine the quality of soil loosening, a multifactorial experiment was conducted to determine the area of soil scattering by a screw working body [19]. In the conducted experimental studies on the determination of the area of dispersion of soil particles by the turn of a helical surface, the variable parameters were as follows: the angle of attack of the helical surface α=20°-30°, the angular speed of rotation of the helical surface ω=0–10 s^{-1} and soil moisture, which is determined by the coefficient of friction f=0.2...0.4. After processing the numerical values, a regression equation was obtained, which determines the area of dispersion of particles S according to the change of the above parameters:

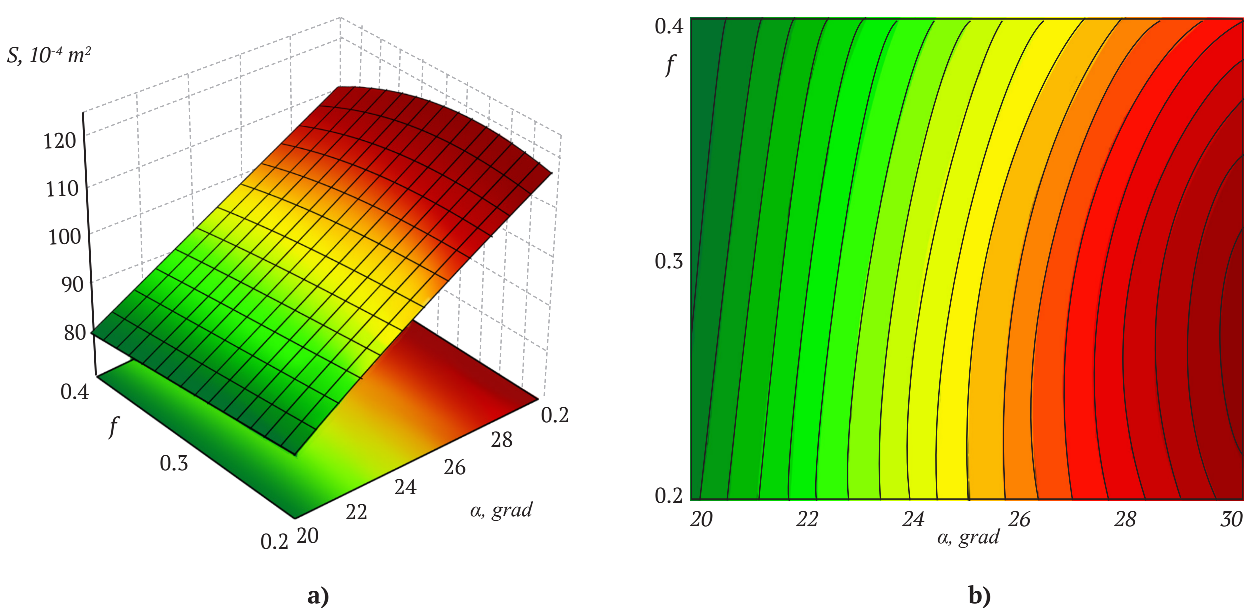

Figure 6. The dependence of the change in the dispersion area of particles S on the angle of attack of the helical surface α and the coefficient of soil friction f

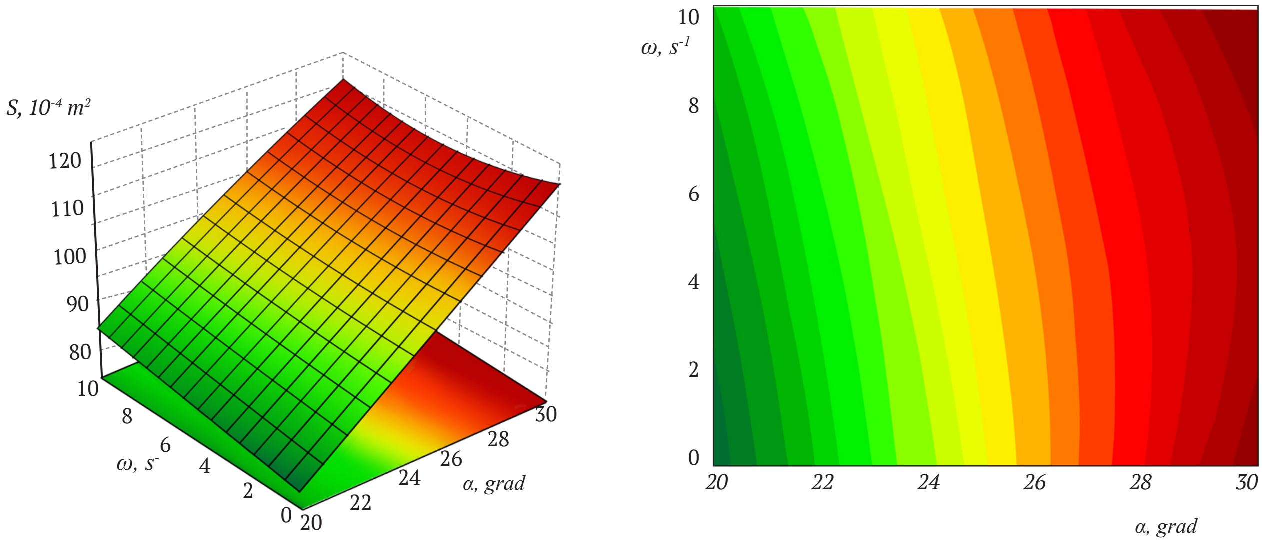

Figure 7. Dependence of the change in the particle dispersion area *S* on the angle of attack of the helical surface *α* and the angular speed of rotation of the helical surface *ω*

$$S=9.97+3.46\cdot\alpha+1.76\cdot\omega-4.64\cdot\alpha\cdot f \quad (21)$$

Having analysed the regression Equation (21), the response surfaces and their two-dimensional cross-sections were constructed, which are presented in Figures 6, 7, and 8 [20].

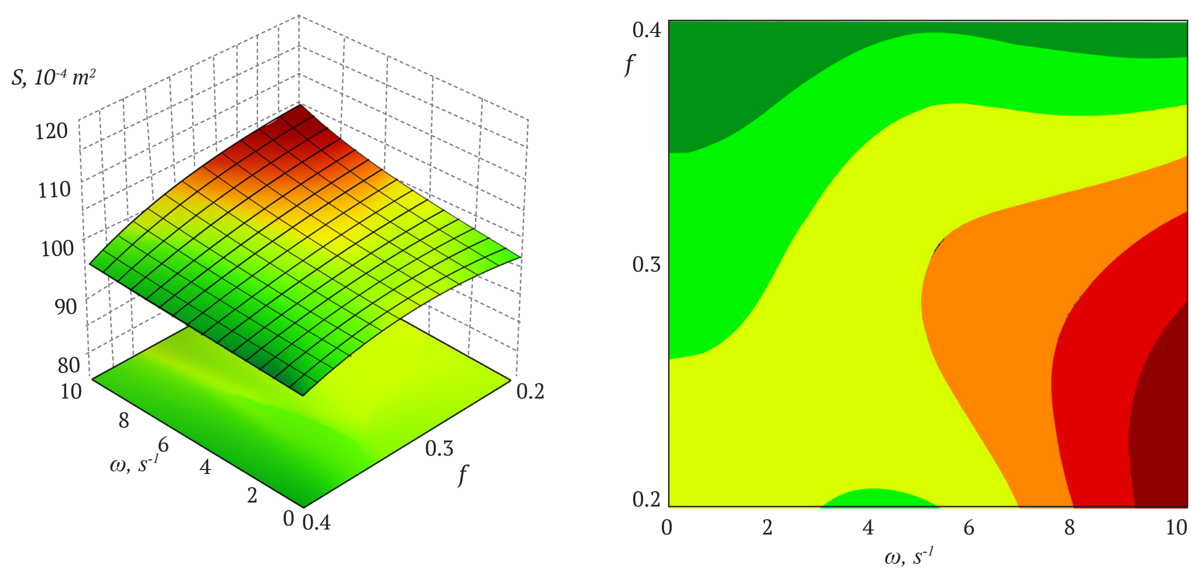

Figure 8. The dependence of the change in the particle dispersion area *S* on the angular velocity of rotation of the helical surface *ω* and the soil friction coefficient *f*

Analysis of the surfaces shows that the dispersion area of particles *S* varies within 70*10⁻⁴...130*10⁻⁴ (m²) depending on the change in the angle of attack of the helical surface *α*, the angular speed of rotation of the helical surface *ω*, and the coefficient of friction *f*. It was established that an increase in the angle of attack of the helical surface *α* leads to an increase in the dispersion area of particles *S* by 1.81 times, and an increase in the angular speed of rotation of the helical surface *ω* to an increase in *S* by 1.36 times; within the limits of the change in the coefficient of friction *f*, the change in *S* is insignificant.

Experimental studies were carried out to determine the effect of soil moisture on the quality of its cultivation, i.e., on the dispersion value of soil particle dispersion. In experimental studies of the operation of the screw working body during soil cultivation, the absolute soil moisture W_a

varied in the range from 10% to 30% at a fixed value of the angle of attack of the screw surface α=20° and the angular speed of the screw working body ω=5 (s^{-1}).

The research results are presented in the form of a graphical dependence, which is presented in Figure 9. It was established that with an increase in the absolute humidity of the soil W_a in the range from 10% to 30%, the size of the scattering area of soil particles S decreases from $98*10^{-4}$ to $86*10^{-4}$ (m^2), i.e., by 1.14 times.

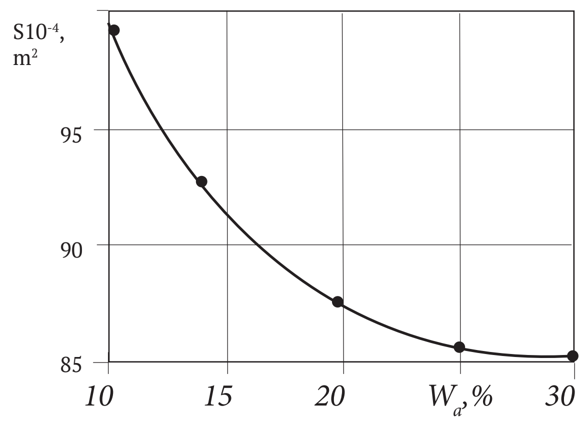

Figure 9. Dependence of the change in the dispersion area of particles *S* on absolute soil moisture W_a

The results of research on determining the quality of soil loosening and determining the area of soil scattering by a screw working body are similar to the results of the study [8], which presents the results of research on determining the quality of soil loosening by a disk working body [21; 22].

Thus, the screw working body works like disk tools. When the blade of the helical surface is in contact with the ground, the available angles of attack and roll are similar to the angles for disc tools. The developed tillage screw working body has an uncomplicated design and low metal consumption.

CONCLUSIONS

As a result of the conducted research, a mathematical model of the movement of soil particles through the helical working surface of the tillage body, which is an expanding helicoid, was developed.

As a result of solving differential equations by the method of numerical integration, it was found that an increase in the angle of attack of the screw working body leads to an increase in the height of the rise of particles and an increase in the area of their dispersal over the helical surface. The value of the coefficient of friction almost does not affect the trajectory of the movement of the particle.

To determine the quality of soil loosening, a multifactorial experiment was conducted to determine the area of scattering of soil particles. It was established that the quality of loosening the soil depends most on the angle of attack of the screw surface and the angular speed of rotation of the working body. The results of studies of the effect of soil moisture on the size of the particle scattering area are also given.

The perspective of this study is to establish the quality of loosening the soil and determine the area of scattering of soil particles depending on the angle of inclination of the rectilinear elements of the helical surface.

REFERENCES

[1] Vasilenko, P.M. (1960). *Theory of particle motion on rough surfaces of agricultural machines*. Kyiv: USHA.

[2] Voytiuk, D.G., & Pilipaka, S.F. (1999). Before determining the trajectories of soil particles on the cylindrical surfaces of the working bodies of tillage implements. *Collection of Scientific Works of the National Agrarian University "Mechanization of Agricultural Production"*, 5, 242-251.

[3] Gutsol, O.P., & Kovbasa, V.P. (2016). *Substantiation of parameters and modes of movement of tillage machines with disk working bodies*. Kyiv: National University of Life and Environmental Sciences of Ukraine.

[4] Socht, K.A., Trubilin, E.I., & Konovalov, V.I. (2014). Disc harrows and cultivators. In *Disc harrows and cultivators* (pp. 16-23). Krasnodar: Kuban State Agrarian University.

[5] Bulgakov, V., Adamchuk, O., Ivanovs, S., & Olt, J. (2021). Experimental investigations on the surface application of superphosphate by the fertiliser spreading tool with inclined axis. *INMATEH - Agricultural Engineering*, 64, 307-316.

[6] Hailis, G.A. (1990). *Calculation of working bodies of tillage machines*. Kyiv: UMK VO.

[7] Bulgakov, V., Pascuzzi, S., Adamchuk, V., Gadzalo, J., Nadykto, V., Olt, J., Nowak, J., & Kaminskiy, V. (2022). Dynamics of temperature variation in soil under fallow tillage at different depths. *Agriculture*, 12, article number 450.

[8] Pylypaka, S., Klendii, M., & Klendii, O. (2018). Particle motion on the surface of a concave soil-tilling disk. *Acta Polytechnica. Journal of Advanced Engineering,* 58(2), 201-208.

[9] Socht, K.A., Trubilin, E.I., & Konovalov, V.I. (2014). Forecasting of technological parameters of disk tillage implements at the stage of their design. In *Disc harrows and cultivators* (pp. 39-53). Krasnodar: Kuban State Agrarian University.

[10] Bulgakov, V.M., Kuvachov, V.P., Solona, O.V., & Boris, M.M. (2021). Experimental studies of the microrelief of the soil surface of the constant technological track. *Machinery, Energy, Transport of Agro-Industrial Complex*, 114(3), 16-23.
[11] Kirichenko, A.K., & Sokht, K.A. (1983). Estimation of uniformity of depth of tillage by the combined unit. *Mechanization and Electrification of Agriculture*, 7, 26-30.
[12] Bulgakov, V., Holovach, I., Nadykto, V., Parakhin, O., Kaletnik, H., Shymko, L., & Olt, J. (2020). Motion stability estimation for modular traction vehicle-based combined unit. *Agronomy Research*, 18(4), 2340-2352.
[13] Bulgakov, V., Pascuzzi, S., Ivanovs, S., Kaletnik, G., & Yanovich, V. (2018). Angular oscillation model to predict the performance of a vibratory ball mill for the fine grinding of grain. *Biosystems Engineering*, 171, 155-164.
[14] Pylypaka, S., Klendii, M., Trokhaniak, V., Kresan, T., Hryshchenko, I., & Pastushenko, A. (2021). External rolling of a polygon on closed curvilinear profile. *Acta Polytechnica*, 61(1), 270-278.
[15] Hevko, B.M., Hevko, R.B., Trokhaniak, O.M., Buriak, M.V., Dzyadykevych, Y.V., & Rozum, R.I. (2018). Improvement of machine safety devices. *Acta Polytechnica,* 58(1), 17-25.
[16] Hevko, R., Rohatynskyi, R., Hevko, M., Lyashuk, O., & Trokhaniak, O. (2020). Investigation of sectional operating elements for conveying agricultural materials. *Research in Agricultural Engineering*, 66(1), 18-26
[17] Hevko, R., Lyashuk, O., Dzyura, V., Dovbush, T., Trokhaniak, O., & Liashko, A. (2021). Experimental studies of the process of loose material transportation by a pneumatic-screw conveyor. *INMATEH – Agricultural Engineering*, 63(1), 479-487.
[18] Tkachenko, I., Hevko, R., Gandziuk, M., Synii, S., & Trokhaniak, O. (2021). Substantiation of the parameters of a horizontal conveyer-cleaner of root crops. *Bulletin of the Transilvania University of Brasov*, 1, 213-222. doi: 10.31926/BUT.FWIAFE.2021.14.63.1.19.
[19] Hevko, R., Zalutskyi, S., Tkachenko, I., Lyashuk, O., & Trokhaniak, O. (2021). Design development and study of an elastic sectional screw operating tool. *Acta Polytechnica*, 61(5), 624-632. doi: 10.14311/AP.2021.61.0624.
[20] Kuvachov, V., Bulgakov, V**.,** Adamchuk, V., Kaminskiy, V., Melnik, V., & Olt, J. (2021). Experimental research into new harrowing unit based on gantry agricultural implement carrier. *Agronomy Research*, 19(1), 126-135.
[21] Bulgakov, V., Trokhaniak, O., Adamchuk, V., Olt, J., & Ivanovs, S. (2022). Experimental studies of flexible sectional screw conveyor torque value. In *Engineering for rural development* (pp. 472-477). Jelgava: Latvia University of Life Sciences and Technologies.
[22] Bulgakov, V., Olt, J., Ivanovs, S., Trokhaniak, O., Gadzalo, Ja., Adamchuk, V., Chernovol, M., Pascuzzi, S., Santoro, F., & Arak, M. (2022). Research of a contact stresses in swivel elements of flexible shaft in screw conveyor for transportation of agricultural materials. *Estonian Academic Agricultural Society,* 1, 1-7.

СПИСОК ВИКОРИСТАНИХ ДЖЕРЕЛ

[1] Василенко П.М. Теория движения частицы по шероховатым поверхностям сельскохозяйственных машин. Киев: УСХА, 1960. 283 с.
[2] Войтюк Д.Г., Пилипака С.Ф. До визначення траєкторій руху частинок грунту по циліндричних поверхнях робочих органів грунтообробних знарядь. *Збірник наукових праць Національного аграрного університету “Механізація сільськогосподарського виробництва”.* Вип. 5. С. 242–251.
[3] Гуцол О.П., Ковбаса В.П. Обґрунтування параметрів і режимів руху ґрунтообробних машин з дисковими робочими органами: монографія. Київ: Нац. ун-т біоресурсів і природокористування України, 2016. 145 с.
[4] Сохт К.А., Трубилин Е.И., Коновалов В.И. Дисковые бороны и лущильники. *Проектирование технологических параметров:* учеб. пособие. Краснодар: КубГАУ, 2014. С. 16–23.
[5] Bulgakov, V., Adamchuk, O., Ivanovs, S., & Olt, J. (2021). Experimental investigations on the surface application of superphosphate by the fertiliser spreading tool with inclined axis. *INMATEH – Agricultural Engineering*. Vol. 64. P. 307–316.
[6] Хайлис Г.А. Расчет рабочих органов почвообрабатывающих машин: учебное пособие. Киев: УМК ВО, 1990. 83 с.
[7] Dynamics of temperature variation in soil under fallow tillage at different depths / V. Bulgakov et al. *Agriculture*. 2022. Vol. 12. Article number 450.
[8] Pylypaka S., Klendii M., Klendii O. Particle motion on the surface of a concave soil-tilling disk. *Acta Polytechnica. Journal of Advanced Engineering*. 2018. Vol. 58, No. 2. P. 201–208.
[9] Сохт К.А. Прогнозирование технологических параметров дисковых почвообрабатывающих орудий на этапе их проектирования. *Дисковые бороны и лущильники*. Краснодар: КубГАУ, 2014. С. 39–53.
[10] Булгаков В.М., Кувачов В.П., Солона О.В., Борис М.М. Експериментальні дослідження мікрорельєфу поверхні грунту постійної технологічної колії. *Техніка, енергетика, транспорт АПК*. 2021. Вип. 114, № 3. С. 16–23.
[11] Кириченко А.К., Сохт К.А. Оценка равномерности глубины обработки почвы комбинированным агрегатом. *Механизация и электрификация сельского хозяйства*. 1983. № 7. С. 26–30.
[12] Motion stability estimation for modular traction vehicle-based combined unit / V. Bulgakov et al. *Agronomy Research.* 2020. Vol. 18, No. 4. P. 2340–2352.
[13] Angular oscillation model to predict the performance of a vibratory ball mill for the fine grinding of grain / V. Bulgakov et al. *Biosystems Engineering*. 2018. Vol. 171. P. 155–164.

[14] External rolling of a polygon on closed curvilinear profile / S. Pylypaka et al. *Acta Polytechnica*. 2021. Vol. 61, No. 1. P. 270–278.
[15] Improvement of machine safety devices / B.M. Hevko et al. *Acta Polytechnica*. 2018. Vol. 58. No. 1. P.17–25.
[16] Investigation of sectional operating elements for conveying agricultural materials / R. Hevko et al. *Research in Agricultural Engineering*. 2020. Vol. 66, No. 1. P. 18–26.
[17] Experimental studies of the process of loose material transportation by a pneumatic-screw conveyor / R. Hevko et al. *INMATEH – Agricultural Engineering*. 2021. Vol. 63, No. 1. P. 479–487.
[18] Substantiation of the parameters of a horizontal conveyer-cleaner of root crops / I. Tkachenko et al. *Bulletin of the Transilvania University of Brasov*. 2021. Vol. 1. P. 213–222. doi: 10.31926/BUT.FWIAFE.2021.14.63.1.19.
[19] Design development and study of an elastic sectional screw operating tool / R. Hevko et al. *Acta Polytechnica*. 2021. Vol. 61, No. 5. P. 624–632. doi: 10.14311/AP.2021.61.0624.
[20] Experimental research into new harrowing unit based on gantry agricultural implement carrier / V. Kuvachov et al. *Agronomy Research*. 2021. Vol. 19, No. 1. P. 126–135.
[21] Experimental studies of flexible sectional screw conveyor torque value / V. Bulgakov et al. *Engineering for rural development*: Contents of proceedings of 21st international scientific conference (Jelgava, 25-27 May 2022). Jelgava, 2022. P. 472–477.
[22] Research of a contact stresses in swivel elements of flexible shaft in screw conveyor for transportation of agricultural materials / V. Bulgakov et al. *Estonian Academic Agricultural Society*. 2022. Vol. 1. P. 1–7.

Сергій Федорович Пилипака[1], Микола Богданович Клендій[2], Тетяна Анатоліївна Кресан[3]

[1]Національний університет біоресурсів і природокористування України
03041, вул. Героїв Оборони, 15, м. Київ, Україна

[2]Відокремлений підрозділ національного університету біоресурсів і природокористування України «Бережанський агротехнічний інститут», Україна
47501, вул. Академічна, 20, м. Бережани, Тернопільська область, Україна

[3]Відокремлений підрозділ національного університету біоресурсів і природокористування України «Ніжинський агротехнічний інститут», Україна
16600, вул. Шевченка, 10, м. Ніжин, Чернігівська область, Україна

Дослідження руху частинки ґрунту по поверхні гвинтового ґрунтообробного робочого органа

Анотація. В статті розглянуто взаємодію частинок ґрунту із гвинтовим ґрунтообробним органом, робоча поверхня якого виконана у вигляді розгортного гелікоїда і суттєво відрізняється від шнека. Крім того, для розгортної поверхні властива технологічність виготовлення робочого органу, оскільки можна розрахувати геометричні розміри плоскої заготовки, яка формується у готовий виріб простим згинанням із мінімальними пластичними деформаціями. Метою дослідження було проведення теоретичних та експериментальних досліджень руху частинок ґрунту по гвинтовій поверхні грунтообробного робочого органу, яка виконана у вигляді розгортного гелікоїда. Математичне моделювання процесів руху частинок ґрунту по гвинтовій поверхні грунтообробного робочого органу описано на базі загальних законів і принципів аналітичної та диференціальної математики, теоретичної та аналітичної механіки. Експериментальні дослідження були проведені із застосуванням методики з елементами математичної статистики, математичних методів оптимального планування багатофакторного експерименту. Аналіз результатів проведених експериментальних та теоретичних досліджень виконано із використанням прикладних комп'ютерних програм та систем. Експериментальні дослідження проводили відповідно до стандартних та самостійно розроблених методик. Результати: розроблено математичну модель руху частинки ґрунту гвинтовою поверхнею ґрунтообробного органу, та встановлено, що при збільшенні величини кута атаки гвинтового грунтообробного робочого органа величина підйому частинок ґрунту зростає і збільшується величина площі їх роззосередження гвинтовою поверхнею. Величина коефіцієнта тертя несуттєво впливає на форму траєкторії руху частинки ґрунту. Якість розпушування ґрунту найбільше залежить від кута атаки гвинтової поверхні та кутової швидкості обертання робочого органу. Матеріали статті можуть бути використані науковцями для подальших досліджень та практиками у виборі ґрунтообробних агрегатів

Ключові слова: розгортний гелікоїд, поверхневий обробіток, прямолінійна твірна, диференціальні рівняння руху, кутова швидкість, кут атаки, коефіцієнт тертя, площа розсіювання

Machinery & Energetics
Vol. 13, No. 2. 2022

Journal homepage:
https://technicalscience.com.ua/en

UDC 621.316.729:621.396.6
DOI: 10.31548/machenergy.13(2).2022.73-82

Valerii Koval[1*], Vitaliy Lysenko[1], Nikolay Kiktev[1], Yurii Pylypenko[2], Oleksandr Samkov[2], Oleksandr Osinskiy[2], Ivan Popov[3]

[1]National University of Life and Environmental Sciences of Ukraine
03041, 15 Heroiv Oborony Str., Kyiv, Ukraine

[2]Institute of Electrodynamics of the National Academy of Sciences of Ukraine
03057, 56 Peremohy Ave., Kyiv, Ukraine

[3]Odessa State Ecological University
65016, 15 Lvivska Str., Odessa, Ukraine

Automated Monitoring of Time Synchronisation Devices and Digital Processing of Vector Measurements of Dynamic Characteristics of SMART Grid Power Systems

Abstract. Currently, customers of energy companies use devices to generate electricity (solar panels, windmills, etc.) and return energy to the grid to save costs or generate income. Therefore, it is urgent to solve the problem of creating an automated system for diagnosing the quality of electricity for consumers who use renewable sources of electricity. The purpose of this study was to improve the efficiency of management in intelligent SMART Grid power systems. To fulfil the said purpose, it was proposed to use an automated system for monitoring synchro signals of PMU microprocessor equipment and software tools for digital processing and statistical analysis of the results of synchronised vector measurements of dynamic characteristics of power grids. Software tools for digital processing and statistical analysis of the obtained vector measurement data were developed. Linear regression, Random Forest Regression, and Ridge regression methods were employed to analyse and predict electricity quality indicators. The results of a comparative analysis of the obtained results of the predictive model were presented. To conduct experimental studies, a laboratory sample of a quality control device for generating synchro signals was developed and manufactured, which directly affects the reliability of digital data from distributed synchronised vector measurements in transient modes (in real time). The multichannel nature of the device increases the performance and reliability of the automated monitoring system. The paper presents the results of experimental studies of the device as a part of the developed laboratory stand, which is connected to the current local IP network of the National University of Life and Environmental Sciences of Ukraine. The practical significance of the conducted experimental studies lies in the establishment of the technical possibility of simultaneous monitoring of time synchronisation signals generated by two GPS receivers. In this case, it is obvious to increase the performance of the developed and manufactured device for monitoring the quality of clock signal generation, compared to a single-channel one. This material can be useful for engineers who design electrical systems connected to renewable energy sources

Keywords: renewable energy sources, synchronised vector measurements, multichannel device, quality control of synchro signal generation, monitoring of synchro signals, Ridge regression model, forecasting of electricity indicators

Article's History: Received: 17.12.2021; Revised: 02.03.2022; Accepted: 27.04.2022.

INTRODUCTION

At present, energy efficiency is one of the main technical indicators that characterise the competitiveness of products, innovative development of the economy, and national security. The need to adapt the Ukrainian economy, including the agro-industrial complex, as one of the main subjects of

Suggested Citation:
Koval, V., Lysenko, V., Kiktev, N., Pylypenko, Yu., Samkov, O., Osinskiy, O., & Popov, I. (2022). Automated monitoring of time synchronisation devices and digital processing of vector measurements of dynamic characteristics of SMART Grid power systems. *Machinery & Energetics,* 13(2), 73-82.

*Corresponding author

the export-forming function, to market energy prices has led to the need to solve the problems of highly efficient use of energy resources. Apart from energy consumption in the electric power industry, the problems of improving the energy efficiency of electricity production and supply are no less relevant. The joint solution of these issues in electric power SMART and MicroGrid systems through the introduction of digital intelligent control tools that operate in real time ensures a positive effect [1-3]. These problems are directly related to the level of automation of electric SMART Grid power systems. In turn, the quality of operation of automated control systems of electric power networks of SMART technologies directly depends on the characteristics of time synchronisation signals used for conducting synchronised vector measurements, as well as on the effectiveness of methods for digital processing and analysis of measurement results data. To find the factual characteristics of time synchronisation signals, it is necessary to have hardware and software tools that ensure their continuous monitoring and processing of the received digital data [1; 4; 5]. The use of distributed synchronised vector measurements in transient modes (in real time) in SMART Grid power systems necessitates the development of software tools for digital processing and statistical analysis of measurement results for the implementation of effective power supply management in the field of intelligent energy [6; 7].

The construction of modern computerised power supply management complexes and networks for the field of intelligent energy based on monitoring the main characteristics in transient modes (in real time) involves the use of synchronised vector measurements [8-10]. The widespread use of functionally oriented PMU microprocessor equipment in the system of distributed synchronised vector measurements provides synchronous measurements of the main characteristics for various sections of the power network distributed in space, values of phase angles of voltages and currents synchronised with a single astronomical time [11; 12].

Thanks to the widespread use of GPS technology, it has become possible to create and implement distributed synchronised vector measurements (which ensure synchronisation of measuring instruments with an accuracy of the order of hundreds of nanoseconds). Information on the instantaneous values of the amplitude and phase, respectively, of voltage and current, registered in the same period (or moment) of time for different sections of the power grid, values of the speed of change of the phase angle of adjacent nodes of the power grid, and a list of other characteristics provides a modern level of knowledge about the properties of power networks and the specific features of the course of dynamic processes, as well as the possibility of direct observations of dynamic characteristics of power supply systems [7; 12; 13]. Notably, one can currently observe the increasing use of distributed synchronised vector measurements, an increase in the range of tasks for which they are used, namely the development of power grids with adaptive relay protection and automation, the detection of "hidden damage" in power grids with adaptive relay protection, the production of online control signals for automated prevention of a decrease in the level of stability in power grids and the elimination of asynchronous modes.

The widespread use of synchronised vector measurement technology in SMART Grid electric power systems can substantially reduce the uncertainty of primary information and improve the quality of processes for assessing the dynamics of electromechanical processes [7; 9]. Important in these processes is the use of software tools for digital processing and statistical analysis of the results of vector measurements, which determine the need for their further research, modernisation, and improvement for the implementation of effective power system management [10; 13].

It is problematic to use GPS signals as a reference sync signal for vector measurements [1; 5; 14]. Synchro signals generated solely by GPS signals cannot provide "high information survivability since they can be distorted, both in normal operation and in emergencies" [15]. The lack of sufficient reliability in providing SMART Grid time synchronisation signals to power systems leads to a decrease in the information reliability of the vector measurement process itself. To detect changes in time synchronisation signals, it is proposed to use computer-integrated systems that provide automated monitoring of time synchronisation devices [15; 16]. This approach will reduce the probability of accidents in smart grid power systems and, as a result, will help improve their energy efficiency. Modelling of dynamic energy consumption management scenarios using the inductive biclusterisation algorithm in the management of renewable energy sources is described in [6]. The web interface for an information system for diagnosing the quality of electricity consumers and monitoring synchronised vector measurements using cloud technologies is described in [17].

The purpose of this study was to develop and experimentally test the automated monitoring tools for time synchronisation devices and upgraded software tools for digital processing and statistical analysis of data from vector measurements of dynamic characteristics of SMART Grid power systems.

MATERIALS AND METHODS

To conduct experimental research in laboratory conditions and on the active IP networks, a developed laboratory stand with a quality control device for the formation of synchronous signals, two GPS receivers, and a reference high-stable thermostated quartz oscillator MXOCS were used. The study was performed in the problem-based research laboratory "Intelligent control systems in the agricultural industry" of the Department of Automation and Robotic Systems named after I. Martynenko (room 141, building 11, NULES of Ukraine). Experimental studies were performed according to the developed methods, structural and functional measurement schemes.

Automated monitoring of time synchronisation devices of distributed SMART Grid vector measurement tools of energy systems. Time synchronisation devices (TSD) of SMART Grid power systems are designed to generate sync signals that have prominent frequency stability. However, during their functioning, TSDs generate essentially quasi-periodic signals, to assess the quality indicators of which it is necessary to conduct measurements. Measurement of time characteristics is based on measurements of the relationships between the reference and controlled signal [18].

The parameter determined during the measurement process is a function called the time interval error function:

$$\mathrm{TIE}_t(\tau)=\mathrm{TI}_t(\tau)-\mathrm{TI}_{REF}(\tau), \quad (1)$$

where the time interval function $\mathrm{TI}_t(\tau)$ is found according to the equation $\mathrm{TI}_t(\tau)=T(t+\tau)-T(t)$.

Function $\mathrm{TI}_t(\tau)$ is a measure of the time interval τ, starting at the moment t, for the signal under study (provided that there is an ideal reference signal) [18]. Under such conditions, the time interval error function will have the following form:

$$\mathrm{TIE}_t(\tau)=\mathrm{TI}_t(\tau)-\tau. \quad (2)$$

In this case, the time interval function $\mathrm{TI}_{REF}(\tau)$ of the reference signal $\mathrm{TI}_{REF}(t)$ should be determined from the equation as follows:

$$\mathrm{TI}_{REF}(\tau)=\mathrm{TI}_{REF}(t+\tau)-\mathrm{TI}_{REF}(t). \quad (3)$$

Automated monitoring lies in performing continuous (24/7) real-time measurements of the parameters of the TSD output signals, transmission, digital processing of measurement results and decision-making based on the obtained data.

The automated monitoring system includes sensors that provide the primary conversion of a physical quantity into an electrical signal. As a result, the time interval is converted into electrical digital signals, which should be represented as digital data of measurement results [5; 15; 16].

Further data processing provides calculation of indicators for comparison with normalised values defined by international recommendations, standards, and technical specifications. For instance, the maximum time interval deviation (TID) corresponding to one measurement period is calculated according to the following formula [18]:

$$MTIE(n\cdot\tau_0)=\max_{1\le k\le N-n}\left[\max_{k\le i\le k+n}x(i)-\min_{k\le i\le k+n}x(i)\right] \quad (4)$$

where τ_0 – is the sampling period; $\tau=n\tau_0$ – is the observation interval; n=1,2,…,N; $\{x_i=x(i\tau_0)$, i=1,2,…$N\}$ –is a sequence of uniform discrete counts of the time error $x(t)$.

The operator solves the tasks of managing the work of SMART Grid energy systems based on the received data of the results of the measurements of the indicators of the time synchronisation signals and comparison with the normalised values. It is possible to increase the performance of the automated monitoring system by increasing the number of channels. Structurally, this possibility is implemented using the developed quality control device for synchronous signals formation (QCDSSF), the scheme of which is presented in Figure 1.

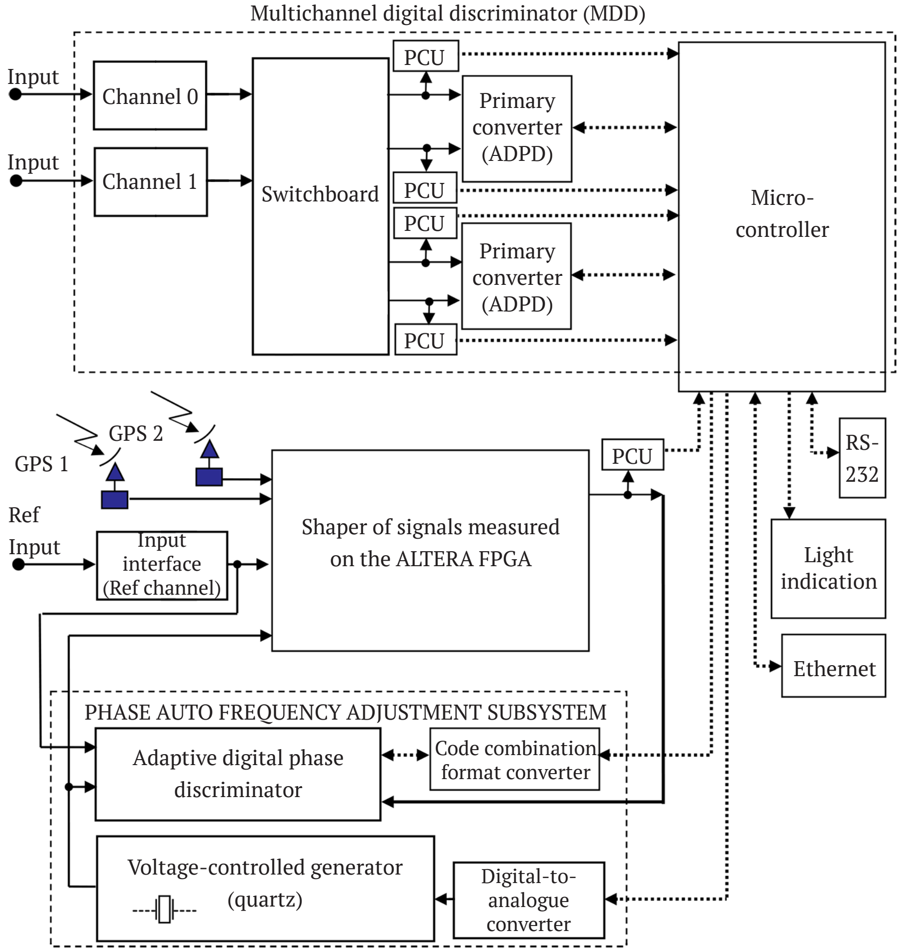

Figure 1. Block diagram of the quality control device for generating synchro signals

The device was built using a multichannel digital discriminator (MDD), the software and hardware implementation of which was performed using the Cyclone IV EP4CE10E22C8N programmable logic circuit. MDD performs the functions of a primary sensor, which provides the primary conversion of the error of the time interval (controlled indicator) into a digital signal in text format. Therewith, in the periodicity control unit (PCU) of the device (Fig. 1) the presence of pulse fronts on the clock interval of the controlled signal is checked. The results of these processes, which are presented in digital format, are processed by a microcontroller and prepared for transmission via RS-232 and Ethernet interfaces.

MDD is implemented using an adaptive digital phase discriminator (ADPD), which is protected by a Ukrainian patent for an invention [19]. The ADPD asynchronously, i.e., at any given time, without synchronising the measurement and reading processes, forms a code combination that determines the time ratio between the reference and controlled signal.

The developed QCDSSF device provides in an automated mode continuous monitoring of time synchronisation signals by performing simultaneous multichannel measurements of the instantaneous value of the deviation of the time interval relative to the reference synchronisation signal, which is formed by a voltage-controlled generator. The results of measurements of several time synchronisation signals (up to two simultaneously) are transmitted in text format via the IP network to a computer, where they are processed using software and presented to the SMART Grid operator of power systems for decision-making.

To conduct experimental studies of the automated monitoring system, a laboratory stand was developed with a quality control device for the formation of synchronous signals, two GPS receivers, and a MXOCS reference high-stable thermostated quartz generator were used. A photo of the laboratory stand is shown in Figure 2.

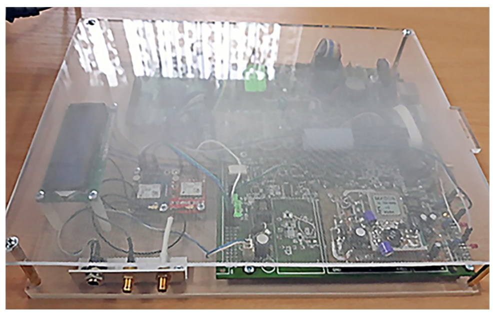

Figure 2. The appearance of a laboratory stand with a quality control device for the synchronous signals formation

The task of experimental studies was to check the technical specifications of the developed device for controlling the quality of clock signal generation. During the study, the accuracy of measurements of the deviation of the time interval of two time synchronisation signals of type 1-PPS (one pulse per second) relative to the reference sync signal, which is connected to the REF input, was checked (Fig. 1). Controlled time synchronisation signals of the 1-PPS type, formed by two GPS receivers, were connected to the corresponding inputs Input 1 and Input 2 of the device. Interaction of the developed laboratory stand with the computer was performed using the current local IP network of the NULES of Ukraine.

Digital processing of the obtained results of vector measurements of dynamic characteristics of SMART Grid power systems. The input information was an array of measured values of the vector format of electrical parameters [20] obtained from the ENIP-2 type PMU vector measurement device. This data was collected primarily for scientific purposes.

For further statistical processing and forecasting, a dataset containing 100 rows and 5 columns was created (Table 1). Digitised graphs are presented in Figure 3.

Table 1. Fragment of the generated data set

No.	f, Hz	I, A	U, V	I2, A
1	49.9803	2.0511	230.705	33.374
2	49.9669	2.0512	230.694	33.375
3	49.9942	0.0513	230.661	33.371
4	49.9982	2.0507	230.629	33.374
5	50.0154	2.0506	230.596	33.375
6	49.961	2.0508	230.552	33.373
7	50.0107	2.051	230.535	33.375
8	49.9887	2.0509	230.508	33.3735
9	49.9905	2.0512	230.469	33.3745
10	49.9715	2.0514	230.442	33.3735
11	49.9701	2.0512	230.42	33.369
12	49.9611	2.0514	230.409	33.375
13	49.9822	2.0513	230.381	33.372
14	49.9847	2.0513	230.359	33.3745
15	49.9821	2.0511	230.337	33.379

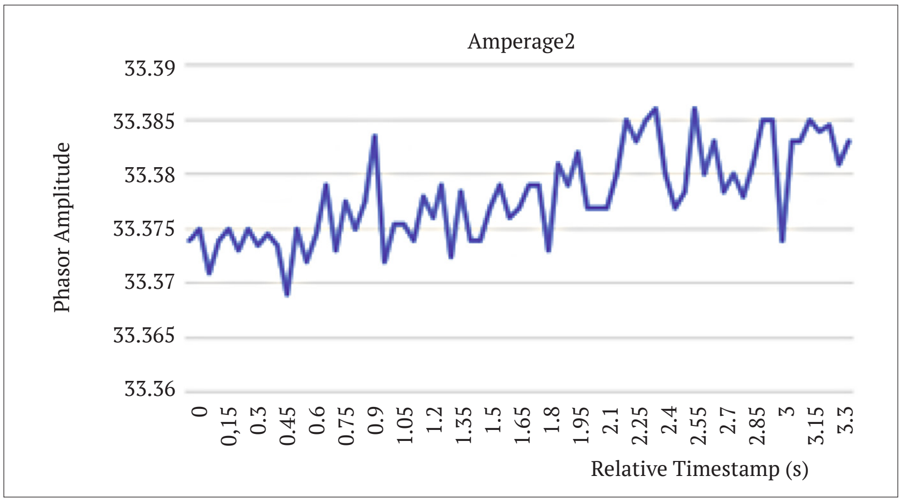

Figure 3. The appearance of a laboratory stand with a quality control device for the synchronous signals formation

Data structure. The data set is the characteristics of electricity (frequency, voltage, current). The dataset comprises a training dataset used to train and tune the model designed to predict values on the test data.

Eventually, the training set was divided into a training sample and a validation sample to evaluate the accuracy and quality of the models. The calculated statistical indicators for frequency, voltage, and current are presented in Table 2.

Table 2. Statistical characteristics of the measured parameters

Statistical characteristics	Frequency	Voltage	Current
Average values:	49.992	33.378	228.884
Median:	49.992	33.377	229.318
Maximum value:	50.024	33.386	230.705

For columns (1) and (2), the value of column (3) was predicted using two methods: KNN and Ridge regression.

The Predict matrix for data processing is presented in Table 3.

Table 3. Matrix for data processing

f, Hz	U, V
50.0228	228.569
49.9793	228.492
50.0041	228.404
50.0248	228.332
50.0233	228.272
49.9803	228.195
49.9734	228.113
49.9666	228.041
50.0249	227.926

Features of software implementation.

Features of the software implementation include:

– data reading and primary processing using the Pandas library;

– plotting graphs using the Matplotlib and Plotly express libraries;

– building a correlation table using the Seaborn library;

– data standardisation, splitting the training set into a training sample and validation sample, implementing classification models using the Scikit-Learn library.

Initially, the data was normalised for the highest accuracy of the calculation. An example of calculation based on normalised data is presented in Figure 4, without normalisation for Ridge regression – in Figure 5.

```
In [208]: from sklearn.linear_model import Ridge
          model = Ridge()
          model.fit(X_train_norm, Y_train)
          model.score(X_train_norm,Y_train)
Out[208]: 0.4774677178673772
```

Figure 4. Code snippet of the programme and calculation based on normalised data

```
In [209]: model.fit(X_train, Y_train)
          model.score(X_train,Y_train)
Out[209]: 0.45478502803711784
```

Figure 5. Code snippet of the programme and calculation based on data without normalisation

According to the normalised data, the accuracy of the model is higher. Columns (1), (2) are frequency and voltage, respectively. Predicted column (3) – current. The results of forecasting using the k-nearest neighbours algorithm (KNN) and the calculation accuracy of the method are presented in Figure 6, the predicted model is presented in Figure 7.

```
In [206]: model.score(X_train_norm, Y_train)
Out[206]: 0.6012872304007943
```

Figure 6. Code snippet of the programme and prediction results using the KNN method

```
In [207]: model.predict(X_prednorm)
Out[207]: array([33.3764, 33.3723, 33.3761, 33.3794, 33.383 , 33.38  , 33.3798,
                 33.3798, 33.3815])
```

Figure 7. Predictive model based on the KNN method

The Ridge regression method and the calculation accuracy of the method are presented in Figure 8. The predicted model is presented in Figure 9. The digital monitoring data obtained during experimental studies was stored in the computer's memory.

```
In [208]: from sklearn.linear_model import Ridge
          model = Ridge()
          model.fit(X_train_norm, Y_train)
          model.score(X_train_norm,Y_train)
Out[208]: 0.4774677178673772
```

Figure 8. Code snippet of the Ridge regression method and method calculation accuracy

```
In [210]: model.predict(pred)
Out[210]: array([33.38373138, 33.38404514, 33.38446656, 33.38480939, 33.38508349,
                 33.3853977 , 33.38576735, 33.38608706, 33.38666182])
```

Figure 9. Predictive model using the Ridge regression method

RESULTS AND DISCUSSION

Figure 10 presents digital monitoring data for time synchronisation signals of two GPS receivers, which were processed using Excel software. Based on the results of experimental studies, graphs of the dependence of time interval deviations (TID) of controlled time synchronisation signals generated by two GPS receivers were constructed. The upper graph presented in Figure 10 displays the results of monitoring the signal generated by the first GPS receiver, and lower graph – the second GPS receiver.

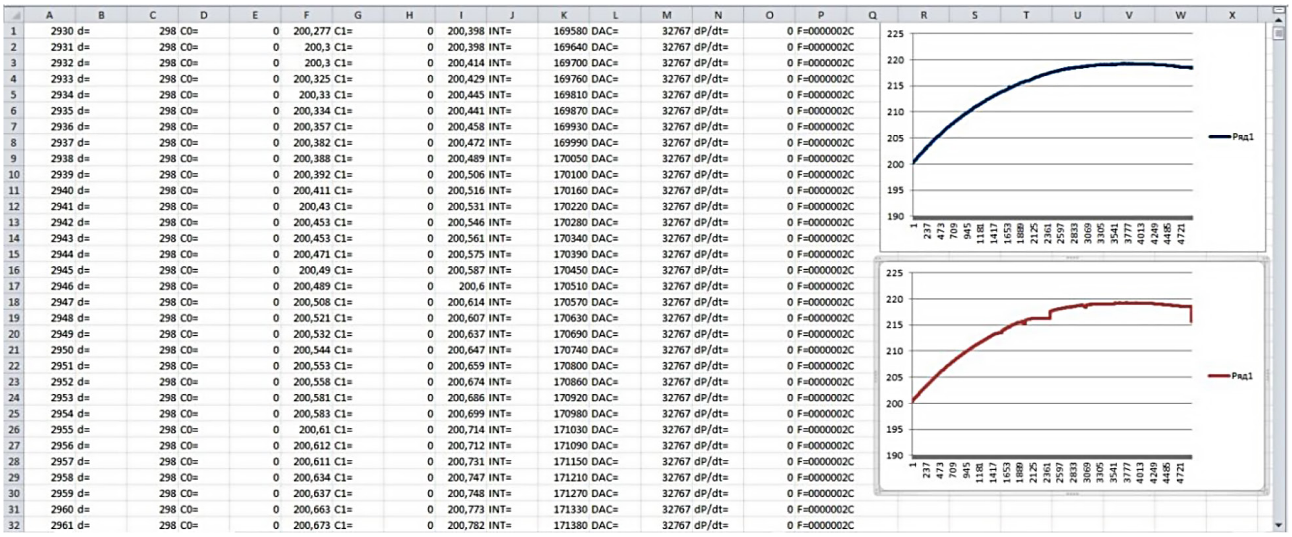

Figure 10. The results of experimental studies of the time synchronisation signals of two GPS receivers using a laboratory sample of the device for quality control of the formation of synchronous signals

Analysis of the results obtained confirms the technical capability of the device to perform simultaneous primary conversion of the deviation of the time interval of two controlled signals into a digital code with a quantisation step of less than 1 nanosecond. This result is sufficient for the practical implementation of the tasks of monitoring SMART Grid time synchronisation signals of power systems, which, according to the international standards IEEE C37.118.1-2011, IEEE C37.118.2-2011, must provide an accuracy of ±1 microsecond for synchronised vector measurements using synchrophasors [5].

Analysing the resulting forecast graph (Fig. 11), according to the normalised data, the accuracy of the Ridge regression model is 10-15% higher than the KNN method.

A diagram of the calculated predicted voltage values compared to the factual values is presented in Figure 12.

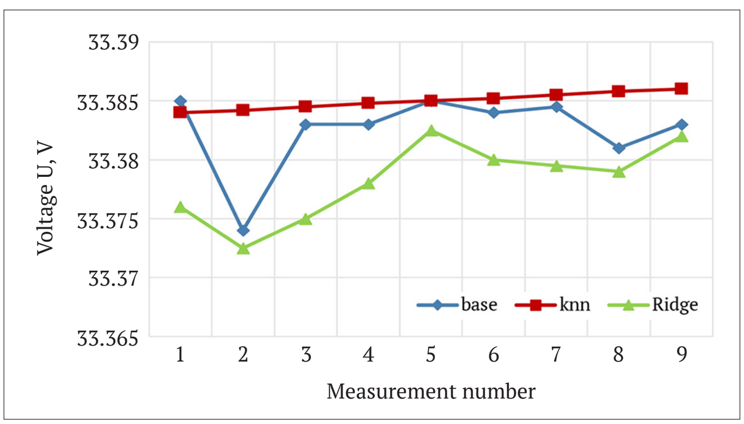

Figure 11. Graphical representation of output and projected data using KNN and Ridge regression methods

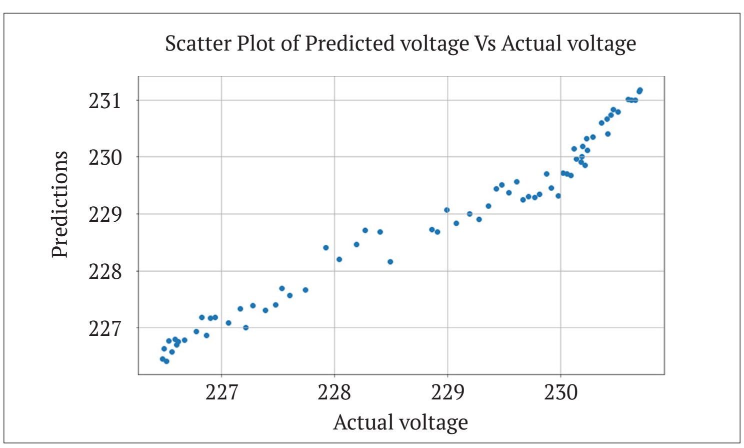

Figure 12. Graphical representation of output and projected data using KNN and Ridge regression methods

Analysing the resulting forecast graph (Fig. 12), according to the normalised data, the accuracy of the Random Forest Regression model is 5-10% higher than linear regression.

This study combined two tasks of diagnosing the quality of electricity vector measurements of SMART Grid power systems:

– conducting experiments on time synchronisation of two GPS receivers based on a previously developed laboratory stand;

– generating a dataset based on the results obtained and digitally processing the dynamic characteristics of electricity quality indicators.

In contrast to the publications [1; 17; 19] that were reviewed, this study presents the created software and hardware for automated diagnostics of digital signal synchronisation devices, which is an advanced system developed in Ukraine and tested in the current network of the National University of Life and Environmental Sciences of Ukraine. With the obtained real data, statistical processing was performed using various methods – KNN and Ridge regression, Random Forest Regression and linear regression, from which the best ones were selected – Ridge regression and Random Forest regression.

CONCLUSIONS

Based on the results obtained the following conclusions can be drawn:

1. Software tools were developed for digital processing and statistical analysis of a training data set in vector format of electrical parameters of SMART Grid energy systems, which provide the construction of a predictive model of electricity parameters, which is necessary for further decision-making.

2. The analysis of the obtained forecast graphs was performed, and it was concluded that according to the normalised data, the accuracy of the Random Forest Regression model is higher by 5-10%, while the accuracy of the Ridge regression model is higher by 10-15%.

3. As a result of experimental studies of the developed and manufactured device for quality control of the formation of synchronising signals as part of a laboratory stand, which is connected to the active local IP network of the NULES of Ukraine, the technical possibility of simultaneous monitoring of time synchronisation signals generated by two GPS receivers has been established. In this case, it is obvious to increase the performance of the developed monitoring device, compared to a single-channel one.

4. A comparative analysis of the obtained values of the deviation of the time interval with a quantisation step of 1 nanosecond and the norm of ±1 microsecond, which is set to the accuracy of the synchronising signals of vector measurements, indicates the practical possibility of solving the problems of monitoring time synchronisation signals with the manufactured device.

In the future, it is planned to develop the project, namely:

– within the framework of the research project, to purchase and connect several types of devices for vector measurements of PMU (synchrophasors) and integration into the information collection system at various facilities;

– to apply optimisation and decision-making methods for quality management at points where renewable generation sources are connected.

REFERENCES

[1] Yang, H., Wu, Q., He, C., & Chu, J. (2019). A high precision time synchronization method for smart grid based on Beidou satellite system. *IOP Conference Series: Materials Science and Engineering*, 490, article number 072006. doi: 10.1088/1757-899X/490/7/072006.

[2] Kopylova, L.O. (2018). *Intelligent automated control system for power consumption and power supply of an industrial enterprise* (Doctoral thesis, National University of Food Technology, Kyiv, Ukraine).

[3] Hatziargyriou, N., & Strbac, G. (2021). *MicroGrids – A possible future energy configuration?* Retrieved from http://www.MicroGrids.eu/micro2000/presentations/10.pdf.

[4] Skok, S., Frlan, K., & Ugarkovicc, K. (2017). Detection and protection of distributed generation from island operation by using PMUs. *Energy Procedia*, 141, 438-442.

[5] Koval, V., Kalian, D., Osinskiy, O., Samkov, O., Khudyntsev, M., & Lysenko, V. (2020). Diagnostics of time synchronization means of the integrated power grid of SMART technologies by using an optimal performance system of automatic frequency adjustment. In *Trends in radioelectronics, telecommunications and computer engineering, TCSET* (pp. 269-276). Lviv: National Forestry University of Ukraine.

[6] Osypenko, V., & Kaplun, V. (2019). Modeling of dynamic energy-management scenarios in local polygeneration microgrids using inductive bi-clustering algorithm. In *International scientific and technical conference on computer sciences and information technologies* (pp. 183-186). Kyiv: Igor Sikorsky Kyiv Polytechnic Institute.

[7] Moksli, R., Rzhepka, G., Jersonmec, Je., & Flenhinger, B. (2011). Application of all available results of synchronized vector measurements. In *International. scientific and technical conf. "Modern directions of development of relay protection systems and automation of power systems"* (pp. 239-240). St. Petersburg: St. Petersburg State University of Economics.

[8] Kyrylenko, O.V., Basok, B.I., Baseyev, Ye.T., & Blinov, I.V. (2020). Power industry of Ukraine and realities of the global warming. *Tekhnichna Elektrodynamika*, 3, 52-61. doi: 10.15407/techned2020.03.052.

[9] Kirilenko, O. (Ed.). (2016). *Intelligent electrical networks: elements and modes*. Kyiv: Institute of Electrodynamics of the National Academy of Sciences of Ukraine.

[10] Stasiuk, O.I., Zheleznyak, A.L., & Goncharova, L.L. (2015). *Mathematical models and methods of computer intellectualization of fast-moving technological processes of railway power supply*. Kyiv: Aspect-polygraph.

[11] Stogniy, B.S., Kyrylenko, O.V., Butkevych, O.F., & Sopel, M.F. (2009). Application of means of monitoring of transitional regimes in UES of Ukraine at the decision of problems of dispatching management. *Technical Electrodynamics*, 7, 27-35.

[12] Butkevich, O.F., Levkonyuk, A.V., & Stasiuk, O.I. (2014). Improving the reliability of monitoring the acceptability of loads of controlled sections of power systems. *Technical Electrodynamics*, 2, 56-57.

[13] Stasiuk, O.I., Honcharova, L.L., & Maksymchuk, V.F. (2014). Methods of organizing intelligent electrical networks of railways based on the concept of SMART Grid. *Information and Control Systems for Railway Transport*, 2, 29-37.

[14] Lo, C.-H., & Ansari, N. (2011). The progressive smart grid system from both power and communications aspects. *IEEE Communications Surveys & Tutorials*. Vol. 14, No. 3. P. 799-821. doi: 10.1109/SURV.2011.072811.00089.

[15] Höller, R., Gridling, G., Horauer, M., Kerö, N., Schmid, U., & Schossmaier, K. (2002). SynUTC – high precision time synchronization over ethernet networks. In *8th workshop on electronics for LHC experiments* (pp. 428-432). Colmar: University of Strasbourg. doi: 10.5170/CERN-2002-003.428.

[16] Wang, D., Jiang, T., Liu, C., Zhou, S., & Yu, S. (2018). Stable radio frequency dissemination via a 1007 km fiber link based on a high-performance phase lock loop. *Optics Express*, 26(19), 24479-24486. doi: 10.1364/OE.26.024479.

[17] Kiktev, N., Kutyrev, A., Khort, D., & Kalivoshko, O. (2021). Web application for an information system for diagnosing the quality of electricity consumers using cloud technologies. *Information Technology and Implementation. CEUR Workshop Proceedings*, 3132, 176-185.

[18] Bregni, S. (2003). *Synchronization of digital telecommunications networks: Translation from English*. Moscow: Mir.

[19] Patent for invention No. 113473, Ukraine. Retrieved from http://uapatents.com/6-113473-adaptivnijj-cifrovijj-fazovijj-diskriminator.html.

[20] Leibovich, P., Issouribehere, F., & Barbero, J. (2019). Synchrophasor communication over Internet: Performance analysis of different methods based on real experiences. In *2019 IEEE power & energy society general meeting* (pp. 10-23). Atlanta: Georgia State University. doi: 10.1109/PESGM40551.2019.8973792.

СПИСОК ВИКОРИСТАНИХ ДЖЕРЕЛ

[1] Yang H., Wu Q., He C., Chu J. A high precision time synchronization method for smart grid based on Beidou satellite system. *IOP Conference Series: Materials Science and Engineering*. 2019. Vol. 490. Article number 072006. doi: 10.1088/1757-899X/490/7/072006.

[2] Копилова Л.О. Інтелектуальна автоматизована система керування електропостачанням та електроспоживанням промислового підприємства: атореф. дис.…канд. техн. наук: 05.13.07. Київ: Національний університет харчових технологій, 2018. 153 с.

[3] Hatziargyriou N., Strbac G. MicroGrids – A possible future energy configuration? URL: http://www.MicroGrids.eu/micro2000/presentations/10.pdf.

[4] Skok S., Frlan K., Ugarkovicc K. Detection and protection of distributed generation from island operation by using PMUs. *Energy Procedia*. 2017. Vol. 141. P. 438–442.

[5] Diagnostics of time synchronization means of the integrated power grid of SMART technologies by using an optimal performance system of automatic frequency adjustment / V. Koval et al. *Trends in radioelectronics, telecommunications and computer engineering, TCSET*: 15th international conference on advanced 2020 (Lviv-Slavske, 25 Feb. 2020). Lviv, 2020. P. 269–276.

[6] Osypenko V., Kaplun V. Modeling of dynamic energy-management scenarios in local polygeneration microgrids using inductive bi-clustering algorithm. *International scientific and technical conference on computer sciences and information technologies* (Kyiv, 17-20 Sept. 2019). Kyiv, 2019. P. 183–186.

[7] Моксли Р., Ржепка Г., Эрсонмец Э., Фленхингер Б. Применение всех доступных результатов синхронизированных векторных измерений. *Современные направления развития систем релейной защиты и автоматики энергосистем*: материалы междунар. науч.-техн. конф. (г. Санкт-Петербург, 03 июня 2011 г.). Санкт-Петербург, 2011. С. 239–240.

[8] Кириленко О.В., Басок Б.І., Базєєв Є.Т., Блінов І.В. Енергетика України та реалії глобального потепління. *Технічна електродинаміка*. 2020. № 3. С. 52–61. doi: 10.15407/techned2020.03.052.

[9] Інтелектуальні електричні мережі: елементи та режими / за ред. О.В. Кириленко. Київ: Ін-т електродинаміки НАН України, 2016. 400 с.

[10] Стасюк О.І., Железняк А.,Л., Гончарова Л.Л. Математичні моделі і методи комп'ютерної інтелектуалізації швидкоплинних технологічних процесів електропостачання залізниці. *Інформаційно-керуючі системи на залізничному транспорті*. 2015. № 1. С. 3–10.

[11] Стогній Б.С., Сопель М.Ф., Варський Г.М., Яковлєва І.В. Трифазні вимірювальні канали напруги та струму, їх вплив на точність вимірювання. *Технічна електродинаміка*. 2014. № 1. С. 81–87.

[12] Буткевич О.Ф, Левконюк А.В., Стасюк О.І. Підвищення надійності моніторингу допустимості завантажень контрольованих перетинів енергостистем. *Технічна електродинаміка*. 2014. № 2. С. 56–57.

[13] Стасюк О.І., Гончарова Л.Л., Максимчук В.Ф. Методи організації інтелектуальних електричних мереж залізниць на основі концепції SMART Grid. *Інформаційно-керуючі системи на залізничному транспорті*. 2014. № 2. С. 29–37.

[14] Lo C.-H., Ansari N. The progressive smart grid system from both power and communications aspects. *IEEE Communications Surveys & Tutorials*. 2011. Vol. 14, No. 3. P. 799–821. doi: 10.1109/SURV.2011.072811.00089.
[15] SynUTC – high precision time synchronization over ethernet networks / R. Höller et al. *8th workshop on electronics for LHC experiments* (Colmar, 9-13 Sept. 2002). Colmar, 2002. P. 428–432. doi: 10.5170/CERN-2002-003.428.
[16] Stable radio frequency dissemination via a 1007 km fiber link based on a high-performance phase lock loop / D. Wang et al. *Optics Express*. 2018. Vol. 26, No. 19. P. 24479–24486. doi: 10.1364/OE.26.024479.
[17] Kiktev N., Osypenko V., Kalivoshko, O., Kutyrev A. Information system for decision-making in the management of renewable energy sources in the microgrid system. *Information Technology and Implementation. CEUR Workshop Proceedings*. 2021. Vol. 3132. P. 176–185.
[18] Брени С. Синхронизация цифровых сетей связи. Москва: Мир, 2003. 456 с.
[19] Leibovich P., Issouribehere F., Barbero J. Synchrophasor communication over Internet: Performance analysis of different methods based on real experiences. *2019 IEEE Power & Energy Society General Meeting* (Atlanta, 4–8 Aug. 2019). Atlanta, 2019. P. 10–23. doi: 10.1109/PESGM40551.2019.8973792.
[20] Патент на винахід № 113473, Україна. URL: http://uapatents.com/6-113473-adaptivnijj-cifrovijj-fazovijj-diskriminator.html.

Валерій Вікторович Коваль[1], Віталій Пилипович Лисенко[1], Микола Олександрович Кіктєв[1], Юрій Володимирович Пилипенко[2], Олександр Всеволодович Самков[2], Олександр Леонідович Осінський[2], Іван Олександрович Попов[3]

[1]Національний університет біоресурсів і природокористування України
03041, вул. Героїв Оборони, 15, м. Київ, Україна

[2]Інститут електродинаміки Національної академії наук України
03057, просп. Перемоги, 56, м. Київ, Україна

[3]Одеський державний екологічний університет
65016, вул. Львівська, 15, м. Одеса, Україна

Автоматизований моніторинг пристроїв синхронізації часу та цифрова обробка векторних вимірювань динамічних характеристик SMART Grid енергосистем

Анотація. В теперішній час клієнти енергокомпаній використовують пристрої для вироблення електроенергії (сонячні панелі, вітряки та ін.) і для економії витрат або для отримання доходу повертають енергію в мережу. Тому актуальним є вирішення задачі створення автоматизованої системи діагностування якості електроенергії споживачів, які використовують відновлювальні джерела електроенергії. Мета дослідження – підвищення ефективності керування в інтелектуальних SMART Grid енергосистемах. Для її реалізації запропоновано використання автоматизованої системи моніторингу синхросигналів мікропроцесорного обладнання PMU та програмних засобів цифрової обробки і статистичного аналізу результатів синхронізованих векторних вимірювань динамічних характеристик енергомереж. Розроблено програмні засоби цифрової обробки та статистичного аналізу отриманих даних векторних вимірювань. Для аналізу та прогнозування показників якості електроенергії використовуються методи лінійної регресії, Random Forest Regression та Ridge regression. Наведено результати порівняльного аналізу отриманих результатів прогнозної моделі. Для проведення експериментальних досліджень розроблено та виготовлено лабораторний зразок пристрою контролю якості формування синхросигналів, від яких безпосередньо залежить достовірність цифрових даних розподілених синхронізованих векторних вимірювань у перехідних режимах (в реальному часі). Багатоканальність пристрою забезпечує підвищення продуктивності та надійності системи автоматизованого моніторингу. Наведено результати експериментальних досліджень пристрою у складі розробленого лабораторного стенду, який підключено до діючої локальної IP-мережі НУБіП України. Практична значущість проведених експериментальних досліджень полягає у встановлені технічної можливості одночасного моніторингу сигналів синхронізації часу, що формуються двома приймачами GPS. У цьому разі очевидним є збільшення продуктивності розробленого та виготовленого пристрою контролю якості формування синхросигналів, в порівнянні з одноканальним. Матеріал може бути корисним інженерам, які проектують електричні системи з підключенням відновлювальних джерел енергетики

Ключові слова: відновлювальні джерела електроенергії, синхронізовані векторні виміри, багатоканальний пристрій, контроль якості формування синхросигналів, моніторинг синхросигналів, модель Ridge regression, прогнозування показників електроенергії

Machinery & Energetics
Vol. 13, No. 2. 2022

Journal homepage:
https://technicalscience.com.ua/en

UDC 621.867
DOI: 10.31548/machenergy.13(2).2022.83-90

Yuriy Romasevych*, Viatcheslav Loveikin, Oleg Malinevsky

National University of Life and Environmental Sciences of Ukraine
03041, 15 Heroiv Oborony Str., Kyiv, Ukraine

The Method of Calculating the Maximum Torque When Jamming the Auger of the Screw Conveyor

Abstract. The designs of screw conveyors contain safety clutches that ensure the avoidance of breakdowns in emergencies (e.g., when the auger is jammed). Therefore, the choice of these clutches is a relevant scientific problem, which is related to the calculation of the maximum torque of the auger. The purpose of this study was to develop a method for calculating the maximum torque when the auger of a screw conveyor is jammed. The method developed in this paper article is based on the use of an artificial neural network trained using the "supervised learning" technology. The training and test data set for the artificial neural network was obtained by conducting machine experiments, each of which consisted in the numerical integration of a nonlinear differential equation and the determination of the value of the maximum torque in the elastic connection of the dynamic system based on the obtained solution. The specified differential equation is obtained based on the equation of motion of the non-jammed part of the conveyor (drive, gears, clutch) and the Kloss equation, which corresponds to the model of the mechanical characteristics of the conveyor asynchronous motor. The statistical significance of the results of an artificial neural network was proved by analysing the values of approximation quality indicators. A brief analysis of the influence of the stiffness of the elastic connection of the dynamic conveyor system and the drive gear ratio, as well as the overloading capacity of the engine on the maximum torque that occurs when the screw is jammed, was performed. The practical significance of the results obtained is related to the software implementation of the method, which allows engineers to effectively select safety clutches upon designing screw conveyors

Keywords: mathematical modelling, approximation, numerical experiments, artificial neural network

Article's History: Received: 02.11.2021; Revised: 25.02.2022; Accepted: 27.04.2022.

INTRODUCTION

Screw conveyors are widely used in modern agricultural and industrial production. This is explained by their high performance, reliability, ease of operation, etc. During the operation of such machines, emergencies may occur that are caused by the jamming of hard particles (cargo, pebbles, etc.) in the gap between the auger edge and the conveyor trough. This case causes the auger to jam and the safety clutch to trigger. Therefore, the correct choice of such a clutch at the stage of conveyor calculations allows avoiding premature failure of the conveyor engine. The main parameter that determines the choice of a particular safety clutch is the maximum torque that it can transmit. Exceeding this torque leads to disconnection of the kinematic connection between the clutch halves and makes it impossible for mechanical gears and the conveyor drive motor to fail.

The calculation of the clutch torque limit value should reflect the main dynamic parameters of the conveyor and its drive parameters. Well-known engineering methods of such calculations only approximately allow considering these factors, which can lead to incorrect choice of the safety clutch. Thus, this issue transcends engineering calculations and is the subject of scientific research. The result of such a study is a scientifically sound method for calculating the maximum drive torque of a screw conveyor when the auger is jammed, which allows considering all significant factors affecting the amount of torque.

To establish the current level of technological developments in the field of designing individual elements of screw conveyors, the website of the German patent office was used [1]. Using this resource, data was obtained on the number of received patents in the world under International Patent Classification (IPC) B65G33/24 "Screw or rotating spiral conveyors. Details", B65G33/34 "Screw or rotating spiral conveyors. Details. Drives". The received data is valid as of 04/16/2022 (Table 1).

Suggested Citation:
Romasevych, Yu., Loveikin, V., & Malinevsky, O. (2022). The method of calculating the maximum torque when jamming the auger of the screw conveyor. *Machinery & Energetics,* 13(2), 83-90.

*Corresponding author

Table 1. Number of patents received in the world by individual classes

Class	Years				
	2018	2019	2020	2021	2022
B65G33/24	856	891	1579	2098	585
B65G33/34	199	272	617	698	138

Source: compiled by the author based on [1]

Analysis of data from Table 1 suggests a substantial increase in the number of patents for both classes since 2020. This trend continued in subsequent years. Admittedly, this reflects the interest of conveyors developers in improving their designs. Certain improvements to screw conveyors should be scientifically sound. Therefore, this study analysed the content of scientific publications related to the design and operation of these machines.

In [2], a model of a screw conveyor is investigated and the influence of the size of a discrete load particle, external and internal friction forces on the main operational and technical parameters of the conveyor was established. The paper also confirms theoretical results by comparing them with experimental data obtained in the laboratory.

In [3], the design of a vertical conveyor screw with a variable diameter was proposed. As shown in this study, this allows increasing the capacity of the conveyor. A common feature of research in [2; 3] is the use of bulk medium models based on the discrete element method.

The study [4] presents a model of a screw conveyor developed in the ANSYS software environment. This research allowed establishing the influence of conveyor parameters on screw vibrations in the vertical and horizontal directions. The results of this study allow avoiding resonant phenomena during the operation of these machines.

Fuzzy logic was used to establish relationships between the technical and operational characteristics of screw conveyors and their parameters in [5]. Here, a rule base was constructed, and a complex functional dependence was obtained on its basis, which allowed obtaining two sets of optimal values for the speed of rotation of the screw, its pitch and the angle of inclination of the conveyor. For the first case, the volumetric capacity of the machine is maximum, and for the second – its energy efficiency.

Thus, the issue of calculating dynamic processes that take place in a screw conveyor is quite an extensive and urgent task. Solving certain aspects of this issue will contribute to more advanced screw conveyor designs. This particularly refers to the problem of determining the maximum value of the conveyor screw torque, since it has a substantial impact on the choice of the safety clutch of its drive.

The purpose of this study was to develop a method for calculating the maximum torque when jamming a screw conveyor auger. Fulfilling this purpose required to solve the following tasks: 1) conduct mathematical modelling of the process of jamming the conveyor auger; 2) conduct numerical experiments and obtain a tabulated function of the maximum torque of the screw conveyor when it is jammed; 3) based on the tabulated function, to train an artificial neural network and prove the statistical significance of the results of its work; 4) assess the influence of individual factors on the value of the maximum torque when the auger of the screw conveyor is jammed and indicate the prospects for further research in this area

MATERIALS AND METHODS

To illustrate the essence of the problem considered in this study, a kinematic diagram of the conveyor is presented below (Fig. 1). It corresponds to typical designs of belt-driven screw conveyors [6-8].

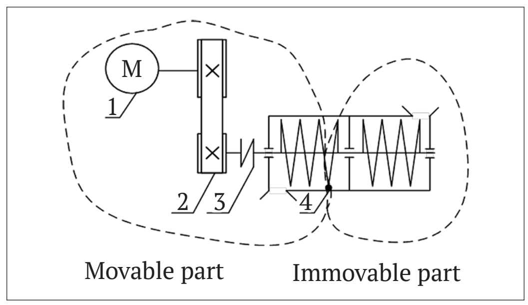

Figure 1. Kinematic scheme of a screw conveyor with a jammed auger

In Figure 1 the following designations are used: 1 – motor; 2 – belt drive (the most elastic element of the drive); 3 – safety clutch; 4 – place of jamming of the conveyor auger. Based on Figure 1, a dynamic model of the movement of a screw conveyor with a jammed auger was developed. For this purpose, the inertial, elastic, and dissipative properties of the dynamic conveyor system, as well as the mechanical characteristics of its drive, were considered (Fig. 2), and when constructing the model, methods of machine dynamics were used [9].

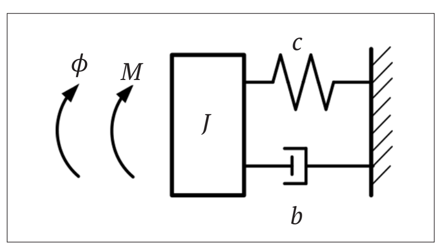

Figure 2. Dynamic model of screw conveyor movement when the auger is jammed: M is the driving torque of the drive; J is the reduced moment of inertia of the drive; b is the reduced drive dissipation factor; c is the reduced drive stiffness coefficient (in the case under study – of the belt drive

In Figure 2, all values are reduced to the auger shaft of the elastic connection of the drive.

When constructing a dynamic model, the following assumptions were used: 1) the part of the auger that continues to move after jamming (from position 3 to 4 in Fig. 1), has an insignificant moment of inertia in comparison with the moment of inertia of the drive, and therefore it is not considered; 2) the part of the auger that continues to move after jamming is an absolutely rigid body; 3) there is no dissipation in the part of the auger that continues to move after jamming.

A mathematical model that corresponds to a dynamic model (Fig. 2), is represented by a second-order differential equation (1):

$$M = J\ddot{\phi} + b\dot{\phi} + c\phi. \tag{1}$$

Driving torque M is created by an asynchronous motor, the mechanical characteristic of which is described by the Kloss equation [10] (2):

$$M = \frac{2\lambda M_n U\eta}{A\dot{\phi} + (A\dot{\phi})^{-1}}, \tag{2}$$

where A is the constant coefficient, the value of which is determined by the drive parameters

$\left(A = \dfrac{60 f_n U}{p\left(\dfrac{60 f_n}{p} - n_n\right)\left(1 + \lambda\sqrt{\lambda^2 - 1}\right)}\right)$; f_n is the rated frequency of the motor supply voltage (f_n=50 Hz); n_n is the rated engine speed, rpm; λ is the engine overload capacity; p is the number of pairs of motor poles; U s the drive gear ratio; η is the drive efficiency.

Substituting (2) in (1) allows obtaining a nonlinear differential equation that cannot be integrated analytically. Therefore, to determine the solution, it is necessary to apply one of the numerical methods [11]. For this, one needs to set the initial conditions for the system's movement. Since this study considered the case when auger jamming occurs when the conveyor is operating in the nominal mode, it is obvious that the elastic connection of the drive c is loaded with the torque of resistance M_0, i.e., $\phi(0)=M_0/s$. To find the angular velocity of the system, it is necessary to substitute M_0 in equation (2) instead of M and solve the resulting quadratic equation with respect to $\dot{\phi}$. To simplify calculations, it was assumed that the torque of resistance M_0 corresponds to the rated engine torque $M_0 = M_n U\eta = \frac{30P_n}{\pi n_n}U\eta$, i.e., the conveyor drive operates in the nominal mode before it gets jammed. From the two roots of the quadratic equation, the authors chose the one that corresponded to the drive motion in the first quadrant of the mechanical characteristic:

$$\dot{\phi}(0) = \frac{\pi}{30pP_nU^3}\Big(n_np\big(P_nU^2\eta\lambda(1+\lambda\sqrt{\lambda^2-1}\big) + \frac{P_nU^2}{n_np}(n_np - 60f)\sqrt{(\eta^2\lambda^2-1)\left(1-\lambda^2+\lambda^4+2\lambda\sqrt{\lambda^2-1}\right)} - 60fP_nU^2\big(\eta\lambda(1+\lambda\sqrt{\lambda^2-1}) - 1\big)\Big) \tag{3}$$

Thus, having found the initial conditions of motion of the system and having the equations of its motion (1), (2), a solution of the equation can be obtained for certain numerical values of system parameters (n_n, P_n, λ, U, c). In this study, it was also assumed that b=0 because, as will be shown later, the duration of the increase in torque to the maximum value during jamming is so insignificant that the influence of dissipative forces can be ignored.

For numerical integration of the nonlinear differential equation (1), a condition was used that sets the moment when the integration stops. This condition corresponds to the zero angular velocity of the dynamic system.

Figure 3 shows the results of integration of equations (1), (2) for the following parameters: n_n=720 rpm, P_n=2.2 kW, λ=2.2, U=10, c=10 kNm/rad. As Figure 3 demonstrates, the duration of the conveyor stop is 0.0283 seconds.

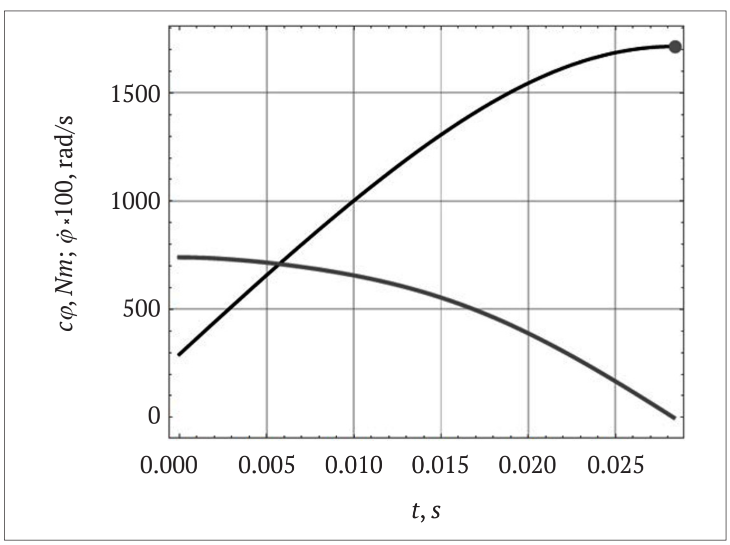

Figure 3. Graphs of changes in the elastic torque and angular velocity of a dynamic system

When the system stops, there is a rapid increase in the elastic torque. To exclude the failure of the mechanical elements of the drive caused by the action of this torque, it is necessary to choose the right safety clutch. However, its definition by numerical integration is irrational. This is explained by the need to attract considerable computational resources, which are spent on direct numerical integration of the corresponding differential equation, tabbing the elastic torque function, and then determining its maximum value $M_{c.max}$ (indicated in Fig. 3 with a grey dot). Therefore, it is advisable to obtain a tabulated function of the maximum values of the elastic torque whose arguments are the parameters n_n, P_n, λ, U, c. In the future, using one of the known approximation methods, one needs to get the function $M_{c.max}=f(n_n, P_n, \lambda, U, c)$.

Thus, building a tabulated function Mc.max is factually a machine experiment. Therewith, the limits of changes in independent factors n_n, P_n, λ, U, c were selected from the conditions of coverage of screw conveyor structures, which are most often found in practice (Table 2).

Table 2. Independent factors of machine experiment and their levels

Independent factor	Unit of measurement	Value
n_n	rpm	720, 900, 1,400, 2,850
P_n	kW	0.75, 1.1, 1.5, 2.2, 3.0
λ	–	1.8, 1.9, 2.0, 2.1, 2.2, 2.3, 2.4, 2.5
U	–	2, 3, 4, 5, 6, 7, 8, 9, 10, 11, 12, 13, 14, 15, 16, 17, 18, 19, 20, 21
c	kNm/rad	1, 2, 3, 4, 5, 6, 7, 8, 9, 10

The moment of inertia of the system was determined according to the expression J=1.3$J_{en}U^2$ (here J_{en} is the moment of inertia of the engine, which for various brands of engines of the AIR series is selected from the catalogue [12]; 1.3 is a coefficient that considers the inertial characteristics of other drive elements: pulleys, connecting clutches, etc.).

Consequently, 32,000 machine experiments were performed and a tabulated function Mc.max was formed. The next step in the study was to find a relationship that would be able to approximate the data obtained with a sufficient degree of accuracy. The classical approach to achieving this goal is to apply regression analysis [13]. However, it did not allow getting the desired model. To illustrate this thesis without delving into the method for calculating regression models, see Table 3, where the main results of this approach are presented (for compactness of writing, independent factors are indicated by symbols x with the corresponding indexes respective to their order).

Table 3. Results of applying regression analysis to calculate the model $M_{c.max}=f(n_n, P_n, \lambda, U, c)$

Model	Value of the determination coefficient R^2
$A_0+\sum_{i=1}^{5}A_i x_i$	0.644
$A_0+\sum_{i=1}^{5}\sum_{j=1}^{5}A_{i.j}x_i x_j$	0.814
$A_0+\sum_{i=1}^{5}\sum_{j=1}^{5}\sum_{k=1}^{5}A_{i.j.k}x_i x_j x_k$	0.863
$A_0+\sum_{i=1}^{5}\sum_{j=1}^{5}\sum_{k=1}^{5}\sum_{q=1}^{5}A_{i.j.k.q}x_i x_j x_k x_q$	0.888

Analysis of R^2 values shows that an increase in the complexity of the regression model does not lead to a substantial improvement in the quality of the approximation. This means that none of the regression models used can qualitatively approximate the tabulated function $M_{c.max}$. Therefore, this approach should be considered ineffective for this task.

An alternative to regression analysis in approximation problems is the use of artificial neural network (ANN) technologies [14]. Based on these considerations, the authors of this study attempted to develop such an ANN that would allow obtaining a high-quality approximation of the tabulated function $M_{c.max}$. For this, the architecture of the ANN was set as follows: it has five inputs (according to the number of independent factors) and one output (value $M_{c.max}$); two hidden layers of the ANN include ten neurons each; the activation function of each neuron is a hyperbolic tangent.

According to the generally accepted approach to ANN training, the overall data sample should be normalised. In this study, the following equation (4) was used:

$$\tilde{x}_i = 2\frac{x_i - x_{i.min}}{x_{i.max} - x_{i.min}} - 1, \tag{4}$$

where $\tilde{x}_i$ is the normalised value of i^{th} independent factor that changes within [-1, 1]; $x_{i.max}$ and $x_{i.min}$ are the maximum and minimum values of the ith independent factor. In the future, the normalised data sample should be divided into training (includes 25,645 elements) and test (includes 6,355 elements), and the individual elements of the original sample with this division are selected randomly so that the trained ANN can cover as many possible sets of parameters of screw conveyors as possible.

ANN training was performed using the ADAM method [15]. The metaeuristic methods ME-D-PSO [16] and RotRing-PSO [17] were used for the same purpose.

RESULTS AND DISCUSSION

The use of these metaeuristic methods [16; 17] leads to almost identical results. They were as follows:

– weight matrix of the first layer W_1=[{-0.11, 0.529, 0.119, 0.227, -0.073}, {-1.397, 0.434, -0.067, -0.05, 0.079}, {0.404, -0.331, 0.09, 0.128, 0.102}, {-0.063, 0.012, -0.017, -0.015, -0.616}, {0.607, 0.197, -0.009, 0.036, 0.084}, {0.126, -0.31, 0.008, 0.004, -0.391}, {0.193, -1.768, -0.019, -0.018, 0.072}, {-0.412, -2.058, -0.019, -0.01, 0.361}, {0.934, -0.288, -0.074, -0.127, 0.182}, {-1.339, -0.04, 0.035, -0.083, -0.11}];

– vector of biases of the first layer B_1=[-0.7, -0.844, 0.072, 0.051, 0.099, -0.14, 0.442, -0.346, -0.733, 0.042];

– weight matrix of the second layer W_2=[{1.517, 0.742, -0.317, -0.172, -3.434, 0.063, 0.552, 0.741, -0.178, 0.307}, {0.526, 0.432, 0.272, 0.171, 0.641, -0.086, 0.584, -0.451, 0.646, 0.336}, {-0.133, 0.034, -0.22, -0.732, 0.733, -0.575, -0.105, -0.309, 0.535, 0.223}, {-0.499, -0.921, 0.296, 0.151, -0.976, 0.502, 0.112, 0.288, -0.742, 0.195}, {0.064, -0.028, -0.257, -0.104, -0.473, 0.257, -0.011, -0.381, -0.169, 0.155}, {-0.57, 0.111, -0.017, -0.1, 0.02, -0.04, -0.456, -0.398, 0.135, -0.952}, {1.345, 2.308, -1.444, -0.673, -0.978, 0.552, -3.741, -0.366, -0.33, 1.042}, {0.047, 1.848, 0.728, 0.821, 0.291, -1.917, -0.143, -2.253, 0.492, 0.517}, {0.668, -0.566, -0.553, 0.585, -1.201, 0.082, 0.543, 0.454, -0.64, -0.266}, {-0.253, -0.536, 0.32, -0.257, -0.474, 0.408, -0.908, -0.11, 0.184, -0.628}];

– vector of biases of the second layer B_2=[-0.054, 0.13, -0.453, 0.447, -0.005, 0.155, -0.502, -0.326, 0.36, 0.008];

– weight matrix of the third layer W_3=[-0.498, 0.986, -0.517, -0.677, -0.913, -1.091, -0.836, 1.337, -0.648, -0.835];

– bias of the third layer B_3=0.103.

The presented numerical data allow reproducing the ANN in software environments (this is relevant for the practical implementation of the research results).

Thus, a trained ANN was obtained that can approximate the tabulated function $M_{c.max}$, i.e., it is a contender for the sought model $M_{c.max}=f(n_n, P_n, \lambda, U, c)$. To determine whether the resulting ANN can represent a model $M_{c.max}$=f(n_n, P_n, λ, U, c), a test sample was used to calculate several statistical indicators of approximation quality (Table 4).

Table 4. Approximation quality indicators using ANN

Statistical indicator	Unit of measurement	Value
Scope of variation	Nm	334.3
Standard deviation	Nm	23.3
Variation coefficient	%	1.7
*Determination coefficient R^2	–	0.9996

Note: *R^2 value was calculated based on a training sample

Analysis of the data from Table 4 shows a fairly high-quality approximation, which is performed using a trained ANN. To evaluate it in more detail, here is Figure 4 (index n shows the item number in the sample).

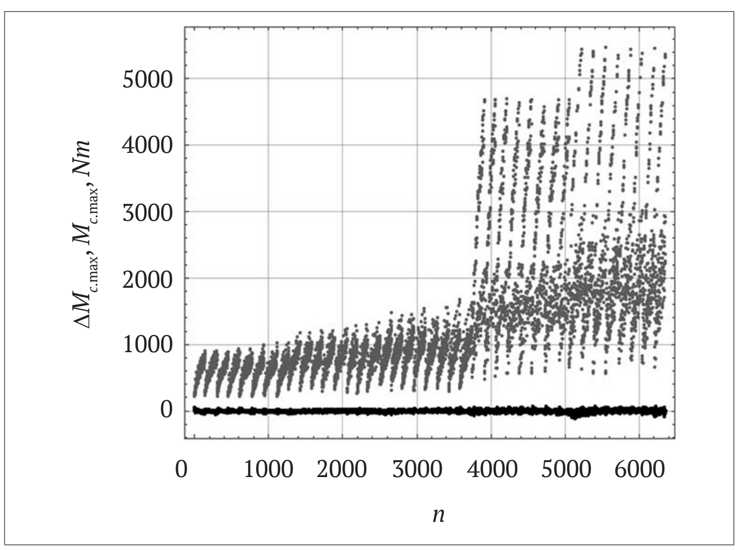

Figure 4. Test sample data (grey points) and absolute approximation error $\Delta M_{c.max}$ (black points)

From Figure 4, it is impossible to follow the dependence of the response on independent factors; however, this dependence is non-linear. This factor prevented the construction of a working regression dependence (Table 3).

Numerical values of indicators (Table 4), as well as a graphical dependency (Fig. 4) allow drawing a conclusion about the acceptability of using a trained ANN to assess the values of $M_{c.max}$. Thus, the results (trained ANN) fully correspond to the methodology for obtaining a dependency model $M_{c.max}=f(n_n, P_n, \lambda, U, c)$, which is described in the previous section.

In practical terms, estimating the value of $M_{c.max}$ must be performed using specially developed software. It can be a separate module, or it can be integrated into a common set of software products that are used by design engineers to build screw conveyors.

To present the results of the work of the trained ANN, calculations of Mc.max were performed for several variants of independent factors *c* and *U* (Fig. 5). It should be recalled that the latter considerably affects the inertial properties of the system.

Figure 5 shows equipotential lines that indicate which levels of $M_{c.max}$ they correspond to. Analysis of graphic dependences presented in Figure 5 show that their nature of change for different λ is somewhat similar. Furthermore, the graphs (Fig. 5) show the influence of *c* and *U* on the value of $M_{c.max}$: an increase in each of them leads to an increase in $M_{c.max}$. It is also worth noting the nonlinear nature of dependencies (Fig. 5).

Comparing the obtained results with those corresponding to the engineering methods of calculating the value of $M_{c.max}$ [18-20], it can be said that the discrepancy is –23.6...34.8%. Such discrepancies can be explained by the fact that engineering methods do not fully consider the dynamic parameters of the system (inertial and elastic properties of the system). Therefore, the results obtained will contribute to further improvement of engineering methods for calculating the elements of transport machines.

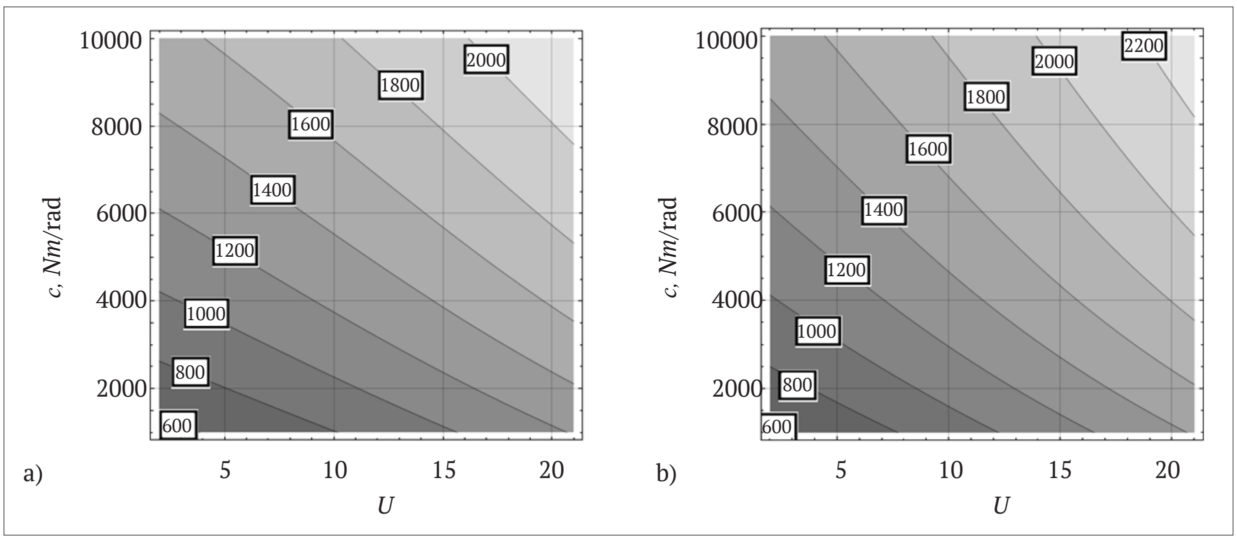

Figure 5. Graphs of dependence of $M_{c.max}$ on *c* and *U*: a) λ=1.8; b) λ=2.5

Summarising the results obtained, the purpose of this scientific study was successfully achieved. The resulting calculation method for $M_{c.max}$ is based on the ANN. The ANN was trained based on data reflecting the influence of the main factors of the transport machine and its drive on the value of $M_{c.max}$.

Returning to considerations regarding the software implementation of this method, its use will lie in entering numerical values n_n, P_n, λ, U, c in the appropriate fields of the software. Based on this data, the software should calculate the value of $M_{c.max}$ and select the appropriate safety clutch for the conveyor drive (or at least offer the user several options for clutches corresponding to the value of $M_{c.max}$).

CONCLUSIONS

1. A dynamic and corresponding mathematical model of the movement of the screw conveyor when it jams was built, which is represented by a nonlinear differential equation of the second order. The edge values of the system movement were obtained, which correspond to the operation of the conveyor in the nominal mode.

2. A series of 32,000 machine experiments was conducted, in which the nominal rotation frequency n_n and power P_n of the conveyor drive motor, the overload capacity of the motor λ, the gear ratio *U* and the combined stiffness *c* of the drive were the independent factors. The result was a tabulated function $M_{c.max}=f(n_n, P_n, \lambda, U, c)$.

3. Based on data of the tabulated function $M_{c.max}=f(n_n, P_n, \lambda, U, c)$, the ANN was trained and the statistical significance of the results of its work was proved. Furthermore, the influence of factors *c*, *U* and λ on the value of $M_{c.max}$ was briefly analysed.

4. The results obtained require validation by conducting experimental studies. If they do not fully reflect all significant factors that affect the value of $M_{c.max}$, it is necessary to include these factors in model (1) and repeat the calculations. The essence of calculations does not change. This represents the prospect of further research in this area.

5. It is proposed to implement the resulting method in the form of software that can be used in the design of screw conveyor drives.

REFERENCES

[1] German Patent and Trade Mark Office. (2022). Retrieved from https://depatisnet.dpma.de/DepatisNet/depatisnet?window=1&space=menu&content=index&action=basis&switchToLang=en.

[2] Karwat, B., Rubacha, P., & Stańczyk, E. (2020). Simulational and experimental determination of the exploitation parameters of a screw conveyor. *Maintenance and Reliability*, 22(4), 741-747. doi: 10.17531/ein.2020.4.18.

[3] Yuan, J., Li, M., Ye, F., & Zhou, Z. (2020). Dynamic characteristic analysis of vertical screw conveyor in variable screw section condition. *Science Progress*, 103(3), 1-16. doi: 10.1177/0036850420951056.

[4] Moorthi, S., Megaraj, M., Nagarajan, L., Karthick, A., Bharani, M., & Patil, P.P. (2022). Dynamic analysis and fabrication of single screw conveyor machine. *Advances in Materials Science and Engineering*, 2022, article number 3843968. doi: 10.1155/2022/3843968.

[5] Özbek, O. (2020). Fuzzy modeling of volumetric efficiency and specific energy consumption in agricultural screw conveyors. *Rural Engineering*, 50(5), 1-8. doi: 10.1590/0103-8478cr2019076.

[6] Screw conveyor catalog & engineering manual. (2022). Retrieved from https://screwconveyor.com/wp-content/uploads/2018/08/Screw-Conveyor-Catalog-SCC_787F.pdf.

[7] Engineering guide. Screw conveyors. (2022). Retrieved from https://www.kwsmfg.com/wp-content/themes/va/pdf/Screw-Conveyor-Engineering-Guide.pdf.

[8] Screw conveyor catalog & engineering manual. (2022). Retrieved from https://orthman.com/wp-content/uploads/2020/09/2005RP-Screw-conveyor-cat-1-31-08.pdf.

[9] Faulkner, L.L., & Earl, L.Jr. (Ed.). *Handbook of machinery dynamics*. (2000). Boca Raton: CRC Press.

[10] Veltman, A., Pulle, D.W.J., & de Doncker, R.W. (2007). *Fundamentals of electrical drives*. Dordrecht: Springer. doi: 10.1007/978-1-4020-5504-1.

[11] Griffiths, D.F., & Higham, D.J. (2010). *Numerical methods for ordinary differential equations*. Dordrecht: Springer. doi: 10.1007/978-0-85729-148-6.

[12] Catalogue of industrial motors series AIR. (n.d.). Retrieved from https://samsnab.com.ua/docs/Katalog-elektrodvigatelei-AIR-TM-ELMO.pdf.

[13] Korn, G.A., & Korn, T.M. (2013). *Mathematical handbook for scientists and engineers: Definitions, theorems, and formulas for reference and review*. New York: Dover Publications.

[14] Anastassiou, G.A. (2011). *Intelligent systems: Approximation by artificial neural networks*. Dordrecht: Springer. doi: 10.1007/978-3-642-21431-8.

[15] Kingma, D.P., & Ba, J. (2015). *Adam: A method for stochastic optimization.* Retrieved from https://arxiv.org/pdf/1412.6980.pdf.

[16] Romasevych, Y., Loveikin, V., & Makarets, V. (2020). Optimal constrained tuning of PI-controllers via a new PSO-based technique. *International Journal of Swarm Intelligence Research*, 11(4), 87-105. doi: 10.4018/IJSIR.2020100104.

[17] Romasevych, Y., Loveikin, V., & Loveikin, Y. (2021). Development of new rotating ring topology of PSO-algorithm. In *IEEE KhPI week on advanced technology, KhPI week 2021* (pp. 79-82). Kharkiv, NTU "KhPI". doi: 10.1109/KhPIWeek53812.2021.9569973.

[18] The most accurate calculating tutorial of screw conveyor specification. (2022). Retrieved from https://vietmfg.com/screw-conveyor-spec.

[19] Screw conveyor components & design. Version 2.20. (2022). Retrieved from https://edisciplinas.usp.br/pluginfile.php/4650272/mod_resource/content/0/Catalogo_Screw_Conveyor_Fabricante.pdf.

[20] Screw conveyor engineering guide. (2022). Retrieved from https://www.kwsmfg.com/wp-content/uploads/SC-Eng-Guide-Screw-Conveyor-Torque.pdf.

СПИСОК ВИКОРИСТАНИХ ДЖЕРЕЛ

[1] German Patent and Trade Mark Office. URL: https://depatisnet.dpma.de/DepatisNet/depatisnet?window=1&space=menu&content=index&action=basis&switchToLang=en.

[2] Karwat B., Rubacha P., Stańczyk E. Simulational and experimental determination of the exploitation parameters of a screw conveyor. *Maintenance and Reliability*. 2020. Vol. 22, No. 4. P. 741–747. doi: 10.17531/ein.2020.4.18.

[3] Yuan J., Li M., Ye F., Zhou Z. Dynamic characteristic analysis of vertical screw conveyor in variable screw section condition. *Science Progress*. 2020. Vol. 103, No. 3. P. 1–16. doi: 10.1177/0036850420951056.

[4] Dynamic analysis and fabrication of single screw conveyor machine / S. Moorthi et al. *Advances in Materials Science and Engineering*. 2022. Vol. 2022. Article number 3843968. doi: 10.1155/2022/3843968.

[5] Özbek O. Fuzzy modeling of volumetric efficiency and specific energy consumption in agricultural screw conveyors. *Rural Engineering*. 2020. Vol. 50, No. 5. P. 1–8. doi: 10.1590/0103-8478cr2019076.

[6] Screw conveyor catalog & engineering manual. URL: https://screwconveyor.com/wp-content/uploads/2018/08/Screw-Conveyor-Catalog-SCC_787F.pdf.

[7] Engineering guide. Screw conveyors. URL: https://www.kwsmfg.com/wp-content/themes/va/pdf/Screw-Conveyor-Engineering-Guide.pdf.
[8] Screw conveyor catalog & engineering manual. URL: https://orthman.com/wp-content/uploads/2020/09/2005RP-Screw-conveyor-cat-1-31-08.pdf.
[9] Handbook of machinery dynamics / L.L. Faulkner, L.Jr. Earl (Eds.). Boca Raton: CRC Press, 2000, 608 p.
[10] Veltman A., Pulle D.W.J., de Doncker R.W. Fundamentals of electrical drives. Dordrecht: Springer, 2007, 345 p. doi: 10.1007/978-1-4020-5504-1.
[11] Griffiths D.F., Higham D.J. Numerical methods for ordinary differential equations. Dordrecht: Springer, 2010. 271 p. doi: 10.1007/978-0-85729-148-6.
[12] Каталог общепромышленных электродвигателей серии АИР. URL: https://samsnab.com.ua/docs/Katalog-elektrodvigatelei-AIR-TM-ELMO.pdf.
[13] Korn G.A., Korn T.M. Mathematical handbook for scientists and engineers: Definitions, theorems, and formulas for reference and review. New York: Dover Publications, 2013. 1152 p.
[14] Anastassiou G.A. Intelligent systems: Approximation by artificial neural networks. Dordrecht: Springer, 2011. 108 p. doi: 10.1007/978-3-642-21431-8.
[15] Kingma D.P., Ba J. Adam: A method for stochastic optimization. URL: https://arxiv.org/abs/1412.6980.
[16] Romasevych Y., Loveikin V., Makarets V. Optimal constrained tuning of PI-controllers via a new PSO-based technique. *International Journal of Swarm Intelligence Research*. 2020, Vol. 11, No. 4. P. 87–105. doi: 10.4018/IJSIR.2020100104.
[17] Romasevych Y., Loveikin V., Loveikin Y. Development of new rotating ring topology of PSO-algorithm. *IEEE KhPI week on advanced technology, KhPI week 2021* (Kharkiv, September 13–17 2021). Kharkiv, 2021. P. 79–82. doi: 10.1109/KhPIWeek53812.2021.9569973.
[18] The most accurate calculating tutorial of screw conveyor specification. URL: https://vietmfg.com/screw-conveyor-spec.
[19] Screw Conveyor components & design. Version 2.20. URL: https://edisciplinas.usp.br/pluginfile.php/4650272/mod_resource/content/0/Catalogo_Screw_Conveyor_Fabricante.pdf.
[20] Screw conveyor engineering guide. URL: https://www.kwsmfg.com/wp-content/uploads/SC-Eng-Guide-Screw-Conveyor-Torque.pdf.

Юрій Олександрович Ромасевич, Вячеслав Сергійович Ловейкін, Олег Дмитрович Маліневський

Національний університет біоресурсів і природокористування України
03041, вул. Героїв Оборони, 15, м. Київ, Україна

Метод розрахунку максимального крутного моменту при заклинюванні шнека гвинтового конвеєра

Анотація. Конструкції гвинтових конвеєрів містять запобіжні муфти, що забезпечують уникнення поломок в аварійних ситуаціях (наприклад, при заклинюванні шнека). Тому вибір цих муфт представляє собою актуальну наукову задачу, яка пов'язана із розрахунком максимального крутного моменту шнека. Метою дослідження є розробка методу розрахунку максимального крутного моменту при заклинюванні шнека гвинтового конвеєра. Розроблений у статті метод ґрунтується на використанні штучної нейронної мережі, навченої за технологією «навчання з учителем». Навчальний і тестовий набір даних для штучної нейронної мережі отримано за допомогою проведення машинних експериментів, кожен з яких полягав у чисельному інтегруванні нелінійного диференціального рівняння та визначенні на основі отриманого розв'язку значення максимального моменту у пружному зв'язку динамічної системи. Вказане диференціальне рівняння отримано на основі рівняння руху незаклиненої частини конвеєра (привод, передачі, муфта) та рівняння Клосса, що відповідає моделі механічної характеристики асинхронного двигуна конвеєра. Було доведено статистичну значимість результатів роботи штучної нейронної мережі шляхом аналізу величин показників якості апроксимації. Проведено короткий аналіз впливу жорсткості пружного зв'язку динамічної системи конвеєра та передаточного числа приводу, а також перевантажувальної здатності двигуна на максимальний момент, що виникає при заклинюванні шнека. Практична значимість отриманих результатів пов'язана із програмною реалізацією методу, яка дасть змогу інженерам ефективно проводити вибір запобіжних муфт при конструювання гвинтових конвеєрів

Ключові слова: математичне моделювання, апроксимація, машинні експерименти, штучна нейронна мережа

Machinery & Energetics
Vol. 13, No. 2. 2022

Journal homepage:
https://technicalscience.com.ua/en

UDC 681.511;681.527
DOI: 10.31548/machenergy.13(2).2022.91-101

Viktor Trokhaniak*

National University of Life and Environmental Sciences of Ukraine
03041, 15 Heroiv Oborony Str., Kyiv, Ukraine

Study of the Influence of the Arrangement of Exhaust Fans Along the Lower Line on the Aerodynamics of the Poultry House

Abstract. Coverage and outbreaks of diseases lead to considerable losses in large-scale poultry farming. New ventilation systems are essential to ensure a safe and uniform indoor environment in large enterprises, especially in the changing climate of global warming. Thus, it is necessary to improve the design of the poultry house, to search for the most effective way of arranging the supply air valves and to improve the aerodynamic parameters of the internal environment of the poultry house in the most effective way of arranging the supply air valves and improving the aerodynamic parameters of the internal environment of the poultry house. Within the framework of this study, computational hydrodynamics modelling of the lateral ventilation system in the poultry house during the winter period of the year was performed. As a result, the temperature of the 3D field, the current lines, and the pressure in the aviary were detected. Supply air valves located 200 mm above the floor were found to perform better than those conventionally installed at 400 mm. Building walls on the inside of the poultry house frame, as well as reducing the height of the floor, improve the aerodynamics of the poultry house. The practical value of the presented study is targeted at poultry farmers with large productive capacities

Keywords: CFD, aerodynamics, aviary, lateral ventilation system, inlet valves

Article's History: Received: 22.10.2021; Revised: 11.02.2022; Accepted: 27.04.2022.

INTRODUCTION

The thermal regime of poultry houses is one of the prognostic factors that determine the productivity of the poultry industry. Poultry breeding must follow zootechnical standards [1]. The thermal regime of the poultry house is established as a result of heat exchange processes occurring both indoors and through its outer walls. It is formed under the influence of heating and ventilation systems, depending on the meteorological parameters of the outside air and the structural characteristics of the poultry house. Thus, the normalised microclimate system has a directly proportional effect on poultry farming, and the final product is the yield of meat.

Figure 1 shows the conventional design of the poultry house. The external walls are made of a concrete frame, the ceiling is not lowered. Thus, the purpose of this study was to improve the design of the poultry house, find the most effective way of arranging the supply air valves, and improve the aerodynamic parameters of the poultry house environment using computational fluid dynamics (CFD).

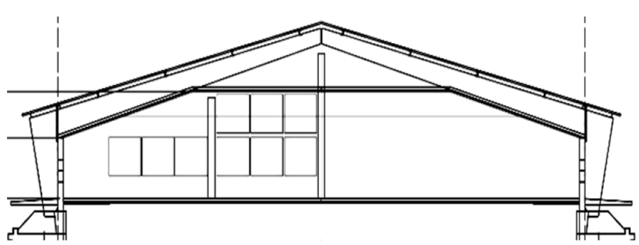

Figure 1. A fragment of the conventional design of the poultry house with inlet valves of the lateral ventilation system

Suggested Citation:
Trokhaniak, V. (2022). Study of the influence of the arrangement of exhaust fans along the lower line on the aerodynamics of the poultry house. *Machinery & Energetics,* 13(2), 91-101.

*Corresponding author

Thus, the development of improved structural solutions of the lateral ventilation system is an urgent issue that needs to be solved.

LITERATURE REVIEW

The publication [2] analysed the influence of height (0.4 m, 0.55 m, 0.7 m, 0.85 m and 1 m) and intervals (6 m, 9 m, 12 m, 15 m and 18 m) of deflectors on the speed and distribution of air in the cage zones. The study shows that the deflectors can considerably direct the downward airflow, increase the air velocity in the cage and passage area by 0.66 m/s and 0.91 m/s, respectively, compared to no deflectors, if the deflectors are 1 m high at 6 m intervals.

Authors of publications [1; 3; 4] proposed to apply a new cooling system in the poultry house using heat exchangers [5] of a distinctive design [6-8]. CFD modelling of air flows and heat and mass transfer in a poultry house is presented. Here, water from underground wells is used as a coolant. Recommendations for choosing the design of ventilation systems in poultry houses are given. In their further studies [9], the authors optimise the height of the exhaust fan. It is shown that it is advisable to install ventilation equipment at a height of 1.5 m. Here, the area of dead air zones and the uneven distribution of air velocities close to the poultry decrease.

To reduce energy consumption and increase the quality of the air environment while providing the necessary conditions for keeping poultry [10], the authors conducted experimental studies and numerical simulations. During the studies, a reduction in energy consumption was achieved to ensure a microclimate during broiler breeding. The quality of the air environment of poultry farms was improved. It allowed reducing feed costs and poultry losses and, as a result, increasing the economic efficiency of production and the quality of finished products.

The authors of the study [11; 12] consider the methods of the lateral mechanical ventilation system to be more effective compared to other methods. In their article, CFD simulations show a wide range of airflow velocity values. Two main conclusions were made based on the air velocity in the room: 1 – excessive heterogeneity in the area where the animals stay; 2 – air movement is insufficient for thermoregulation of poultry.

CFD solutions for various flow configurations and poultry house shapes are presented in [13]. The effects of transverse and longitudinal ventilation are combined with changes in the directions of incoming air flows, as well as with a different cross-sectional shape obtained using valves. This paper considers the construction of the poultry house in such a way that the walls are located on the outside of the concrete frame. This design worsens the aerodynamics in the middle of the poultry house. There are a lot of stagnant air zones. Due to the high overlap, heat in winter is concentrated above the poultry. This accompanies an increase in energy costs for heating the room.

MATERIALS AND METHODS

According to the terms of reference, an engineering calculation of air exchange in the winter period of the year was performed. To remove carbon dioxide, moisture vapour, and harmful substances, it was necessary to ensure an airflow of about 155 thousand m^3/h at an external temperature of -10°C.

The geometry of the poultry house was built in true size. To reduce the calculation time inside the building, symmetry was applied. That is, modelling was carried out only for half of the poultry house building. The calculation was carried out at an airflow rate of 30 kg/s. The temperature of the outside air was taken as -10°C and the heat release parameters were entered. The walls were concrete and insulated with 35 kg/m^3 foam, 60/150/60 mm thick, respectively. The building was covered with polyurethane with a thickness of 100 mm, 45 kg/m^3. The floor was insulated with polystyrene foam with a thickness of 45 kg/m^3, 100 mm thick on a width of 2 m from the wall along the perimeter of the poultry house, 50 mm on the rest of the area. The length of the poultry house was 120 m, the width was 22.36 m (Fig. 2). The average number of poultry was 41,000, the weight of the poultry was 3.3 kg. The poultry was a source of heat and corresponded to +41°C. Wlotpowietrza 857x337 mm 3000-VFG and Przepustowocs 2900 v^3/h ventilation valves were applied. They were placed on the side walls, a total of 79 pcs. (Fig. 5a). The first ten ventilation valves were installed at a height of 0.2 m from the floor (Fig. 3b, Fig. 5a). The rest of the valves were located at a height of 0.4 m from the floor (Figs. 3a, 4(H5), 5a). One of the design concepts was to install a spoiler at an angle of inclination of 75° from the vertical line above the supply air valves (Fig. 4 (A20)). The length of the spoiler was 0.08 m (L9). Munters EM50 1.5 Hp exhaust fans were used, 18 pcs in total. During winter, 6 pieces were specially prepared (Fig. 5b). As a rule, they are located in the upper row, shifted closer to the centre. Such fans can withstand a maximum long-term load of up to 56 Pa.

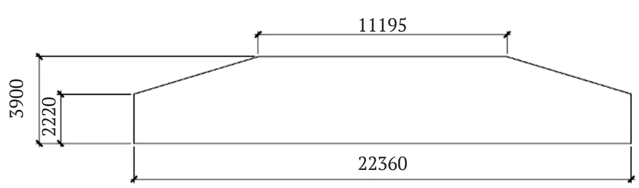

Figure 2. The proposed cross-sectional scheme of the structural dimensions of the poultry house

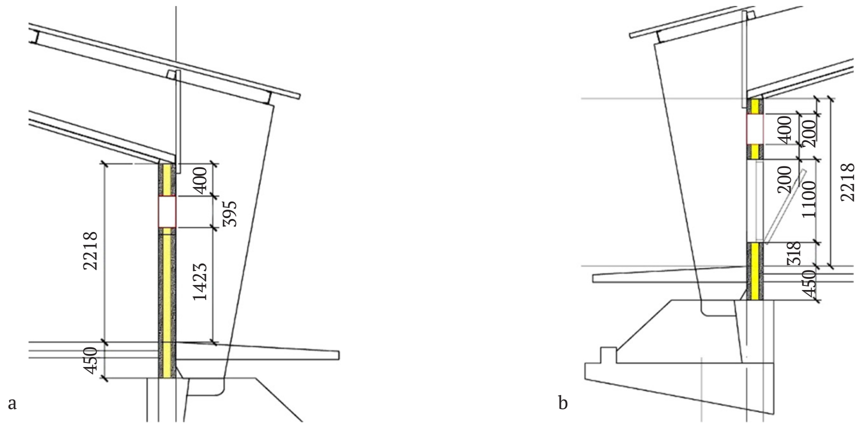

Figure 3. The proposed cross-sectional scheme of the structural dimensions of the poultry house: a – small valves, b – tunnel ventilation valves

Figure 4 schematically presents the angle of the valve from the side. The ventilation scheme was built in such a way that the airflow in winter reached the centre of the building to normalise the aerodynamic parameters of the poultry house. This method allowed reducing the loss of fresh air pressure in the poultry house. Thus, the following structural changes were made: the width of the building was increased from 21 m to 22.36 m. Figure 4 shows the maximum valve opening of 0.1 m (H16). Numerical simulations were performed at valve openings of 0.1 m, 0.066 m, and 0.049 m, respectively.

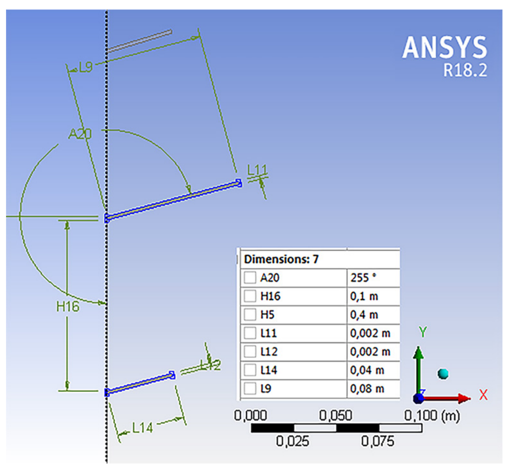

Figure 4. Angles of inclination of intake valves and spoiler

(a)

(b)

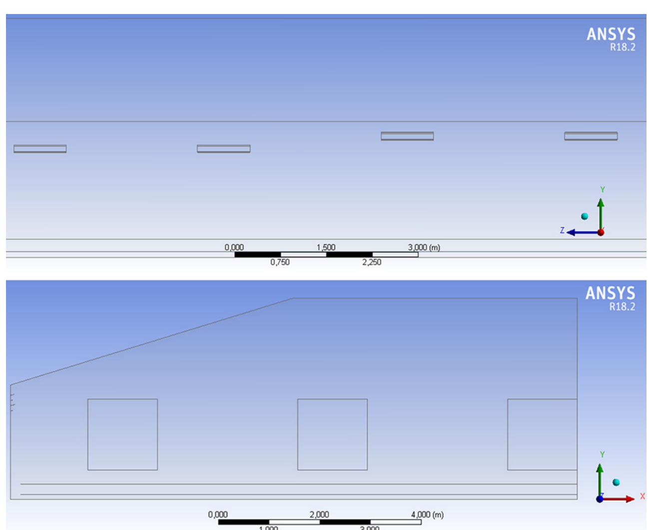

Figure 5. Side (a) and rear (b) walls of the poultry house

The number of elements and faces was quite numerous (Table 1). Given the large dimensions of the building, the size of the element and face was not significantly increased due to limitations of computer performance and design power.

Table 1. Parameters of building a mesh for a poultry house

Configuration options	Indicator
Orthogonal quality indicator	0.24
Number of elements, pcs	3813129
Number of nodes, pcs	4005901
Method	CutCell
Maximum face size, m	0.11
Minimum face size, m	0.0275
Minimum size of the supply valve element, m	0.0276
Minimum element size of exhaust fans, m	0.05

Figure 6 presents the frontal and side views of the formed poultry house mesh, fresh air openings, and entrance gate. The mesh was slightly reduced relative to the rest of the wall area (Table 1). Such measures were applied to obtain a better hydrodynamic calculation. Furthermore, the net was compacted close to the floor, as the poultry was placed there. Using the finite element method, a 3D computational mesh was built in the ANSYS Meshing software complex, aimed at solving the problems of hydrodynamics and heat exchange in the poultry house [2; 4].

(a)

(b)

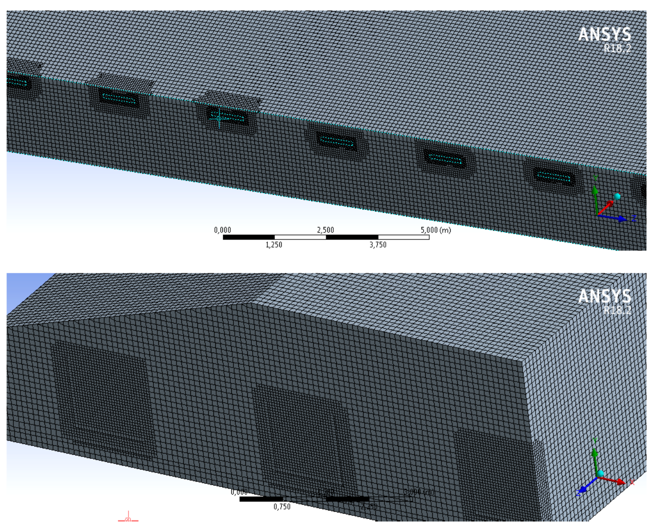

Figure 6. Side view (a) and rear view (b) of the walls of the poultry house

The construction of various meshes for CFD models allowed choosing the optimal and high-quality ones, which allowed obtaining reliable and accurate results of calculating the ventilation of the poultry house. The simulation was carried out without the use of an added heating system.

The flow of a viscous liquid or gas (air) was described by a system of equations that included continuity equations and momentum equations in projections onto the coordinate axis. If the flow of the medium was followed by heat transfer, then the energy conservation equation (heat transfer equation) was added to the aforementioned system of equations.

The mathematical model was based on Navier-Stokes equations [14; 15] and energy transfer equations for convective currents [15-17]. The Spalart-Allmaras turbulence model was used in the calculations [18; 19] and the discrete ordinate radiation model [20; 21].

RESULTS AND DISCUSSION

The results of CFD 3D simulation of the poultry house allowed comparing three modifications of the opening of the valves in the case of the lateral ventilation system of the poultry house. Before numerical modelling, a three-dimensional mesh was created using the finite element method [2; 4] in ANSYS Meshing.

Figures 7-15 show the results of CFD modelling of the poultry house on two sections along the length of the building – 10.3 m and 52.3 m with different valve openings from 0.1 m to 0.049 m.

Figures 7-9 present values of pressure loss in fresh air valves. It is shown that the smallest pressure loss is 24.3 Pa when the valve is opened 0.1 m, and the largest is 55.68 Pa at 0.049 m, respectively.

Figures 10-15 show the hydrodynamics of the airflow in the poultry house.

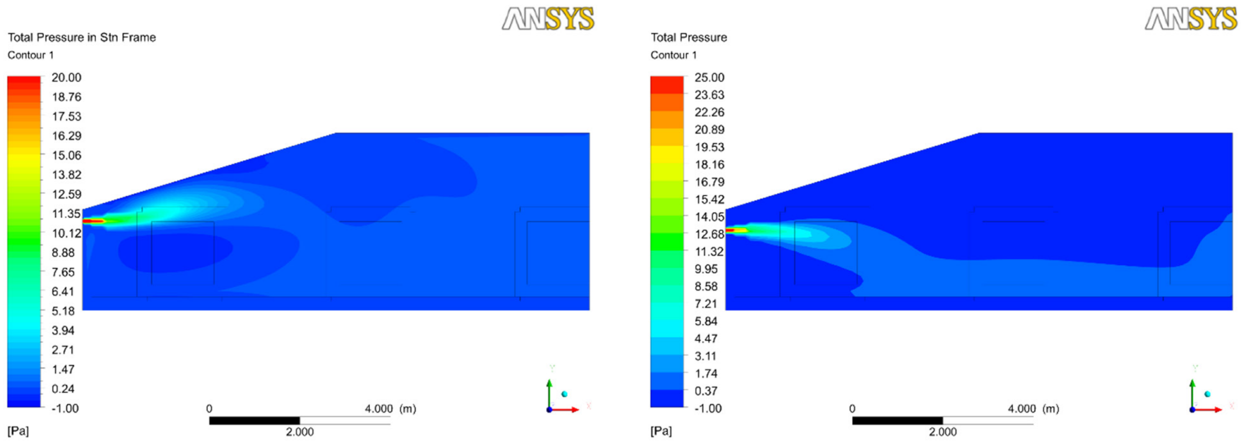

(a) (b)

Figure 7. Pressure loss (Pa) in the fresh air valve of the poultry house when the valve is opened 0.1 m at a distance from the front-end wall: a – 10.3 m; b – 52.3 m

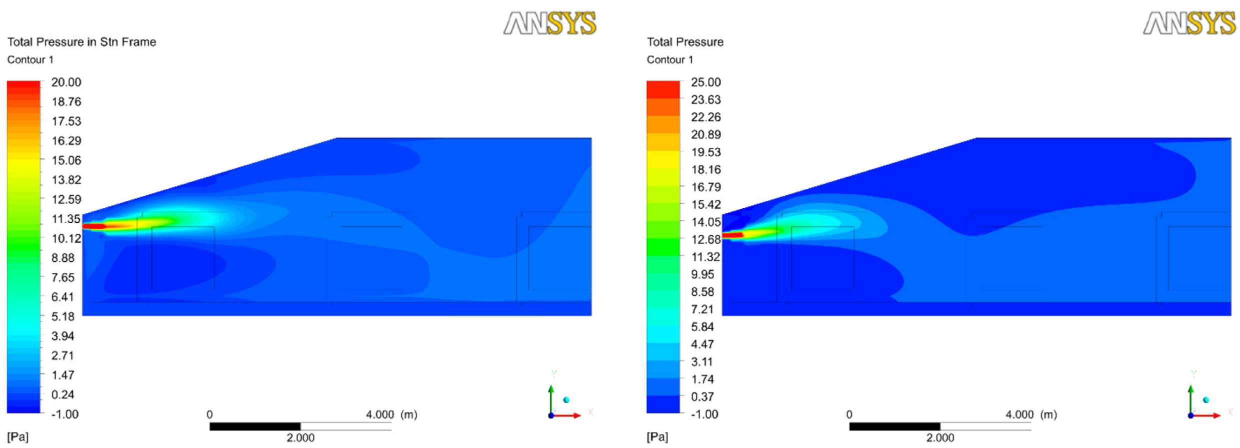

(a) (b)

Figure 8. Pressure loss (Pa) in the fresh air valve of the poultry house when the valve is opened is 0.066 m at a distance from the front-end wall: a – 10.3 m; b – 52.3 m

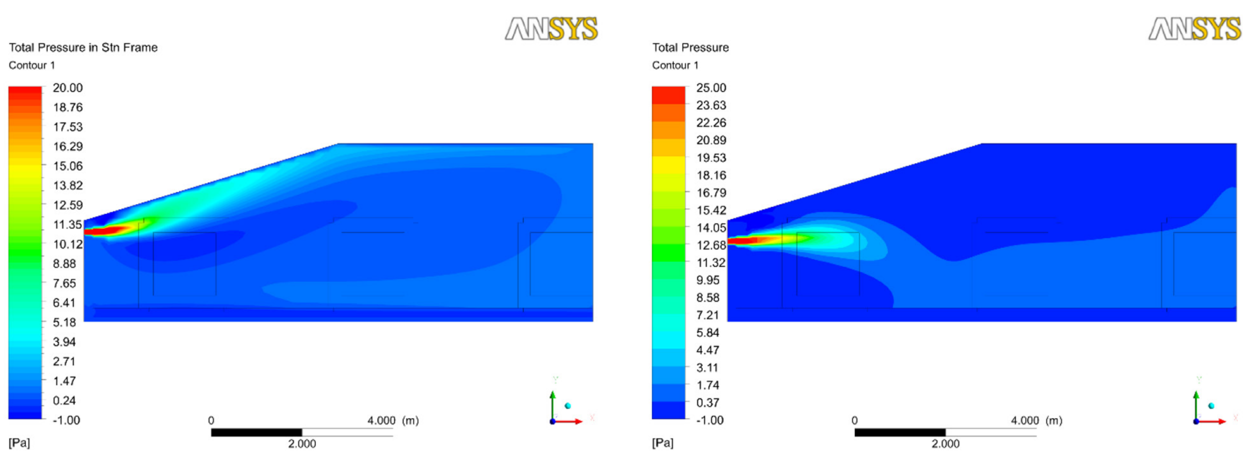

(a) (b)

Figure 9. Pressure loss (Pa) in the fresh air valve of the poultry house when the valve is opened is 0.049 m at a distance from the front-end wall: a – 10.3 m; b – 52.3 m

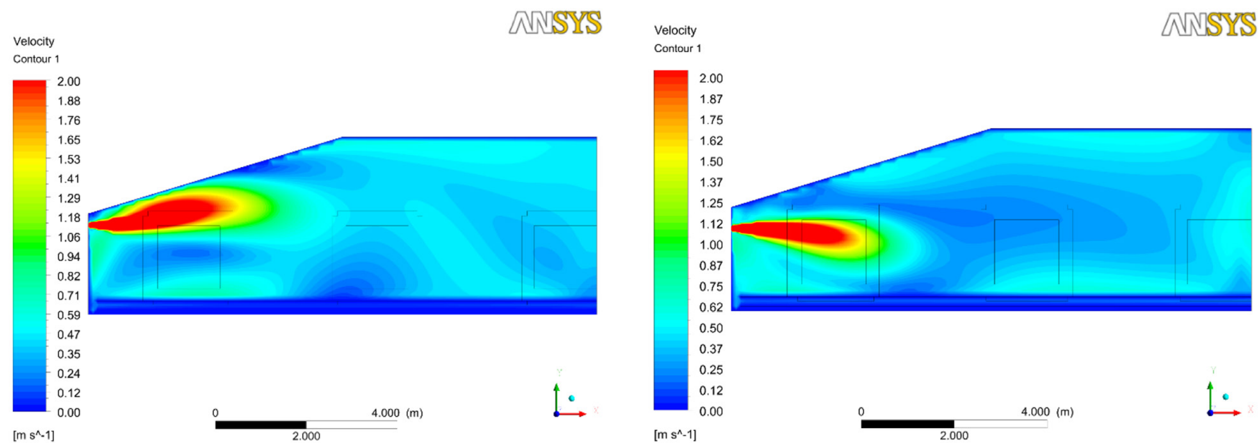

(a) (b)

Figure 10. Velocity field (m/s) in the poultry house when the valve is opened 0.1 m at a distance from the front-end wall: a – 10.3 m, b – 52.3 m

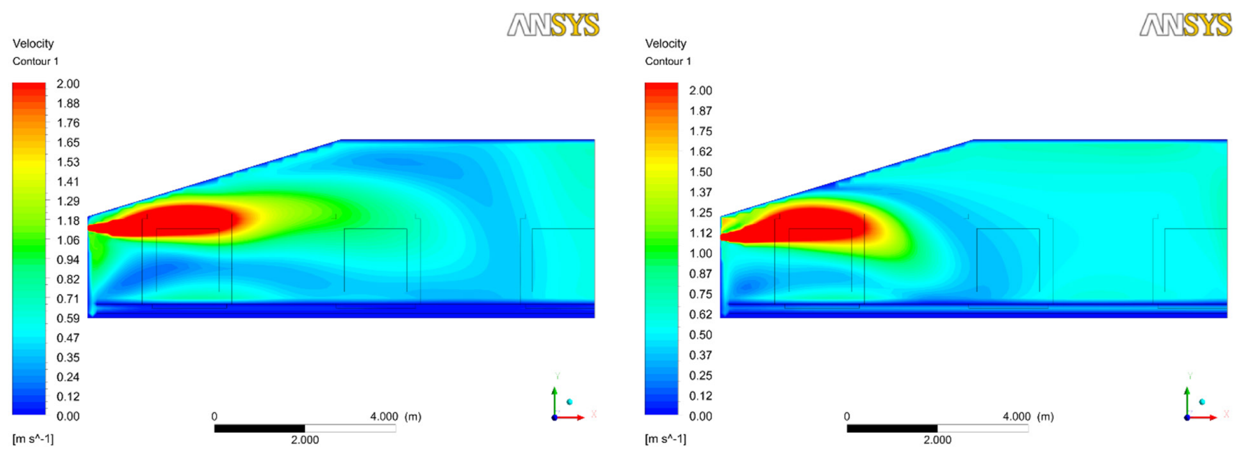

(a) (b)

Figure 11. Velocity field (m/s) in the poultry house when the valve is opened 0.066 m at a distance from the front-end wall: a – 10.3 m; b – 52.3 m

As already mentioned, the airflow is directed upwards by fresh air valves. However, due to low pressures and velocities at the entrance, passing a third of the building, the air falls. The valves are located at a height of 200 mm from the floor (Fig. 12a, Fig. 15a). The air moves smoothly close to the floor area and is directed to the centre of the building. Valves found at a height of 400 mm from the floor cannot provide the same effect. This can be caused by disturbance due to the large airspace of the building. The average entry speed for diverse types of air ranges from 6.39 m/s to 9.62 m/s.

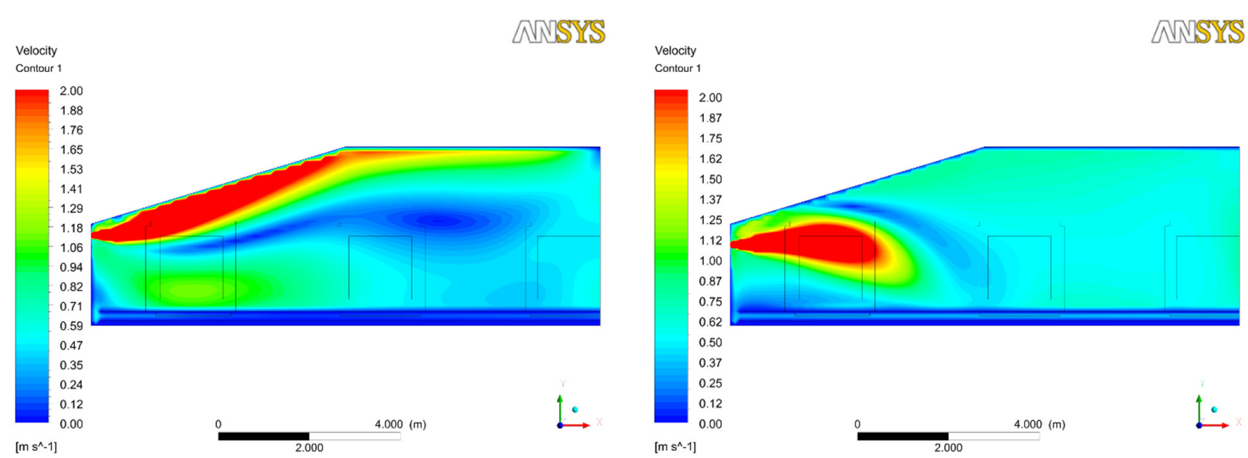

(a) (b)

Figure 12. The field of velocities (m/s) in the poultry house when the valve is opened is 0.049 m at a distance from the front-end wall: a – 10.3 m; b – 52.3 m

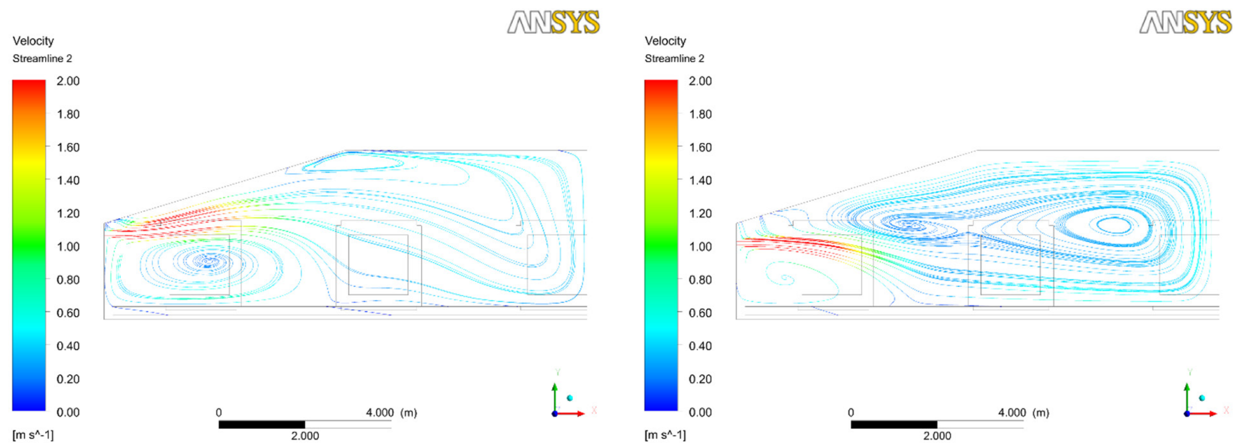

(a) (b)

Figure 13. Stream lines (m/s) in the poultry house when the valve is opened 0.1 m at a distance from the front-end wall: a – 10.3 m; b – 52.3 m

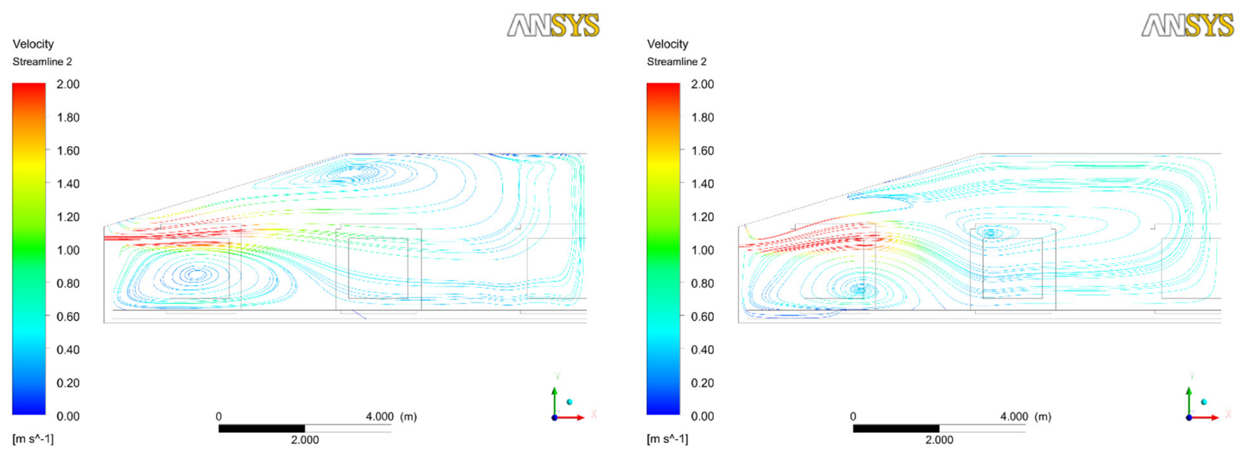

(a) (b)

Figure 14. Stream lines (m/s) in the poultry house when the valve is opened 0.066 m at a distance from the front-end wall: a – 10.3 m; b – 52.3 m

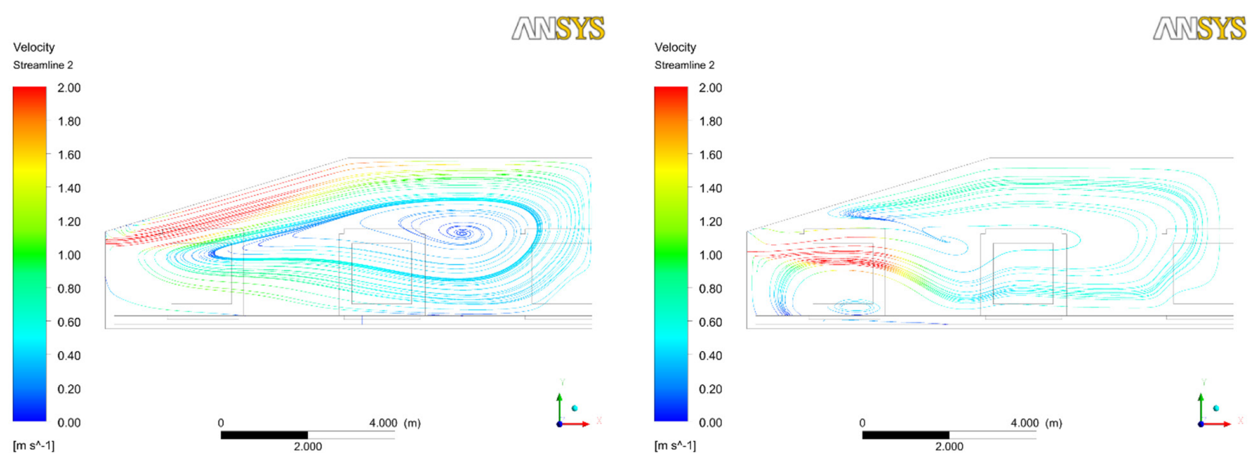

(a) (b)

Figure 15. Stream lines (m/s) in the poultry house when the valve is opened 0.049 m at a distance from the front-end wall: a – 10.3 m; b – 52.3 m

Figure 16 shows the velocity field in the poultry house at a height of 0.7 m from the floor level. These results can help estimate the airspeed over the poultry. The average speed of air movement ranges from 0.54 m/s to 0.66 m/s. Only near the exhaust fans, the speed is slightly higher at 2 m/s. The bulk of the poultry does not feel discomfort. In [9], the authors optimised the height of the exhaust fan. The set height is 1.5 m. However, these studies show that installing exhaust fans at a height of 0.8 m is more effective (Fig. 16).

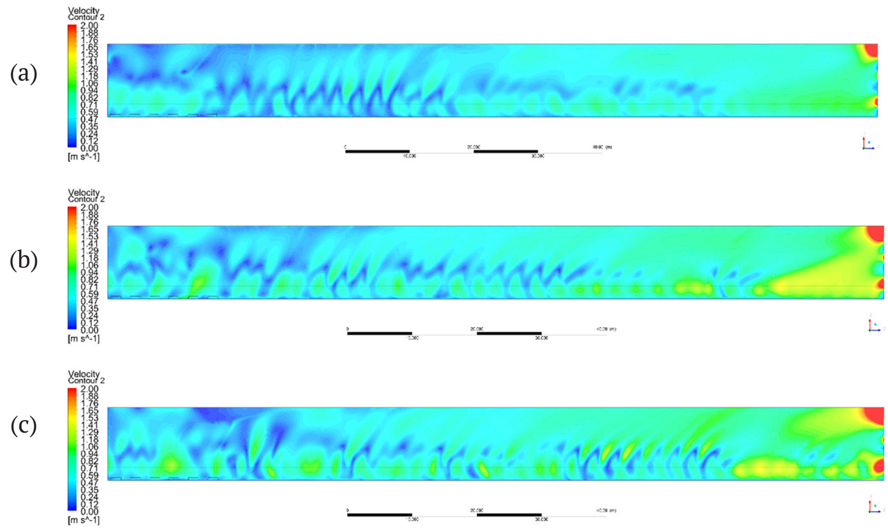

Figure 16. Field of velocities (m/s) in the poultry house at a height of 0.7 m from the floor level when the valve is opened: a – 0.1 m; b – 0.066 m; c – 0.049 m

Figure 17 presents 3D streamlines in the poultry house. The results show that valves that are located at a height of 400 mm are not effective. The middle exhaust fan is practically not used. A large load falls on the side fan, which is arranged close to the wall. The main load is taken by the fan, which is in the centre of the building.

Table 2 presents more detailed information about the CFD simulation results.

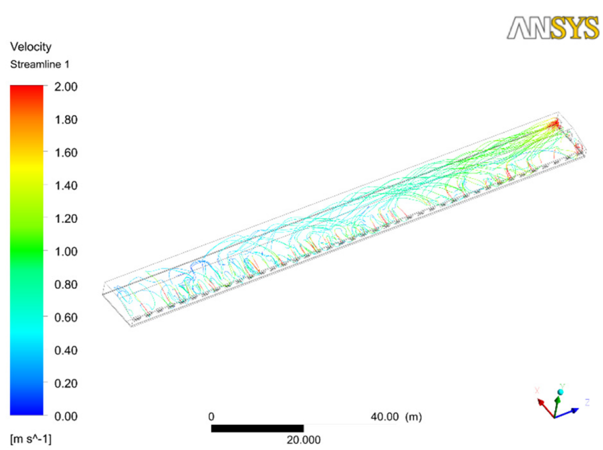

Figure 17. 3D stream lines (m/s) in the poultry house when the valve is opened 0.049 m

Table 2. Average indicators of air in the poultry house

Parameter	Dimensions	Result		
Valve opening distance	m	0.1	0.066	0.049
Consumption of incoming air for half of the poultry house	kg/s	30	30	30
Valve inlet pressure	Pa	24.332	43.41	55.684
Outlet fan pressure	Pa	-1.23	-2.215	-3.132
Air temperature at the valve Inlet	K	263.947	263.927	263.975
Fan outlet air temperature	K	273.778	273.91	273.148
Valve inlet air velocity	m/s	6.388911	8.518548	9.625959
Fan outlet air velocity	m/s	5.904209	7.946565	9.010783
Air velocity at a height of 0.7 m from the floor level	m/s	0.54181	0.63328	0.657591
Air density at the valve Inlet	kg/m^3	1.337423	1.337529	1.337287
Air density at the fan outlet	kg/m^3	1.289433	1.288785	1.292457

In winter, the density of fresh air is higher than in summer. Thus, with a lateral ventilation system, it is difficult to supply air to the centre of the poultry house. The main volume of air is directed to the centre of the room and mixed. Thus, according to studies [11; 12] it is confirmed that the lateral ventilation system is more effective compared to others. As a result of higher quality indicators of the microclimate in the poultry house, the consumption of feed, the loss of the poultry population decreases and, as a result, the economic efficiency of production increases, which is confirmed by the authors [10; 22].

At the next stage of designing the side ventilation system, the authors suggest considering that the supply air valves should be located at a height of at least 200 mm from the ceiling level.

CONCLUSIONS

Based on the conducted research, the project of the poultry house was improved. Spoilers are suggested to be placed above the supply air valves at an angle of 75° from the vertical line; installation of external walls on the inner side of the concrete frame; increasing the width of the poultry house to 22.36 m; lowering the floor height to 3.9 m above the floor level.

Thanks to CFD, the effective arrangement of supply air valves and the improvement of aerodynamic characteristics in the construction of the poultry house were investigated. It was found that the smallest pressure loss is 24.3 Pa when opening the valve 0.1 m, and the largest losses are 55.68 Pa at 0.049 m, respectively.

Conducted studies show that valves located at a height of 200 mm from the floor are much more efficient. Valves that are located at a height of 400 mm from the floor cannot provide the same effect.

The prospect of further research is the inclusion in the model of the cooling and heating system, depending on the season. Thus, the improvement of the microclimate system of the poultry house as a whole. Furthermore, for more efficient air supply, the length of the spoiler will be increased, the overlap model will be more detailed, and other measures will be taken to improve the microclimate in the air environment of the poultry house.

REFERENCES

[1] Trokhaniak, V.I. (2018). *Power saving system in poultry-houses with usage of soil low-potential energy*. Kyiv: Komprint.

[2] Cheng, Q.Y., Li, H., Rong, L., Feng, X.L., Zhang, G.Q., & Li, B.M. (2018). Using CFD to assess the influence of ceiling deflector design on airflow distribution in hen house with tunnel ventilation. *Computers and Electronics in Agriculture*, 151, 165-174. doi: 10.1016/j.compag.2018.05.029.

[3] Gorobets, V.G., Trokhaniak, V.I., Antypov, I.O., & Bohdan, Yu.O. (2018). The numerical simulation of heat and mass transfer processes in tunneling air ventilation system in poultry houses. *INMATEH: Agricultural Engineering*, 55(2), 87-96.

[4] Gorobets, V.G., & Bohdan Yu.O. (2017). Computer modeling and experimental study of heat transfer and hydrodynamics in the channels of compact shell-and-tube heat exchangers. *Energy and Automation*. 4, 38-59.

[5] Gorobets, V.G., Bohdan, Yu.O., Trokhaniak, V.I., & Antypov, I.O. (2018). Experimental studies and numerical modelling of heat and mass transfer process in shell-and-tube heat exchangers with compact arrangements of tube bundles. *MATEC Web of Conferences*, 240, article number 02006. doi: 10.1051/matecconf/201824002006.

[6] Gorobets, V., Bohdan, Y., Trokhaniak, V., Antypov, I., & Masiuk, M. (2019). Summarizing of Nusselt numbers and Euler numbers in depending of Reynolds number for the compact tube bundle of small diameter tubes by experimental and numerical methods of researches. *XII International Conference on Computational Heat, Mass and Momentum Transfer*, 128, article number 04003. doi: 10.1051/e3sconf/201912804002.

[7] Slimene, M.B., Poncet, S., Bessrour, J., & Kallel, F. (2022). Numerical investigation of the flow dynamics and heat transfer in a rectangular shell-and-tube heat exchanger. *Case Studies in Thermal Engineering*, 32, article number 101873. doi: 10.1016/j.csite.2022.101873.

[8] Gorobets, V.G., & Trokhanyak, V.I. (2014). Modeling of transfer processes and thermal-hydraulic efficiency of a shell heat exchanger with a compact arrangement of pipe beams. *Scientific Bulletin of National University of Life and Environmental Sciences of Ukraine. "Technologies and Power Engineering"*, 194(2), 147-155.

[9] He, S., Wang, M., Tian, W., Qiu, S., & Su, G.H. (2022). Development of an OpenFOAM solver for numerical simulations of shell-and-tube heat exchangers based on porous media model. *Applied Thermal Engineering*, 210, article number 118389.

[10] Gorobets, V.G., Trokhaniak, V.I., Rogovskii, I.L., Titova, L.L., Lendiel, T.I., Dudnyk, A.O., & Masiuk, M.Y. (2018). The numerical simulation of hydrodynamics and mass transfer processes for ventilating system effective location. *INMATEH: Agricultural Engineering*, 56(3), 185-192.

[11] Trokhaniak, V.I., Rutylo, M.I., Rogovskii, I.L., Titova, L.L., Luzan, O.R., & Bannyi, O.O. (2019). Experimental studies and numerical simulation of speed modes of air environment in a poultry house. *INMATEH Agricultural Engineering*, 59(3), 9-18. doi: 10.35633/INMATEH-59-01.

[12] Bustamante, E., Calvet, S., Estelles, F., Torres, A.G., & Hospitaler, A. (2017). Measurement and numerical simulation of single-sided mechanical ventilation in broiler houses. *Biosystems Engineering*, 160, 55-68.

[13] Pourvosoghi, N., Nikbakht, A.M., Sharifian, F., & Najafi, R. (2018). Numerical analyses of air velocity and temperature distribution in poultry house using computational fluid dynamics. *INMATEH: Agricultural Engineering*, 56(3), 109-118.

[14] Zajicek, M., & Kic, P. (2012). Improvement of the broiler house ventilation using the CFD simulation. *Agronomy Research*, 10(1), 235-242.

[15] Khmelnik, S.I. (2018). *Navier-Stokes equations. On the existence and the search method for global solutions*. Raleigh: Mathematics in Computers.

[16] Antypov, I.O. (2016). Development of means for intensification of heat exchange processes in heat accumulators based on accumulative phase transition materials. *Energy and Automation*, 2, 110-119.

[17] Marzouk, S.A., Abou, A.M.M., El-Fakharany, M.K., & El-Said, E.M.S. (2022). A comparative numerical study of shell and multi-tube heat exchanger performance with different baffles configurations. *International Journal of Thermal Sciences*, 179, article number 107655. doi: 10.1016/j.ijthermalsci.2022.107655.

[18] Allmaras, S.R., Johnson, F.T., & Spalart, P.R. (2012). Modifications and clarifications for the implementation of the Spalart-Allmaras Turbulence model. In *7th international conference on computational fluid dynamics* (pp. 9-13). Melbourne: Melbourne Institute of Technology.

[19] Nordanger, K., Holdahl, R., Kvamsdal, T., Kvarving, A.M., & Rasheed, A. (2015). Simulation of airflow past a 2D NACA0015 airfoil using an isogeometric incompressible Navier-Stokes solver with the Spalart-Allmaras turbulence model. *Computer Methods in Applied Mechanics and Engineering*, 290, 183-208. doi: 10.1016/j.cma.2015.02.030.

[20] ANSYS. Fluent theory guide. Release 18.2. (2017). Retrieved from https://www.luis.uni-hannover.de/fileadmin/software-lizenzen/Ueberlassung/ANSYS18.2_ReleaseNotes.pdf.

[21] Moreno, J., Casado, C., & Marugán, J. (2019). Improved discrete ordinate method for accurate simulation radiation transport using solar and LED light sources. *Chemical Engineering Science*, 205, 151-164. doi: 10.1016/j.ces.2019.04.034.

[22] Babilya, M.I., Shender, I.O., Pogodin, A.I., Bilanych, V.S., & Studenyak, I.P. (2020). Mechanical Properties of Superionic Composites Based on (Cu1−xAgx)7SiS5I. *Scientific Herald of Uzhhorod University. Series "Physics"*, (48), 7-13.

СПИСОК ВИКОРИСТАНИХ ДЖЕРЕЛ

[1] Троханяк В.І. Система енергозбереження у пташниках із використанням низькопотенціальної енергії ґрунту. Київ: ЦП «Компринт», 2018. 386 с.

[2] Using CFD to assess the influence of ceiling deflector design on airflow distribution in hen house with tunnel ventilation / Q.Y. Chengeta et al. *Computers and Electronics in Agriculture*. 2018. Vol. 151. P. 165–174. doi: 10.1016/j.compag.2018.05.029.

[3] Gorobets V.G., Trokhaniak V.I., Antypov I.O., Bohdan Yu.O. The numerical simulation of heat and mass transfer processes in tunneling air ventilation system in poultry houses. *INMATEH: Agricultural Engineering*. 2018. Vol. 55, No. 2. P. 87–96.

[4] Горобець В.Г., Богдан Ю.О. Компьютерное моделирование и экспериментальное исследование теплообмена и гидродинамики в каналах компактных кожухотрубных теплообменников. *Енергетика та автоматика*. 2017. Вип. 4. С. 38–59.

[5] Gorobets V.G., Bohdan Yu.O., Trokhaniak V.I., Antypov I.O. Experimental studies and numerical modelling of heat and mass transfer process in shell-and-tube heat exchangers with compact arrangements of tube bundles. *MATEC Web of Conferences*. 2018. Vol. 240. Article number 02006. doi: 10.1051/matecconf/201824002006.

[6] Summarizing of Nusselt numbers and Euler numbers in depending of Reynoldsnumber for the compact tube bundle of small diameter tubes by experimental and numerical methods of researches / V. Gorobets et al. *XII International Conference on Computational Heat, Mass and Momentum Transfer*. 2019. Vol. 128. Article number 04003. doi: 10.1051/e3sconf/201912804002.

[7] Slimene M.B., Poncet S., Bessrour J., Kallel F. Numerical investigation of the flow dynamics and heat transfer in a rectangular shell-and-tube heat exchanger. *Case Studies in Thermal Engineering*. 2022. Vol. 32. Article number 101873. doi: 10.1016/j.csite.2022.101873.

[8] Горобець В.Г., Троханяк В.І. Моделювання процесів переносу та теплогідравлічна ефективність кожухотрубного теплообмінника з компактним розташуванням пучків труб. *Науковий вісник Національного університету біоресурсів і природокористування України. Серія «Техніка та енергетика АПК»*. 2014. Вип. 194, Ч. 2. С. 147–155.

[9] Development of an OpenFOAM solver for numerical simulations of shell-and-tube heat exchangers based on porous media model / S. He et al. *Applied Thermal Engineering*. 2022. Vol. 210. Article number 118389.

[10] The numerical simulation of hydrodynamics and mass transfer processes for ventilating system effective location / V.G. Gorobets et al. *INMATEH: Agricultural Engineering*. 2018. Vol. 56, No. 3. P. 185–192.

[11] Experimental studies and numerical simulation of speed modes of air environment in a poultry house / V.I. Trokhaniak et al. *INMATEH Agricultural Engineering*. 2019. Vol. 59, No. 3. P. 9–18. doi: 10.35633/INMATEH-59-01.

[12] Measurement and numerical simulation of single-sided mechanical ventilation in broiler houses / E. Bustamante et al. *Biosystems Engineering*. 2017. Vol. 160. P. 55–68.

[13] Pourvosoghi N., Nikbakht A.M., Sharifian F., Najafi R. Numerical analyses of air velocity and temperature distribution in poultry house using computational fluid dynamics. *INMATEH: Agricultural Engineering*. 2018. Vol. 56, No. 3. P. 109–118.

[14] Zajicek M., Kic, P. Improvement of the broiler house ventilation using the CFD simulation. *Agronomy Research*. 2012. Vol. 10, No. 1. P. 235–242.
[15] Khmelnik S.I. Navier-Stokes equations. On the existence and the search method for global solutions. Raleigh: Mathematics in Computers, 2018. 134 p.
[16] Антипов Є.О. Розробка засобів для інтенсифікації процесів теплообміну в акумуляторах теплоти на основі акумулюючих матеріалів фазового переходу. *Енергетика та автоматика*. 2016. № 2. С. 110–119.
[17] Marzouk S.A., Abou Al-Sood M.M., El-Fakharany M.K., El-Said E.M.S. A comparative numerical study of shell and multi-tube heat exchanger performance with different baffles configurations. *International Journal of Thermal Sciences*. 2022. Vol. 179. Article number 107655. doi: 10.1016/j.ijthermalsci.2022.107655.
[18] Allmaras S.R., Johnson F.T., Spalart P.R. Modifications and clarifications for the implementation of the Spalart-Allmaras Turbulence model. *7th international conference on computational fluid dynamics*. Melbourne, 2012. P. 9–13.
[19] Simulation of airflow past a 2D NACA0015 airfoil using an isogeometric incompressible Navier–Stokes solver with the Spalart–Allmaras turbulence model / K. Nordanger et al. *Computer Methods in Applied Mechanics and Engineering*. 2015. Vol. 290. P. 183–208. doi: 10.1016/j.cma.2015.02.030.
[20] ANSYS. Fluent theory guide. Release 18.2. URL: https://www.luis.uni-hannover.de/fileadmin/software-lizenzen/Ueberlassung/ANSYS18.2_ReleaseNotes.pdf.
[21] Moreno J., Casado C., Marugán J. Improved discrete ordinate method for accurate simulation radiation transport using solar and LED light sources. *Chemical Engineering Science*. 2019. Vol. 205. P. 151–164. doi: 10.1016/j.ces.2019.04.034.
[22] Babilya, M.I., Shender, I.O., Pogodin, A.I., Bilanych, V.S., & Studenyak, I.P. Studenyak Mechanical Properties of Superionic Composites Based on (Cu1−xAgx)7SiS5I. *Scientific Herald of Uzhhorod University. Series "Physics"*. 2020. Vol 48. P. 7-13.

Віктор Іванович Троханяк

Національний університет біоресурсів і природокористування України
03041, вул. Героїв Оборони, 15, м. Київ, Україна

Дослідження впливу розташування витяжних вентиляторів по нижній лінії на аеродинаміку пташника

Анотація. Охоплення та спалах захворювань призводять до значних втрат у великомасштабному птахівництві. Нові вентиляційні системи необхідні для забезпечення безпечного та однорідного внутрішнього середовища на великих підприємствах, особливо в мінливих кліматичних умовах глобального потепління. Таким чином, необхідно вдосконалити конструкцію пташника, провести пошук найбільш ефективного способу влаштування клапанів припливного повітря та покращити аеродинамічні показники внутрішнього середовища пташника у найбільш ефективного способу влаштування клапанів припливного повітря та покращення аеродинамічних показників внутрішнього середовища пташника. У рамках цього дослідження було проведено моделювання обчислювальної гідродинаміки бічної системи вентиляції в пташнику в зимовий період року. В результаті температура 3D поля, були виявлені поточні лінії та тиск у пташнику. Встановлено, що клапани припливного повітря, розташовані на висоті 200 мм від підлоги, працюють краще, ніж ті, які традиційно встановлюються на висоті 400 мм. Зведення стін з внутрішньої сторони каркаса пташника, а також зменшення висоти підлоги покращують аеродинаміку пташника. Практична цінність представлених досліджень направлена для пташників з великими продуктивними потужностями

Ключові слова: CFD, аеродинаміка, пташник, бокова система вентиляції, припливні клапана

Machinery & Energetics
Vol. 13, No. 2. 2022

Journal homepage:
https://technicalscience.com.ua/en

UDC 636.082
DOI: 10.31548/machenergy.13(2).2022.102-108

Leonid Chervinsky*, Ivan Radko, Vitalii Nalyvaiko, Oleksandr Okushko

National University of Life and Environmental Sciences of Ukraine
03041, 15 Heroiv Oborony Str., Kyiv, Ukraine

The Results of Experimental Studies of the Passage of Light Energy under the Skin of Animals Along Individual Hairs

Abstract. This paper presents new scientific results of experimental studies that refute the generally accepted fact that the coat solely protects animals from the effects of solar energy. The purpose of this study was to confirm the fact of the spread of optical radiation energy under the animal's skin along individual hairs, as light guides. The authors of this study experimentally determined the optically conductive structure of an individual wool hair, the components of the transmission parameter of an individual wool hair, namely the coefficient of light transmission inside the wool hair, the coefficient of attenuation of internal light transmission by the substance of the wool hair, the coefficient of losses in the middle of the cylinder of the wool hair due to the beam scattered in the internal structure and the refractive index of its outer shell. Based on the use of methods of photometry and geometric optics, theoretically substantiated and experimentally obtained results regarding the establishment of a mathematical dependence of the total amount of optical radiation energy entering the hair cylinder on the value of the angle of incidence of the beam on the surface of the hair, the cleanliness of the inner core of the cylinder structure, the length of the light-conducting section to the surface of the skin, as well as the refractive index of its outer shell. Based on the results of experimental studies, mathematical dependencies were obtained that describe the spectral light-conducting properties of an individual hair, as well as the distribution of energy emitted in the thickness of the skin along the entire length from the point of penetration into the hair and to the follicle – the place of use of optical energy in photobiological processes. The obtained results of experimental studies of the passage of optical radiation energy along the length of a single hair into the body of an animal are of practical importance for photobiologists investigating the effect of optical radiation from the Sun on biological objects of animal origin

Keywords: solar energy, irradiation of animals, skin-fur cover, light transmission, hair

Article's History: Received: 05.01.2022; Revised: 08.03.2022; Accepted: 27.04.2022.

INTRODUCTION

Breeding of animals and birds is impossible without sunlight, which has a wide range of biological effects. Analysis of modern scientific research [1-3] shows that each of the radiation spectra has its special biological effect on the structure of the animal's body. Ultraviolet radiation has an anti-rickets and healing effect, light of the visible spectrum of assorted colours causes an exciting or calming effect, and infrared radiation causes a thermal effect and improves the physical condition of the animal and its assimilation of food [4; 5].

It is customary to believe that the main part of the Sun's energy passes into the animal's body through the skin and fur [6; 7]. Moreover, only the protective function against excess solar energy is assigned to the wool or hair cover.

It is known that the skin covering of biological objects of animal origin is divided into two main layers: the surface layer of dehydrated dead cells (epidermis) and the actual skin of the animal (corium or dermis), which consists of interconnected living cells of various functions [1; 8; 9].

Research into the ways of the influence of the Sun's energy on the skin and hair covering of biological objects of animal origin (animals and birds) has been carried out since the middle of the 20th century. The studies of several scientists [10-12] substantiated that individual hairs of the animal coat can be a kind of living light guides of optical radiation that falls on the surface of the animal and falls on the skin-fur coat and passes through the skin and along individual hairs into its thickness to the places of biologically

Suggested Citation:
Chervinsky, L., Radko, I., Nalyvaiko, V., & Okushko, O. (2022). The results of experimental studies of the passage of light energy under the skin of animals along individual hairs. *Machinery & Energetics,* 13(2), 102-108.

*Corresponding author

active subcutaneous structures, where it takes part in relevant photobiological processes.

It is known that the internal structure of individual hairs depends on many factors, which can be defined as the main ones – species, age, breed, constitutional, and seasonal [1; 13; 14].

The analysis of the results of scientific research [15-17] regarding the ways of the influence of different spectra of optical radiation upon irradiating biological objects of animal origin, namely pigs, as animals with a fur coat made of the thickest individual hairs, shows that the diameter of individual hairs (bristles) is ten fractions of a millimetre, and their optical conductivity can be measured effortlessly and accurately on modern optical spectrophotometers and other optical measuring devices.

Considering these facts, namely, the possibility of the effect of optical energy of different spectra, which indirectly passes through the wool cover, as through separate light channels, is an urgent scientific problem that is still understudied.

The purpose of this study was to establish the possibility of the passage of optical energy radiation into the biologically active structures of the skin of the body of a biological object of animal origin through individual hairs in the form of light channels. Establishing the quantitative value of the light conductivity of the wool coat during photobiological processes in the body of irradiated animals, obtaining analytical dependencies describing the processes of passage, absorption, and reflection of optical energy of various spectral composition, as well as determining the effectiveness of the effect of absorbed energy by irradiating the wool coat constitute new knowledge for understanding the full the mechanism of interaction of the energy of optical radiation of the Sun with irradiated animals.

MATERIALS AND METHODS

When conducting experimental research, individual wool (hair) of white pigs was used. Optical quantum generators (lasers) with monochromatic radiation of the near-infrared, visible, and long-wave ultraviolet spectra of biological action (630 nm, 532 nm, 445 nm) and a universal spectrophotometer of the SF-4 type were used to investigate the light conductivity of individual hairs. Registration of radiation at the exit of the end of a single hair, as a light guide, was carried out using a special device built based on a sensitive galvanometer with a photomultiplier (FEU-118A) of a wide range of sensitivity. To obtain a reliable signal regarding the measurement of the radiation that passed to the receiving window of the sensitive photoelectric multiplier, a separate hair was tightly wrapped with a rubber seal. Studies were performed in no less than tenfold repetition [18; 19].

The data of the experimental study of the light conductivity of individual wools were conducted based on the use of methods and means of fibre optics. At present, fibre optics for transmitting information over long distances is widely developed. Developed methods for calculating fibre optics [18; 19]. To find the energy of the spectrum of optical radiation affecting the body of animals through the wool cover, it is possible to use such approaches, but with certain limitations.

The optical fibre is a long cylinder with an outer coating with a high refractive index and a core transparent to optical radiation.

The main parameter characterising the efficiency of optical energy propagation in optical fibres is the spectral coefficient of light conductivity, which is determined according to the following correlation:

$$\tau = \frac{\Phi_\lambda}{\Phi_{\lambda 0}}\,, \tag{1}$$

where Φ_λ and $\Phi_{\lambda 0}$ are optical energy fluxes with a wavelength, respectively, passing inside the cylinder through the light guide and the flux falling on the surface of its cylinder from the outside.

Passing through a material medium, the intensity of optical radiation always decreases, i.e., a certain amount of it is lost. These losses in the material occur through the scattering and absorption of photons emitted by the molecules of the material structure itself.

As a rule, such losses are divided into losses in the material (substance) itself and light (optical). The more heterogeneous the structure of the light guide, the greater the radiation loss in it.

If one considers a single wool as a light guide of optical radiation, then given the above, the correlation of the transmission coefficient depending on the geometric parameters, the structure of the wool and the structure can be described by the following mathematical expression

$$\tau_0 = \tau_1 \cdot \tau_2 \cdot \tau_3, \tag{2}$$

where τ_1 is the geometric transmission coefficient, which determines the effective light transmission inside the wool cylinder.

$$\tau_1 = \frac{sin^2\psi_0}{sin^2\psi_1} \tag{3}$$

where Ψ_0 is the limiting angle of incidence of the beam on the surface of the wool, at which such a beam completely penetrates inside; Ψ_1 is the angle at which the beam is completely reflected from the surface of the animal's fur at the point of its incidence.

$$sin\psi_1 = \frac{S_0}{\sqrt{1 - L^2 \cdot D^{-2}}} \tag{4}$$

where S_0 is the area of the wool surface that is irradiated at the point of incidence of the beam itself; L is the length of the light-conducting wool particle; D is the cross-sectional diameter of the wool.

The coefficient τ_2, which characterises the weakening (scattering) of internal light transmission on the cellular structures of wool:

$$\tau_2 = 10^{-\varepsilon \cdot P}, \tag{5}$$

where ε is an indicator showing the absorption of radiation by the wool material; P is the beam path length inside the wool when it is repeatedly reflected inside the cylinder.

$$P = L \cdot sec\psi_1 = \frac{L}{\sqrt{1 - sin^2\psi_1 \cdot n_c^{-2}}} \tag{6}$$

where n_c is an indicator showing the angle of refraction of the beam that falls in the middle of the wool cylinder; L is the length of the light-conducting part of the hair.

The coefficient τ_3, which characterises the loss of light transmission inside the wool cylinder by scattering the beam itself in its internal structures:

$$\tau_3 = \rho_r^{\eta}, \tag{7}$$

where ρ_r is the coefficient characterising the single reflection of the beam from the inner surface of the wool; η is the number of reflections on single internal structures of the wool material.

If there is a core in the hair, which is observed in many species and breeds of animals, such number of reflections will be determined according to the following correlation:

$$\eta = L \cdot D_c^{-1} \cdot tg\psi_0 = \frac{L \cdot sin\psi_1}{D_c \cdot \sqrt{n_c^2 - sin^2\psi_1}} \tag{8}$$

where n_c is an indicator that characterises the angle of refraction of the incident beam; D_c is the cross-sectional diameter of the wool core.

Considering the above, the loss of light transmission of the core in the wool can be determined according to the following correlation:

$$\tau_3 = \rho_{\text{в}}^{\frac{L \cdot sin\psi_1}{D_c \cdot \sqrt{n_c^2 - sin^2\psi_1}}} \tag{9}$$

Having found the light transmittance components of an individual hair, it is possible to find the total light transmittance according to the following correlation:

$$\tau_0 = \tau_1 \cdot \tau_2 \cdot \tau_3 = \frac{sin^2\psi_0}{sin^2\psi_1} \cdot 10^{-\varepsilon P} \cdot \rho_{\text{в}}^{\frac{L \cdot sin\psi_1}{\sqrt{n_c^2 - sin^2\psi_1}}} \tag{10}$$

Thus, expression 10 shows that the amount of optical radiation energy entering the skin through a cylinder of individual wool depends on the angle of incidence of the beam on the surface of the wool, the transparency of the internal structure of its cylinder, the length of the light-conducting part and the refractive index of its outer shell.

Notably, the above correlation characterises the light conductivity of wool of a simple structure and comprises a light-conducting core and a protective cladding. In real conditions, especially in winter, in most animals, the formation of the axial core (brain) is observed inside the hair. Therefore, in the case under study, it is better to consider the wool as a fibre optic cable made of three coaxial cylinders. Furthermore, the inner cylinders will also be light conducting with different transmission coefficients (Fig. 1).

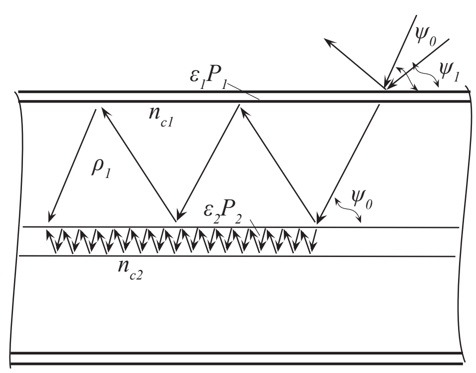

Figure 1. Schematic representation of optical radiation propagating inside a cored hair

The light conductivity of such wool will be determined by the product of the light conductivities of the "brain" core and the inner cylinder:

$$\tau = \tau_{01} \cdot \tau_{02} = \frac{sin^2\psi_0}{sin^2\psi_1} 10^{-\varepsilon_1 \cdot P_1} \cdot \rho_{\text{в}}^{\frac{L \cdot sin\psi_1}{D_c \cdot \sqrt{n_{c1}^2 - sin^2\psi_1}}} \times$$
$$\times \frac{sin^2\psi_0{}'}{sin^2\psi_1{}'} \cdot 10^{-\varepsilon_2 P_2} \cdot \rho_{\text{в}}^{\frac{L sin\psi_1{}'}{D_c \cdot \sqrt{n_{c2}^2 - sin^2\psi_1}}} \tag{11}$$

The determination of the total light transmission coefficient of individual hairs can be performed according to the correlation (11), while this correlation is inherent in determination under the condition of conducting research on the primary mechanism of action of optical radiation that enters the follicles through these hairs.

In the conditions of the industrial use of optical radiation in the cultivation of biological objects of animal origin, namely animals and poultry, in the case when the entire skin and fur cover is exposed to radiation, then in this case it is appropriate to use simplified calculations.

Losses in the optical path comprise losses that occur at the interface between the cladding and the core. If the beam of optical radiation is of sufficient intensity I_{e0}, then in this case, the light intensity I_{el}, which propagates at a distance l from the entry point (according to the Bouguer-Lambert-Behr law), is determined according to the following correlation:

$$I_{el} = I_{e0} e^{-\alpha_t \cdot l} \tag{12}$$

where l is the distance from the point of incidence of the optical beam to the point from which energy is measured in the light guide; $\alpha_t - \alpha_s + \alpha_a$ is an indicator that represents attenuation during radiation in the light guide; α_s is an indicator that factors in attenuation by scattering the energy of the beam from the outside through the cladding; α_a is the rate of attenuation of the incident energy inside the light guide by its absorption.

Given that the hair is fixed in the skin at one end (follicle), and its length and diameter increase with the age of the animal, in this case, the practical interest lies only in the determination of the radiation energy that is scattered in the thickness of its skin along the entire length of the hair before it will come out of the follicle.

Such radiation, which passed through the hair cylinder into the follicle, is scattered through its spherical surface in the thickness of the skin and takes part in photobiological reactions, can be determined from the following correlation:

$$dI_s(l)=I_e(l)\cdot\alpha_s\cdot dl=I_{e0}\,e^{-\alpha_t\cdot l}\cdot\alpha_s\cdot dl \qquad (13)$$

where $dI_s(l)$ is the intensity of optical radiation, which is scattered over a length dl along the surface of the wool at a distance l from the point of entry of the radiation into the cylinder of the wool.

The spectral intensity of radiation absorption along the entire length of the wool cylinder can be written as follows:

$$I_e(l,\gamma)=I_{e0}(\gamma)\cdot e^{-\alpha_t(\gamma)\cdot l} \qquad (14)$$

The intensity of radiation scattering by hair into the skin environment is determined from the following correlation:

$$I_{s(l_2-l_1)\gamma}=I_{e0}(\gamma)\cdot\frac{\alpha_s(\gamma)}{\alpha_t(\gamma)}\left(1-e^{-\alpha_t(\gamma)\cdot(l_2-l_1)}\right), \qquad (15)$$

and accordingly, the very intensity of radiation absorption by hair in the depth of the skin is determined by the following correlation:

$$I_{\alpha(l_2-l_1)\gamma}=I_{e0}(\gamma)\cdot\frac{\alpha_\alpha(\gamma)}{\alpha_t(\gamma)}\left(1-e^{-\alpha_t(\gamma)\cdot(l_2-l_1)}\right). \qquad (16)$$

The correlations (14), (15), (16) describe the spectral light-conducting properties of hair and their distribution of radiation energy along its entire length from the point of penetration into the hair to the follicle and in the depth of the animal's skin.

RESULTS AND DISCUSSION

Experimental studies, as mentioned above, were carried out on the original setup. The results of the conducted experimental studies to determine the transmission efficiency of monochromatic laser radiation (with a wavelength of 445 nm) depending on the place of incidence of the laser beam on the surface of the fur along the entire length of the hair are presented in Figure 2 [20].

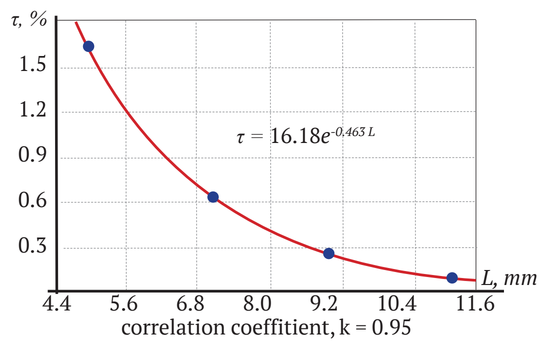

Figure 2. Experimental and mathematical correlation of the light conductivity of a single bristle on its length towards radiation and perpendicular to its side surface [20]

Figure 2 shows that the process of propagation of optical radiation inside the cylinder of individual hair has an exponential form, which indicates a complex non-linear biological structure of the cylinder core. Similar studies were conducted with the optical radiation of lasers of 630 and 532 nanometres. To find the correlation of the light transmission of a hair and the diameter of its cylinder, the study used hair from various parts of the animal's body, as well as from animals of the same breed and of different ages. As an example, the spatial image of optical radiation inside the cylinder of an individual hair depending on the wavelength of optical radiation λ and the length of the light-conducting part of the hair L is presented in Figure 3.

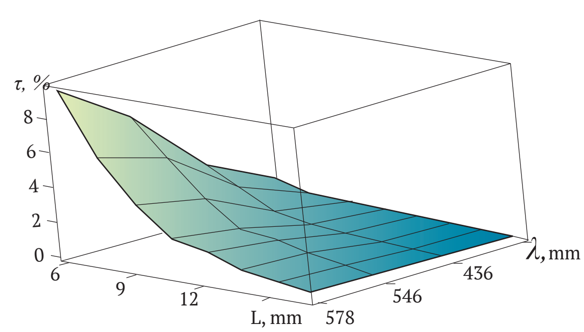

Figure 3. Expanded spatial picture of the correlation of the light conductivity of a hair on its spectral composition of optical radiation and the length of the light-conducting particle (distance to its skin) [9; 20]

The obtained results confirmed the hypothesis of some authors [8; 11; 21;22] that the fur coat of animals not only protects them from the harmful effects of the external environment but can also be a regulator of this effect. The exponential nature of the obtained correlations corresponds to the biological laws of nature and partially confirms their probability and reliability.

CONCLUSIONS

1. When studying the effectiveness of the penetration of optical radiation under the skin of a biological object of an animal origin along separate hairs, like a bundle of light guides, it is advisable to use the known laws of fibre optics in calculations and research.

2.It was experimentally established and theoretically substantiated that the light-conducting capacity of a single hair increases with the increase in the wavelength of the spectrum of optical radiation, i.e., infrared radiation has a higher penetrating power than ultraviolet radiation.

3. The closer the beam of radiant light falls on the surface of the hair to the growth area of the individual hair from the surface of the skin of the biological object of animal origin, the more optical energy will flow through the cylinder of the hair to its follicle under the skin. Thus, optical energy enters directly into the perifollicular environment of the skin, saturated with cells of nerve endings and blood capillaries. Such energy takes part in photobiological processes much more effectively than the energy that enters directly through the surface of the skin between the hairs.

4. Explanation and substantiation of the mechanism of the propagation of optical radiation energy inside the cylinder of a single individual hair is of scientific and practical importance in biological studies of the role of the skin and hair of biological objects of animal origin in their life and development and in the further study of the ways and mechanism of the influence of optical radiation energy on them, as well as for the possibility of effective dosing of optical irradiation of animals and poultry that are grown on large farms with a lack of sunlight.

REFERENCES

[1] Cooper, C.E., & Withers, P.C. (2008). Animal physiology. In *Encyclopedia of ecology* (pp. 228-237). Amsterdam: Elsevier.

[2] Lundsgaard, N.U., Cramp, R.L., & Franklin, C.E. (2021). Ultraviolet-B irradiance and cumulative dose combine to determine performance and survival. *Journal of Photochemistry and Photobiology B: Biology*, 222, article number 112276.

[3] Sousa, A.P.C., Gurgel, C.A., Ramos, E.A.G., Trindade, R.F., Valverde, L.F., Carneiro, T.S., Cangussú, M.C.T., Pinheiro, A.L.B., & Santos, J.N. (2014). Infrared LED light therapy influences the expression of fibronectin and tenascin in skin wounds of malnourished rats – A preliminary study. *Acta Histochemica*, 116(7), 1185-1191.

[4] Middelburg, T.A., de Bruijnb, H.S., van der Ploeg, A., Neumann, H.A.M., & Robinson, D.J. (2013). The effect of light fractionation with a 2-h dark interval on the efficacy of topical hexyl-aminolevulinate photodynamic therapy in normal mouse skin. *Photodiagnosis and Photodynamic Therapy*, 10(4), 703-709.

[5] Munem, M., Djuphammar, A., Sjölander, L., Hagvall, L., & Malmberg, P. (2021). Animal – free skin permeation analysis using mass spectrometry imaging. *Toxicology in Vitro*, 71, 245-251.

[6] Kim, C.-H., Cheong, K.A., & Lee, A.-Y. (2013). 850 nm light-emitting-diode phototherapy plus low-dose tacrolimus (FK-506) as combination therapy in the treatment of dermatophagoides farinae-induced atopic dermatitis-like skin lesions in NC/Nga mice. *Journal of Dermatological Science*, 72(2), 142-148.

[7] Dimaki, A., Kyriazi M., Leonis, G., Sfiniadakis, I., Theodoros, G., Papaioannou, E., Vassilios, I., & Rallis, R.M. (2019). Diabetic skin and UV light: Protection by antioxidants. *European Journal of Pharmaceutical Sciences*, 127, 1-8.

[8] Li, J., Shaoab, Y., Chenc, X., Wangab, X., Wangab, Q., Wangd, Y, Zhue, Y., Yua, H., Hanab, L., & Tianab, F. (2022). Dual-excitation red-emissive carbon dots excited by ultraviolet light for the mitochondria-targetable imaging and monitoring of biological process in living cells. *Journal of Photochemistry and Photobiology A: Chemistry*, 425, 15-23.

[9] Akhtar, S., Smedowskic, A., Masmalib, A. Alkanaanb, A., Khan, A.A., Almutle, E., Mofty, H.K., Al-Debasi, H.I., Samivel, R., & Almubrad, T. (2022). Effect of Ultraviolet-A and Riboflavin treatment on the architecture of the center and periphery of normal rat cornea: 7 days post treatment. *Experimental Eye Research*, 219, article number 109064.

[10] Maliszewska, I., & Goldeman, W. (2021). Pentamidine enhances photosensitization of Acinetobacter baumannii using diode lasers with emission of light at wavelength of λ=405 nm and λ=635 nm. *Photodiagnosis and Photodynamic Therapy*, 34, 12-21.

[11] Ivanov, V.V., Tyunina, P.S., & Savinova, M.S. (1967). Research of the permeability of the bristles of pigs of different ages to ultraviolet rays. *Bulletin of Yakutsk State University*, 7, 89-94.

[12] Butov, G.P. (1980). Optical properties of wool, feather and skin covers of animals and poultry. *Gorki, Automation and Electrification of Agricultural Production*, 63, 68-72.

[13] Graeme, E. (2021). Glass photobiomodulation: A review of the molecular evidence for low level light therapy. *Journal of Plastic, Reconstructive & Aesthetic Surgery*, 74(5), 1050-1060.

[14] Nakashima, Y., Ohta, S., & Wolf, M. (2017). Blue light-induced oxidative stress in live skin free radical. *Biology and Medicine*, 108, 300-310.

[15] Pavlov, V.F., & Melnik, I.L. (1963). Penetration of ultraviolet rays through the wool into the body of cattle and horses. In *Use of ultraviolet radiation in animal husbandry* (pp. 91-95). Moscow: Publishing House of the Academy of Sciences of the USSR.

[16] Park, I.-S., Mondal, A., Chung, P.-S., & Ahn, J.C. (2015). Prevention of skin flap necrosis by use of adipose-derived stromal cells with light-emitting diode phototherapy. *Cytotherapy*, 17(3), 283-292.
[17] Weihrauch, D., Keszler, A., Lindemer, B., Krolikowski, J., & Nicole, L. (2021). Lohr red light stimulates vasodilation through extracellular vesicle trafficking. *Journal of Photochemistry and Photobiology, B: Biology*, 220, 354-364.
[18] Chervinsky, L.S. (2020). The ways and effects of ultraviolet radiation on the human and animal body. *Tissue Optics and Photonics*, 11363, article number 113630I. doi: 10.1117/12.2552719.
[19] Sattarov, D.S. (1973). *Fiber optics*. Leningrad: Mechanical Engineering.
[20] Chervinsky, L.S. (2018). Rationale and definition of the criteria of the efficiency of the biological activity of optical radiation on animal organism. *Korean Journal of Food & Health Convergence*, 4(3), 1-5.
[21] Ripoll, J., & Ntziachristos, V. (2011). Light, sound, chemistry… action: State of the art optical methods for animal imaging Drug. *Discovery Today: Technologies*, 8(2-4), e79-e86.
[22] Bobyr, S. (2021). Theoretical Aspects of Hydrogen Diffusion in Metals. *Scientific Herald of Uzhhorod University. Series "Physics"*, (50), 31-38.

СПИСОК ВИКОРИСТАНИХ ДЖЕРЕЛ

[1] Cooper C.E., Withers P.C. Encyclopedia of ecology. *Animal physiology*. Amsterdam: Elsevier, 2008. P. 228–237.
[2] Lundsgaard N.U., Cramp R.L., Franklin C.E. Ultraviolet-B irradiance and cumulative dose combine to determine performance and survival. *Journal of Photochemistry and Photobiology B: Biology*. 2021. Vol. 222. Article number 112276.
[3] Infrared LED light therapy influences the expression of fibronectin and tenascin in skin wounds of malnourished rats – A preliminary study / A.P.C. Sousa, et al. *Acta Histochemica*. 2014. Vol. 116, No. 7. P. 1185–1191.
[4] The effect of light fractionation with a 2-h dark interval on the efficacy of topical hexyl-aminolevulinate photodynamic therapy in normal mouse skin / T.A. Middelburg et al. *Photodiagnosis and Photodynamic Therapy*. 2013. Vol. 10, No. 4. P. 703–709.
[5] Animal – free skin permeation analysis using mass spectrometry imaging / M. Munem et al. *Toxicology in Vitro*. Vol. 71. 2021. P. 245–251.
[6] Kim C.-H., Cheong K.A., Lee A.-Y. 850 nm light-emitting-diode phototherapy plus low-dose tacrolimus (FK-506) as combination therapy in the treatment of dermatophagoides farinae-induced atopic dermatitis-like skin lesions in NC/Nga mice. *Journal of Dermatological Science*. 2013. Vol. 72, No. 2. P. 142–148.
[7] Diabetic skin and UV light: Protection by antioxidants / A. Dimaki, et al. *European Journal of Pharmaceutical Sciences*. 2019. Vol. 127. P. 1–8.
[8] Dual-excitation red-emissive carbon dots excited by ultraviolet light for the mitochondria-targetable imaging and monitoring of biological process in living cells / J. Li et al. *Journal of Photochemistry and Photobiology A: Chemistry*. 2022. Vol. 425. P. 15–23.
[9] Effect of Ultraviolet-A and Riboflavin treatment on the architecture of the center and periphery of normal rat cornea: 7 days post treatment / S. Akhtar et al. *Experimental Eye Research*. 2022. Vol. 219. Article number 109064.
[10] Maliszewska I., Goldeman W. Pentamidine enhances photosensitization of Acinetobacter baumannii using diode lasers with emission of light at wavelength of λ=405 nm and λ=635 nm. *Photodiagnosis and Photodynamic Therapy*. 2021. Vol. 34. P. 12–21.
[11] Іванов В.В., Тюніна П.С., Савінова М.С. Дослідження проникнення щетини свиней різного віку для ультрафіолетових змін. *Вісник Якутського державного університету*. 1967. № 7. С. 89–94.
[12] Бутов Г.П. Оптические свойства шерстяного, перьевого и кожного покровов животных и птицы. *Автоматизация и электрификация сельскохозяйственного производства*. 1980. № 63. С. 68–72.
[13] Graeme E. Glass photobiomodulation: A review of the molecular evidence for low level light therapy. *Journal of Plastic, Reconstructive & Aesthetic Surgery*. 2021. Vol. 74, No. 5. P. 1050–1060.
[14] Nakashima Y., Ohta S., Alexander M. Wolf Blue light-induced oxidative stress in live skin Free Radical. *Biology and Medicine*. 2017. Vol. 108. P. 300–310.
[15] Павлов В.Ф., Мельник І.Л. Проникнення ультрафіолетових променів через шерсть в організм великої рогатої худоби і коней. *Використання ультрафіолетового випромінювання в тваринництві*. Київ: Видавництво АН УРСР, 1963. С. 91–95.
[16] Prevention of skin flap necrosis by use of adipose-derived stromal cells with light-emitting diode phototherapy / I.S. Park et al. *Cytotherapy*. 2015. Vol. 17, No. 3. P. 283–292.
[17] Red light stimulates vasodilation through extracellular vesicle trafficking / D. Weihrauch, et al. *Journal of Photochemistry and Photobiology B: Biology*. 2021. Vol. 220. P. 354–364.
[18] Chervinsky, L.S. (2020). The ways and effects of ultraviolet radiation on the human and animal body. *Tissue Optics and Photonics*, 11363, article number 113630I. doi: 10.1117/12.2552719
[19] Саттаров Д.С. Волоконна оптика. Ленинград: Машиностроитель, 1973. 254 с.

[20] Chervinsky L.S. Rationale and definition of the criteria of the efficiency of the biological activity of optical radiation on animal organism. *Korean Journal of Food & Health Convergence*. 2018. Vol. 4, No. 3. P. 1–5.
[21] Ripoll J., Ntziachristos V. Light, sound, chemistry… action: state of the art optical methods for animal imaging. *Drug. Discovery Today: Technologies*. 2011. Vol. 8, No. 2–4. P. e79–e86.
[22] Bobyr, S. (2021). Theoretical Aspects of Hydrogen Diffusion in Metals. *Scientific Herald of Uzhhorod University. Series "Physics"*. 2021. Vol 50. P. 31-38.

Леонід Степанович Червінський, Іван Петрович Радько, Віталій Адамович Наливайко, Олександр Володимирович Окушко

Національний університет біоресурсів і природокористування України
03041, вул. Героїв Оборони, 15, м. Київ, Україна

Результати експериментальних досліджень проходження енергії світла під шкіру тварин по окремим шерстинам

Анотація. В статті наведено нові наукові результати експериментальних досліджень, які спростовують загально прийнятий факт вважати, що шерстинний покрив лише захищає тварини від впливу енергії Сонця. Метою даних досліджень є підтвердження факту поширення енергії оптичного випромінювання під шкіру тварини по окремим шерстинам, як світлопроводах. Експериментально визначено оптичнопровідну структуру окремої шерстини, складові параметра пропускання окремо взятої шерстяної волосини, а саме коефіцієнт світлопропускання усередину шерстяної волосини, коефіцієнт послаблення внутрішнього світлопропускання речовиною шерстяної волосини, коефіцієнт втрат в середині циліндру шерстяної волосини за рахунок променю, що розсіюється у внутрішній структурі і коефіцієнту заломлення її зовнішньої оболонки. На основі використання методів фотометрії та геометричної оптики теоретично обґрунтовано і експериментально отримано результати щодо встановлення математичної залежності загальної величини енергії оптичного випромінювання, що надходить по циліндру шерстинки від значення кута падіння променю на поверхню шерстинки, чистоти внутрішнього осердя структури циліндру, довжини світлопровідної ділянки до поверхні шкіри, а також коефіцієнту заломлення її зовнішньої оболонки. На основі результатів експериментальних досліджень отримано математичні залежності, що описують спектральні світло провідні властивості окремої шерстинки, а також розподіл енергії, що випромінюється в товщі шкіри по всій довжині від місця проникнення у шерстинку і до фолікули – місця використання оптичної енергії в фотобіологічних процесах. Отримані результати експериментальних досліджень проходження енергії оптичного випромінювання по довжині окремої шерстинки в тіло тварини, мають важливе практичне значення для фотобіологів, що досліджують дію оптичного випромінювання Сонця на біологічні об'єкти тваринного походження

Ключові слова: сонячна енергія, опромінення тварин, шкіряно-шерстинний покрив, світлопропускання, шерстинка

ТЕХНІКА ТА ЕНЕРГЕТИКА

Науковий журнал

Том 13, № 2. 2022

Заснований у 2010 р. Виходить чотири рази на рік

Оригінал-макет видання виготовлено у відділі науково-технічної інформації
Національного університету біоресурсів і природокористування України

Редагування англомовних текстів:
С. Воровський, К. Касьянов

Комп'ютерна верстка:
К. Сосєдко

Підписано до друку 27 квітня 2022 р. Формат 60*84/8
Умов. друк. арк. 12,8
Наклад 50 прим.

Адреса видавництва:
Національний університет біоресурсів і природокористування України
вул. Героїв Оборони, 15, м. Київ, 03041, Україна
E-mail: info@technicalscience.com.ua
www: https://technicalscience.com.ua/uk

MACHINERY & ENERGETICS

Scientific Journal

Volume 13, No. 2. 2022

Founded in 2010. Published four times per year

The original layout of the publication is made in the Department of Scientific and Technical Information of National University of Life and Environmental Sciences of Ukraine

Editing English-language texts:
S. Vorovsky, K. Kasianov

Desktop publishing:
K. Sosiedko

Signed for print of April 27, 2022. Format 60*84/8
Conventional printed pages 12.8
Circulation 50 copies

Editors Office Address:
National University of Life and Environmental Sciences of Ukraine
03041, 15 Heroiv Oborony, Kyiv, Ukraine
E-mail: info@technicalscience.com.ua
www: https://technicalscience.com.ua/en